

**CHARACTERIZATION OF HYDROPHILIC-RICH PHASE MIMIC IN DENTIN ADHESIVE AND
COMPUTER-AIDED MOLECULAR DESIGN OF WATER COMPATIBLE VISIBLE LIGHT
INITIATORS**

BY

©2016

Farhana Abedin

Submitted to the graduate degree program in Bioengineering and the Graduate Faculty of the University
of Kansas in partial fulfillment of the requirements for the degree of Doctor of Philosophy

Chairperson Dr. Paulette Spencer

Co-chairperson Dr. Kyle Camarda

Dr. Qiang Ye

Dr. Anil Misra

Dr. Jennifer Laurence

Dr. Trent J. Herda

Date Defended: April 27th, 2016

The Dissertation Committee for Farhana Abedin

Certifies that this is the approved version of the following dissertation:

CHARACTERIZATION OF HYDROPHILIC-RICH PHASE MIMIC IN DENTIN ADHESIVE AND
COMPUTER-AIDED MOLECULAR DESIGN OF WATER COMPATIBLE VISIBLE LIGHT
INITIATORS

Chairperson Dr. Paulette Spencer

Co-chairperson Dr. Kyle Camarda

Date Approved: May 6th, 2016

ABSTRACT

The clinical lifetime of moderate-to-large dental composite restorations is lower than dental amalgam restorations. With the imminent and significant reduction in the use and availability of dental amalgam, the application of composite for the restoration of teeth will increase. Since composite has a higher failure rate, the increased use of composite will translate to an increase in the frequency of dental restoration replacement, overall cost for dental health and discomfort for patients. The composite is too viscous to bond directly to the tooth and thus, a low viscosity adhesive is used to form the bond between the composite and tooth. The bond at the adhesive/tooth is intended to form an impervious seal that protects the restored tooth from acids, oral fluids and bacteria that will undermine the composite restoration. The integrity of the adhesive/tooth bond (the exposed tooth structure is largely composed of enamel and dentin) plays an important role in preventing secondary caries which undermine the composite restoration. This study focuses on the durability of etch-and-rinse dental adhesives.

As the adhesive infiltrates the demineralized dentin matrix, it undergoes phase separation into hydrophobic- and hydrophilic-rich phases. The hydrophilic-rich phase contains the conventional hydrophobic photo-initiator system (camphorquinone/ethyl 4-(dimethylamino)benzoate) and cross-linker both in inadequate concentrations. This may compromise the polymerization reaction and the cross-linking density of this phase, making it vulnerable to failure. The goal of this study is to characterize the hydrophilic-rich phase of the dental adhesive by monitoring its polymerization kinetics and glass transition temperature under the presence of an iodonium salt (reaction accelerator), and varying water concentration, photo-initiator concentration and light intensity. The final goal is to develop a computational framework for designing water compatible visible light photosensitizers specifically for the hydrophilic-rich phase of dental adhesives.

It was observed that the degree of conversion of the hydrophilic-rich mimics is dominated by the photo-initiator concentration and not the cross-linker. A secondary rate maxima was observed in the case of hydrophilic-rich phase mimics which was associated with the formation of microgels during polymerization. A polymerization mechanism involving polymerization- and solvent-induced phase separation was proposed for the hydrophilic-rich mimics. The hydrophilic dental resins were sensitive to light intensity, i.e. at low light intensities the degree of conversion of the hydrophilic resin was reduced substantially in the presence of camphorquinone/ethyl 4-(dimethylamino)benzoate as photo-initiators, whereas a substantial degree of conversion was observed for the hydrophobic resin even at these lower light intensities. The addition of iodonium salt in the hydrophilic resin significantly improved the degree

of conversion of the hydrophilic resin at low light intensities. These studies also showed that the iodonium salt could lead to enhanced cyclization and shorter polymer chain lengths within the hydrophilic-rich phase. For the physically separated hydrophilic-rich phase specimens, it was observed that in the presence of the conventional photo-initiator system (camphorquinone/ethyl 4-(dimethylamino)benzoate), there was no polymerization, mostly due to the insufficient partition concentrations of the photo-initiator components within this phase. The addition of iodonium salt in this case significantly improved the degree of conversion but it was still significantly lower. These studies indicated that the overall polymerization efficiency of the hydrophilic-rich phase was lower than the hydrophobic-rich phase. The lower polymerization efficiency of the hydrophilic-rich phase led to a phase that lacks integrity; the hydrophilic-rich phase could be infiltrated by oral fluids and cariogenic bacteria. The infiltration of these noxious agents at the interface between the material and tooth could pave the way for enhanced degradation of the tooth structure (collagen and mineral) as well as the adhesive polymer. Novel photosensitizer molecules were proposed to improve the polymerization efficiency of this phase. Computer-aided molecular design (CAMD) was employed to obtain the new photosensitizers. These photosensitizers were capable of improving the degree of conversion of the hydrophilic-rich phase. An enhanced degree of conversion of the hydrophilic-rich phase would lead to a better seal at the adhesive/dentin interface and higher bond strength.

Computer-aided molecular design (CAMD) is a fast and inexpensive technique compared to the conventional trial-and-error method to rationally design products. For this case, hydrophilic molecules with photosensitizing capability in the visible range were selected and several target properties of these molecules were determined. The target properties for this design were: octanol/water partition coefficient, relative normalized photon absorption efficiency, molar extinction coefficient at 480 nm, degree of conversion and polymerization rate of the hydrophilic-rich phase. These data for the target properties were used to develop quantitative structure property relationships (QSPRs). These correlations and structural constraints were used to develop a mixed integer non-linear program, which was solved via an optimization algorithm, minimizing the difference between the properties of the solutions and the target values. Four candidate novel molecular structures for the photosensitizer were proposed, which were predicted to be hydrophilic in nature and exhibit a substantial degree of conversion within the hydrophilic-rich phase. All these molecules contained iminium ions, which suggested that this specific feature could play a vital role in the formation of efficient radicals. This investigation clearly indicates that the hydrophilic-rich phase forms a weak region and provides several directions towards fortifying this phase against failure.

ACKNOWLEDGEMENTS

This work would not have been possible without the support and guidance from Dr. Spencer, Dr. Ye and Dr. Camarda. I will remain indebted to them for all the achievements accomplished here. I am extremely grateful to Dr. Ye for providing me with the guidance to learn experimental and analysis techniques. I also would like to express my gratitude to Dr. Misra, Dr. Laurance and Dr. Herda for being my committee members.

I would like to thank Ranganathan Parthasarathy and Viraj Singh for their support and advice. I am grateful to Dr. Song and Dr. Ge for helping me with my experiments and their invaluable suggestions. I also would like to thank Holly J. Good and all other lab assistants for helping me with my project. I am grateful to Banu Taktak and Sarah VanOosten for helping me with the UV-vis spectroscopy study. I am also thankful to Brock Roughton for his support and help with the computer-aided molecular design project. I would like to thank Jenny Ding and Jen Welch for their support and help with various processes while I was working at the Bioengineering Research Center.

Lastly, I would like to thank my parents and my husband, Md Rajib Anwar for their inspiration and support which has led me to pursue a PhD degree. This research was supported by the research grants from National Institutes of Health (NIH)/National Institute for Dental and Craniofacial Research (NIDCR), R01DE022054 (PS, JSL) and R01DE025476-01 (PS, CT), Bethesda, MD.

CONTENTS

ABSTRACT.....	iii
CONTENTS.....	vi
1. INTRODUCTION AND BACKGROUND.....	1
1.1 Introduction.....	1
1.2 Motivation.....	2
1.3 Background.....	8
1.3.1 Dental Adhesive.....	8
1.3.2 Computer-aided molecular design.....	12
1.3.2.1 Molecular descriptors.....	13
1.3.2.2 Quantitative Structure Property Relationship (QSPR).....	15
1.3.2.3 Computer-aided molecular design problem formulation (CAMD)	16
1.4 Specific aim.....	18
1.4.1 Specific Aim 1: Characterization of hydrophilic-rich phase.....	19
1.4.2 1.4.2 Specific Aim 2: Development of a framework for computer-aided molecular design (CAMD) of water compatible visible light photosensitizer	20
1.5 Innovation.....	21
PART I: CHARACTERIZATION OF HYDROPHILIC-RICH PHASE OF DENTAL ADHESIVE.....	24
2. POLYMERIZATION KINETICS OF HYDROPHOBIC- VERSUS HYDROPHILIC-RICH PHASES & EFFECT OF CROSS-LINKER/PHOTOSENSITIZER CONCENTRATIONS ON THE POLYMERIZATION OF HYDROPHILIC-RICH PHASE MIMICS.....	25
2.1 Introduction.....	25
2.2 Materials and methods.....	26
2.2.1 Preparation of hydrophobic- and hydrophilic-rich phase mimics.....	26
2.2.2 Fourier Transform Infrared Spectroscopy (FTIR).....	28
2.2.3 Photopolymerization kinetics study.....	29
2.2.4 Viscosity measurement.....	30
2.2.5 Statistical analysis.....	30
2.3 Results.....	31
2.3.1 Difference in photopolymerization kinetics of hydrophobic- and hydrophilic- rich phase mimics.....	31
2.3.2 Polymerization kinetics results for hydrophilic-rich phase mimics containing standard PI concentration.....	32
2.3.3 Polymerization kinetics results of hydrophilic-rich phase mimics containing reduced concentration of PI.....	34

2.4	Discussion.....	35
2.5	Conclusion.....	38
3.	IMPACT OF WATER CONCENTRATION ON THE PHOTO-POLYMERIZATION OF HYDROPHILIC-RICH MIMICS AND ITS POLYMERIZATION MECHANISM.....	39
3.1	Introduction.....	39
3.2	Materials and methods.....	39
3.2.1	Polymerization kinetics study.....	41
3.2.2	Differential scanning calorimetry (DSC).....	42
3.2.3	Determination of glass transition temperature (T_g) of the hydrophilic-rich mimics.....	43
3.2.4	Determination of viscosity.....	44
3.3	Results.....	44
3.3.1	Polymerization kinetics of hydrophilic-rich mimics.....	44
3.3.2	Viscosity of the hydrophilic-rich mimics.....	46
3.3.3	Glass transition temperatures (T_g) of hydrophilic-rich mimics.....	47
3.4	Discussions.....	49
3.5	Conclusion.....	53
4.	IMPACT OF LIGHT INTENSITY ON THE PHOTO-POLYMERIZATION AND NETWORK FORMATION OF HYDROPHOBIC- AND HYDROPHILIC METHACRYLATE DENTAL RESINS.....	56
4.1	Introduction.....	56
4.2	Materials and methods.....	56
4.2.1	Photopolymerization kinetics study using FTIR.....	57
4.2.2	Glass transition temperature using DSC.....	59
4.2.3	Statistical analysis.....	59
4.3	Results.....	59
4.3.1	Polymerization of dental hydrophobic and hydrophilic resins.....	59
4.3.2	Glass transition temperature (T_g) of adhesive polymers from hydrophobic and hydrophilic resins.....	64
4.4	Discussion.....	65
4.5	Conclusion.....	71
5.	IMPACT OF PHOTO-INITIATOR PARTITION AND INCORPORATION OF IODONIUM SALT ON THE PHOTO-POLYMERIZATION OF PHYSICALLY PHASE SEPARATED DENTAL ADHESIVE.....	73
5.1	Introduction.....	73
5.2	Materials and methods.....	73
5.2.1	Preparation of physically separated hydrophilic- and hydrophobic-rich phases.....	73

5.2.2	Polymerization kinetic of physically separated hydrophobic- and hydrophilic-rich phase.....	75
5.2.3	High performance liquid chromatography (HPLC).....	75
5.2.3.1	Reverse-phase chromatography.....	75
5.2.3.2	HPLC for determining partition concentrations of PI components in hydrophobic- and hydrophilic-rich phase.....	76
5.2.4	Statistical analysis.....	78
5.3	Results.....	78
5.3.1	Polymerization kinetics result.....	78
5.3.2	Results from high performance liquid chromatography (HPLC).....	81
5.4	Discussion.....	82
5.5	Conclusion.....	85
PART II: COMPUTATIONAL DESIGN OF WATER COMPATIBLE PHOTSENSITIZER FOR DENTAL ADHESIVE APPLICATION.....		87
6.	DYES AS PHOTSENSITIZERS FOR DENTAL ADHESIVES.....	88
6.1	Introduction.....	88
6.2	Materials and methods.....	89
6.2.1	Rational selection of photosensitizer molecules to form the model building set.....	89
6.2.2	Preparation of hydrophobic- and hydrophilic-rich phases.....	90
6.2.3	Polymerization kinetics study.....	91
6.2.4	Determination of molar extinction co-efficient (ξ).....	91
6.2.5	Photon absorption efficiency.....	92
6.3	Results.....	93
6.3.1	Polymerization kinetics study.....	93
6.3.2	Molar extinction coefficient of photosensitizers.....	98
6.3.3	Photon absorption efficiency.....	98
6.4	Discussion.....	100
6.5	Conclusion.....	101
7.	COMPUTER-AIDED MOLECULAR DESIGN (CAMD) OF WATER-COMPATIBLE VISIBLE LIGHT PHOTSENSITIZER FOR DENTAL ADHESIVE APPLICATIONS.....	102
7.1	Introduction.....	102
7.2	Materials and methods.....	102
7.2.1	Forward problem: Target properties and model building set.....	102

7.2.2	Connectivity indices as topological descriptors.....	103
7.2.3	Development of quantitative structure property relationships (QSPRs).....	106
7.2.4	Inverse problem: CAMD formulation and Tabu Search.....	109
7.2.4.1	Optimization formulation and objective function.....	112
7.2.4.2	Tabu Search algorithm.....	112
7.2.4.3	Selection of target values for the properties.....	114
7.3	Results and discussion.....	114
7.3.1	Quantitative structure property relationships (QSPRs).....	114
7.3.2	Candidate photosensitizers from CAMD.....	116
7.4	Conclusion.....	116
8.	CONCLUSIONS AND FUTURE DIRECTIONS.....	119
	REFERENCES.....	122
	NOMENCLATURE.....	131
	APPENDIX: A. SOURCE FOR CALCULATION OF CONNECTIVITY INDICES AND VALENCE CONNECTIVITY INDICES IN MATLAB®	133
	APPENDIX: B. MOLECULAR STRUCTURES OF SUB-GROUPS USED IN CAMD.....	141
	APPENDIX: C. CHANGES MADE TO THE EXISTING “CARBOHYDRATE EXCIPIENT DESIGNER” TO ADAPT IT FOR THE DESIGN OF PHOTSENSITIZER.....	146

LIST OF FIGURES

Figure 1.1 Formation of hydrophobic- and hydrophilic-rich phases during phase separation of the dental adhesive (Abedin et al., 2016).....	6
Figure 1.2. Molecular structures of the major components in dental adhesive resin.....	9
Figure 1.3. Schematic showing steps involved in CAMD.....	14
Figure 1.4. Schematic describing the entire proposed project. Specific aim 1 will determine the experimental conditions necessary for carrying out photo-polymerization kinetics experiments in specific aim 2. In specific aim 2, relevant properties such as degree of conversion, rate of polymerization, molar extinction coefficient and PAE for various molecules in the model building set will be determined. The data collected in specific aim 2 will be used to develop correlations (QSPRs) with molecular descriptors. The QSPRs, structural constraints and optimization algorithm will be used to predict molecules with desired properties.....	22
Figure 2.1. Ternary phase diagram showing the phase boundary line as dashed line and formulations investigated. The circles show formulations with standard concentrations of photo-initiators and the squares exhibit formulations with reduced concentration (Abedin et al., 2015c).....	27
Figure 2.2. Schematic showing the steps for preparing samples at the miscibility limit.....	29
Figure 2.3. Polymerization kinetics results for hydrophobic-rich mimic (HB45PB) and hydrophilic-rich mimic (HB95PB) showing (a) degree of conversion versus time and (b) rate of polymerization against time. (c) Viscosity measurement showing that the hydrophobic-rich mimic is significantly viscous compared to the hydrophilic-rich mimics (Abedin et al., 2015c).....	32
Figure 2.4. Polymerization kinetics results of hydrophilic-rich mimics at miscibility limit with standard PI concentration exhibiting (a) degree of conversion against time and (b) rate of polymerization against time (Abedin et al., 2015c).....	33
Figure 2.5. Polymerization kinetics results of hydrophilic-rich mimics at miscibility limit with reduced PI concentration exhibiting (a) degree of conversion against time. (b) Comparative rate of polymerization against time is shown for HB95PB and HB95PB-QTX with standard and reduced PI concentration (Abedin et al., 2015c).....	34
Figure 3.1. Schematic showing preparation of hydrophilic-rich mimics below the miscibility limit.....	40
Figure 3.2. Ternary phase diagram showing the hydrophilic-rich mimics investigated in triangles and circles (Abedin et al., 2014).....	41

Figure 3.3. (a) 3-D surface plot for the C=C bond at 1637 cm^{-1} (b) 3-D surface plot for D-O bond for D_2O during polymerization (c) Band ratio of C=C at 1637 cm^{-1} to C=O at 1716 cm^{-1} decreasing during monitoring the polymerization kinetics <i>in-situ</i> and D_2O profile remaining almost constant (Abedin et al., 2014).....	42
Figure 3.4. (a) Reversible heat flow signal from MTDSC for HB95NR showing both the 1 st and 2 nd heating cycles (b) First derivative of the reversible heat flow versus temperature curve for HB95NR and the peaks represent the glass transition temperature (T_g) (Abedin et al., 2014).....	44
Figure 3.5. Polymerization kinetics result for formulations made from neat resin containing 95 wt% HEMA. (a) DC against time as a function of D_2O content. (b) Rate of polymerization of the formulation against time as a function of D_2O content showing the presence of secondary rate maxima. (c) Average initial and secondary rate maxima as a function of D_2O content (Abedin et al., 2014).....	45
Figure 3.6. Polymerization kinetics result for formulations made from neat resin containing 99 wt% HEMA. (a) DC against time as a function of D_2O content. (b) Rate of polymerization of the formulation against time as a function of D_2O content showing the presence of secondary rate maxima (Abedin et al., 2014).....	46
Figure 3.7. Variation of viscosity as a function of D_2O content. The triangles represent formulations prepared from HB95NR and the circles represent those from HB99NR (Abedin et al., 2014).....	48
Figure 3.8. Glass transition temperature for the first heating cycle of formulations prepared from (a) HB95NR and (b) HB99NR (Abedin et al., 2014).....	48
Figure 3.9. Schematic showing possible polymerization mechanism in case of (a) neat resins where PIPS was responsible for the microgel precipitation and (b) formulation with more than 30 wt% D_2O where PIPS and SIPS both are responsible for the microgel precipitation. The final structure will consist of higher and lower cross-linked regions as indicated by the two glass transition temperatures in the graph shown as inset. The final structure as shown by the schematic H will contain water droplets facilitating plasticization and hydrolysis of ester linkages (Abedin et al., 2014).....	54
Figure 4.1. Representative results of polymerization kinetics study for hydrophobic resins, (a, b) HB45NR2PI and (c, d) HB45NR3PI. Variation of (e) rate maxima and (f) DC at 1 h with light intensity for the hydrophobic resins (Abedin et al., 2015b).....	60
Figure 4.2. Representative results of the polymerization kinetics study for the hydrophilic formulations (a, b) HB95NR2PI and (c, d) HB95NR3PI. Variation of (e) initial rate maxima, (f) secondary rate maxima and (g) DC at 2 h with light intensity for the hydrophilic resins (Abedin et al., 2015b).....	62
Figure 4.3. Variation of final DC at 24 h obtained using pan samples for hydrophilic resins, HB95NR2PI and HB95NR3PI (Abedin et al., 2015b).....	63

Figure 4.4. DSC results for formulations (a) HB45NR2PI, (b) HB45NR3PI, (c) HB95NR2PI and (d) HB95NR3PI. The results shown here are average of all the samples per intensity (Abedin et al., 2015b).....	66
Figure 4.5. Schematic of possible polymer structures for (a) HB45NR2PI and (b) HB45NR3PI (Abedin et al., 2015b).....	70
Figure 4.6. Schematic of possible polymer structures for (a) HB95NR2PI and (b) HB95NR3PI (Abedin et al., 2015b).....	72
Figure 5.1. Schematic showing steps for preparing hydrophobic- and hydrophilic-rich phases (Abedin et al., 2016).....	74
Figure 5.2. Schematic showing major components for high performance liquid chromatography (HPLC).....	76
Figure 5.3. Chromatograms of (a) hydrophobic- and (b) hydrophilic-rich phases prepared from resin containing DPIHP, showing DPIHP peak after subtraction (Abedin et al., 2016)....	78
Figure 5.4. Representative polymerization kinetics result for the hydrophobic-rich phase showing (a) DC against time and (b) rate maxima against time (Abedin et al., 2016).....	79
Figure 5.5. Representative polymerization kinetics result for the hydrophilic-rich phase showing (a) DC against time and (b) rate maxima against time (Abedin et al., 2016).....	80
Figure 5.6. Chromatograms of hydrophobic- and hydrophilic-rich phases for (a), (b) DMAEMA and (c), (d) EDMAB (Abedin et al., 2016).....	81
Figure 5.7. Chromatograms of DPIHP for the (a) hydrophobic-rich phase and (b) hydrophilic-rich phase (Abedin et al., 2016).....	82
Figure 6.1. Molecular structures of photosensitizers in the model building set.....	94
Figure 6.2. (a) Emission spectrum of LCU Dentsply Spectrum® 800 (SN 9169 Dentsply, Konstanz, Germany) (Eacute et al., 2008) and (b) representative absorption spectrum of the photosensitizer Eosin Y disodium salt.....	95
Figure 6.3. Polymerization kinetic result of hydrophilic-rich phase showing (a) DC versus time and (b) polymerization rate against time. The polymerization rate of the hydrophilic-rich phase representing fluorescein sodium salt and methylene blue chloride are not shown because their DC is very low.....	96
Figure 6.4. Polymerization kinetic result of hydrophobic-rich phase showing (a) DC versus time and (b) polymerization rate against time. The polymerization rate of the hydrophobic-rich phase representing fluorescein sodium salt is not shown because its DC is very low.....	97
Figure 6.5. (a) Absorption spectrum and (b) graph showing the product of emission spectrum of the LCU and absorption spectrum of each photosensitizer molecule in the model building	

set. The concentration of the solution was 9 μM except in case of QTX and victoria blue B. In case of the latter two the concentration was 27 μM	99
Figure 7.1. Molecular structure of molecules in the model building set for log P.....	104
Figure 7.2. (a) Molecular structure and (b) hydrogen suppressed graph of new fuchsin.....	105
Figure 7.3. Schematic showing steps for the forward problem of CAMD.....	109
Figure 7.4. Variation of C_p statistic with the number of descriptors in the models for (a) $\ln(\xi)$ (b) log P (c) relative normalized PAE (d) degree of conversion (DC) and (e) rate of polymerization (RT).....	110
Figure 7.5. Variation of predicted value with experimental value for (a) $\ln(\xi)$ (b) log P (c) relative normalized PAE (d) degree of conversion (DC) and (e) rate of polymerization (RT)..	117
Figure 7.6. Structures of four best candidate photosensitizer molecules given by CAMD for dental adhesive application.....	118

LIST OF TABLES

Table 2.1: Composition of formulations with standard concentration of photo-initiator (Abedin et al., 2015c).....	28
Table 2.2 Composition of formulations containing reduced concentration of photo-initiators (Abedin et al., 2015c).....	29
Table 2.3. Summary of degree of conversion and rate of polymerization of formulations containing standard concentration of PI (Abedin et al., 2015c).....	31
Table 2.4. Polymerization kinetics result for hydrophilic-rich phase mimics with reduced PI concentration (Abedin et al., 2015c).....	35
Table 3.1. Composition of the hydrophilic-rich mimics investigated (Abedin et al., 2014).....	40
Table 3.2. Summary of polymerization kinetics results (Abedin et al., 2014).....	47
Table 3.3 Average T_g of formulations investigated here for the first and second heating cycle (Abedin et al., 2014).....	49
Table 4.1 Composition of the neat resin formulations studied (Abedin et al., 2015b).....	57
Table 4.2 Light intensity of the LCU and its corresponding reading on the light intensity meter (Abedin et al., 2015b).....	58
Table 4.3. Summary of polymerization kinetics result showing DC at 2 h, initial rate maxima and secondary rate maxima for all the formulations (Abedin et al., 2015b).....	64
Table 4.4. Average glass transition temperature (T_g) for each formulation at various light intensities. The T_g is reported for the second heating/cooling cycle (Abedin et al., 2015b).....	65
Table 5.1. Composition of each components in the resin mixture prior to collection of the two phases by centrifugation (Abedin et al., 2016).....	74
Table 5.2. Degree of conversion and rate maxima for hydrophobic-rich phase (Abedin et al., 2016).....	80
Table 5.3. Degree of conversion and rate maxima for hydrophilic-rich phase (Abedin et al., 2016).....	81
Table 5.4. Partition concentration of DMAEMA, DPIHP and EDMAB in hydrophobic- and hydrophilic-rich phase (Abedin et al., 2016).....	82
Table 6.1. Components of PI and their approximate wt% in the final mixture before phase separation.....	90

Table 6.2. Composition of mixture before phase separation for each type of photosensitizer in the model building set.....	92
Table 6.3. Average DC and polymerization rate of the hydrophilic-rich phase for each photosensitizer in the model building set.....	96
Table 6.4. Average DC and polymerization rate of the hydrophobic-rich phase for each photosensitizer in the model building set.....	97
Table 6.5. Average molar extinction coefficient and peak wavelength of photosensitizers in the model building set.....	98
Table 6.6. Summary of average relative normalized PAE of each photosensitizer in the model building set.....	99
Table 7.1. Summary of log P of molecules in the model building set.....	103
Table 7.2. Summary of connectivity indices of the molecules used to develop QSPRs.....	107
Table 7.3. Summary of valence connectivity indices of the molecules used to develop QSPRs	108
Table 7.4. Summary of the properties for the candidate molecules.....	116

CHAPTER 1: INTRODUCTION AND BACKGROUND

1.1 Introduction

Dentists are increasingly using composite as opposed to dental amalgam for direct restoration of posterior teeth. The reasons for the widespread use of composite restorations include:

- Global effort to reduce mercury containing products
- Concern for release of mercury from the amalgam restoration to the oral environment
- Esthetic appeal since composite restoration's color is close to that of the tooth

Dental composite materials usually consist of dimethacrylate monomer, fillers, coupling agents and an initiator system (Ferracane, 2011). The fillers are inorganic in nature and typically made of radiopaque glass, quartz, ceramics or metal alkoxides such as titanium (IV) and zirconium (IV) ethoxide (Klapdohr and Moszner, 2005). Fillers play an important role in the radiopacity, abrasion resistance, flexural modulus and thermal coefficient of expansion of the restoration (Klapdohr and Moszner, 2005). The composite formulation is highly viscous which poses significant difficulty in bonding it directly to the tooth structure, and hence a low viscosity adhesive serves as the bridge between the tooth structure and composite material (Spencer *et al.*, 2010).

Dental adhesive can be classified as either etch-and-rinse or self-etch adhesives (Moszner and Hirt, 2012). The etch-and-rinse adhesive can either be applied in two or three steps (Moszner and Hirt, 2012). In both the cases, an acid etchant, typically 32-37% phosphoric acid with pH ranging from 0.1 to 0.4, is used to demineralize the dentin (Moszner and Hirt, 2012). The next step for the three step etch-and-rinse adhesive is the application of primer followed by the adhesive (Moszner and Hirt, 2012). For the two step etch-and-rinse adhesive, the primer and adhesive are applied together (Moszner and Hirt, 2012). Primers cause the collagen of the demineralized dentin to expand to facilitate infiltration of the adhesive (Moszner and Hirt, 2012). Primers usually contain solvents and the less viscous monomethacrylate monomer, 2-hydroxyethylmethacrylate (HEMA) (Moszner and Hirt, 2012). The self-etch adhesive contain acidic monomers which demineralize and simultaneously prime the dentin (Moszner and Hirt, 2012). Self-etch adhesives can be applied in one or two steps (Moszner and Hirt, 2012). In the two step self-etch system, the primer and adhesive are applied separately, and in the one step system they are combined (Moszner and Hirt, 2012).

The composition of dentin is approximately 50% mineral, 30% collagen and 20% water by volume (Pashley *et al.*, 2011a). During demineralization the portion occupied by mineral is replaced by water, making the dentin very hydrated. Under these conditions the demineralized dentin will consist of 70% water and 30% collagen.

Despite the increased use of the dental composite restoration, its clinical lifetime (particularly class II composite restorations) is inferior to the conventional amalgam restoration. Usually, the bond integrity between the enamel and the adhesive is strong, but the bond between the dentin and the adhesive (adhesive/dentin interface) is vulnerable to failure (Spencer *et al.*, 2010). Failure at the adhesive/dentin (a/d) interface is considered one of the primary reasons for clinical failure of composite restorations.

During infiltration through the wet demineralized dentin, the adhesive undergoes phase separation into the hydrophobic- and hydrophilic-rich phases. In this investigation, the characteristics of the hydrophilic-rich phase of dentin adhesives are examined, in detail, to understand the myriad of factors that contribute to the failure of this material. From this study, factors which require alteration or modification to improve the bond integrity of the a/d interface are identified. Modification of the photo-initiator system is recommended by proposing possible candidate hydrophilic photosensitizers which can be incorporated into the current adhesive formulation. The candidate water compatible visible light photosensitizers are obtained rationally via computer-aided molecular design (CAMD).

1.2 Motivation

Nearly 60% of all dental operative work represents replacement of failed dental restorations (Bernardo *et al.*, 2007). It was reported that the failure rate for posterior composite restorations was 43% compared to 8% for amalgam restorations (Levin *et al.*, 2007). In another study, it was reported that after 4.6 years, the mean failure rate per annum was 2.9% for resin-composite restoration and 1.6% for amalgam (Kopperud *et al.*, 2012). In the former study, it was found that the major reason for failure of class II composite restorations was secondary caries, and among the patients with composite restorations secondary caries accounted for 73.9% of failed restorations (Kopperud *et al.*, 2012). The mean replacement time for composite restorations is 5.7 years (Burke *et al.*, 2001) and for the conventional amalgam the lifetime ranges from 8.3 to 15 years (Bernardo *et al.*, 2007; Burke *et al.*, 2001).

Despite the high failure rate, the use of composite restorations is on the rise. The reasons for the increased use of composite restorations include the global effort to reduce mercury containing products,

the esthetic appeal of composites, i.e. a color that approximates the natural color of teeth, and toxicity concerns regarding the release of mercury from the dental amalgam. As the number of patients with composite restorations increases, it is expected that there will be a concomitant increase in failed restorations. Secondary decay that develops at the margins of the composite/tooth interface undermines the restoration. It was observed that the risk for developing secondary caries was 3.5 times higher in the case of patients with composite restorations as compared to patients with the conventional amalgam (Bernardo *et al.*, 2007). The increase in secondary decay and increased failure of composite restorations could lead to an increase in pain, discomfort, time away from work and school, and increased treatment costs.

Ionescu *et al.* demonstrated that the surface properties of composite restorations such as roughness, played an important role in the biofilm formation of oral cariogenic bacteria *Streptococcus mutans*, and increasing the resin concentration in the restoration could be favorable for biofilm formation (Ionescu *et al.*, 2012). Another study indicated that the adhesion of *Streptococcus mutans* could be dependent on the type of monomer in the resin (Hahnel *et al.*, 2008). Moreover, each replacement is responsible for an increase in the size of the cavity, which indicates that patients with composite restoration may undergo frequent replacement leading ultimately to a total loss of tooth structure (Spencer *et al.*, 2010). Frequent replacement of restorations is detrimental especially for younger patients. It has been reported that more than 50% of children ranging from 6 to 8 years suffer from caries, and in the case of 15 year old patients this becomes 78% (NIH, 2000).

The increased use of composite restoration translates to an increase in the replacement of failed restorations. Increased replacement means higher cost. This has the potential to contribute to the burden of medical expenditures worldwide. It was reported that in 1984 the cost of dental filling replacement in the U.S. alone amounted to \$5 billion and in 1991 it was 100 million pounds in the UK (Jokstad *et al.*, 2001). All of these factors point to the urgency to improve the clinical lifetime of dental composite restorations.

Accumulation of cariogenic bacteria such as *Streptococcus mutans* at the margins between the restoration and tooth leads to secondary caries (Spencer *et al.*, 2010). Past investigations have shown that the weak region leading to failure of composite restorations is the a/d interface (Spencer *et al.*, 2010). The adhesive resin usually contains methacrylate based monomers, and its key function is to prevent exposure of the demineralized dentin from the oral environment. Several factors were identified which hinder the adhesive from achieving an ideal seal between the demineralized dentin and oral environment.

These factors include poor photopolymerization (Cadenaro *et al.*, 2005; Santini and Miletic, 2008), water sorption leading to reduced bond strength (Carrilho *et al.*, 2005; Ito *et al.*, 2005; Malacarne *et al.*, 2006; Tay *et al.*, 2003; Toledano *et al.*, 2007; Ye *et al.*, 2008), incomplete infiltration (Hashimoto *et al.*, 2011; Pashley *et al.*, 2011b; Wang and Spencer, 2003), phase separation (Eliades *et al.*, 2001; Spencer and Wang, 2002; Toledano *et al.*, 2012; Van Landuyt *et al.*, 2005), enzymatic and hydrolytic degradation of ester linkages (Malacarne *et al.*, 2006; Santerre *et al.*, 2001; Tay *et al.*, 2003). Incomplete infiltration leaves regions of exposed collagen that are prone to degradation by hydrolysis and host-derived matrix metalloproteinases (MMPs). MMPs potentially undermine the bond integrity of the a/d interface (Hashimoto *et al.*, 2011; Pashley *et al.*, 2011a; Pashley *et al.*, 2004).

Water sorption causes plasticization of the adhesive polymer over time, lowering the a/d bond strength, and eventually compromising the seal between dentin and adhesive. Exposure of the adhesive to water causes hydrolytic degradation of the ester linkages enhancing the diffusion of the oral fluid containing deleterious agents into the a/d interface. Salivary enzymes further enhance the degradation of the ester linkages. Degradation of ester linkages results in the release of methacrylic acid which leads to inflammation and a decrease in the pH of the surrounding tissue (Grinstein *et al.*, 1991; Lardner, 2001). Further deterioration is promoted by the release of acids as a result of metabolism on fermentable carbohydrates by cariogenic bacteria near the inflammation site. Low pH can enhance the dissolution of the mineral from the surrounding tooth and lead to loss of tooth structure.

Limited polymerization results in a weak a/d bond and leaves behind unreacted residual monomers which may leach causing cytotoxicity in the surrounding tissue. The mono-methacrylate component, HEMA, has been associated with apoptosis, interference with the production of reactive oxygen species (ROS) and expression of type I collagen by gingival fibroblasts (Chang *et al.*, 2005; Falconi *et al.*, 2007; Paranjpe *et al.*, 2005; Spagnuolo *et al.*, 2006). Decreased polymerization could also lead to loosely cross-linked regions. The final consequence of these events is enhanced diffusion of oral fluid in the a/d interface facilitating the colonization of *Streptococcus mutans* and other cariogenic bacteria followed by successful establishment of a biofilm. The cumulative effect may be failure of the composite restoration.

During application of the adhesive resin, the collagen fibrils within the demineralized dentin were kept hydrated to prevent them from collapsing. This improves the infiltration of the adhesive. As the adhesive resin infiltrates the collagen matrix, it undergoes phase separation into hydrophobic- and hydrophilic-rich phases (Spencer and Wang, 2002). Previous investigation on the partitioned components

of the adhesive showed that the major components of the hydrophilic-rich phase were water and the mono-methacrylate component, i.e. 2-hydroxyethylmethacrylate (HEMA); the crosslinker and conventional photo-initiating components were present in minor quantities in this phase (Ye *et al.*, 2012)..

The adhesive resin infiltrates the collagen matrix forming a hybrid layer as shown in Figure 1.1 (Abedin *et al.*, 2016). The hybrid layer is composed primarily of collagen fibrils and variable distribution of the adhesive resin components (Figure 1.1). Other components of the hybrid layer are water, solvent and isolated mineral particles. The hydrophilic-rich phase represents a major part of the hybrid layer. Lack of cross-linker within the hydrophilic-rich phase means formation of loosely cross-linked regions within this phase (Figure 1.1). The lack of a photo-initiating system within the hydrophilic-rich phase leads to poor polymerization. Loosely cross-linked regions and a weak a/d bond due to poor polymerization will facilitate the diffusion of oral fluid, paving the way for colonization of cariogenic bacteria at the margin, and promote further hydrolytic/enzymatic degradation of the adhesive and cytotoxicity at the surrounding tissue. Hence, this region is vulnerable to failure and further investigation is needed to address this important clinical problem.

Incorporation of hydrophilic esterase resistant cross-linker and water compatible visible light photo-initiator system may improve the lifetime of this phase. Hydrophilic cross-linker and photo-initiator will partition in higher concentration within the hydrophilic-rich phase. Higher concentrations of cross-linker and photo-initiator will enhance the polymerization and cross-linking density of the hydrophilic-rich phase. Also, an esterase resistant cross-linker will delay the enzymatic degradation of the hydrophilic-rich phase yielding a durable a/d bond.

As a first step towards improving the clinical lifetime of dental composite restoration, the rational design of water compatible visible light photosensitizers has been proposed here. The reason for designing photosensitizers first is that it is vital to achieve substantial polymerization for the hydrophilic-rich phase. The design and development of a hydrophilic photosensitizer can offer immediate benefit to the current adhesive formulations.

Although cross-linkers and photo-initiators that are hydrophilic in nature are warranted, there is a lack of rational approach for selecting or designing candidate hydrophilic cross-linkers and photo-initiators. Even though the hydrophilic-rich phase plays a vital role in the failure of the a/d interface, the characteristics of this phase remain vastly underexplored.

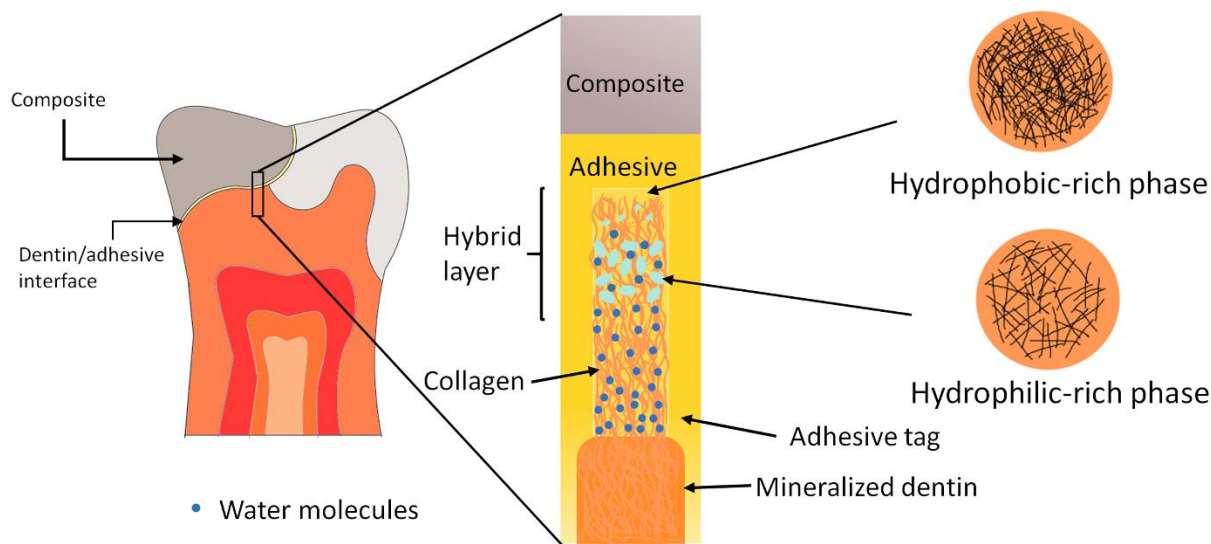


Figure 1.1 Formation of hydrophobic- and hydrophilic-rich phases during phase separation of the dental adhesive (Abedin *et al.*, 2016)

The lack of detailed characterization has created a gap in knowledge regarding the performance of the widely used photo-initiator system and monomers within this phase. Most of the previous studies involve formulations that represent the hydrophobic-rich phase (Cadenaro *et al.*, 2009; Catel *et al.*, 2012; Catel *et al.*, 2009; Ely *et al.*, 2012; Ganster *et al.*, 2008; Lima *et al.*, 2013; Park *et al.*, 2010; Park *et al.*, 2008; Podgórski, 2012).

Therefore, in this study the hydrophilic-rich phase is characterized to understand the impact of water concentration, light intensity and presence of iodonium salt on the photopolymerization kinetics, rate of polymerization, microstructure and thermal behavior of this phase. The former investigation is then combined with a rational approach to design candidate efficient molecules of water compatible visible light photosensitizer by optimization of molecular structures for several relevant properties simultaneously using computer aided molecular design (CAMD). This is significant because characterization of the hydrophilic-rich phase will help in the identification and isolation of those factors that adversely impact the polymerization of this phase. Structural information from the proposed photosensitizer molecules using CAMD can be used to synthesize novel efficient hydrophilic visible light photosensitizers. The newly designed molecules will enhance the photopolymerization of the hydrophilic-rich phase. The potential benefits of enhanced polymerization include improved durability at the a/d interface and reduced cytotoxicity arising from the monomer leaching.

The aim of this research will significantly contribute to advancing the field of dental material development. It will provide insight regarding factors impacting the polymerization kinetics of the current adhesive system in a highly hydrated environment and possible polymerization mechanism in the hydrophilic-rich phase. This will be valuable for the design of next generation dental adhesive systems. Some of the properties of photosensitizer which are critical to its function are: intensity of the absorbed light, the range of excitation wavelength, electron transfer ability, photophysical and photochemical processes. These are intrinsic to the photo-initiating system. Therefore, it is possible that the newly designed photosensitizer molecules can be applicable for polymers other than methacrylate-based polymers.

The proposed candidate photosensitizer molecules may also be used in other fields such as tissue engineering (Almeida *et al.*, 2011; Anseth *et al.*, 1999; Chen *et al.*, 2012; Davis *et al.*, 2003; Valmikinathan *et al.*, 2012; Wang *et al.*, 2013), coatings (Allen, 1996; Bose and Bogner, 2010; Fouassier *et al.*, 2003), bioprinting (Malda *et al.*, 2013), and photoimaging and holographic recordings (Fouassier and Morlet-Savary, 1996; Gao and Yang, 2000; Monroe and Weed, 1993). Photopolymerizable monomers are often employed for synthesizing implants because they provide the flexibility to handle difficult to reach areas at the defect site (Anseth *et al.*, 1999). Photo-cross-linkable hydrogels have been studied for application as scaffolds in treating irregular neural tissue defects, cell encapsulation for regeneration and also for drug delivery (Almeida *et al.*, 2011; Chen *et al.*, 2012; Davis *et al.*, 2003; Ishihara *et al.*, 2006; Valmikinathan *et al.*, 2012). Tissue adhesives which are used for wound healing and repairing are sometimes required to be polymerized in the presence of cells (Wang *et al.*, 2013). Use of visible light photo-initiator system to polymerize these types of implants, scaffolds, and drug delivery vehicles reduces the potential of photo damage to cells and drugs. Use of 100% water based coatings in paint can reduce the release of volatile organic compounds (VOC) (Fouassier *et al.*, 2003) and hence the newly designed candidate photosensitizers can be used for such coatings. Moreover, use of visible light instead of UV for curing creates a safer working environment. These water-compatible visible light candidate photosensitizers can also find applications in pharmaceutical coatings where the product contains drugs sensitive to UV light.

The molecular structure of the monomer plays an important role in the polymerization reaction. It was observed that some photosensitizers such as Eosin Y were able to trigger photopolymerization of both methacrylate and non-methacrylate based monomers (Beyazit *et al.*, 2014; Encinas *et al.*, 2009; Mallavia *et al.*, 1994); there were also reports that in the presence of camphorquinone/ethyl-4-dimethylaminobenzoate photo-initiator system, homo-polymerization of acrylic acid and N-

vinylpyrrolidone did not occur, but introduction of triethyleneglycol dimethacrylate monomer resulted in the polymerization reaction (Jakubiak *et al.*, 2000). Polymerization of a monomer is largely dependent on its reactivity. If the proposed candidate photosensitizers fail to work in the absence of methacrylate based monomers, they can at least be used for various applications where one of the monomers belongs to the methacrylate group. The computer-aided design (CAMD) framework that has been exhibited here can be implemented for design of other types of molecules, and the QSPRs that have been developed here can be used by scientists attempting to predict properties for similar types of molecules. Overall, the present investigation is significant not only for the community working on the development of new dental materials but also for the broader field of materials science.

1.3 Background

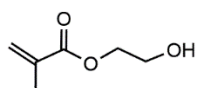
1.3.1 Dental Adhesive

The major components of etch-and-rinse dental adhesives are: monomethacrylate monomer (usually 2-hydroxyethylmethacrylate (HEMA)), di-methacrylate monomer such as bisphenol A glycerolate dimethacrylate (BisGMA), 1,6-bis-[2-methacryloyloxyethoxycarbonylamino]-2,4,4-trimethylhexane (UDMA), triethyleneglycol dimethacrylate (TEGDMA), and photo-initiating system. The di-methacrylate monomer acts as the cross-linker imparting mechanical strength to the polymeric adhesive. The most widely used photo-initiating system consists of: camphorquinone (CQ) and ethyl 4-(dimethylamino)benzoate (EDMAB). Sometimes iodonium salt is added within the photo-initiating system as a reaction accelerator. The chemical structures of the monomers and components in the photo-initiators are shown in the Figure 1.2. Here, CQ acts as the photosensitizer and EDMAB as the co-initiator (reducing agent).

The primary composition of most commercially available dental adhesive resin is 45:55 wt% HEMA/BisGMA (Ye *et al.*, 2007a). A ternary phase diagram for HEMA, BisGMA and water was developed in the past to determine the miscibility of the components (Ye *et al.*, 2011). Most of the previous studies on dental adhesives involve adhesive formulations representing the hydrophobic-rich phase. It was shown previously that the infiltration of the cross-linker decreased along the length of the hybrid layer (Wang and Spencer, 2003). Wang *et al.* investigated the compatibility of co-initiators with HEMA in the wet environment, but the maximum water content they studied was far below the quantity that may arise within the hydrophilic-rich phase (Wang *et al.*, 2006).

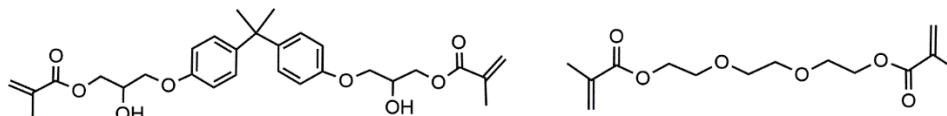
Ye and colleagues studied the polymerization kinetics of HEMA/BisGMA (40:60 wt%) adhesive monomers in the presence of varying concentrations of ethanol up to 40 wt% (Ye *et al.*, 2007a). This former study reported that increased concentration of ethanol led to a decrease in the ultimate tensile strength and modulus of elasticity, whereas the degree of conversion remained similar (Ye *et al.*, 2007a). In a separate study, it was observed that the iodonium salt could improve the photopolymerization of the dental monomers and the incorporation of a hydrophilic initiator could be beneficial in improving the photopolymerization of dental adhesives in an over-wet condition (Ye *et al.*, 2009). In the former study, the water content within formulations was kept limited to only 8.3 wt% which mimicked the hydrophobic-rich phase (Ye *et al.*, 2009). This does not mean that addition of the iodonium salt always improves the polymerization reaction since another study has shown that in the presence of methacrylate phosphonic acid monomer, the iodonium salt has a reverse effect (Besse *et al.*, 2013).

Monomethacrylate monomer:



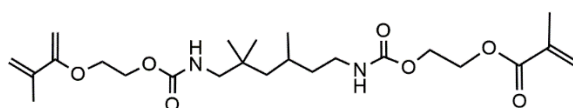
2 - hydroxyethyl methacrylate (HEMA)

Dimethacrylate monomer:



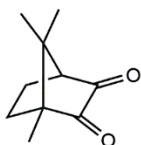
Bisphenol A glycerolate dimethacrylate (BisGMA)

Triethyleneglycol dimethacrylate (TEGDMA)

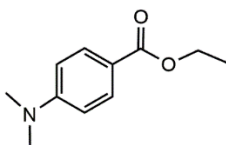


1,6-bis-[2-methacryloyloxyethoxycarbonylamino]-2,4,4-trimethylhexane (UDMA)

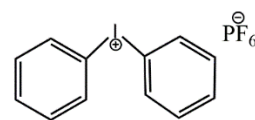
Photo-initiating Components:



Camphorquinone (CQ)



Ethyl 4-(dimethylamino)benzoate (EDMAB)



Diphenyliodonium hexafluorophosphate (DPIHP)

Figure 1.2. Molecular structures of the major components in dental adhesive resin

Ely *et al.* conducted a polymerization kinetics study of a monomer blend of BisGMA, HEMA and TEGDMA using the hydrophilic photosensitizer 2-hydroxy-3-(3,4-dimethyl-9-oxo-9H-thioxanthen-2-yl-oxy)-N,N,N-trimethyl-1-propanaminium chloride (QTX) (Ely *et al.*, 2012). The monomer blend in the former study consisted of 50 wt% BisGMA, 25 wt% TEGDMA and 25 wt% HEMA (Ely *et al.*, 2012). The effect of various combinations of photoinitiator systems on the polymerization of HEMA/BisGMA in equal ratio, in the presence of 10 wt% deuterium oxide (D₂O) was investigated in the past as well (Sodré *et al.*, 2015). The photosensitizers used in this study were CQ, phenanthrenequinone (PQ), trimethylbenzoyl-diphenyl-phosphine oxide (TPO), and bisacyl-phosphine oxide (BPO) (Sodré *et al.*, 2015).

Although most of the studies in the past are concerned with hydrophobic-rich formulations, there have been a few studies on formulations which are close to the hydrophilic-rich phase (He *et al.*, 2006, 2008; Li and Lee, 2005). These investigations involved methacrylate-based hydrogels with composition similar to the dental adhesive hydrophilic-rich phase (He *et al.*, 2006, 2008; Li and Lee, 2005). Li *et al.* studied the polymerization kinetics of HEMA/DEGDMA in a molar ratio of 100/1 in the presence of water content of 60% at maximum (Li and Lee, 2005). He *et al.* investigated the photopolymerization kinetics and microstructure of a methacrylic acid (MAA) and TEGDMA co-polymer where the cross-linker (TEGDMA) was present in 1 mol% (He *et al.*, 2006). Here, the polymerization reaction was carried out in the presence of 50 wt% of solvent mixture which was made up of ethanol and water in varying ratios (He *et al.*, 2006). In another study, He *et al.* investigated the impact of light intensity on a similar formulation of MAA/TEGDMA (He *et al.*, 2008).

Most of the studies regarding the effect of light intensity on the polymerization of dental monomers were concerned with dental composite and not the adhesive. Several authors studied the effect of light intensity on the volumetric shrinkage and hardness of dental composites (Davidson-Kaban *et al.*, 1997; Discacciati *et al.*, 2004). It was observed that light intensity (200 and 400 mW/cm²) had a significant impact on the Vickers hardness of the dental composite but very little on the volumetric polymerization shrinkage (Discacciati *et al.*, 2004). In another study, it was observed that higher light intensity (700 mW/cm²) was accompanied by increased shrinkage leading to marginal gap (Davidson-Kaban *et al.*, 1997).

There were several investigations regarding the impact of irradiation time and ramp curing on the degree of conversion (DC) and shrinkage of dental composites (Emami *et al.*, 2003; Hofmann *et al.*, 2002; Silikas *et al.*, 2000). It was observed that total overall energy which was the product of exposure time and light intensity played an important role rather than the light intensity itself (Emami *et al.*, 2003). In the

former study, the authors reported that dental composites with similar DC, Young's modulus and volumetric shrinkage could be obtained by maintaining constant total energy (Emami *et al.*, 2003). The total energy can be kept constant by manipulating the exposure time and light intensity. This study indicated that the formation of reactive species for polymerization depends on the concentration of useful photons (Emami *et al.*, 2003). Lovell *et al.* showed that the DC and rate of polymerization of the comonomers, BisGMA and TEGDMA increased with light intensity (Lovell *et al.*, 1999). In this study, it was found that at 25°C, there was a proportional relationship between the rate of polymerization and light intensity raised to the power 0.6 (Lovell *et al.*, 1999).

The impact of various light curing units (LCUs) on the polymerization of commercially available dental composites were explored in the past (Franco *et al.*, 2007; Hofmann *et al.*, 2002; Lee *et al.*, 2013; Lohbauer *et al.*, 2005). The spectral absorbance of the photosensitizer within the resin played an important role in the efficiency of the LCU. It was observed that light intensity exhibited very little effect on network formation during the copolymerization of BisGMA/TEGDMA (Lovell *et al.*, 2001b). The final flexural strength for similar DC of viscous dimethacrylate resin showed very little change for different light intensities (Lovell *et al.*, 2001b). In this study, two types of LCU were used: Quartz-tungsten-halogen light (QTH) at an intensity of 200 mW/cm² and xenon-plasma-arc light (PAC) at 2000 mW/cm² (Lovell *et al.*, 2003).

There were a few studies regarding the impact of light intensity on the polymerization of dental adhesives. Ye *et al.* investigated the effect of light intensity on the polymerization of commercially available adhesives; Single Bond, One-up Bond F and Adper Prompt (Ye *et al.*, 2007b). Here, it was shown that the DC of the hydrophilic adhesive (Adper Prompt) depended on the light intensity (Ye *et al.*, 2007b). In another study, it was found that the shear bond strengths of commercial adhesives (Imperva Fluoro Bond, Mac Bond II, Fluoro Bond Shake-One, One-up Bond F Plus) were significantly lower at a low light intensity such as 150 mW/cm² (Yamamoto *et al.*, 2006). The formulations studied here mostly represented the hydrophobic-rich phase which would be rich in the cross-linker concentration.

There were a few investigations which focused on the effect of light intensity on formulations representing the hydrophilic-rich phase of dental adhesives, the latter being rich in water and mono-methacrylate component. He *et al.* reported that for a MAA/TEGDMA hydrogel in presence of solvent, high UV light intensity could have a negative impact on the photopolymerization, and the light intensity impacted the onset of macrogelation (He *et al.*, 2008). Moreover, the authors proposed the structure formation for MAA/TEGDMA copolymer in presence of solvent and the various stages of the structure

formation were proposed to be: initiation, microgel, cluster formation, macrogelation, and post gelation (He *et al.*, 2008). It was also noted in this study that important factors that could impact the intra- and intermolecular reaction of growing chains were: light intensity, monomer concentration, solvent concentration and type, and curing temperature (He *et al.*, 2008). In another study on dilute HEMA/DEGDMA systems, it was observed that higher light intensity delayed macrogelation and also had an impact on the reaction profile (Li and Lee, 2005).

In general, the use of higher light intensity is proposed for dental composite resin since enhanced light intensity is accompanied by an increase in the mechanical properties and depth of cure of the restoration (Dennison *et al.*, 2000). During the curing of dental adhesives using LCU, the light intensity may vary along the hybrid layer. Previous studies indicated a decrease in the light intensity with the increase in the distance from the tip of LCU, leading to an adverse impact on the polymerization of composite resins (Price *et al.*, 2000; Rueggeberg and Jordan, 1993). It is possible that the decrease in light intensity along the depth of the hybrid layer can impair the photopolymerization of the hydrophilic-rich phase.

Although the hydrophilic-rich phase is a weak region that is prone to failure, the behavior of this phase has been largely ignored. Detailed study of this phase may lead to the identification of factors that contribute to clinical failure of the composite restoration. In this study, the difference in the polymerization kinetics of model hydrophobic- and hydrophilic-rich mimics has been determined. The impact of various factors such as concentration of cross-linker versus photo-initiator, water content, light intensity, partition of photo-initiator components, and incorporation of iodonium salt on the photopolymerization and structure formation of model hydrophilic-rich phases have been investigated.

1.3.2 Computer-Aided molecular design (CAMD)

Several researchers have synthesized novel cross-linker monomers for dental adhesives, but there have been a few systematic approaches to the design of novel monomers (Catel *et al.*, 2012; Park *et al.*, 2008; Podgórski, 2012; Venkatasubramanian *et al.*, 1994). Eslick *et al.* demonstrated a framework for rationally designing cross-linker monomers for dental adhesives by a computational approach (Eslick *et al.*, 2009). The search space for novel molecules with desired characteristics is huge, but a rational design methodology such as computer-aided molecular design (CAMD) can explore this enormous search space in a much shorter time. CAMD suggests molecular structures with desired properties and is able to conduct a search over a much larger space than the conventional trial-and-error experimental method.

CAMD is an inexpensive and efficient technique to discover structures with desired properties. Previously, new photo-initiators in the visible range have also been explored (Ganster *et al.*, 2008) and others have studied the efficacy of various photosensitizers in dental adhesives (Ely *et al.*, 2012; Musanje *et al.*, 2009; Schneider *et al.*, 2009; Schneider *et al.*, 2008). The use of systematic approaches for optimal photo-initiator systems in dental adhesives has not been explored. Since one of the factors that may impair the photopolymerization of the hydrophilic-rich phase is the lack of photosensitizer within this phase, a framework for designing water-compatible visible light photosensitizers computationally is demonstrated here. The proposed novel candidate photosensitizer molecules may indicate structures which are novel and important in improving the photopolymerization of the hydrophilic-rich phase.

CAMD consists of a forward and inverse problem. In the forward problem, molecules of interest are selected to form the model building set, and then relevant properties are either experimentally determined or obtained from the literature. Using molecular descriptors which are numerical quantities defining structures, correlations between the relevant properties and descriptors are determined which are called quantitative structure property relationships (QSPRs). In the inverse problem, novel candidate molecules are designed by solving an optimization problem which is formulated using the QSPRs, structural constraints and objective function. A schematic that describes the steps in CAMD is presented in the Figure 1.3. This approach has been utilized before to design products such as pharmaceuticals, biologics, catalysts, polymers, refrigerants, solvent mixtures (Eslick *et al.*, 2009; Folić *et al.*, 2008; Gani *et al.*, 1991; Roughton *et al.*, 2012a; Venkatasubramanian *et al.*, 1994).

1.3.2.1 Molecular Descriptors

Molecular descriptors are numerical representations of the structure of molecules. Connectivity indices are topological descriptors which take into account the connectivity within the molecular structure as well as the electronic configuration (Bicerano, 2002). Connectivity indices were first proposed by Randić *et al.* (Randić, 1975). These topological indices are able to capture structural 2D information. Connectivity indices were employed to predict properties for pharmaceutical products, catalysts, polymers, cross-linked polymers (Bicerano, 2002; Camarda and Maranas, 1999; Chavali *et al.*, 2004; Eslick *et al.*, 2009; Keir and Hall, 1986; Roughton *et al.*, 2012b; Siddhaye *et al.*, 2000). Roughton *et al.* used connectivity indices to estimate glass transition temperatures and Gordon-Taylor constants of carbohydrate excipients, and these expressions were used in a CAMD framework to minimize protein aggregation (Roughton *et al.*, 2012b). Eslick *et al.* also used connectivity indices to predict properties such as tensile strength, elastic

modulus, glass transition temperature and rate of polymerization of cross-linked polymers (Eslick *et al.*, 2009).

The calculation of connectivity indices of various orders will be discussed later. Group contribution is another method to develop estimates for properties. In this method, the structure of a compound/mixture is described in terms of the functional groups and the number of times of their occurrence in it (Gani *et al.*, 1991). UNIFAC is a group contribution method which has been used in the past to predict various properties such as activity coefficients (Fredenslund *et al.*, 1975; Larsen *et al.*, 1987). The equation used for determining the primary property using a group contribution method is given below (Sheldon *et al.*, 2005):

$$P = p_o + \sum_{i \in G} n_i p_i \quad 1.1$$

where P represents the primary property, G is the set of all groups, n_i is the number of times the group type i occurs, p_o and p_i represent the coefficients obtained by linear regression

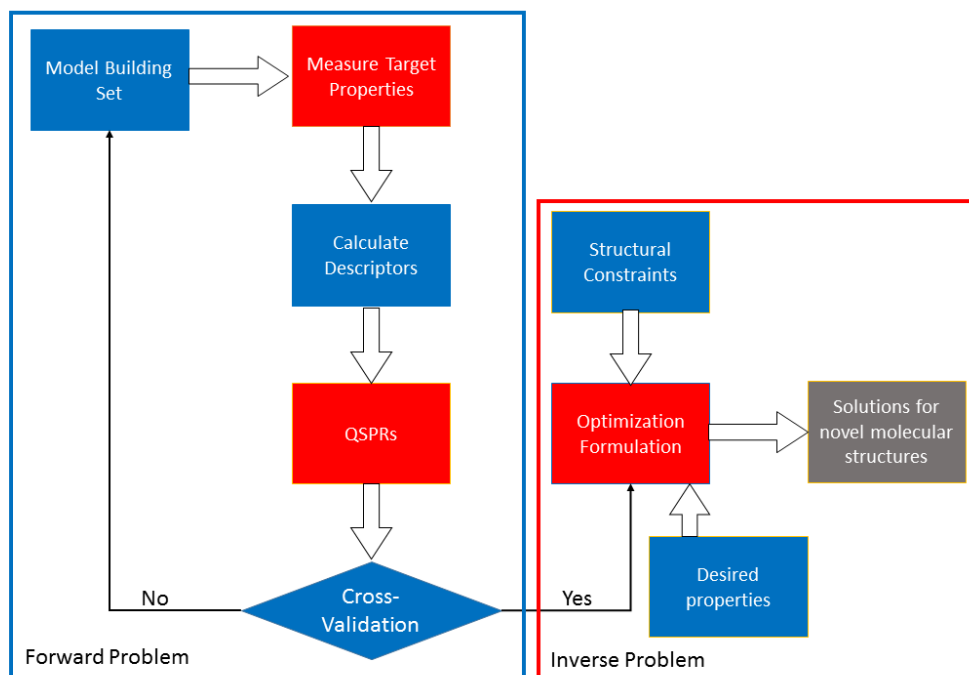


Figure 1.3. Schematic showing steps involved in CAMD

Sheldon *et al.* utilized a group contribution method to estimate primary properties such as Abraham's hydrogen-bond basicity and acidity, and secondary properties which included Hildebrand

solubility parameter, macroscopic surface tension, dipole moment refractive index and dielectric constant of compounds which could be denoted using UNIFAC groups (Sheldon *et al.*, 2005). Other properties such as critical pressure, critical volume, normal boiling and melting temperatures of pure organic compounds were predicted in the past using the group contribution method (Marrero and Gani, 2001). Here, higher order groups were utilized to improve the accuracy of the property prediction and inclusion of such groups took into account factors such as isomerism and complex structures (Marrero and Gani, 2001). Group contribution was successfully employed to design solvents for reactions (Folić *et al.*, 2008; Struebing *et al.*, 2013). Gani *et al.* employed the group contribution method as well as first and second order connectivity indices to compensate for contribution of missing groups in a method they called GC⁺ (Gani *et al.*, 2005). Connectivity indices possess additional structural information compared to the group contribution approaches (Camarda and Maranas, 1999).

Three dimensional descriptors are able to take into account spatial information of molecules, and hence are useful in predicting properties which are dependent on the conformation of the molecule such as bioactivity or stereospecific interactions (Estrada, 1995). Since topological indices define 2D representation of molecular structures, there have been attempts to extend some of them to include spatial information. For example, the Wiener number was modified to include geometric distances rather than graph theoretical distances, and it was observed that the performance of the 3D Wiener number was superior to the 2D Wiener number for prediction of enthalpy functions of lower alkanes (Bogdanov *et al.*, 1989). Randić *et al.* proposed novel molecular descriptors that include molecular geometry (Randić, 1995). Here, molecular distances were used to determine higher order interatomic distances (Randić, 1995). Topological indices extended to include 3D molecular description are convenient in terms of ease of calculation. Consonni *et al.* proposed novel 3D descriptors called GETAWAY (Geometry, Topology, and Atom-Weight Assembly) and used them to derive quantitative structure property relationships (QSPRs) for physicochemical properties of octane isomers (Consonni *et al.*, 2002).

1.3.2.2 Quantitative Structure Property Relationships (QSPRs)

A quantitative structure property relationship (QSPR) is a mathematical function that correlates the structure of the molecules in a model building set to a property. In other words, the property to be predicted in a CAMD problem needs to be dependent on the structure of the molecule. The most common approach to obtain QSPR is by linear regression. This will yield several regression models and the selection of model is made based on the lack of fit and overfitting. Criteria like Mallows' C_p statistics and Akaike information criterion (AIC) can be employed to understand this (Roughton *et al.*, 2012b). These criteria

provide a score to each model by giving penalties for underfitting and addition of predictors (descriptors). Model with optimal score should be selected. For example, model with lowest Mallows's C_p statistic should be chosen. Model search can be carried out by exhaustive means, forward or backward method. For the exhaustive search models, all possible combinations of predictors are obtained (Roughton *et al.*, 2012b). In case of the forward method, predictors are added successively until there is no further improvement in the model. For the backward method, the model search begins with all the available predictors and then they are removed successively until there is no additional improvement. It is also important to cross-validate the model to understand its predictive capability. Cross-validation can be carried out by leaving out each data point and correlating the remaining data points with the same descriptors and using this correlation to predict the property of the data point that was left out. This is repeated for each data point. This method of cross-validation is called leave-one-out (LOOCV). Hence, in LOOCV the number of folds is equivalent to the total number of data points. For K-fold cross-validation, the total number of data points is divided into equal folds and equal number of data points are left out from each fold. Predictive capability of a model can be evaluated from predictive squared correlation coefficient, Q^2 . For LOOCV, it can be calculated using equation 1.2 and a model with good predictive capability will have Q^2 very close to the correlation coefficient, R^2 .

$$Q^2 = 1 - \frac{\sum_{i=1}^m (\hat{Y}_i - Y_i)^2}{\sum_{i=1}^m (\bar{Y} - Y_i)^2} \quad 1.2$$

where m is the total number of data points, \hat{Y}_i is the predicted value of the i^{th} data point which was left-out during cross-validation, Y_i is the value of the i^{th} data point obtained from the correlation and \bar{Y} is the average of all the data points

1.3.2.3 Computer-aided molecular design problem formulation (CAMD)

The aim of CAMD is to minimize the difference between the property of the candidate molecule and the target value. A general form of the optimization formulation is given below:

$$\text{Minimize } s = \sum_M \frac{1}{P_m^{scale}} |P_m - P_m^{Target}|$$

$$P_m = f_m(\chi)$$

$$\chi = g(a_{i,j}, w_i) \quad 1.3$$

$$h_c(a_{i,j}, w_i) \geq 0$$

where P_m is the property m obtained from the QSPR designated as $f_m(\chi)$, χ are the connectivity indices obtained from the function g ; $a_{i,j}$ and w_i are adjacency matrix and identity vector respectively, h_c represents structural molecular constraints, P_m^{Target} is the target value for the property m , P_m^{Scale} is the scaling factor.

The vital steps in the inverse problem of CAMD are (Gani *et al.*, 1991):

- Selection of molecular sub-groups which will form the building blocks
- Combination of the building blocks to yield feasible chemical compounds
- Prediction of relevant properties for the newly generated compound
- Selection of compounds that possess the desired relevant properties

The last step discussed above form the solution method for the optimization problem which can be achieved via deterministic means, stochastic method or enumeration techniques (Eljack and Eden, 2008).

Deterministic Method: This approach requires gradient information which is used to solve the objective function mathematically (Eljack and Eden, 2008). Property constraints are used as bounds within which the solution is limited. Mixed integer non-linear problems can be solved via this method, but it can be computationally expensive and does not guarantee a global optimal solution (Eljack and Eden, 2008). Roughton *et al.* employed deterministic method to design ionic liquids for separation process (Roughton *et al.*, 2012a).

Stochastic Method: It is an iterative technique which does not require the gradient information for obtaining solutions (Eljack and Eden, 2008). This technique provides near optimal solutions, and move from one solution to another can be made by following certain rules based on the type of technique used. Stochastic approach provides multiple local optimal solutions and does not guarantee global optimal solution as well. Some examples of stochastic methods are: simulated annealing, genetic algorithm, Tabu Search, swarm algorithm and so forth. Tabu Search had been used in the past for polymer design (Camarda and Maranas, 1999; Eslick *et al.*, 2009), and Venkatasubramaniam *et al.* exhibited a polymer design framework using genetic algorithm (Venkatasubramanian *et al.*, 1994). Roughton *et al.* also utilized Tabu Search for designing carbohydrate excipient (Roughton *et al.*, 2012b).

Enumeration Technique: In this method, molecules are generated using combinatorial approach, and then they are checked whether they fall within the constraints and their properties match with the desired target values (Eljack and Eden, 2008). This method may lead to combinatorial explosion making it inferior

compared to the other two techniques. Gani *et al.* exhibited a systematic approach using this technique for designing molecules (Gani *et al.*, 1991).

1.4 Specific Aim

With the increasing trend towards the use of dental composites as opposed to dental amalgam, it is anticipated that there will be an increase in failed restorations and a corresponding increase in replacement therapy. The increase in replacement therapy could lead to increased pain, discomfort, time away from school and work, and cost. The primary causes of failure of dental composite restorations are: secondary caries, fracture and marginal defects (Deligeorgi *et al.*, 2001; Kopperud *et al.*, 2012; Opdam *et al.*, 2007). Increased colonization of oral cariogenic bacteria on composite surface also enhances the risk of developing secondary caries (Brambilla *et al.*, 2012). The a/d interface has been identified as the weak link in the composite restoration. This region is particularly vulnerable to clinical failure and progress in the development of durable dental adhesives has been slow (Donovan *et al.*, 2015). Water compatible photo-initiators and esterase resistance monomers have been identified as a means of improving the longevity of composite restorations (Spencer *et al.*, 2010; Ye *et al.*, 2009).

Most of the current studies fail to address the hydrophilic-rich phase of the dental adhesive arising after phase separation in the wet, oral environment. Therefore, there is a definite gap in knowledge in terms of understanding how the existing photo-initiators and dental monomers perform during the polymerization reaction in the presence of excess moisture, and how various factors related to photopolymerization may impact this phase. Moreover, there is also a lack of rational design approach for selecting and designing candidate photo-initiators and cross-linkers that will provide the optimum performance under wet conditions. These gaps are preventing the understanding of approaches to improve the lifetime of composite restorations, and development of optimal dental photo-initiators and monomers suitable for the over-wet environment.

The goal in the long run is to design and synthesize a water compatible photosensitizer and esterase resistant cross-linker monomer that will give enhanced durability and cross-linking density to the hydrophilic-rich phase. The current objective of this study is to characterize the model hydrophilic-rich phase of dental adhesive and use that knowledge to develop an efficient computer aided molecular design (CAMD) approach that will predict the structures of new water compatible photosensitizer molecules reducing the need for trial and error experimental method. In addition, characterization of the hydrophilic-rich phase will yield factors related to photopolymerization in over wet conditions that need

to be addressed to improve the polymerization reaction in this phase. The overall hypothesis of this work is that optimization of photosensitizer structures for several properties simultaneously will yield novel and superior candidate visible light photosensitizer molecules suitable for over wet conditions. Selected factors related to photopolymerization (photo-initiator concentration, water content, light intensity or accelerator) will have substantial impact on the polymerization reaction in the hydrophilic-rich phase. These factors may impair the performance of the hydrophilic-rich phase. The rationale is that characterization of the hydrophilic-rich phase may allow identification of critical factors related to the poor polymerization of adhesives in wet environments. Investigation of several properties of photosensitizers and polymerization kinetics of the hydrophilic-rich phase of dental adhesives can be used to develop quantitative models containing structure property correlations (QSPRs), which along with combinatorial optimization algorithms can be used to design efficient water compatible photosensitizer. The structural information can be extracted from the proposed molecules to synthesize a water compatible visible light photosensitizer which will provide the platform to design and synthesize a water compatible esterase resistant cross-linker.

1.4.1 Specific Aim 1: Characterization of hydrophilic-rich phase

The objective of this aim will be to characterize the hydrophilic-rich phase in terms of polymerization kinetics and polymer structure of model hydrophilic-rich phase of dental adhesive under various conditions. The conditions are: water content, light intensity, photo-initiator concentration and presence of accelerator. The hypothesis is that the rate of polymerization, degree of conversion and the polymer structure may vary with the water composition and photo-initiator concentration in the hydrophilic-rich phase, light intensity during curing, and the presence of accelerator such as iodonium salt; whereas variation of these conditions will not deteriorate/impact the performance of the hydrophobic-rich phase. The rationale of this aim is that evaluation of the performance of the current adhesive/photo-initiator system in model hydrophilic-rich phase under various experimental conditions (factors) will provide insight into the reaction mechanism of the hydrophilic-rich phase, identify factors responsible for impairing its performance, determine experimental conditions suitable for polymerization kinetics study in the specific aim 2, and deliver the target values for degree of conversion and rate of polymerization of hydrophilic-rich phase in the specific aim 2. The experimental conditions that need to be determined for specific aim 2 include the time for which the polymerization kinetics study needs to be carried out to reach the final degree of conversion, the minimum light intensity to obtain a substantial degree of conversion, whether water content exhibits significant impact on the degree of conversion and

whether an accelerator is necessary for the physically separated hydrophilic-rich mimics to reach a substantial degree of conversion. The outcomes of this aim are polymerization mechanism for the hydrophilic-rich phase, impact of various water content, photo-initiator concentration, light intensity and accelerator on the polymerization kinetics of the hydrophilic-rich phase and its structure formation, experimental conditions necessary for kinetics study in specific aim 2 and the target values for the rate of polymerization and degree of conversion of the hydrophilic-rich phase that will be used in specific aim 2.

The approach will be to monitor polymerization kinetics *in situ* by using Fourier transform infrared spectrophotometer (FTIR) and to analyze the resultant polymer structure with differential scanning calorimetry (DSC). A time resolved spectrum collector will be used for continuous collection of infrared spectra. This technique is simple and allows higher spectral resolution for the time resolved data collection. Simplified model of dentin adhesive containing approximately 45 wt% hydrophilic monomethacrylate component, HEMA and 55 wt% hydrophobic dimethacrylate component, BisGMA can be used to represent BisGMA based commercial adhesive (Ye *et al.*, 2007a). Commercial adhesive formulations contain other additives, e.g. solvents, stabilizers and copolymer of polyacrylic and polyitaconic acids. A simplified model for the dental adhesive will be used for the kinetic studies to eliminate the effect of other additives on the polymerization kinetics. The simplified model will consist of hydrophilic HEMA, hydrophobic BisGMA and the most widely used photo-initiator system, CQ and EDMAB. Most of the model dental adhesive composition that will be investigated in this aim will be at or below their miscibility limit for water. This means the solutions are in a single phase and hence miscible. The ternary phase diagram for the simplified model of dental adhesive was constructed by Ye and colleagues (Ye *et al.*, 2011). Single phase solutions at miscibility limit represent formulations which reside on the phase boundary line. Solutions on the phase boundary line contain maximum water content, and further addition of water will cause the solution to separate into two phases.

1.4.2 Specific Aim 2: Development of a framework for computer-aided molecular design (CAMD) of water compatible visible light photosensitizer

The objective of this aim is to conduct experimental investigations of several specific properties for various photosensitizer molecules, develop quantitative structure property relationships (QSPRs), use the QSPRs in an optimization problem and finally, solve this problem to predict candidate molecular structures with desired properties. Properties that will be investigated include molar extinction coefficient, photon absorption efficiency (PAE), octanol/water partition coefficient (log P), and the degree of conversion/rate of polymerization of hydrophilic-rich phase in presence of the selected

photosensitizers. It is hypothesized that the molecular structure and functional groups in a photosensitizer molecule will have an impact on these properties. We also hypothesize that the QSPRs developed are capable of predicting the properties of similar molecules, and that simultaneous optimization for multiple properties will give efficient water compatible photosensitizer molecules for dental application. The rationale is that these properties will correlate with topological descriptors which describe the structures of the molecules and optimization of the molecular structures for multiple properties by CAMD is a quick and cost effective means to design superior candidate photosensitizer molecules with desired properties.

The approach in accomplishing this aim will be to rationally select photosensitizer molecules to form the model building set and to measure the specific properties. The specific properties are linked to the photo-polymerization reaction or to the availability of the photosensitizer in the hydrophilic-rich phase. The properties will be correlated with the molecular structures by linear regression. The optimization problem will be formulated as a mixed integer non-linear program (MINLP) which will be solved via stochastic method, Tabu Search. The outcome of this aim is a property database for molecules in the model building set, validated correlations (QSPRs) between structural descriptors and properties, and predicted novel water compatible photosensitizer molecules with properties close to the target values.

1.5 Innovation

In this project, characterization of model hydrophilic-rich phase of dental adhesive in terms of polymerization kinetics and polymer structure was performed under various experimental conditions, and a framework to rationally design novel water compatible photosensitizers with an absorption peak in the visible range have been proposed. The specific aims are linked to each other as shown in Figure 1.4. Current techniques for designing dental photo-initiators rely heavily on trial and error experiments. These experiments are expensive, time-consuming and fail to address several properties simultaneously. The CAMD technique is a fast and inexpensive method to predict candidate photosensitizer molecular structures which will possess properties close to the target values. This method is able to traverse a larger search space within a short time, and optimize molecular structures for several properties simultaneously using a combinatorial optimization algorithm. This method offers advantages over the current trial and error technique where the actual search space is vast but only a very small fraction of the unknown space is explored. Although this method has been used by our group and others to design polymers and small molecules, (Eslick *et al.*, 2009; Roughton *et al.*, 2012a), the novelty of this project lies in the use of this method for the design of water compatible visible light photosensitizer molecules for dental applications.

Previous investigators have employed various design methodologies for organic photosensitizers but these methods were significantly different from the proposed approach (Biswas *et al.*, 2014; Park *et al.*, 2009; Tamilavan *et al.*, 2014; Wang *et al.*, 2008). Moreover, most of these studies were focused on applications in dye sensitized solar cells. The systematic design approach for photosensitizer molecules with particular focus on dental applications has not been attempted before. Previous investigations on photosensitizers include a narrow search space, such as modifying an existing molecule with only a few groups based on a hypothesis. The proposed CAMD method designs molecules from a large number of building blocks (molecular sub-groups) and hence a larger search space can be explored compared to the traditional trial and error approach. The CAMD method quantitatively determines the best possible solutions by minimizing the difference between predicted and target property values.

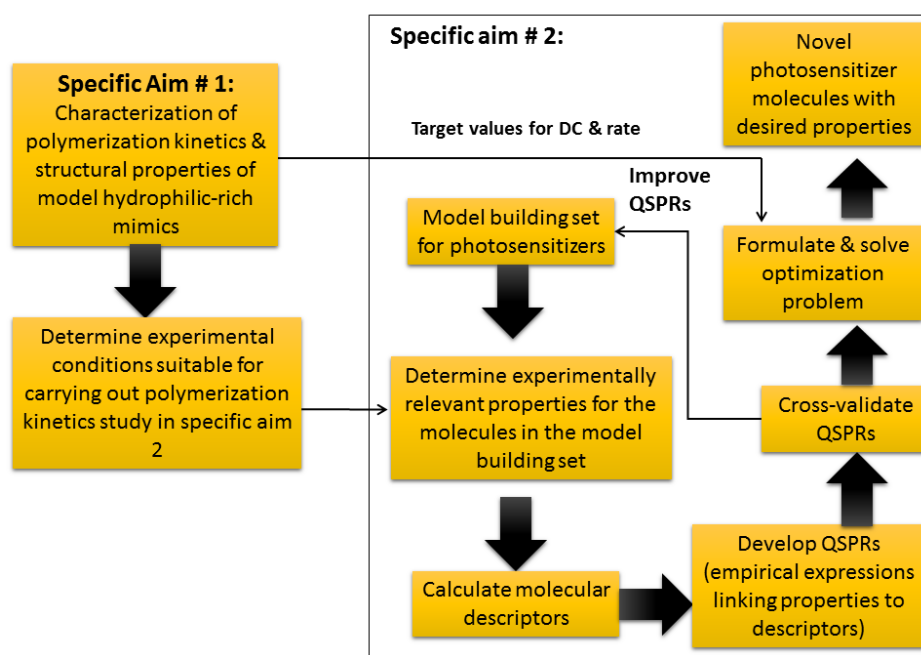


Figure 1.4. Schematic describing the entire proposed project. Specific aim 1 will determine the experimental conditions necessary for carrying out photo-polymerization kinetics experiments in specific aim 2. In specific aim 2, relevant properties such as degree of conversion, rate of polymerization, molar extinction coefficient and PAE for various molecules in the model building set will be determined. The data collected in specific aim 2 will be used to develop correlations (QSPRs) with molecular descriptors. The QSPRs, structural constraints and optimization algorithm will be used to predict molecules with desired properties

Although phase separation of the adhesive has been identified as a key factor in the loss of integrity at the a/d interface, there have been limited investigations of the hydrophilic-rich phase. This is the first study to provide detailed characterization of the polymerization kinetics and structural features of the hydrophilic-rich phase. This study delivers quantitative information about the impact of various experimental conditions on the polymerization kinetics of dental adhesives in model hydrophilic-rich compositions. This project is significant because it will provide possible molecular structures of efficient water compatible photosensitizers, and information from these structures can be used for synthesis of a water compatible visible light photosensitizer in the future. This project is innovative because it demonstrates a) the impact of water on the photo-polymerization and the polymer structure of model hydrophilic-rich mimics of dental adhesives, and this information has been used to propose a possible reaction mechanism involving polymerization- and solvent-induced phase separations (PIPS and SIPS) b) whether light intensity has any effect on the polymerization kinetics and polymer structure of model hydrophilic-rich mimics of dental adhesives c) effect of photo-initiator concentration on the polymerization of hydrophilic-rich mimics d) impact of an accelerator such as iodonium salt on the photo-polymerization kinetics of the physically separated hydrophilic-rich phase and e) rational design framework by using computer-aided molecular design (CAMD) to predict novel photosensitizer molecular structures which possess desired properties for use in dental applications. The molecular structures proposed by CAMD will give valuable insight regarding possible structural features that could impart desirable properties.

PART I: CHARACTERIZATION OF HYDROPHILIC-RICH PHASE OF DENTAL ADHESIVE

CHAPTER 2: POLYMERIZATION KINETICS OF HYDROPHOBIC- VERSUS HYDROPHILIC-RICH PHASES & EFFECT OF CROSS-LINKER/PHOTOSENSITIZER CONCENTRATIONS ON THE POLYMERIZATION OF HYDROPHILIC-RICH PHASE MIMICS

(This chapter is based on the journal article: Abedin F., Ye Q., Parthasarathy R., Misra A., Spencer P., Polymerization behavior of hydrophilic-rich phase of dentin adhesive, Journal of Dental Research, 2015, 94(3), 500-507)

2.1 Introduction

The first step in the characterization of the hydrophilic-rich phase is to understand the difference in the polymerization behavior of the hydrophilic-rich and hydrophobic-rich phases. As mentioned earlier, there is limited control over the quantity of water within the demineralized dentin matrix. The adhesive which is expected to infiltrate this wet, demineralized dentin matrix will experience phase separation. Results from a previous study indicated that the hydrophobic dimethacrylate cross-linker (BisGMA) and photo-initiator components (CQ and EDMAB) partition in a lower concentration within the hydrophilic-rich phase that arises along the hybrid layer (a composite of demineralized dentin and adhesive resin) (Ye *et al.*, 2012). Therefore, it is important to understand whether the cross-linker or photo-initiator concentration exhibits greater influence on the photopolymerization of the hydrophilic-rich phase. In this chapter, two objectives were investigated as given below (Abedin *et al.*, 2015c):

1. To determine whether the hydrophobic-rich phase and the hydrophilic-rich phase exhibit similar polymerization kinetics
2. To understand whether the concentration of cross-linker, BisGMA or photo-initiator concentration possesses greater influence on the photopolymerization of the hydrophilic-rich phase

The study is based on etch-and-rinse dental adhesive systems. Neat resins containing 45 wt% monomethacrylate monomer, HEMA and 55 wt% di-methacrylate monomer, BisGMA are representative of a simplified version of the commercially available dental adhesive resins (Ye *et al.*, 2007a). Therefore, the formulation that mimicked the hydrophobic-rich phase was prepared from HEMA/BisGMA neat resin containing 45wt% HEMA. Based on past investigations, it is known that the hydrophilic-rich phase lacks in the cross-linker, and hence the formulations that mimicked the hydrophilic-rich phase were prepared from HEMA/BisGMA neat resins containing 95 wt%, 99 wt%, 99.5 wt% and 100 wt% HEMA. These dilute formulations represented mimics for the hydrophilic-rich phase within the hybrid layer. The hydrophobic- and hydrophilic-rich phases were at the miscibility limit, which was attained by adding deuterium oxide

(D₂O) to the neat resins. Increasing concentrations of HEMA for the neat resins to prepare hydrophilic-rich phases means higher concentration of D₂O within the mimics and lower concentration of the cross-linker, BisGMA. Hence, the polymerization kinetics study of the hydrophilic-rich phase mimics will yield how the cross-linker influenced the photopolymerization reaction, since all formulations contained an equal concentration of photo-initiators (standard PI concentration). To determine the influence of the photo-initiator concentration on the polymerization of the hydrophilic-rich phase, the mimics were prepared to contain standard and reduced concentrations of the photo-initiator. It was reported that 0.5 wt% of photo-initiator was sufficient to initiate photopolymerization of a dental adhesive (Musanje *et al.*, 2009; Ye *et al.*, 2007a), and hence for the standard concentration of photo-initiator, 0.5 wt% of each photo-initiator component was used to prepare the mimics. The overall hypotheses investigated in this chapter are as follows (Abedin *et al.*, 2015c):

Null Hypothesis 1:

- The polymerization kinetics (degree of conversion and rate of polymerization) are similar for both hydrophobic- and hydrophilic-rich phase mimics.

Null Hypothesis 2:

- Cross-linker and photo-initiator concentrations both will have an equal influence to obtain substantial polymerization of the hydrophilic-rich phase mimics.

2.2 Materials and methods

2.2.1 Preparation of hydrophobic- and hydrophilic-rich phase mimics

The monomers used to prepare the neat resins consisted of 2-hydroxyethyl methacrylate (HEMA) obtained from Acros Organics, Geel, Belgium and bisphenol A glycerolate dimethacrylate (BisGMA) from Polysciences, Washington, PA, USA. The photo-initiators used were: camphorquinone (CQ) and ethyl 4-(dimethylamino)benzoate (EDMAB); both were from Sigma Aldrich, Milwaukee, WI, USA. CQ was used as the hydrophobic photosensitizer and EDMAB as the hydrophobic co-initiator (reducing agent). In this study a hydrophilic photosensitizer, [3-(3,4-Dimethyl-9-oxo-9H-thioxanthen-2-yloxy)-2-hydroxypropyl]trimethylammonium chloride (QTX) was also used which was purchased from Sigma Aldrich, St. Louis, MO, USA.

The neat resin for the hydrophobic-rich phase was prepared by adding appropriate amount of HEMA to the photo-initiator components, CQ and EDMAB. The mixture was then vortexed until the photo-

initiators dissolved. The cross-linker, BisGMA, was added such that the BisGMA was 55 wt% and HEMA 45wt% in the resin. The photo-initiator components were 0.5 wt% each based on the total mass of the mixture. After adding the cross-linker, the mixture was agitated overnight to form a homogeneous solution. The hydrophobic-rich mimic was prepared by adding deuterium oxide (D_2O) to the neat resin dropwise until one drop changed the mixture from clear to turbid. The mixture was then titrated with the neat resin dropwise until it turned clear. The photo-initiator components were replenished based on the amount of D_2O added. Addition of hydrophobic photo-initiators turned the mixture turbid again. Neat resin was added again dropwise until the solution turned clear. The neat resins for the hydrophilic-rich phase also consisted of HEMA/BisGMA, and were prepared such that they contained 95 wt%, 99 wt%, 99.5 wt% and 100 wt% of HEMA. The hydrophilic-rich phase mimics were prepared in the same way as the hydrophobic-rich phase mimic.

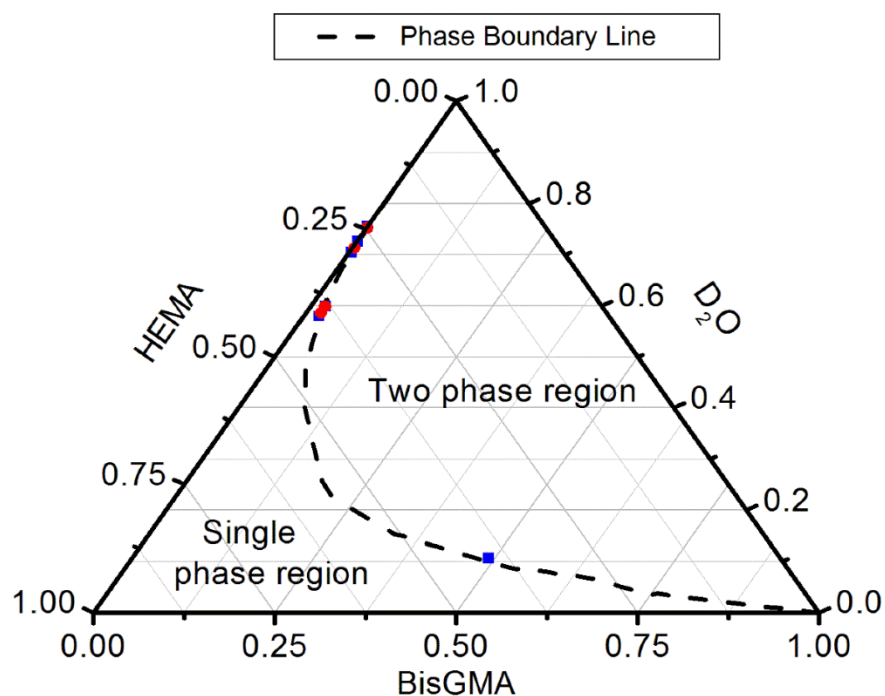


Figure 2.1. Ternary phase diagram showing the phase boundary line as dashed line and formulations investigated. The circles show formulations with standard concentrations of photo-initiators and the squares exhibit formulations with reduced concentration (Abedin *et al.*, 2015c).

These solutions are one-phase solutions and lie on the phase boundary line of the BisGMA/HEMA/D₂O ternary phase diagram as shown in Figure 2.1. This meant that these solutions contained maximum D₂O at the miscibility limit. Formulations with an overall 0.5 wt% photo-initiator components contained standard concentrations of photo-initiators. Table 2.1 exhibits the composition of formulations with a standard concentration of photo-initiators. A formulation partially containing hydrophilic photosensitizer (QTX) was also prepared similarly. In this case, CQ was partially replaced with QTX such that the standard solution contained 0.25 wt% CQ and 0.25 wt% QTX.

For the formulation name, HB stands for HEMA/BisGMA and the number immediately after HB represents the wt% of HEMA in the neat resin, while PB stands for the phase boundary line. Figure 2.2 shows the steps for preparing standard formulations at the miscibility limit in D₂O.

Table 2.1: Composition of formulations with standard concentration of photo-initiator (Abedin *et al.*, 2015c)

Formulation Name	HEMA in Neat Resin (wt)%	wt% of HEMA	wt% of BisGMA	wt% of D ₂ O at Miscibility
HB45PB	45.0	40.26 ± 0.06	49.12 ± 0.04	10.62 ± 0.09
HB95PB	95.0	39.95 ± 0.50	2.09 ± 0.03	57.97 ± 0.52
HB95PB-QTX	95.0	38.08 ± 0.08	2.00 ± 0.01	59.92 ± 0.09
HB99PB	99.0	29.17 ± 1.37	0.29 ± 0.02	70.54 ± 1.39
HB99.5PB	99.5	27.20 ± 1.50	0.14 ± 0.01	72.67 ± 1.50
HB100PB	100	24.47 ± 0.11	N/A	75.53 ± 0.11

CQ and EDMAB are both 0.5 wt% each in the formulations above. Only in case of HB95PB-QTX, CQ and QTX are both 0.25 wt% each, and EDMAB is 0.5 wt%.

Hydrophilic-rich phases with reduced concentrations of photo-initiators were prepared as described above, but the photo-initiators were not replenished after addition of the D₂O. This meant that with increasing concentration of the HEMA in the neat resin and D₂O in the hydrophilic-rich phase, the concentration of photo-initiator (PI) decreased as shown in Table 2.2. The formulation with reduced concentration of PI and partially containing QTX, was prepared similarly.

2.2.2 Fourier Transform Infrared Spectroscopy (FTIR)

Fourier Transform Infrared Spectroscopy (FTIR) is a vibrational absorption technique. It allows identification of chemical groups based on their characteristic vibrational frequency. In this technique, the chemical groups remain in their ground electronic state and transition from ground vibrational state to the first excited vibrational state is detected (Holde *et al.*, 2006). The vibration energies of chemical groups

are within the infrared region. The vibrational modes of chemical groups that can be excited by infrared light include in-plane stretching (in-phase and out-of-phase), in-plane bending (in-phase and out-of-phase) and in-phase out-of-plane bending (Holde *et al.*, 2006). For a molecule to have an infrared (IR) spectra, it must have a dipole moment. Dipole transitions due to vibrations result in the IR spectrum. The chemical groups for which the IR spectra was monitored were C=C at 1637 cm^{-1} and C=O at 1716 cm^{-1} . Under ATR mode, the sample was placed on a diamond crystal and the infrared light was passed through the sample only a few micrometers before being bounced back to the detector.

Table 2.2 Composition of formulations containing reduced concentration of photo-initiators (Abedin *et al.*, 2015c)

Formulation Name	wt% of HEMA in Neat Resin	wt% of HEMA	wt% of BisGMA	wt% of D ₂ O at Miscibility	wt% of CQ	wt% of QTX	wt% of EDMAB
HB95PB	95.0	39.15 ± 0.36	2.07 ± 0.03	58.34 ± 0.38	0.22 ± 0.01	N/A	0.22 ± 0.01
HB95PB-QTX	95.0	37.98 ± 0.24	2.00 ± 0.01	59.61 ± 0.25	0.10 ± 0.01	0.10 ± 0.00	0.21 ± 0.01
HB99PB	99.0	28.32 ± 0.45	0.29 ± 0.01	71.10 ± 0.46	0.14 ± 0.01	N/A	0.15 ± 0.00
HB99.5PB	99.5	24.46 ± 0.30	0.13 ± 0.00	75.15 ± 0.30	0.13 ± 0.01	N/A	0.13 ± 0.00

Preparation of samples at miscibility limit:

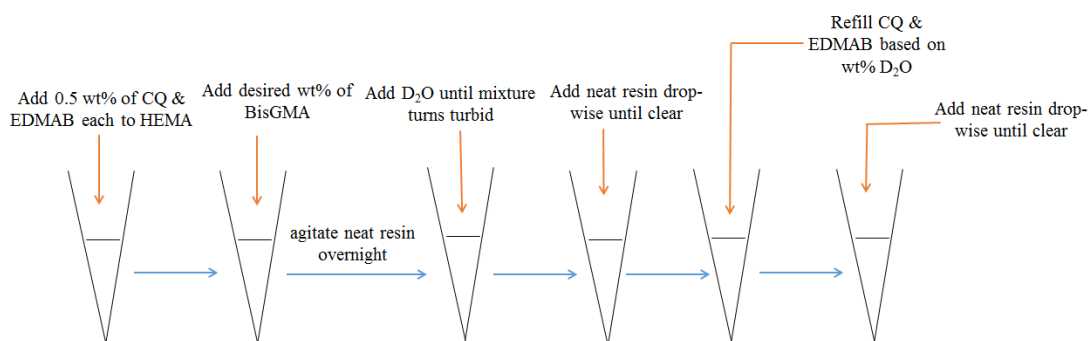


Figure 2.2. Schematic showing the steps for preparing samples at the miscibility limit with standard PI concentration

2.2.3 Photopolymerization kinetics study

The polymerization kinetics was monitored *in-situ* using a Fourier Transform Infrared Spectrophotometer (FTIR), PerkinElmer Spectrum 400, Waltham, MA, USA. A time-resolved spectrum

collector was used to observe the polymerization kinetics. 30 μL of each formulation was added on the internal reflectance crystal, and a transparent plastic coverslip was placed on top of the sample. The coverslip was sealed at the four edges using tapes (Abedin *et al.*, 2014; Abedin *et al.*, 2015c). This prevented the evaporation of D_2O which would otherwise increase the viscosity of the sample, and hence interfere with the polymerization kinetics. The sample was then cured for 40 s using a dental curing light, Spectrum 800, Milford, DE, USA. The data was collected at a resolution of 4 cm^{-1} in the ATR mode (Ye *et al.*, 2007a; Ye *et al.*, 2007b). The D_2O profile was monitored continuously to ensure that there was no evaporation of D_2O (A sample D_2O profile is shown in Chapter 3). The band ratio intensities of C=C at 1637 cm^{-1} to C=O at 1716 cm^{-1} was monitored, and the degree of conversion (DC) was evaluated using equation 2.1 (Abedin *et al.*, 2015c).

$$DC = \left(1 - \frac{\text{Absorbance}_{1637\text{ cm}^{-1}}^{\text{sample}} / \text{Absorbance}_{1716\text{ cm}^{-1}}^{\text{sample}}}{\text{Absorbance}_{1637\text{ cm}^{-1}}^{\text{monomer}} / \text{Absorbance}_{1716\text{ cm}^{-1}}^{\text{monomer}}}\right) \times 100\% \quad 2.1$$

The rate of polymerization was determined from the first derivative of time versus DC graph using Microcal Origin (Version 6.0, Microcal Software, Northampton, MA). The formulations were prepared using D_2O instead of water (H_2O) because the latter showed spectral features at the same wavelength where the C=C bond was monitored.

2.2.4 Viscosity measurement

The viscosities of the experimental formulations were determined using a Brookfield DV-II+Pro viscometer (Brookfield, Middleborough, MA, USA). A cone/plate set up was used for the measurements. A fixed volume of 0.5 mL of the formulation was placed onto the viscometer and the viscosity was determined at various shear rates and at a temperature of $25.0 \pm 0.2^\circ\text{C}$.

2.2.5 Statistical Analysis

Three samples per formulation were prepared, and hence the polymerization kinetics was monitored in triplicate for each formulation. The viscosity measurement of each formulation was also performed in triplicate. To understand whether there was a significant difference in the viscosity, DC and rate of polymerization between hydrophobic- and hydrophilic-rich phases, a one-way analysis of variance (ANOVA) and a t-test at $\alpha = 0.05$ were carried out.

2.3 Results

2.3.1 Difference in photopolymerization kinetics of hydrophobic- and hydrophilic-rich phase mimics

It was observed that there was a significant difference in the degree of conversion and rate of polymerization between the hydrophobic- (HB45PB) and hydrophilic-rich phases ($P < 0.001$) as shown in Figures 2.3 (a) and (b) (Abedin *et al.*, 2015c). Figures 2.3 (a) and (b) exhibit representative polymerization kinetic results for HB45PB and HB95PB. From Figure 2.3 (a), it could be seen that the hydrophobic-rich phase mimic (HB45PB) polymerized much faster than the hydrophilic-rich phase (HB95PB). HB45PB reached approximately 80% degree of conversion in about 2 minutes, whereas the hydrophilic-rich phase mimic (HB95PB) took longer (about 70 to 90 minutes) to reach approximately 90% degree of conversion. The initial rate of polymerization was also significantly higher for the HB45PB compared to the HB95PB as exhibited by Figure 2.3 (b) ($P < 0.001$). It could also be seen that HB95PB exhibited secondary rate maximum which was absent for the HB45PB. Table 2.3 summarizes the degree of conversion and rate of polymerization for both hydrophobic- and hydrophilic-rich phase mimics containing the standard concentration of PI (Abedin *et al.*, 2015c). From Table 2.3, it was observed that all hydrophilic-rich phase mimics (HB95PB, HB95PB-QTX, HB99PB, HB99.5PB and HB100PB) showed secondary rate maxima in contrast to the hydrophobic-rich phase mimic (HB45PB).

Table 2.3. Summary of degree of conversion and rate of polymerization of formulations containing standard concentration of PI (Abedin *et al.*, 2015c)

Formulation Name	Degree of Conversion	Initial Rate Maxima of Polymerization ($s^{-1} \times 10^4$)	Post Polymerization Rate Maxima ($s^{-1} \times 10^4$)	Appearance after Polymerization
HB45PB	0.80 ± 0.07	297 ± 25	N/A	Translucent
HB95PB	$0.94 \pm 0.03^{**}$	$16.1 \pm 5.4^{\#}$	3.4 ± 0.3	Turbid White
HB95PB-QTX	0.83 ± 0.03	$21.5 \pm 0.5^{\#}$	2.0 ± 0.8	Turbid White
HB99PB	$0.95 \pm 0.01^{**}$	$15.9 \pm 3.3^{\#}$	2.1 ± 0.3	Turbid White
HB99.5PB	$0.97 \pm 0.03^{**}$	$14.9 \pm 2.9^{\#}$	2.4 ± 0.1	Turbid White
HB100PB	0.78 ± 0.18	$14.3 \pm 3.3^{\#}$	1.4 ± 0.5	Translucent

**Degree of conversion of hydrophilic-rich phase is significantly different (one way ANOVA analysis at $\alpha=0.05$) from control hydrophobic-rich phase (HB45PB)

[#]Initial rate of polymerization of hydrophilic-rich phase is significantly different (one way ANOVA analysis at $\alpha=0.05$) from control hydrophobic-rich phase (HB45PB)

Therefore, the null hypothesis about the polymerization kinetics being similar for both the hydrophobic- and hydrophilic-rich phases was rejected since they are significantly different. From Figure 2.3 (c), it was

also observed that the viscosity of the HB45PB was significantly higher compared to the hydrophilic-rich phases.

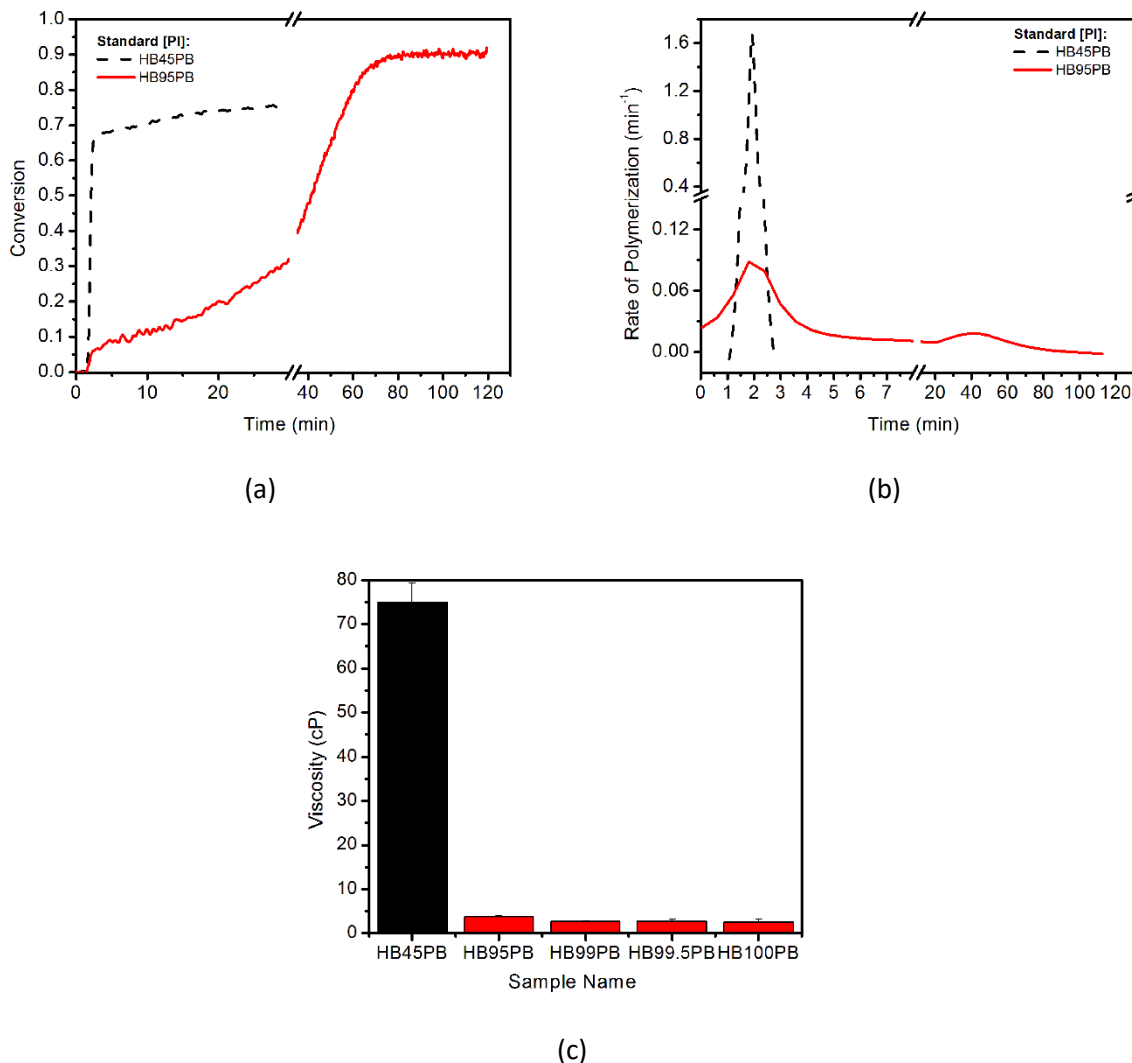


Figure 2.3. Polymerization kinetics results for hydrophobic-rich mimic (HB45PB) and hydrophilic-rich mimic (HB95PB) showing (a) degree of conversion versus time and (b) rate of polymerization against time. (c) Viscosity measurement showing that the hydrophobic-rich mimic is significantly viscous compared to the hydrophilic-rich mimics (Abedin *et al.*, 2015c).

2.3.2 Polymerization kinetics results for hydrophilic-rich phase mimics containing standard PI concentration

It was observed that the average degree of conversion of the hydrophilic-rich phase mimics, HB95PB, HB99PB and HB99.5PB ranged from 94% to 97% after 2 h (Table 2.3) (Abedin *et al.*, 2015c). The average degree of conversion at 2 h for HB95PB-QTX was 83% and that for HB100PB was 78% (Abedin *et al.*, 2015c). From Table 2.3, it could be seen that as the BisGMA concentration decreased in the hydrophilic-rich phase mimics with increasing hydrophilicity, the degree of conversion remained substantial. For the hydrophilic-rich formulations containing CQ as the photosensitizer (HB95PB, HB99PB, HB99.5PB and HB100PB), a slight decreasing trend for the initial rate of polymerization was observed as the cross-linker concentration was reduced (Table 2.3). These results indicated that the concentration of the cross-linker (BisGMA) possessed very little influence on the degree of conversion although it could have some impact on the reactivity of the formulation. Despite the slight decrease in the initial polymerization rate with decreasing BisGMA concentration, the degree of conversion remained substantial. Figure 2.4 shows the representative polymerization kinetic results of hydrophilic-rich phase mimics containing the standard concentration of PI. All the hydrophilic-rich phase mimics exhibited secondary rate maxima which led to a substantial degree of conversion as shown by Figure 2.4 (a) and (b). HB100PB exhibited the lowest secondary rate maxima when compared to the hydrophilic-rich mimics containing BisGMA (Abedin *et al.*, 2015c).

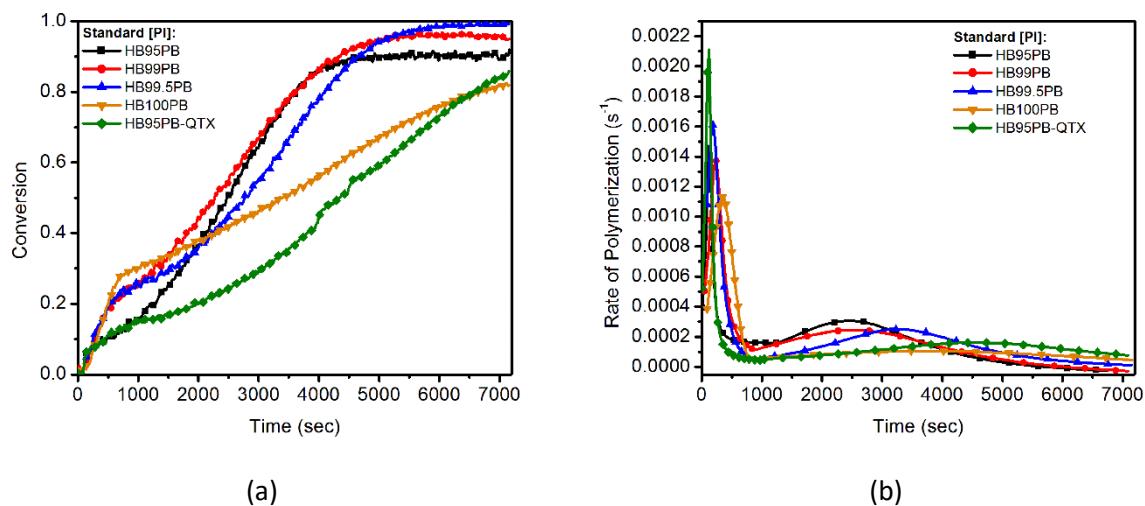


Figure 2.4. Polymerization kinetics results of hydrophilic-rich mimics at miscibility limit with standard PI concentration exhibiting (a) degree of conversion against time and (b) rate of polymerization against time (Abedin *et al.*, 2015c).

2.3.3 Polymerization kinetics results of hydrophilic-rich phase mimics containing reduced concentration of PI

Table 2.4 provides a summary of the photopolymerization kinetics study for hydrophilic-rich mimics with the reduced concentration of PI. Figure 2.5 shows representative polymerization kinetics result for hydrophilic-rich mimics with the reduced concentration of PI. It could be seen from Table 2.4 and Figure 2.5 (a), that the degree of conversion at 2 h was substantially poor for the hydrophilic-rich mimics with reduced PI concentration containing CQ as the photosensitizer only (HB95PB, HB99PB, HB99.5PB, HB100). These samples did not exhibit any secondary rate maxima, indicating an absence of post-polymerization (Table 2.5). Figure 2.5 (b) exhibits comparative results for the rate of polymerization in case of corresponding formulations with standard and reduced PI concentrations.

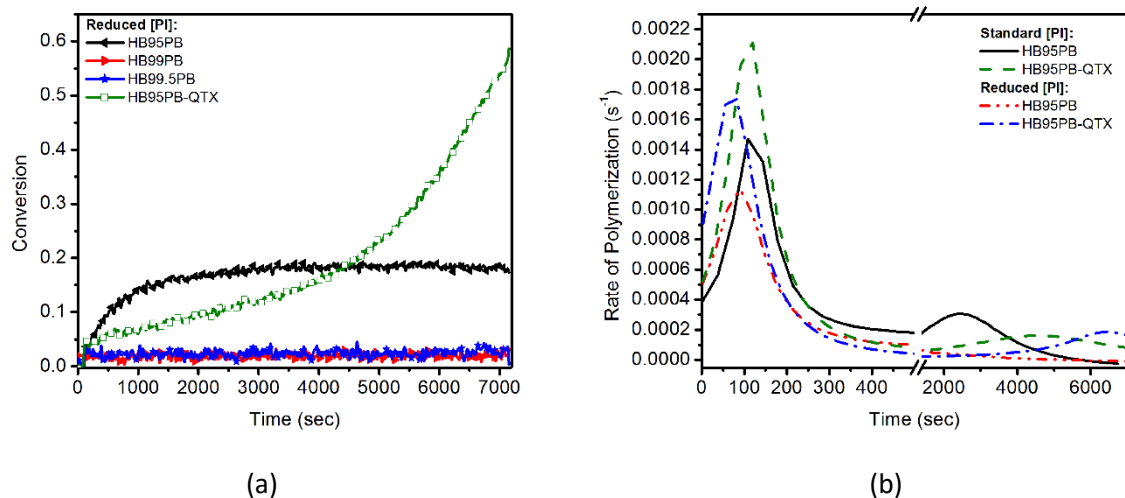


Figure 2.5. Polymerization kinetics results of hydrophilic-rich mimics at miscibility limit with reduced PI concentration exhibiting (a) degree of conversion against time. (b) Comparative rate of polymerization against time is shown for HB95PB and HB95PB-QTX with standard and reduced PI concentration (Abedin *et al.*, 2015c).

The hydrophilic-rich mimic containing CQ/QTX as the photosensitizer exhibited a substantial degree of conversion even when present in reduced concentrations (Table 2.4 and Figure 2.5 (a)). From Figure 2.5 (b), it could be observed that this formulation also exhibited a delayed secondary rate maxima which enabled it to reach a substantial degree of conversion. Comparing corresponding hydrophilic-rich mimics containing CQ as the photosensitizer in Table 2.3 and 2.4, it was seen that the concentration of

the photo-initiator had a significant influence on the degree of conversion. QTX is more hydrophilic in nature compared to the CQ. The negative impact of the reduced PI concentration on the DC could be overcome by improving the compatibility of the photosensitizer within the formulation as indicated by the sample HB95PB-QTX. Even then, reducing the concentration of PI for HB95PB-QTX led to a significant decrease in the DC (one-way ANOVA, $P < 0.05$) as indicated in Table 2.3 and 2.4. Therefore, the null hypothesis that the cross-linker and PI concentrations both equally influence the degree of conversion (DC) of the hydrophilic-rich phase was rejected since the cross-linker concentration exhibited limited influence whereas the PI concentration had a significant impact on the DC.

Table 2.4. Polymerization kinetics result for hydrophilic-rich phase mimics with reduced PI concentration (Abedin *et al.*, 2015c)

Formulation Name	Degree of Conversion	Initial Rate Maxima of Polymerization (s^{-1}) $\times 10^4$	Post Polymerization Rate Maxima (s^{-1}) $\times 10^4$	Appearance after Polymerization
HB95PB	0.24 ± 0.06	13.7 ± 3.3	N/A	Transparent
HB95PB-QTX	0.57 ± 0.13	16.2 ± 1.0	1.7 ± 0.4	Turbid White
HB99PB	0.02 ± 0.01	11.3 ± 4.3	N/A	Transparent
HB99.5PB	0.03 ± 0.01	13.2 ± 1.7	N/A	Transparent

2.4 Discussion

With very little control over water within the demineralized dentin, the adhesive resin will undergo phase separation into hydrophobic- and hydrophilic-rich phases. This study investigated formulations that mimicked the possible hydrophobic- and hydrophilic-rich phases arising within the demineralized dentin. In this investigation, the commercial adhesive was not used to avoid the complexity due to the presence of entities other than monomers and photo-initiators.

The high initial rate of polymerization for the hydrophobic-rich phase was due to the gel effect (Norrish and Smith, 1942). The gel effect, also known as the auto-acceleration, is common for a viscous system (Ye *et al.*, 2008; Ye *et al.*, 2007a; Ye *et al.*, 2007b). The hydrophobic-rich phase is rich in the cross-linker concentration allowing it to form a highly cross-linked network. This results in an increase in the viscosity and hence limits the diffusion of reactive species. In other words, the termination reaction becomes diffusion limited, leading to a decrease in the termination rate and hence an increase in the polymerization rate (Zhang *et al.*, 2008). The viscosity of the hydrophilic-rich mimics was significantly

lower than the hydrophobic-rich mimic (Figure 2.3 (c)). This is because the hydrophobic-rich phase possesses higher concentration of the viscous BisGMA, whereas the hydrophilic-rich phase mostly consists of the less viscous D₂O and HEMA. This indicates that the reactive species are able to diffuse more freely within the hydrophilic-rich mimics compared to the hydrophobic-rich mimics. Hence, the termination rate is higher for the hydrophilic-rich mimics. Moreover, the monomer concentration is much lower within the hydrophilic-rich mimics. Therefore, the possibility of the creation of free radicals to initiate polymerization is lower for hydrophilic-rich mimics. A higher termination rate and lower monomer concentration can be attributed to the significantly lower initial polymerization rate for the hydrophilic-rich mimics compared to the hydrophobic-rich mimic despite both having standard photo-initiator concentration. It is also possible that BisGMA can impart higher reactivity to the formulation. This may also contribute to the higher initial rate for the hydrophobic-rich mimic since it contains significantly higher concentration of BisGMA.

The bimodal rate of polymerization has been reported for methacrylate based system (Anseth *et al.*, 1994; Horie *et al.*, 1975; Yu *et al.*, 2001). According to Horie *et al.*, the reactivity of pendant double bonds is lower than free monomers during the polymerization, and later during the reaction the pendant double bonds begin to react forming cross-linked regions called microgels (Horie *et al.*, 1975). These double bonds become trapped within the microgels and cause secondary gel effect resulting in the secondary rate maxima (Horie *et al.*, 1975). Here, it is possible that the secondary rate maximum is due to trapped reactive species within the microgels (Chapter 3 contains detailed discussion on possible origins of the secondary rate maxima).

The hydrophilic-rich mimic without containing BisGMA (HB100PB) exhibited the lowest secondary rate maximum. In this case, the polymer is linear (polyHEMA) and the microgel formation is possibly due to cyclization reaction, which can be soluble initially within the co-solvent system (i.e. HEMA and D₂O). As a result, fewer reactive species are entrapped in the microgel system. This can result in a lower secondary rate maxima.

Previous investigation by Gao *et al.* showed that the number of radicals generated per unit volume is enhanced with increasing concentration of the photo-initiator (Gao and Nie, 2007). Hence, for the hydrophilic-rich mimics containing reduced concentration of the photo-initiator, the availability of effective free radicals or reactive species is decreased. The lack of effective free radicals or reactive species may have been responsible for the inhibition of post-polymerization or a secondary gel effect within the 2 h. It can be seen in Table 2.4 that the initial polymerization rate for the hydrophilic-rich mimics with

reduced PI concentration are similar, but the DC for the mimics HB95PB and HB95PB-QTX (reduced PI) is higher. The PI and monomer concentrations are higher for HB95PB and HB95PB-QTX (reduced PI) compared to the other mimics with reduced PI concentration leading to enhanced generation of effective radicals and reactivity. This can account for the higher DC for these two mimics. QTX is more water soluble than CQ (Ye *et al.*, 2009) and hence it is possible that for HB95PB-QTX the radicals are able to diffuse more freely due to their enhanced compatibility with the surrounding solution. This may result in the entrapment of more radicals in the microgels even when the PI is present in a lower concentration. This could lead to a higher initial polymerization rate and delayed secondary gel effect for HB95PB-QTX even when the PI concentration was reduced.

The polymerization kinetics study can be impacted by several factors such as evaporation of the D₂O, sample thickness, light intensity and dissolved oxygen. The cover slips were sealed to prevent evaporation of the D₂O and during this study the volume of the sample was kept constant at 30 μ L to ensure uniform sample thickness throughout. The total incident light energy on the sample was kept constant by maintaining the light intensity at 550 mW/cm² and exposure time at 40 s. It is possible that the hydrophilic-rich mimics contain dissolved oxygen due to the presence of D₂O in large quantities. This dissolved oxygen can interfere with the polymerization kinetics. In case of the HB100PB, the viscosity was very low, and the sample contained a high concentration of D₂O, increasing the possibility of dissolved oxygen interfering with the polymerization kinetics. This could have resulted in the high standard deviation for DC in case of the HB100PB. The experimental setting for the polymerization kinetics study is not representative of the clinical setting, since the investigations have been conducted under limited D₂O evaporation and oxygen diffusion. Under clinical conditions, diffusion of oxygen will have a significant negative impact on the polymerization kinetics.

Even though the hydrophilic-rich mimics with the standard PI concentration have undergone substantial DC, reducing the possibility of leaching of HEMA/low-molecular-weight degradants and improving the bond integrity at the margin, the resultant polymer will still be loosely cross-linked. This means that over time the polymer becomes more prone to degradation and plasticization, compromising the a/d bond integrity. Degradation also results in leaching of HEMA and low-molecular-weight degradants which may elicit cytotoxic effects.

2.5 Conclusion

The current study investigates the polymerization behavior of hydrophilic-rich phase mimics of dental adhesives compared to the hydrophobic-rich phase mimic, and whether cross-linker or PI concentration plays an important role in the substantial DC of hydrophilic-rich mimics. The results from this study are summarized below:

- The efficiency of polymerization reactions for the hydrophilic-rich phase mimics is very low compared to the hydrophobic-rich mimics.
- The hydrophilic-rich mimics exhibit secondary rate maxima, which is absent in the hydrophobic-rich mimic.
- The PI concentration has a significant impact on the DC of the hydrophilic-rich mimics, although the BisGMA concentration may impact the reactivity of the polymerization reaction.
- The compatibility of the PI plays an important role in the DC of the hydrophilic-rich mimics.
- Incorporation of water compatible photo-initiator within the current dental adhesive formulation will improve the DC of the hydrophilic-rich mimics under clinical conditions since PI concentration and compatibility of PI are both important factors to reach higher DC.

CHAPTER 3: IMPACT OF WATER CONCENTRATION ON THE PHOTO-POLYMERIZATION OF HYDROPHILIC-RICH MIMICS AND ITS POLYMERIZATION MECHANISM

(This chapter is based on the journal article: Abedin F., Ye Q., Good H. J., Parthasarathy R., Spencer P., Polymerization- and solvent-induced phase separation in hydrophilic-rich dentin adhesive mimic, Acta Biomaterialia, 2014, 10, 3038-3047)

3.1 Introduction

The previous chapter discussed the differences in the polymerization kinetics of the hydrophilic-rich and hydrophobic-rich phases. As mentioned earlier, the polymerization efficiency of the hydrophilic-rich mimics was lower and these samples exhibited a secondary gel effect. Since the water content and resin concentration may vary along the hybrid layer, it is also important to understand the influence of water content on the polymerization of the hydrophilic-rich phase. In this study, the water concentration is varied from 0 wt% until the miscibility limit, where the formulation lies on the phase boundary line of the HEMA/BisGMA/Water ternary phase diagram. The formulations investigated were also mimics for the hydrophilic-rich phase, and they consisted of mostly deuterium oxide (D_2O) and HEMA, while the concentration of the cross-linker, BisGMA was kept low. The concentration of the PI was kept constant for all the formulations.

3.2 Materials and Methods

The mimics were prepared from HEMA (ACROS Organics)/BisGMA (Polysciences, Washington, PA, USA) monomers in the ratio of 95/5 wt% and 99/1 wt%. The PI system used in this study consisted of CQ and EDMAB from Aldrich, Milwaukee, WI, USA. To prepare the neat resin, CQ and EDMAB were added to a specific quantity of HEMA such that each of the PI components was 0.5 wt% based on the total weight of the neat resin. The mixture was vortexed until the PI components dissolved and then BisGMA was added so that the desired HEMA to BisGMA ratio was obtained. The mixture was agitated overnight to obtain a homogeneous solution. For the preparation of hydrophilic-rich mimics under the phase boundary line, the desired amount of D_2O was added to the neat resin. The PI components were added based on the mass of D_2O to keep the final concentration of the PI constant at 0.5 wt%. Figure 3.1 shows the steps to prepare the hydrophilic-rich formulations under the phase boundary line. The preparation method for the mimics at the miscibility limit or on the phase boundary line were discussed in Chapter 2 and illustrated in Figure 2.2. The miscibility was identified using cloud point detection (Spencer and Wang, 2002). The mimics at the miscibility limit represent a one-phase solution containing maximum D_2O , and further addition of the D_2O would lead to separation into two phases. Table 3.1 exhibits the concentration

of the components in the hydrophilic-rich mimics studied here. Figure 3.2 shows all the formulations prepared on a ternary phase diagram of HEMA/BisGMA/water.

The formulations without D₂O are denoted as HBxNR where ‘HB’ means HEMA/BisGMA, ‘x’ is the wt% of HEMA and ‘NR’ stands for the neat resin. The mimics below the phase boundary line are denoted as HBxD₂Oy where ‘x’ represents the wt% of HEMA in the neat resin from which the mimic is made and ‘y’ is the wt% of D₂O in the mimic. The sample notation for the mimic on the phase boundary line is HBxPB where ‘x’ was the wt% of HEMA in the neat resin from which the mimic is prepared and ‘PB’ means phase boundary.

Preparation of samples below miscibility limit:

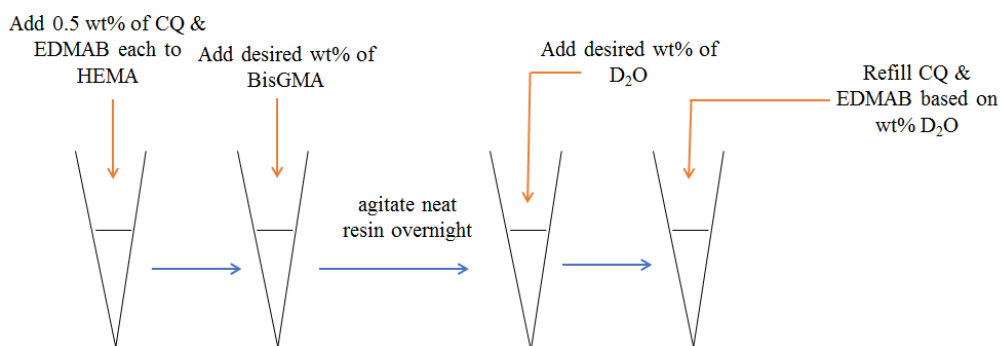


Figure 3.1. Schematic showing preparation of hydrophilic-rich mimics below the miscibility limit

Table 3.1. Composition of the hydrophilic-rich mimics investigated (Abedin *et al.*, 2014)

Name of Formulation	wt% HEMA	wt% BisGMA	wt% D ₂ O
Formulation prepared from HEMA/BisGMA (95/5 wt%) neat resin:			
HB95NR	94.95 ± 0.02	5.05 ± 0.02	0.0 ± 0.0
HB95D ₂ O10	84.95 ± 0.47	4.51 ± 0.04	10.54 ± 0.50
HB95D ₂ O20	75.35 ± 0.60	4.00 ± 0.06	20.65 ± 0.65
HB95D ₂ O30	65.92 ± 0.50	3.51 ± 0.07	30.57 ± 0.56
HB95D ₂ O50	46.91 ± 0.22	2.50 ± 0.02	50.60 ± 0.23
HB95PB	39.95 ± 0.50	2.09 ± 0.03	57.97 ± 0.52
Formulation prepared from HEMA/BisGMA (99/1 wt%) neat resin:			
HB99NR	98.99 ± 0.01	1.01 ± 0.01	0.0 ± 0.0
HB99D ₂ O20	78.55 ± 0.86	0.81 ± 0.01	20.64 ± 0.86
HB99D ₂ O30	69.06 ± 0.13	0.71 ± 0.01	30.23 ± 0.13
HB99D ₂ O50	49.00 ± 0.25	0.51 ± 0.01	50.49 ± 0.26
HB99PB	29.2 ± 1.4	0.29 ± 0.02	70.5 ± 1.4

CQ and EDMAB concentrations were kept constant to 0.5 wt% each

3.2.1 Polymerization kinetics study

The polymerization behavior of the hydrophilic-rich mimics was assessed using the procedure described in Chapter 2. Briefly, the polymerization kinetics was monitored for 2 h using a Perkin-Elmer Spectrum 400 Fourier Transform Infrared spectrophotometer in ATR sampling mode at a resolution of 4 cm^{-1} . The details of the FTIR spectroscopy were discussed in Chapter 2. The sample volume was kept constant at $30\ \mu\text{L}$ and the cover slip was sealed at the edges to prevent evaporation of D_2O . The sample was cured for 40 s at 550 mW/cm^2 using a Spectrum[®] 800, Dentsply, Milford, DE, USA (Abedin *et al.*, 2014).

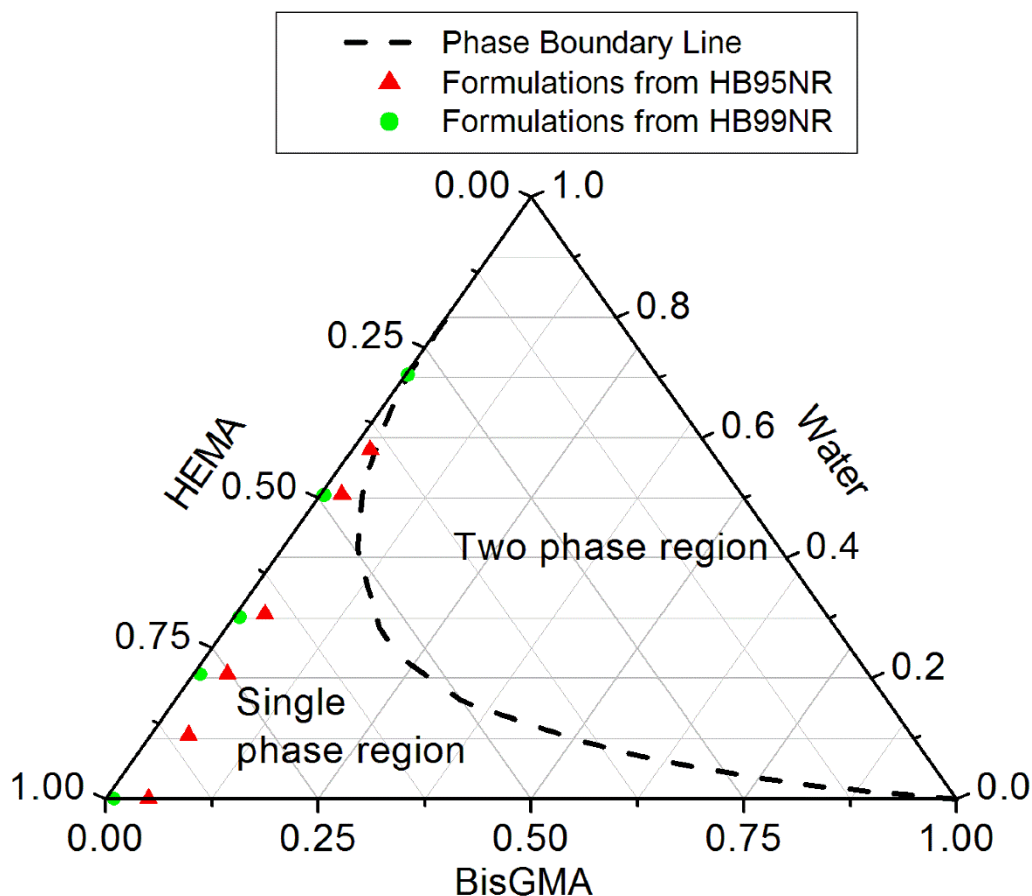


Figure 3.2. Ternary phase diagram showing the hydrophilic-rich mimics investigated in triangles and circles (Abedin *et al.*, 2014)

The intensity for C=C at 1637 cm^{-1} and C=O at 1716 cm^{-1} were monitored and equation 2.1 was used to calculate the degree of conversion (DC), and the rate of polymerization was obtained from the first derivative of the time-DC curve using Microcal Origin (Version 6.0, Microcal Software, Northampton, MA).

D₂O instead of water was used in this study to avoid spectral interference by water at 1637 cm⁻¹ where the C=C was monitored. It was important to monitor the D₂O profile to ensure that there was no evaporation, since this could change the viscosity of the sample and interfere with the polymerization kinetics. Figure 3.3 shows an example D₂O profile for the formulation HB99PB. It could be seen that the intensity band ratio of C=C at 1637 cm⁻¹ to C=O at 1716 cm⁻¹ decreased as the sample polymerized whereas the D₂O profile remained almost constant (Figure 3.3). The slight decrease in the D₂O profile during the initial stage of polymerization may be due to the diffusion of D₂O from the center of the ATR crystal to the surrounding area during curing. Three samples for each formulation were prepared and investigated for their polymerization kinetics.

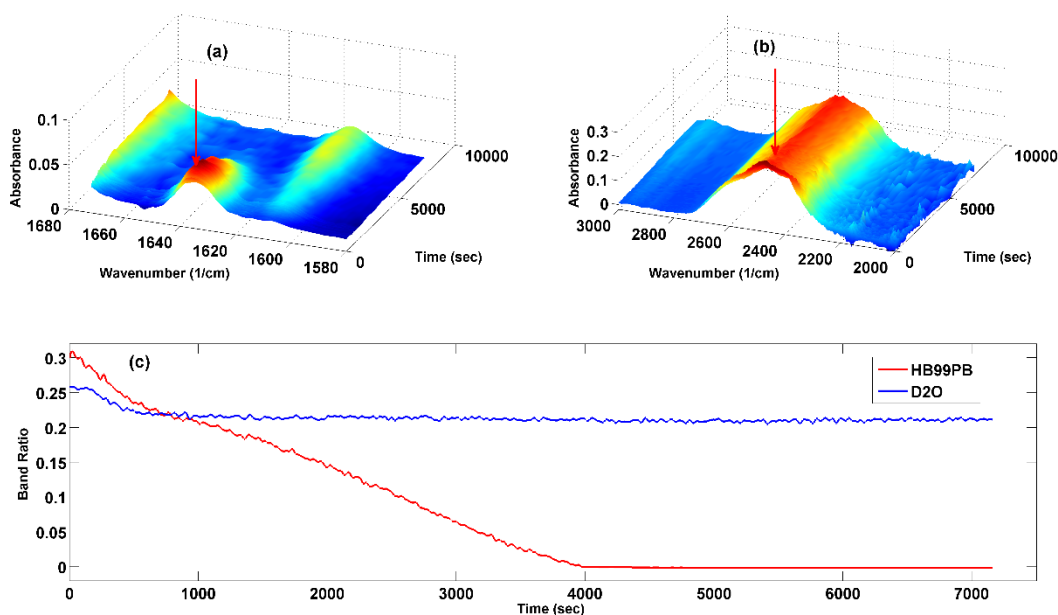


Figure 3.3. (a) 3-D surface plot for the C=C bond at 1637 cm⁻¹ (b) 3-D surface plot for D-O bond for D₂O during polymerization (c) Band ratio of C=C at 1637 cm⁻¹ to C=O at 1716 cm⁻¹ decreasing during monitoring the polymerization kinetics *in-situ* and D₂O profile remaining almost constant (Abedin *et al.*, 2014)

3.2.2 Differential scanning calorimetry (DSC)

In the DSC technique, the difference in the heat flow rate between the sample and a reference is measured as a function of temperature. For the conventional DSC technique, the sample and the reference are subjected to a controlled heating or cooling rate, resulting in a linearly

increasing/decreasing temperature with time (Menczel and Prime, 2014; Thomas, 2005). This results in a single heat flow versus temperature/time data. The obtained data from the conventional technique is the total heat flow at any time or temperature. For the modulated temperature DSC (MTDSC), along with the linear heating/cooling rate, a modulated temperature signal is also applied simultaneously. Usually the temperature is varied sinusoidally with time (Menczel and Prime, 2014; Thomas, 2005). The total heat flow can be associated with changes in heat capacity and time/temperature dependent thermal events as given by the equation below (Thomas, 2005):

$$\frac{dQ}{dt} = C_p \frac{dT}{dt} + f(T, t) \quad 3.1$$

where dQ/dt is the heat flow rate, C_p is the heat capacity, T is temperature, t is time and $f(T, t)$ includes kinetic events which are dependent on both time and temperature

MTDSC, unlike conventional DSC, is able to separate heat flow associated with heat capacity (reversible component) and kinetic events such as chemical reactions, cold crystallization and evaporation (non-reversible component). The transitions that represent the reversible component include the glass transition temperature and melting. The reversible component of MTDSC is not the same as a thermodynamic reversible process (Menczel and Prime, 2014; Thomas, 2005). The advantage of MTDSC is that it allows increased sensitivity of the reversible heat flow signal as a result of reduced noise level, and separation of overlaying reversible and non-reversible transitions leading to a more accurate analysis.

3.2.3 Determination of glass transition temperature (T_g) of the hydrophilic-rich mimics

The glass transition temperatures (T_g) of the hydrophilic-rich mimics were determined using a TA Instruments Model Differential Scanning Calorimetry (DSC) Q200. The samples for DSC were prepared by adding each formulation to an aluminum low-mass DSC pan until it was filled to the brim. Then the pan was covered using a glass coverslip. The sample was then light cured for 40 s at 550 mW/cm² using Spectrum® 800, Dentsply, Milford, DE, USA. The samples were left overnight. The glass coverslips were removed and the specimens were placed in a vacuum chamber at 37°C. The specimens were weighed at specific time intervals until consecutive masses were almost the same value. Three specimens per formulation were prepared. The T_g for each specimen was determined by employing modulated temperature DCS method (MTDSC). This method had been used for determining the T_g for dental adhesives before (Ye *et al.*, 2007a). MTDSC was carried out in the presence of purged nitrogen gas at 40 ml/min. The temperature was perturbed with a sinusoidal amplitude of 2°C every 60 s. There were two heating/cooling cycles at 3°C/min and the temperature range for each cycle was -10°C to 200°C. The T_g

was determined from the first derivative of the temperature against reversible heat flow graph. The analysis was carried out using Universal Analysis Software (TA Instruments, New Castle, DE) (Abedin *et al.*, 2014). Figure 3.4(a) shows an example of the reversible heat flow signal for the sample HB95NR in case of both 1st and 2nd heating cycles and the peaks observed in Figure 3.4(b) represent the glass transition temperatures. Three samples per formulation were prepared to carry out the MTDSC.

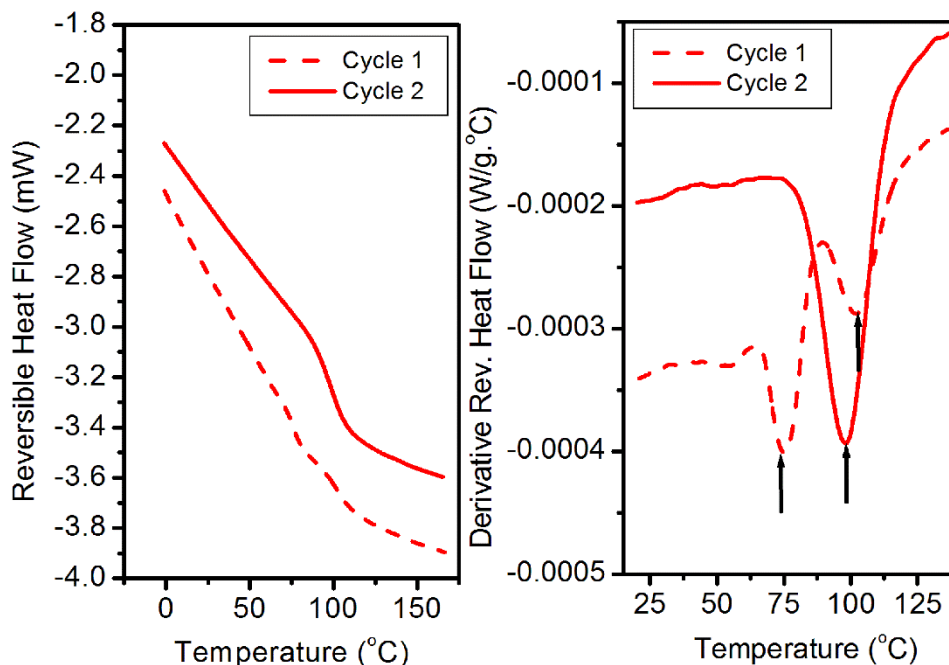


Figure 3.4. (a) Reversible heat flow signal from MTDSC for HB95NR showing both the 1st and 2nd heating cycles (b) First derivative of the reversible heat flow versus temperature curve for HB95NR and the peaks represent the glass transition temperature (T_g) (Abedin *et al.*, 2014)

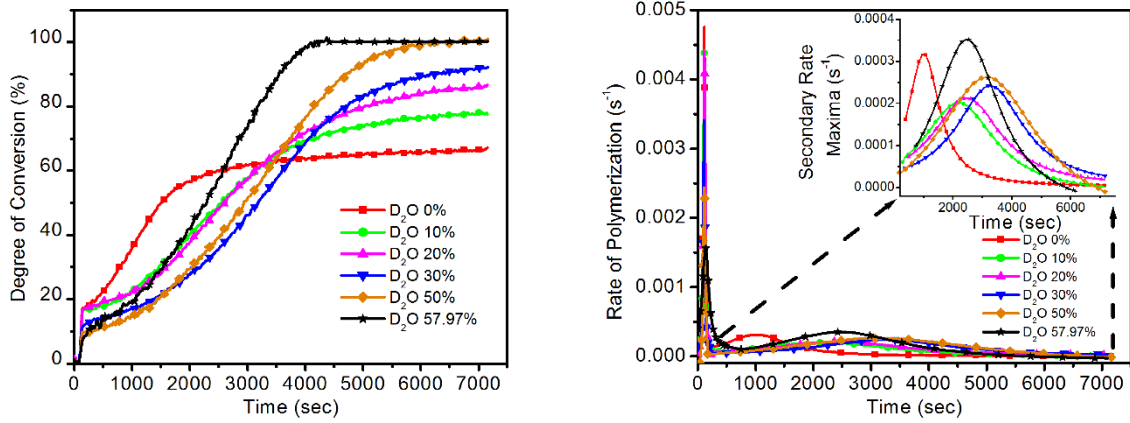
3.2.4 Determination of viscosity

The viscosities of the experimental formulations were determined using a Brookfield DV-II+Pro viscometer (Brookfield, Middleborough, MA, USA). A cone/plate set up was used for the measurements. A fixed volume of 0.5 mL of the formulation was placed onto the viscometer and the viscosity was determined at various shear rates and at a temperature of $25.0 \pm 0.2^\circ\text{C}$.

3.3 Results

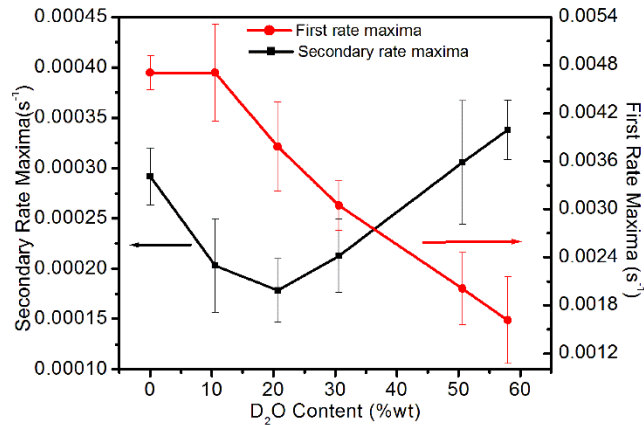
3.3.1 Polymerization kinetics of hydrophilic-rich mimics

The miscibility limit for the formulation prepared from HB95NR was found to be approximately 57.96 wt% D₂O and that from HB99NR was 70.5 wt%. All the formulations exhibited a substantial degree of conversion. Figures 3.5 and 3.6 show the polymerization kinetics of representative samples made from HB95NR and HB99NR respectively. It could be seen that there was a decreasing trend of initial rate maxima as wt% of D₂O was increased (Figure 3.5 (c)).



(a)

(b)



(c)

Figure 3.5. Polymerization kinetics result for formulations made from neat resin containing 95 wt% HEMA. (a) DC against time as a function of D₂O content. (b) Rate of polymerization of the formulation against time as a function of D₂O content showing the presence of secondary rate maxima. (c) Average initial and secondary rate maxima as a function of D₂O content (Abedin *et al.*, 2014)

For the formulations prepared from HB95NR, the secondary rate maxima decreased as the D₂O content was increased, and lower secondary rate maxima was observed when the D₂O content ranged from 10 wt% - 30 wt% as shown in Figure 3.5 (c). For the formulations made from HB99PB, the lowest secondary rate maxima was observed when the D₂O content was 20 wt%. From Figure 3.5 (b) and 3.6 (b), it was observed that all the formulations exhibited secondary rate maxima. Table 3.2 summarizes the average DC, initial and secondary rate maxima of all the formulations investigated here.

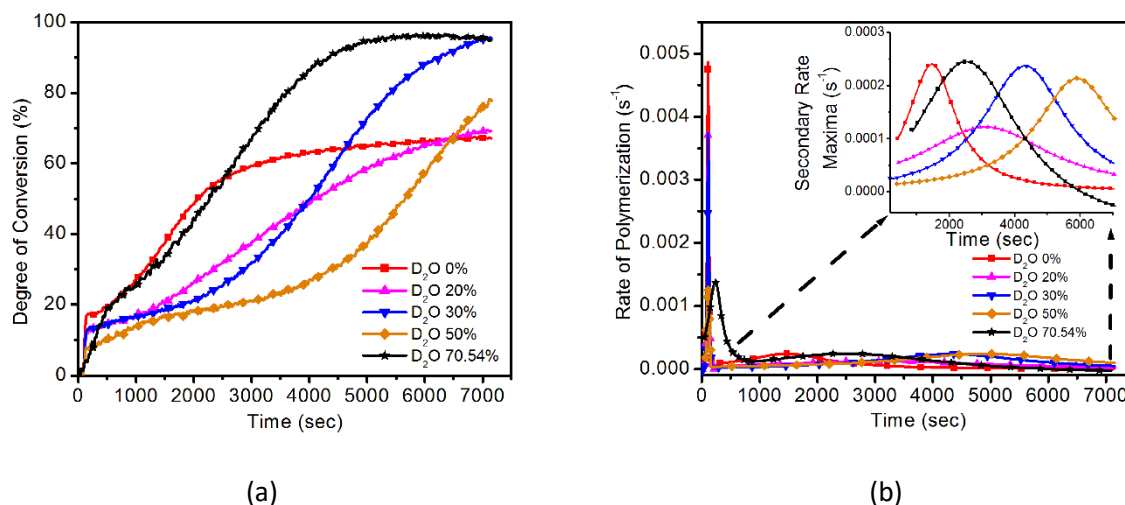


Figure 3.6. Polymerization kinetics result for formulations made from neat resin containing 99 wt% HEMA. (a) DC against time as a function of D₂O content. (b) Rate of polymerization of the formulation against time as a function of D₂O content showing the presence of secondary rate maxima (Abedin *et al.*, 2014)

3.3.2 Viscosity of the hydrophilic-rich mimics

The viscosity of the formulations was reduced as the concentration of D₂O was increased. The viscosity of the formulation prepared from HB95NR was less than that of the corresponding formulation from HB99NR with a similar concentration of D₂O. The concentration of BisGMA was higher in the formulations made from HB95NR compared to the corresponding formulations from HB99NR containing similar D₂O content. This may have contributed to the higher viscosity in the case of formulations prepared using HB95NR versus those from HB99NR. Figure 3.7 illustrated the variation of viscosity as a function of D₂O content for formulations prepared from HB95NR and HB99NR. The viscosity of formulations prepared from the HB95NR varied from 3.8 cP to 8.2 cP, and in case of the formulations from the HB99NR it varied from 2.8 cP to 6.6 cP.

Table 3.2. Summary of polymerization kinetics results (Abedin *et al.*, 2014)

Formulation Name	Degree of Conversion (DC)	Initial Rate Maxima (s^{-1}) $\times 10^4$	Secondary Rate Maxima (s^{-1}) $\times 10^4$	Appearance after Polymerization
Formulations prepared from neat resin with 95 wt% HEMA:				
HB95NR	66.0 \pm 0.9	47.0 \pm 2.1	2.9 \pm 0.3	Clear
HB95D ₂ O10	78.6 \pm 6.9	47.0 \pm 6.0	2.0 \pm 0.5	Almost clear
HB95D ₂ O20	87.3 \pm 2.5	37.8 \pm 5.6	1.8 \pm 0.3	Almost clear
HB95D ₂ O30	78 \pm 12	30.5 \pm 3.2	2.1 \pm 0.4	Translucent
HB95D ₂ O50	99.5 \pm 0.8	20.1 \pm 4.5	3.0 \pm 0.6	Turbid white
HB95PB	94 \pm 3	16.1 \pm 5.4	3.4 \pm 0.3	Turbid white
Formulations prepared from neat resin with 99 wt% HEMA:				
HB99NR	67.5 \pm 2.2	46.1 \pm 2.9	2.3 \pm 0.5	Clear
HB99D ₂ O20	63.3 \pm 9.9	34.9 \pm 2.6	1.0 \pm 0.2	Almost clear
HB99D ₂ O30	95.1 \pm 2.3	35.9 \pm 4.8	2.3 \pm 0.1	Translucent
HB99D ₂ O50	88 \pm 11	20.0 \pm 6.3	2.2 \pm 0.2	Turbid white
HB99PB	95 \pm 1	15.9 \pm 3.3	2.1 \pm 0.3	Turbid white

3.3.3 Glass transition temperatures (T_g) of hydrophilic-rich mimics

A representative MTDSC result of the first heating cycle for formulations prepared from HB95NR and HB99NR is shown in Figure 3.8 (a) and (b) respectively. The peaks observed in the first derivative of reversible heat flow represented the T_g . The presence of two peaks for the first heating cycle indicated a heterogeneous structure within the polymer, most likely arising due to poorer and higher cross-linked regions. From the Figure 3.8 (a) and (b), it could be seen that the two peaks approached each other as the D₂O content was increased and merged to form one peak at approximately 50 wt% D₂O, indicating that increased D₂O concentration led to reduced heterogeneity within the polymer.

At the miscibility limit, two peaks were observed again indicating increased heterogeneity within the polymers. Table 3.3 summarizes the glass transition temperatures (T_g) of all the formulations investigated here for both the heating cycles. The second heating cycle for the HB95NR is shown in the Figure 3.4, and from here it can be seen that there is only one T_g .

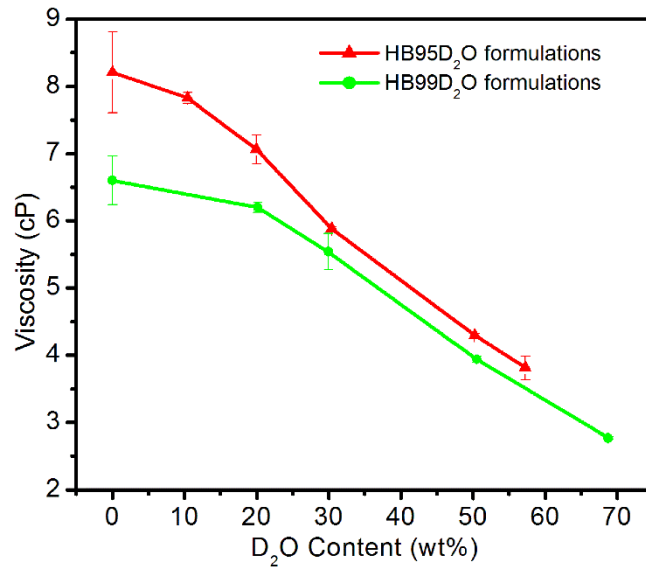


Figure 3.7. Variation of viscosity as a function of D₂O content. The triangles represent formulations prepared from HB95NR and the circles represent those from HB99NR (Abedin *et al.*, 2014)

The second cycle of MTDSC exhibited a single T_g for all the formulations, and it could be possible that during the second heating cycle rearrangement within the polymer led to a more homogeneous structure, resulting in a single T_g . Hence, the second heating cycle provides an approximate average T_g of the structure.

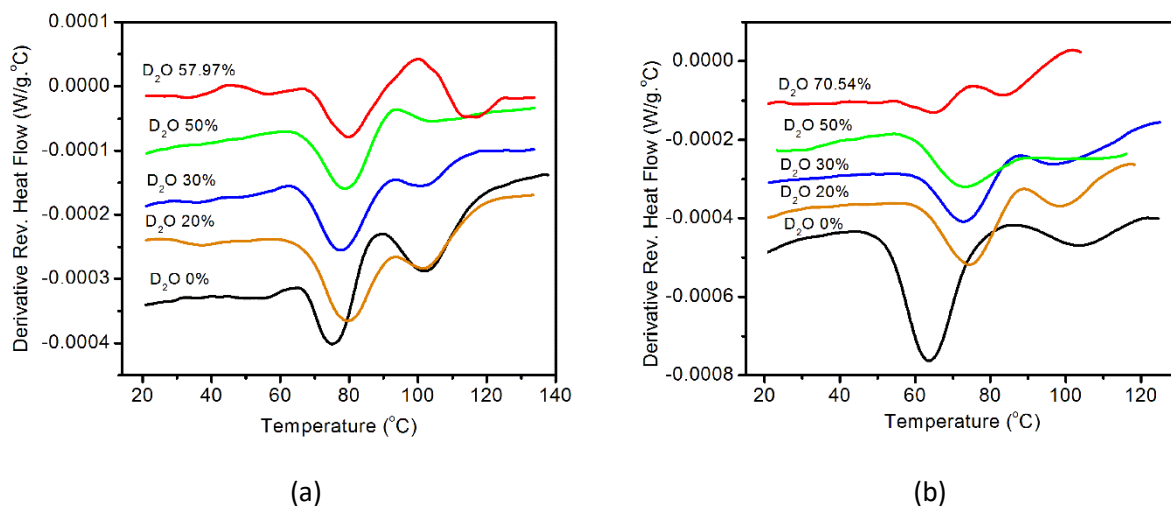


Figure 3.8. Glass transition temperature for the first heating cycle of formulations prepared from (a) HB95NR and (b) HB99NR (Abedin *et al.*, 2014)

Table 3.3 Average T_g of formulations investigated here for the first and second heating cycle (Abedin *et al.*, 2014)

Formulation Name	First T_g for Initial Heating Cycle ($^{\circ}\text{C}$)	First T_g for Initial Heating Cycle ($^{\circ}\text{C}$)	T_g for Second Heating Cycle ($^{\circ}\text{C}$)
Formulations prepared from neat resin with 95 wt% HEMA:			
HB95NR	76 ± 0.5	106.0 ± 3.4	102.7 ± 3.5
HB95D ₂ O20	76.9 ± 3.6	103.4 ± 7.1	106.6 ± 1.6
HB95D ₂ O30	79.2 ± 3.1	101.2 ± 1.4	105.0 ± 3.3
HB95D ₂ O50	80.3 ± 1.9	N/A	104.0 ± 2.7
HB95PB	78.5 ± 0.5	108.8 ± 6.8	105.1 ± 2.2
Formulations prepared from neat resin with 99 wt% HEMA:			
HB99NR	63.2 ± 3.1	101.8 ± 0.6	93.4 ± 1.6
HB99D ₂ O20	72.0 ± 1.5	98.1 ± 0.7	98.7 ± 1.9
HB99D ₂ O30	76.3 ± 2.7	99.2 ± 1.8	99.1 ± 1.5
HB99D ₂ O50	79.7 ± 3.6	N/A	101.1 ± 2.8
HB99PB	71 ± 8	87.3 ± 7.7	101.0 ± 1.9

3.4 Discussion

Bimodal rate of polymerization has been observed in the past for the methacrylate system (Anseth *et al.*, 1994; Cook, 1993; Horie *et al.*, 1975; Yu *et al.*, 2001). According to the authors, microgels were associated with the secondary gel effect or autoacceleration or Trommsdorff effect. Microgels are regions of higher cross-linked density or degree of conversion (DC). Yu *et al.* suggested that trapped pendant double bonds within the microgels became active at some point during the reaction, triggering the secondary gel effect and hence the secondary rate maxima (Yu *et al.*, 2001). Horie *et al.* also suggested that accumulation of pedant double bonds being less reactive than free radicals or propagating polymer radicals led to a secondary rate maxima (Horie *et al.*, 1975). In this case, it is possible that isolated regions of higher cross-linking density and/or DC form which are the microgels, and since the viscosity of the system is very low, reactive species are able to diffuse into the microgels. As the sample continued to polymerize, the microgels could precipitate out as they phase separate from the monomers and solvent, trapping the reactive species. These reactive species within the microgels become reactive some time

during the reaction, triggering a secondary Trommsdorff effect which results in the secondary rate maxima.

In the case of the neat resins (HB95NR and HB99NR), it could be possible that the microgels were smaller in size as the polymer would be more soluble in the monomer compared to the solvent, D₂O. Hence, the diffusion path for the reactive species into the microgels might be shorter for the neat resins, which could cause the secondary rate maxima to appear earlier. As more D₂O was added, the size of the microgels enhanced causing the diffusion path to increase. With the addition of D₂O, the monomer concentration reduced although the mobility of reactive species increased. These factors may delay the appearance of the secondary rate maxima. In case of the formulation at the miscibility limit, immediate precipitation of microgels might occur right after curing, which could cause the secondary rate maxima to appear earlier than the formulation containing 50 wt% despite slower diffusion and lower monomer concentration.

As D₂O concentration rises, the monomer concentration reduces which may cause the secondary rate maxima to decrease until the D₂O concentration reaches 20 wt%, despite the increased mobility of the reactive species. Moreover, for formulations containing less than 20 wt%, the microgels are more soluble in the D₂O since it is present in such a low concentration. This may cause the reactive species to readily diffuse out of the microgels and reduce their availability for the secondary gel effect. The transparent appearance of these formulations also indicates limited precipitation of the microgels. Beyond 20 wt% D₂O, the microgels precipitate out rapidly in larger size and quantity, since increasing the concentration of D₂O decreases the solubility of the microgels in the solvent. This facilitates entrapment of more reactive species in close proximity within the microgels, despite the reduced monomer concentration. The increase in the mobility of the reactive species due to reduced viscosity as more and more D₂O is added also facilitates diffusion of reactive species into the microgels. Hence, the secondary rate maxima increases with D₂O content when its concentration is beyond 20 wt% for formulations prepared from HB95NR. Similar results were observed in case of the formulations from HB99NR. The appearance of the polymer changes from translucent to turbid as D₂O content is increased from 30 wt% indicating precipitation of larger microgels in micron-scale. Therefore, the increase in the secondary rate maxima is due to increased precipitation of larger microgels and higher mobility of reactive species. This also accounts for the very high DC at 2 h for formulations close to the miscibility limit (i.e. 50 wt% D₂O and at the phase boundary). Based on the polymerization kinetics result (i.e. appearance of secondary rate

maxima) and the presence of two T_g for the first heating cycle, a possible polymerization mechanism for the hydrophilic-rich mimics has been proposed as discussed in the subsequent section.

The proposed mechanism involves polymerization-induced phase separation (PIPS) and solvent-induced phase separation (SIPS) (Abedin *et al.*, 2014). PIPS is defined as the separation of polymer from monomers in a mixture of non-reactive components and reactive monomers (Luo, 2006). PIPS was used to prepare multiphase composite materials (Keizer *et al.*, 2003) and polymer-dispersed liquid crystals (Boots *et al.*, 1996) which possessed applications in optical switches, variable transmittance windows and reflective displays (Nwabunma *et al.*, 2000). SIPS is the separation of polymer into solvent- and polymer-rich phases (Bailey *et al.*, 2011). Figure 3.9 exhibits the proposed polymerization mechanism for the dilute methacrylate-based hydrophilic-rich mimics of dental adhesives.

Figure 3.9 (a) shows the possible polymerization mechanism for the neat resin. It is possible that isolated regions of higher cross-linking density and/or DC form after the first Trommsdorff effect, and these regions are the microgels or polymer particles. Reaction within the microgels causes an increase in their size and finally the microgels reach their solubility limit in the monomer and separate from the surrounding monomers due to PIPS (schematic B of Figure 3.9 (a)). The lower viscosity of the hydrophilic neat resin compared to the hydrophobic neat resin facilitates diffusion of reactive species into the microgels. The latter continues to grow until their growth becomes diffusion limited, and at one point, the microgels become swollen with the diffused reactive species. The trapped reactive species within the microgels trigger the second Trommsdorff effect (region BD of the conversion against time graph). The microgels continue to polymerize forming regions of higher cross-linked density and/or DC whereas the surrounding matrix also continues to polymerize forming regions of lower cross-linked density and/or DC. Later during the reaction (region CD of the conversion against time graph), the microgels start forming network with the surrounding matrix as shown by the schematic C in Figure 3.9 (a). The final structure (schematic D) will be a polymer network with regions of higher and lower cross-linked density and/or DC (Abedin *et al.*, 2014). In case of formulations containing less than 20 wt% D_2O , the precipitation of microgels is most likely due to PIPS.

Figure 3.9 (b) exhibits the polymerization mechanism for dilute hydrophilic-rich mimics containing very high D_2O content. Schematic E in Figure 3.9 (b) shows a homogenous solution of monomers and D_2O . After the first Trommsdorff effect, microgels form which are isolated regions of higher cross-linking density and/or DC as mentioned earlier. As the polymerization continues, the miscibility of the microgels or polymer in the monomer and the solvent (D_2O) mixture exceeds the miscibility limit. Hence, the

microgels precipitate out due to both PIPS and SIPS as shown by the schematic F in Figure 3.9 (b). Diffusion and entrapment of reactive species within the microgels trigger the second Trommsdorff effect as discussed earlier (region FH of conversion against time graph). The surrounding matrix and microgels continue to polymerize, forming regions of higher and lower cross-linking density and/or DC. Later during the reaction (region GH of the conversion against time graph), the microgels start to form a network with the surrounding matrix as shown by schematic G in Figure 3.9 (b). During this time the miscibility of the polymer representing the surrounding matrix in D₂O exceeds its miscibility limit resulting in the separation of the D₂O from the matrix as droplets. The final structure may consist of regions of higher and lower cross-linked density and/or DC with D₂O droplets dispersed within the loosely cross-linked matrix as shown by the schematic H in Figure 3.9 (b). In case of formulations containing more than 30 wt% D₂O, the precipitation of microgels is most likely due to the SIPS. The two glass transition temperatures shown as an inset within the polymerization kinetics graphs in Figure 3.9 (a) and (b) arises from the loosely and denser cross-linked regions in the final structure. A previous study has also indicated that heterogeneity in dental polymer structures can arise due to diffusion limitations and microgel formation (Lovell *et al.*, 2001a). Primary cyclization is defined as the intramolecular reaction between double bond and a radical on the same propagating chain (Lovell *et al.*, 2001a). Primary cyclization can promote microgel formation without enhancing the cross-linking density.

The MTDSC study here indicates that as the D₂O content is increased, the two glass transition temperatures approach each other and merge to form one at 50 wt% of D₂O. This means that the heterogeneity within the final structure decreases with the addition of D₂O. In other words, the difference in the cross-linking density between the microgels and surrounding matrix reduces as more and more D₂O is added and becomes equivalent at 50 wt% D₂O. It is possible that with increasing D₂O, the microgel formation is mostly due to the primary cyclization causing the difference in the cross-linking density between the microgels and surrounding matrix to reduce, and resulting in the glass transition temperatures approaching each other and finally merging to show one T_g. At the miscibility limit, immediate precipitation of microgels occur due to the SIPS and this may cause a slightly higher crosslinking density within microgels compared to the surrounding (enhance the heterogeneity slightly) resulting in two glass transition temperatures. The two glass transition temperatures for the hydrophilic-rich mimics studied here are still close indicating that primary cyclization played the major role in the microgel formation, and that its contribution increased with the D₂O content until the miscibility limit at which immediate separation of polymer-rich phase (microgels) slightly decreased its contribution.

The T_g of polyHEMA is approximately 100°C (Coşkun *et al.*, 1997; Kopecek, 2009). Since the second T_g was very close to 100°C, it could be possible that the higher cross-linked regions were mostly polyHEMA with some cross-linking. As mentioned earlier, the first T_g observed represented loosely cross-linked regions which could be mostly polyHEMA. It could be possible that the retention of D₂O and monomer within the polymer structure led to plasticization reducing the T_g . Since the formulations containing high D₂O concentration exhibited very high DC, it could be that residual monomers were lower, allowing the first T_g to be slightly higher than that for the corresponding neat resin. For these former formulations, mostly D₂O could be responsible for the plasticization. The lower DC could have contributed to lower T_g for the neat resins. The second heating cycle provided an approximate average T_g for the samples. Rearrangements within the sample led to a more homogeneous structure yielding only one T_g . Considering the samples containing D₂O, the T_g during the second heating cycle was around 105°C for samples prepared from HB95NR and 100°C for those made from HB99NR. The T_g during the second heating cycle was slightly lower for the neat resins compared to their corresponding formulations with D₂O.

The DC for the neat resin was lower due to limited microgel formation and higher viscosity, restricting the motion of monomers/reactive species. As mentioned in Chapter 2, dissolved oxygen within the formulation could have interfered with the polymerization kinetics leading to a higher standard deviation for the polymerization rate. Although the experiments have not been conducted at the physiological temperature and the polymerization kinetics studies have been carried out under limited oxygen unlike during clinical conditions, this study indicates that the hydrophilic-rich phase of dental adhesive forms a vulnerable region for failure. The retention of D₂O droplets or its evaporation leading to pores within the loosely cross-linked regions could be detrimental, since this could promote/enhance diffusion of oral fluid into the a/d interface, leading to plasticization, degradation and secondary caries. The final result of penetration of oral fluid and the subsequent events is the failure of the a/d bond and hence the dental composite restoration. Inclusion of a hydrophilic cross-linker could significantly improve the durability of the loosely cross-linked regions by reducing the pore/water droplet size or displacing the water droplets through formation of cross-links. This would also reduce the gaps between chains restricting the diffusion of the oral fluid.

3.5 Conclusion

This study indicates how moisture in the wet demineralized dentin can negatively impact the structure of the dental adhesive. The following summarizes the results from this investigation:

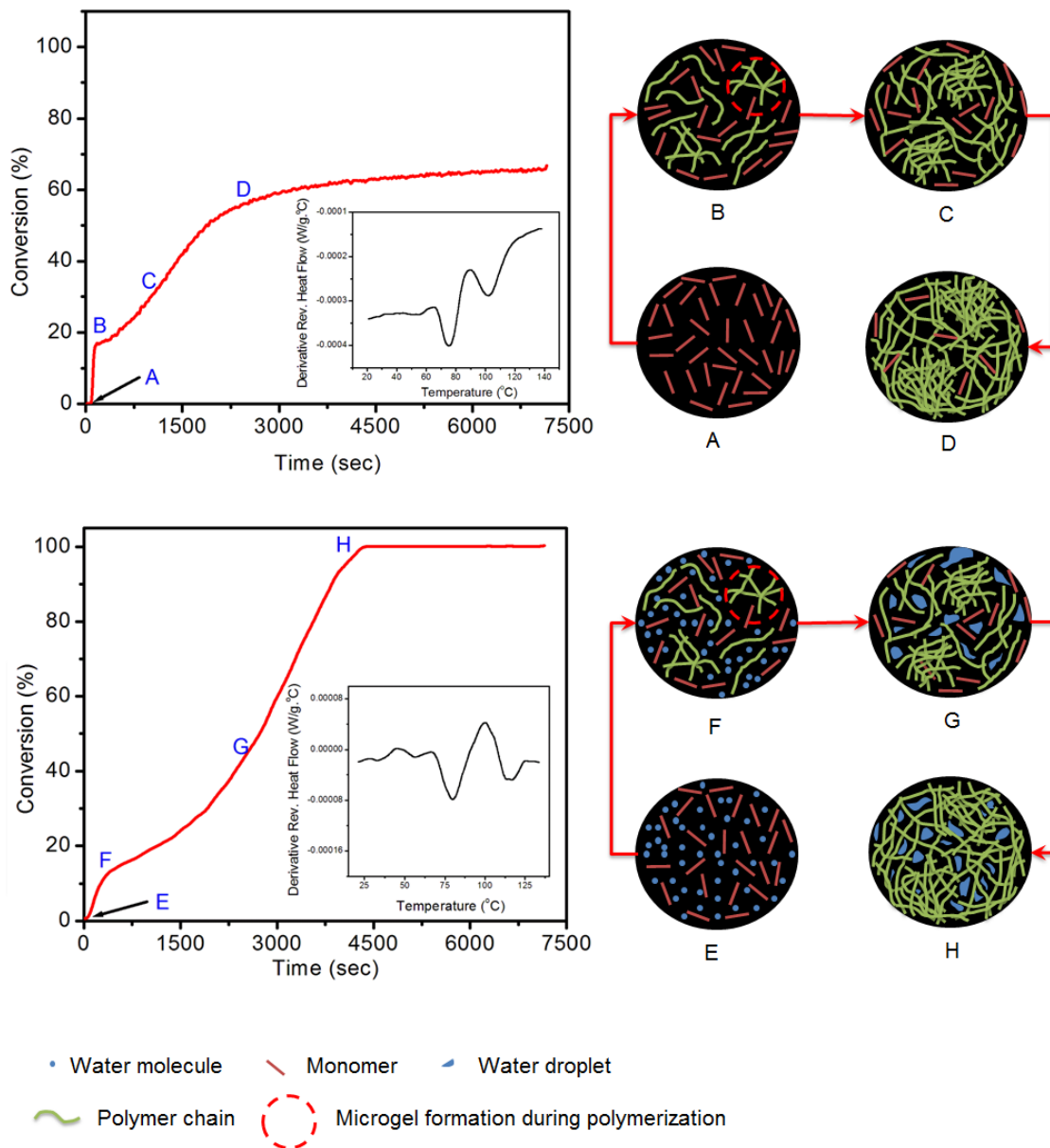


Figure 3.8. Schematic showing possible polymerization mechanism in case of (a) neat resins where PIPS was responsible for the microgel precipitation and (b) formulation with more than 30 wt% D₂O where PIPS and SIPS both are responsible for the microgel precipitation. The final structure will consist of higher and lower cross-linked regions as indicated by the two glass transition temperatures in the graph shown as inset. The final structure as shown by the schematic H will contain water droplets facilitating plasticization and hydrolysis of ester linkages (Abedin *et al.*, 2014)

- Water concentration can influence the DC and rate of polymerization because of a decrease in the monomer concentration and the enhanced mobility of reactive species with increasing D₂O concentration, and the extent of precipitation of microgels due to PIPS and SIPS.
- The initial rate of polymerization showed a decreasing trend with increasing D₂O concentration, since this was accompanied by a decrease in the monomer concentration.
- A decreasing trend for the secondary rate maxima with increasing D₂O concentration was observed until 20 wt% of D₂O. After that, the secondary rate maxima showed an increasing trend until the miscibility limit, mostly due to the enhanced formation of microgels of larger size and increased mobility of reactive species.
- Two polymerization mechanisms, one involving PIPS, and the other involving both PIPS and SIPS were proposed. The former mechanism was applicable for formulations without D₂O or with very little D₂O, and the latter was valid for formulations with high D₂O content or at the miscibility limit.
- The structure of hydrophilic-rich mimics is heterogeneous with densely and loosely cross-linked regions, giving rise to two glass transition temperatures.
- The heterogeneity reduced with increased D₂O content since the two glass transition temperatures approached each other until they merged at 50 wt% D₂O. This was mostly because the microgel formation was dominated by primary cyclization rather than increased cross-linking density.
- The retention of water droplets and the loosely cross-linked regions within the hydrophilic-rich mimics could promote penetration of the oral fluid, and hence this study indicates that incorporation of water compatible cross-linker may improve the durability of the hydrophilic-rich phase of dental adhesive.

CHAPTER 4: IMPACT OF LIGHT INTENSITY ON THE PHOTO-POLYMERIZATION AND NETWORK FORMATION OF HYDROPHOBIC- AND HYDROPHILIC METHACRYLATE DENTAL RESINS

(This chapter is based on the journal article: Abedin F., Ye Q., Camarda K., Spencer P., Impact of light intensity on the polymerization kinetics and network structure of model hydrophobic and hydrophilic methacrylate based dental adhesive resin, Journal of Biomedical Materials Research Part B, 2015)

4.1 Introduction

The composition of the infiltrated dental adhesive within the hybrid layer represents very closely to the hydrophilic-rich phase, containing varying concentrations of the cross-linker, mono-methacrylate monomer (HEMA) and photoinitiator (PI). The primary components of the hydrophilic-rich phase are water and HEMA (Ye *et al.*, 2012). The cross-linker and PI are present in minor concentrations within this phase. The intensity of the curing light varies along the length and breadth of the hybrid layer. There were very few studies which investigated the impact of light intensity on the polymerization and polymer structure of formulations that mimic the hydrophilic-rich phase (He *et al.*, 2008; Li and Lee, 2005). In this chapter, the impact of light intensity was investigated for dental resin formulations which closely represented the hydrophobic- and hydrophilic-rich phases. In this study, the hydrophilic dental resin was represented with formulations containing a high concentration of HEMA and a very low concentration of the cross-linker. Unlike the hydrophilic-rich phase, no water or D₂O was added to the hydrophilic resins. This approach avoided experimental complications such as evaporation. Two types of PI systems (2PI and 3PI) were employed to prepare the formulations, and the concentration of each PI component was kept constant to 0.5 wt%. This experimental design eliminated confounding variables such as differences in PI concentration which could also impact the polymerization. Hence, the elimination of D₂O and keeping the PI concentration constant allowed the evaluation of only the effect of light intensity on the polymerization. The use of two types of PI systems provided the opportunity to compare the performance of these systems.

4.2 Materials and methods

The 2PI system used in this study consisted of camphorquinone (CQ) and the ethyl 4-(dimethylamino) benzoate (EDMAB) and both were obtained from Aldrich, Milwaukee. The 3PI system had diphenyliodonium hexafluorophosphate (DPIHP) as a reaction accelerator in addition to the CQ and EDMAB. DPIHP was also obtained from Aldrich, Milwaukee. The resins were prepared using 2-

hydroxyethyl methacrylate (HEMA) from Acros Organics and Bisphenol A glycerolate dimethacrylate (BisGMA) from Polysciences, Washington, PA.

The resin formulations were prepared in the same way as the neat resins discussed in Chapters 2 and 3. Briefly, for the hydrophobic resin the components of the PI system were added to HEMA and the mixture was vortexed until the components dissolved. Then, the BisGMA was added to the solution so that HEMA and BisGMA were 45:55 wt%. The mixture was left to agitate overnight to produce a homogeneous solution. The PI components were added so that they were 0.5 wt% based on the total weight of the solution. The hydrophilic resin was prepared similarly, but the HEMA and BisGMA were mixed in the ratio of 95:5 wt%. Three hydrophobic resin formulations were prepared for each PI system and hence in total there were six hydrophobic resin formulations. Similarly there were six hydrophilic resin formulations. Table 4.1 shows the composition of the resins studied here. The formulations were named as HBxNRyPI, where HB stands for HEMA/BisGMA, x is the wt% of HEMA in the resin, NR means ‘neat resin’ and y is 2 or 3 based on the type of PI system.

Table 4.1 Composition of the neat resin formulations studied (Abedin *et al.*, 2015b)

PI system	Name of formulation	wt% HEMA	wt% BisGMA
2PI*	HB45NR2PI	44.96 ± 0.03	55.04 ± 0.03
	HB95NR2PI	94.96 ± 0.06	5.04 ± 0.06
3PI#	HB45NR3PI	45.00 ± 0.01	55.00 ± 0.01
	HB95NR3PI	94.98 ± 0.01	5.02 ± 0.01

* The 2PI system was made up of 0.5 wt% CQ and EDMAB each
 # The 3PI system contained 0.5 wt% CQ, EDMAB and DPIHP each

4.2.1 Photopolymerization kinetics study using FTIR

The polymerization kinetics of the hydrophobic and hydrophilic resins were monitored *in-situ* when cured at various light intensities. As mentioned earlier, the polymerization kinetics was investigated using a Fourier Transform Infrared Spectrophotometer (FTIR), Perkin-Elmer Spectrum 400 at a resolution of 4 cm⁻¹ in ATR sampling mode. The sample volume for the polymerization study was 30 μL and the sample was covered with a plastic coverslip. The edges of the coverslip were taped to limit the diffusion of atmospheric oxygen into the sample which could negatively impact the polymerization reaction. A halogen light curing unit (LCU), Spectrum® 800 Dentsply, Milford DE, with a peak emission wavelength at 488 nm (Eacute *et al.*, 2008) was employed to cure the samples. The LCU has a built in system to vary the

light intensity from 300 mW/cm² to 800 mW/cm² (Abedin *et al.*, 2015b). The samples for the polymerization kinetics study were cured at 25, 50, 100, 229, 455 and 679 mW/cm² (Abedin *et al.*, 2015b). To cure samples below the 229 mW/cm² light intensity, the distance between the sample and the tip of the LCU was varied so that the desired intensity could be attained. The distance yielding the required light intensity below 229 mW/cm² (25, 50 and 100 mW/cm²) was first determined by adjusting the distance between the tip of the LCU and a light intensity meter. The distances were recorded, and were then used to set the distance between the sample and the LCU tip to cure samples below 229 mW/cm². The intensity on the display of the LCU read differently from that shown by the intensity meter. For the higher intensities, the LCU was set at 300, 550 and 800 mW/cm² and the corresponding readings were recorded from the intensity meter. Table 4.2 shows the intensity on the display of the LCU and the corresponding reading on the light intensity meter. The samples cured at 229 mW/cm², 455 mW/cm² and 679 mW/cm² were achieved by setting the intensity of the LCU at 300 mW/cm², 550 mW/cm² and 800 mW/cm² respectively. All the samples were cured for 40 s. The intensities of C=C at 1637 cm⁻¹ and C=O at 1716 cm⁻¹ was monitored and the equation 2.1 was used to calculate the degree of conversion (DC). The polymerization kinetics of the hydrophilic resins was monitored for 2 h whereas that of the hydrophobic resin was monitored for 1 h. Previous studies had shown that the hydrophobic resin reaches final DC well before 1 h (Ye *et al.*, 2008).

Table 4.2 Light intensity of the LCU and its corresponding reading on the light intensity meter (Abedin *et al.*, 2015b)

Light intensity on the display of the LCU (mW/cm ²)	Corresponding light intensity read by the visible light intensity meter (mW/cm ²)
300	229
550	455
800	679

The final DC of the hydrophilic resins was determined by preparing pan samples and storing them in the dark at room temperature for 24 h after curing. The resins were transferred to an aluminum low-mass DSC pan until it was filled to the brim. Then, the pan was covered with a plastic coverslip and the sample was cured at the desired light intensity for 40 s. After storage for about 24 h, the cover slip was removed, and the intensities of C=C at 1637 cm⁻¹ and C=O at 1716 cm⁻¹ were determined in ATR mode for the top and bottom surfaces of each sample. Equation 2.1 was used to determine the DC for the pan

samples. There were 3 samples per formulation and per intensity for both the kinetic and the final DC studies.

4.2.2 Glass transition temperature using DSC

Specimens for the DSC study were prepared in the same way as the pan samples used for determining the final DC of the hydrophilic resins. DSC specimens for the hydrophobic resins were cured at 100, 229, 455 and 679 mW/cm². Specimens from the hydrophilic resins were prepared for all six intensities mentioned above. The coverslips were removed from the samples after 24 h storage in the dark. The pan samples for DSC were stored in a vacuum chamber at 37°C. The weight of the samples was measured after specific time intervals until the difference between two consecutive weights was less than 0.3 mg. The pressure within the vacuum chamber facilitated evaporation of unreacted monomers and thus minimized the monomer content in the samples before the DSC test. As discussed in chapter 3, modulated DSC (MTDSC) was used to determine the glass transition temperature (T_g) of the samples (Abedin *et al.*, 2014; Ye *et al.*, 2007a). The parameters for the MTDSC were the same as those described in the chapter 3. Briefly, two heating/cooling cycles were carried out under purged nitrogen gas at 40 mL/min. The temperature was increased from -10°C to 200°C, and a sinusoidal temperature modulation with an amplitude of 2°C was applied every 60 s. Only the second heating cycle was analyzed for each specimen using the Universal Analysis Software (TA Instruments, New Castle, DE) since it gave an approximate average T_g for the sample. There were 3 DSC samples for the hydrophobic resins per intensity and 6 per intensity in the case of the hydrophilic resins.

4.2.3 Statistical Analysis

The DC, rate of polymerization and T_g at various light intensities for the formulations were compared using one-way analysis of variance (ANOVA) and t-test at $\alpha = 0.05$ using Microcal Origin (Version 6.0, Microcal Software, Northampton, MA).

4.3 Results

4.3.1 Polymerization of dental hydrophobic and hydrophilic resins

The hydrophobic-rich phase exhibited a sufficient degree of conversion when cured at all the light intensities studied here. The DC at various light intensities (at 1 h) for HB45NR2PI was similar but that for HB45NR3PI was significantly different (one-way ANOVA, $p < 0.0001$). A slight decreasing trend in DC at 1 h with light intensity >229 mW/cm² was observed for the formulation HB45NR3PI. The rate maxima at

various light intensities were significantly different for the formulations HB45NR2PI and HB45NR3PI (one-way ANOVA, $p < 0.0001$). The representative results for the hydrophobic formulations are shown in Figure 4.1.

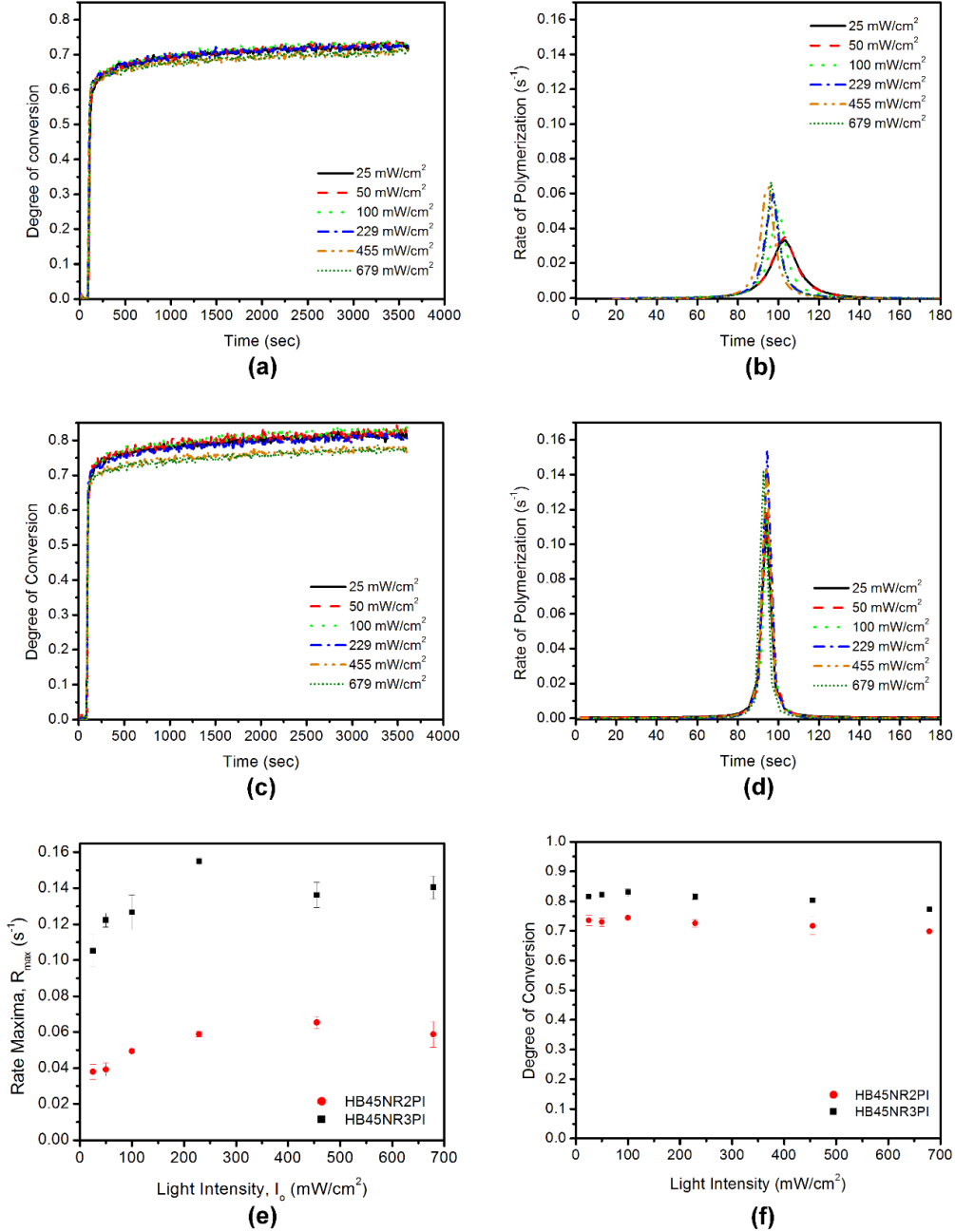


Figure 4.1. Representative results of polymerization kinetics study for hydrophobic resins, (a, b) HB45NR2PI and (c, d) HB45NR3PI. Variation of (e) rate maxima and (f) DC at 1 h with light intensity for the hydrophobic resins (Abedin *et al.*, 2015b)

In Figure 4.1(e) for HB45NR2PI, the initial rate maxima exhibited an increasing trend with light intensity until 455 mW/cm². At a light intensity of 455 mW/cm² the initial rate maxima for HB45NR2PI reached a plateau. In case of the HB45NR3PI, the rate maxima showed an increasing trend until 229 mW/cm². At higher intensities the rate maxima for HB45NR3PI decreased. No significant difference was observed between the rate maxima at 455 and 679 mW/cm² (Two sample t-test, $p < 0.05$) in the case of the HB45NR3PI.

For the hydrophilic formulations (HB95NR2PI and HB95NR3PI), a significant difference in the DC at 2 h and rate maxima at various light intensities was observed (one-way ANOVA, $p < 0.0001$). Figure 4.2 exhibits representative polymerization kinetics results for the hydrophilic formulations. For HB95NR2PI, an increasing trend in DC at 2 h was observed until 455 mW/cm², and at higher light intensity (679 mW/cm²) there was a slight decrease in the DC. At low light intensities such as 25, 50 and 100 mW/cm², the DC at 2 h was substantially lower (Figure 4.2(a)). An increasing trend in the initial rate maxima was observed for this formulation until 229 mW/cm², and then it became almost constant. Although post polymerization leading to a secondary rate maximum was observed for both the 2PI and 3PI hydrophilic formulations, in the case of HB95NR2PI, the secondary rate maxima were observed only at higher light intensities (229, 455 and 679 mW/cm²) as shown in Figure 4.2(b). A significant difference in the secondary rate maxima at various light intensities was observed for this formulation (one-way ANOVA, $p < 0.0002$). An increasing trend in the secondary rate maxima was observed until 455 mW/cm², and at 679 mW/cm² it decreased.

In the case of the formulation, HB95NR3PI the DC at 2 h was sufficiently high at all light intensities. This is in distinct contrast to the observations made for the corresponding 2PI system. The DC at 2 h for HB95NR3PI showed an increasing trend until 100 mW/cm² and at higher intensities it reached a plateau. There was no significant difference in the DC at 2 h for intensities higher than 100 mW/cm² in the case of HB95NR3PI (Two sample t test, $p < 0.05$). An increasing trend in the initial rate maxima with light intensity was observed for the formulations, HB95NR3PI as shown in Figure 4.2(e). Unlike the hydrophilic 2PI formulation, a secondary rate maximum was observed at all light intensities in the case of the HB95NR3PI. A significant difference in the secondary rate maxima at various light intensities was observed for the HB95NR3PI (one-way ANOVA, $p < 0.0001$). The secondary rate maxima exhibited an increasing trend with light intensity for the formulation HB95NR3PI until 229 mW/cm² (Figure 4.2(f)). At intensities higher than 229 mW/cm², the secondary rate maxima reached a plateau and no significant difference was observed

(Two sample t test, $p < 0.05$). The time for the secondary rate maxima to appear decreased with the increase in the light intensity.

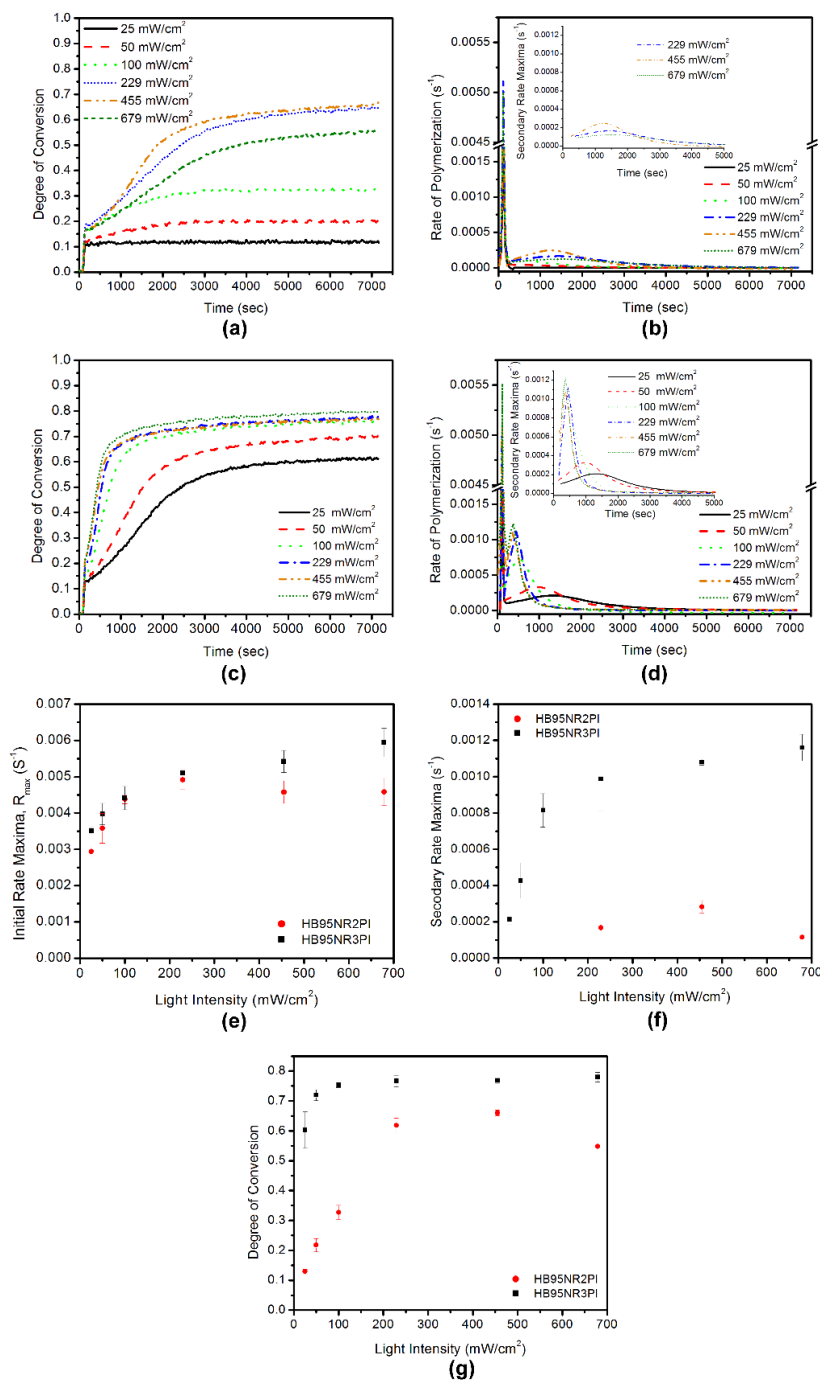


Figure 4.2. Representative results of the polymerization kinetics study for the hydrophilic formulations (a, b) HB95NR2PI and (c, d) HB95NR3PI. Variation of (e) initial rate maxima, (f) secondary rate maxima and (g) DC at 2 h with light intensity for the hydrophilic resins (Abedin *et al.*, 2015b)

From Table 4.3, it can be seen that the DC at 2 h for HB95NR3PI was substantially higher than that for the HB95NR2PI. The presence of iodonium salt exhibited a significant influence on the polymerization of the hydrophilic resin. For example, a substantial degree of conversion and the presence of secondary rate maxima at lower light intensities (25, 50 and 100 mW/cm²) were observed in case of HB95NR3PI. From Table 4.3, it can be seen that the secondary rate maxima were substantially higher for the HB95NR3PI when compared to the corresponding rate for the HB95NR2PI but the initial rate maxima remained of the same order for both the formulations.

The final DC of the hydrophilic resins was measured 24 h after curing using pan samples. Figure 4.3 shows the final DC for both hydrophilic formulations. For HB95NR2PI, significant difference in the final DC at various light intensities was observed (one-way ANOVA, $p < 0.05$). For this formulation, an increasing trend in the final DC with light intensity was observed. For this formulation, the final DC measured at 24 h at low light intensities (25, 50 and 100 mW/cm²) was higher than the corresponding DC from the kinetic study which was measured until 2 h. The final DC for HB95NR2PI at low light intensities (25, 50 and 100 mW/cm²) was lower than the final DC at higher light intensities (229, 455 and 679 mW/cm²). This showed that low light intensities had a negative impact on the final DC of the hydrophilic 2PI resin. The corresponding DC at 2 h from the kinetic study and the final DC at 24 h using the pan samples were similar at light intensities 229 and 455 mW/cm² for the formulation HB95NR2PI.

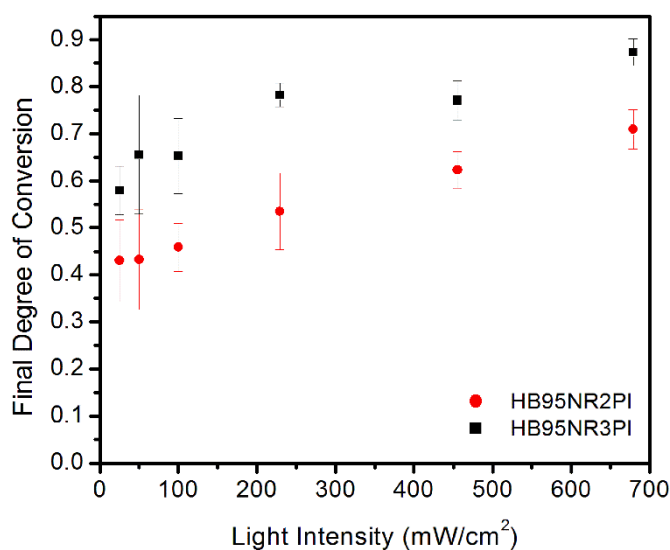


Figure 4.3. Variation of final DC at 24 h obtained using pan samples for hydrophilic resins, HB95NR2PI and HB95NR3PI (Abedin *et al.*, 2015b)

Table 4.3. Summary of polymerization kinetics result showing DC at 2 h, initial rate maxima and secondary rate maxima for all the formulations (Abedin *et al.*, 2015b)

Light Intensity (mW/cm ²)	Degree of Conversion (DC)				Initial Rate Maxima (s ⁻¹) × 10 ⁴				Secondary Rate Maxima (s ⁻¹) × 10 ⁴	
	HB45NR2 PI	HB45NR3 PI	HB95NR 2PI	HB95NR 3PI	HB45NR 2PI	HB45NR 3PI	HB95NR 2PI	HB95NR 3PI	HB95NR 2PI	HB95NR 3PI
25	0.736	0.816	0.129	0.603	379.0	1052.1	29.4	35.1	N/A	2.14
	± 0.018	± 0.003	± 0.008	± 0.061	± 41.4	± 89.9	± 1.6	± 0.9		± 0.27
50	0.729	0.822	0.217	0.720	391.4	1222.8	35.8	39.8	N/A	4.27
	± 0.013	± 0.003	± 0.022	± 0.018	± 35.7	± 39.2	± 4.1	± 2.9		± 0.98
100	0.744	0.829	0.327	0.753	493.3	1266.3	43.8	44.2	N//A	8.15
	± 0.007	± 0.012	± 0.024	± 0.008	± 15.7	± 96.9	± 1.3	± 3.2		± 0.93
229	0.726	0.816	0.618	0.767	587.9	1548.9	49.2	51.1	1.67	9.88
	± 0.013	± 0.009	± 0.024	± 0.019	± 14.3	± 19.5	± 2.5	± 0.9	± 0.02	± 1.79
455	0.717	0.803	0.660	0.768	652.8	1362.7	45.8	54.2	2.82	10.80
	+ 0.030	± 0.005	± 0.009	± 0.009	± 33.8	± 70.6	± 3.1	± 3.0	± 0.35	± 0.17
679	0.698	0.773	0.548	0.780	587.3	1404.3	45.8	59.5	1.15	11.6
	± 0.009	± 0.004	± 0.007	± 0.017	± 71.5	± 63.6	± 3.7	± 3.9	± 0.08	± 0.72

For this formulation, the DC from the kinetic study at 679 mW/cm² was lower than the final DC at 24 h.

In the case of the formulation HB95NR3PI, the corresponding DC at 2 h from the kinetic study was similar to the final DC at 24 h. An increasing trend in the final DC with light intensity was observed for HB95NR3PI. A significant difference in the final DC cured at various light intensities was observed in the case of HB95NR3PI (one-way ANOVA, $p < 0.05$).

4.3.2 Glass transition temperature (T_g) of adhesive polymers from hydrophobic and hydrophilic resins

Table 4.4 exhibits the average glass transition temperature, T_g of the formulations studied here for the second heating/cooling cycle. Figure 4.4 shows the DSC results for the formulations studied here and represents the average result of all the samples per intensity for every formulation. No significant difference in the T_g at various light intensities was observed for the formulations, HB45NR2PI and HB95NR2PI (one-way ANOVA, $p < 0.05$), indicating that the light intensity had very little impact on the T_g of samples prepared from 2PI resins when given sufficient time for polymerization. In contrast, a

significant difference in T_g at various light intensities was observed for the 3PI resins (one-way ANOVA, $p < 0.05$). In the case of the HB45NR3PI, a slight increase in the T_g with the light intensity was observed.

Table 4.4. Average glass transition temperature (T_g) for each formulation at various light intensities. The T_g is reported for the second heating/cooling cycle (Abedin *et al.*, 2015b)

Sample Name	Glass Transition Temperature, T_g (°C)					
	25 mW/cm ²	50 mW/cm ²	100 mW/cm ²	229 mW/cm ²	455 mW/cm ²	679 mW/cm ²
HB45NR2PI	N/A	N/A	126.7± 1.1	127.7 ± 1.7	127.3± 1.3	123.4 ± 3.8
HB45NR3PI	N/A	N/A	131.0± 1.1	130.9 ± 1.5	135.1± 2.9	135.9 ± 2.4
HB95NR2PI	103.6±0.4	102.5±1.2	103.9± 1.0	101.0 ± 1.8	102.1± 2.2	101.4 ± 3.7
HB95NR3PI	96.3 ± 2.8	96.7 ± 3.3	93.7 ± 1.3	90.4 ± 3.4	94.2 ± 1.2	98.3 ± 1.7

For the formulations HB45NR2PI and HB45NR3PI, it was observed that the T_g for the 3PI resin was higher than the corresponding T_g of the 2PI resin. On the other hand, for the formulations HB95NR2PI and HB95NR3PI, a trend of slightly lower T_g was observed for the 3PI resin when compared to the corresponding T_g of the 2PI resin.

4.4 Discussion

The polymerization kinetic study was carried out for 1 h in the case of the hydrophobic resins because previous studies indicated that 1 h was sufficient for these formulation to reach the final DC (Ye *et al.*, 2008). In the case of the hydrophilic resins, it was observed previously that these resins took longer to reach the final DC (Abedin *et al.*, 2015c), and hence the kinetic study was carried out for 2 h instead of 1 h. Since some of the samples prepared from the hydrophilic resins continued to polymerize after 2 h, the final DC in this case was determined using pan samples which were allowed 24 h for post polymerization.

DPIHP, which is used here as a reaction accelerator oxidizes ketyl and aminoalkyl radicals generating phenyl radicals (Cook and Chen, 2011). The ketyl radicals participate in the termination reaction whereas the phenyl radicals take part in the initiation of the polymerization reaction. The oxidation of ketyl and aminoalkyl radicals to phenyl radicals indicates that the DPIHP reduces back electron transfer within the CQ/EDMAB exciplex (Cook and Chen, 2011). The oxidation of ketyl radicals also results in the regeneration of CQ which can absorb photons again. Therefore, the concentration of radicals participating in the initiation is much higher for the 3PI system compared to the 2PI system. Cook *et al.* proposed the possible radical formation steps for the CQ system (Cook and Chen, 2011).

In the case of the formulation HB45NR3PI, at higher light intensities such as 455 mW/cm² and 679 mW/cm², the concentration of the generated radicals can be very high. For a highly viscous system like the HB45NR3PI, very high concentration of radicals can cause them to become trapped in close proximity, allowing them to terminate each other. This can lead to a decrease in the concentration of effective radicals at higher light intensities.

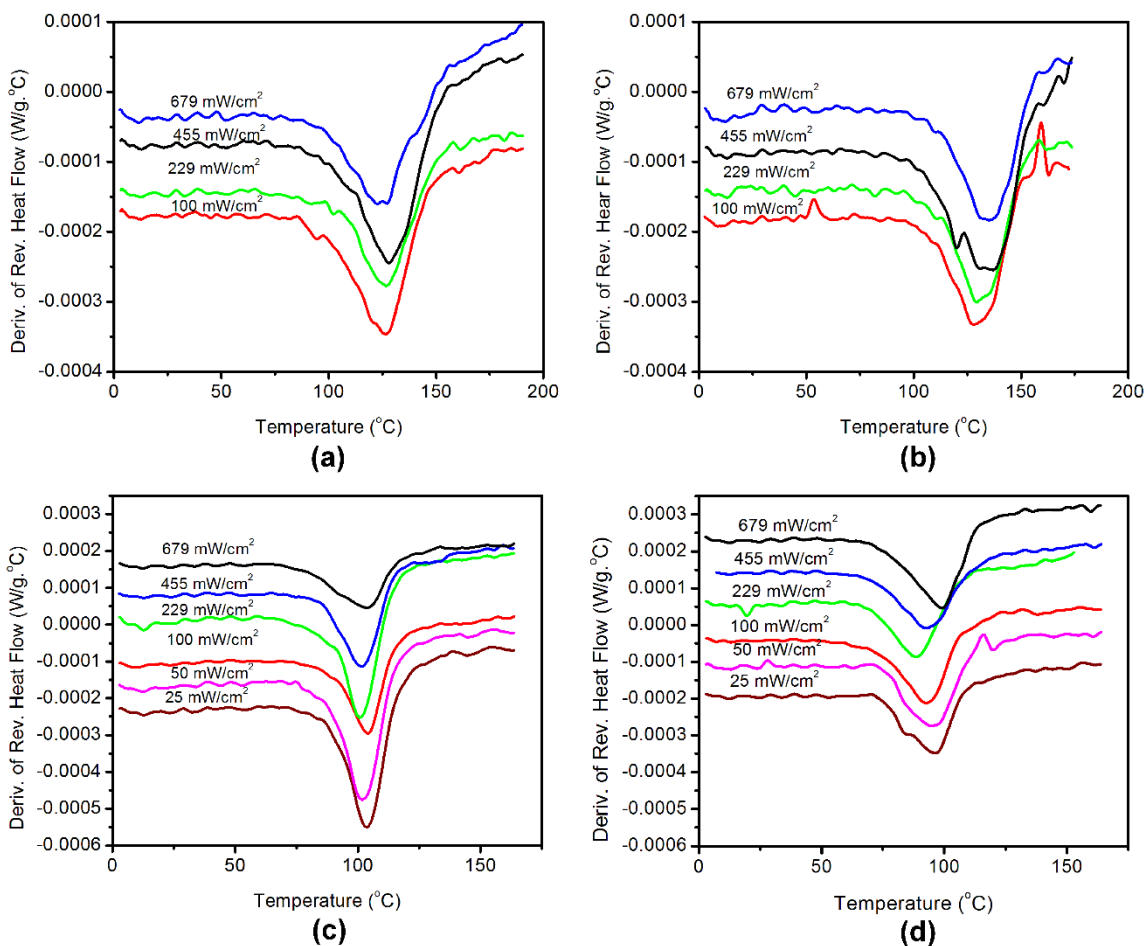


Figure 4.4. DSC results for formulations (a) HB45NR2PI, (b) HB45NR3PI, (c) HB95NR2PI and (d) HB95NR3PI. The results shown here are average of all the samples per intensity (Abedin *et al.*, 2015b)

These events may account for the decrease in the rate of polymerization for light intensities >229 mW/cm² for the HB45NR3PI. Most likely the termination of radicals by each other may lead to a constant concentration of the radicals at light intensities 455 mW/cm² and 679 mW/cm² for the HB45NR3PI, and this could result in the rate maxima reaching a plateau for these intensities. This event could also explain the decreasing trend of DC beyond 229 mW/cm² for HB45NR2PI.

The viscosity of the hydrophilic formulations before and after autoacceleration is much lower than that of the hydrophobic formulations. Therefore, the reactive species within the hydrophilic formulation do not experience the restricted movement that occurs in the hydrophobic formulation. This implies that the rate of the termination reaction within the hydrophilic formulation is much higher. The higher termination reaction rate will lead to a lower initial polymerization rate for the hydrophilic resins as compared to that for the corresponding hydrophobic resins, despite both having the same concentration of photo-initiators. For the hydrophobic resins, the restriction of motion for the reactive species is induced by the high viscosity and cross-linking density.

In the case of HB95NR2PI, at low light intensities such as 25, 50 and 100 mW/cm², the generation of radicals is much lower, and since the termination rate is higher, the overall concentration of effective radicals decreases, leading to a low DC at 2 h. An increase in the light intensity is accompanied by an increase in the overall concentration of effective radicals resulting in the increasing trend of the initial rate maxima until 229 mW/cm² and DC at 2 h until 455 mW/cm². Previous investigations attributed this to microgels with a secondary gel effect leading to the secondary rate maxima (Abedin *et al.*, 2014; Abedin *et al.*, 2015c; Horie *et al.*, 1975). For the HB95NR2PI, a low concentration of radicals at low light intensities leading to inadequate reactive species could account for the absence of secondary rate maxima at 25, 50 and 100 mW/cm². For this formulation, as the light intensity is increased to 455 mW/cm², the increase in the concentration of the effective radicals trapped within the microgels could cause the secondary rate maxima to increase. At a high light intensity, i.e. 679 mW/cm², it is possible that excessive radicals are formed and that they become trapped in close proximity within the microgels. This may lead to the termination of the radicals within the microgels, decreasing the overall concentration of the reactive species within the microgels and reducing the secondary gel effect. Hence, at this light intensity, the secondary rate maximum is much lower for the HB95NR2PI. This shows that for the 2PI hydrophilic resin, very high light intensity reduces the secondary gel effect which was also observed for the MAA/TEGDMA system (He *et al.*, 2008).

For HB95NR2PI, the final DC at 24 h was higher than the DC at 2 h from the kinetic study because the trapped unreacted species within the polymer system triggered a post polymerization reaction in the dark increasing the DC (Gao and Nie, 2007; Lovell *et al.*, 2001a). This was noticeable in the case of low light intensities. The final DC at 24 h for the HB95NR2PI was still less at lower light intensities (25, 50 and 100 mW/cm²) when compared to that at higher light intensities. This indicates that lower light intensity exhibits a negative impact on the DC of the hydrophilic 2PI resin. An increasing trend in the final DC at 24

h with increasing light intensity implies that the concentration of effective radicals for post polymerization increases with the light intensity. Although the DC at 2 h for HB95NR2PI at 679 mW/cm² was lower than that at 455 mW/cm², the trapped radicals were sufficient to continue the post polymerization leading to a higher final DC at 24 h in the case of 679 mW/cm².

For the formulation HB95NR3PI, the generation of radicals was much higher than the HB95NR2PI for reasons discussed earlier. Higher concentration of effective radicals could result in the higher initial rate maxima and secondary rate maxima for the HB95NR3PI as compared to the HB95NR2PI. This could also account for the presence of the secondary rate maxima at lower light intensities such as 25, 50 and 100 mW/cm² for the 3PI hydrophilic resin. For the HB95NR3PI, the increase in the initial and secondary rate maxima with increasing light intensities indicates that the overall concentration of effective radicals is enhanced with light intensity, although the formation of excessive radicals may induce increased termination of the radicals. It was observed that for HB95NR3PI, the DC at 2 h from the kinetic study increased until 100 mW/cm² and very little difference in DC was observed for higher light intensities. On the other hand, the final DC at 24 h for HB95NR3PI exhibited an increasing trend with light intensity, indicating that trapped radicals led to post polymerization, and higher light intensity induced enhanced concentration of these trapped radicals. Despite the increasing trend of the final DC at 24 h for HB95NR3PI, the DC at 2 h from the kinetic study was similar to the corresponding final DC, showing that the 3PI hydrophilic formulation reached almost final DC in 2 h. The secondary rate maxima for the 3PI hydrophilic resin were substantially higher than that of the 2PI hydrophilic resin. This showed that the excess radicals generated due to the iodonium salt in the case of the HB95NR3PI mostly led to an enhanced secondary gel effect within the microgels.

No significant difference in T_g at various light intensities was observed for the 2PI hydrophobic and hydrophilic formulations, indicating that light intensity had little or no impact on the cross-linking density. Lovell *et al.* also exhibited similar results for BisGMA/TEGDMA system (Lovell *et al.*, 2001b). Although there were significant differences in the T_g of samples cured at various light intensities for the HB45NR3PI, the differences were minimal indicating slight variations in the cross-linking density. When the T_g of corresponding samples of HB45NR2PI and HB45NR3PI were compared, the T_g was higher for the latter formulation.

A previous investigation indicated that higher initiation rate could result in a shorter polymer chain length (Lovell *et al.*, 2001b). Due to the increased concentration of effective radicals for the 3PI system, the initiation/secondary rate was higher which could lead to shorter kinetic chains compared to

the corresponding 2PI system. Despite the shorter chain lengths in HB45NR3PI samples, the T_g is higher because it polymerizes to a highly cross-linked network. The highly crosslinked network is attributed primarily to the high concentration of the multi-functional monomer, BisGMA. Therefore, the T_g for the hydrophobic resins is dominated by the cross-linking density rather than the chain length implying that the shorter chains do not significantly impact the network for the hydrophobic formulations. Similar results have been reported by other investigators (Lovell *et al.*, 2001b). The higher T_g for the HB45NR3PI compared to the HB45NR2PI could be due to the enhanced cross-linking density for the former case. The slight increase in the T_g with light intensity for the HB45NR3PI could be attributed to minor increase in the cross-linking density.

For the hydrophilic resins with low viscosity and high concentration of the mono-functional monomers, the chain length can have a significant impact on the polymer network. In this case, the T_g can be dominated by the chain length, since the cross-linking density is low. A high initiation/secondary rate for the HB95NR3PI compared to the HB95NR2PI could result in a shorter chain formation for the former case. A high initiation/secondary rate could also enhance intramolecular cyclization for the HB95NR3PI leading to a higher DC compared to the HB95NR2PI. Cyclization could also enhance microgel formation but reduce the overall cross-linking density. A previous study on a MAA/TEGDMA system containing 50 wt% solvent also showed that higher polymerization rates enhanced the intramolecular cyclization (He *et al.*, 2008). Shorter polymer chains and possibly lower cross-linking density could account for the decreasing trend in T_g for HB95NR3PI compared to that of the corresponding samples of HB95NR2PI. In the case of HB95NR2PI, the T_g remained almost unchanged with light intensity, indicating that it had a very little impact on the chain length and cross-linking density. In the case of HB95NR3PI, there were minor differences in the T_g of samples cured at various light intensities, indicating that variation in the light intensity led to subtle changes in the polymer structure. The first heating/cooling cycles for the DSC study exhibited two T_g values, indicating the presence of higher and lower cross-linked regions within the polymer structure for both the hydrophobic and hydrophilic resins. In Chapter 3, it was also shown that two such phases (microgels and matrix) were present within the polymer structure of the hydrophilic-rich phase of a dental adhesive (Abedin *et al.*, 2014).

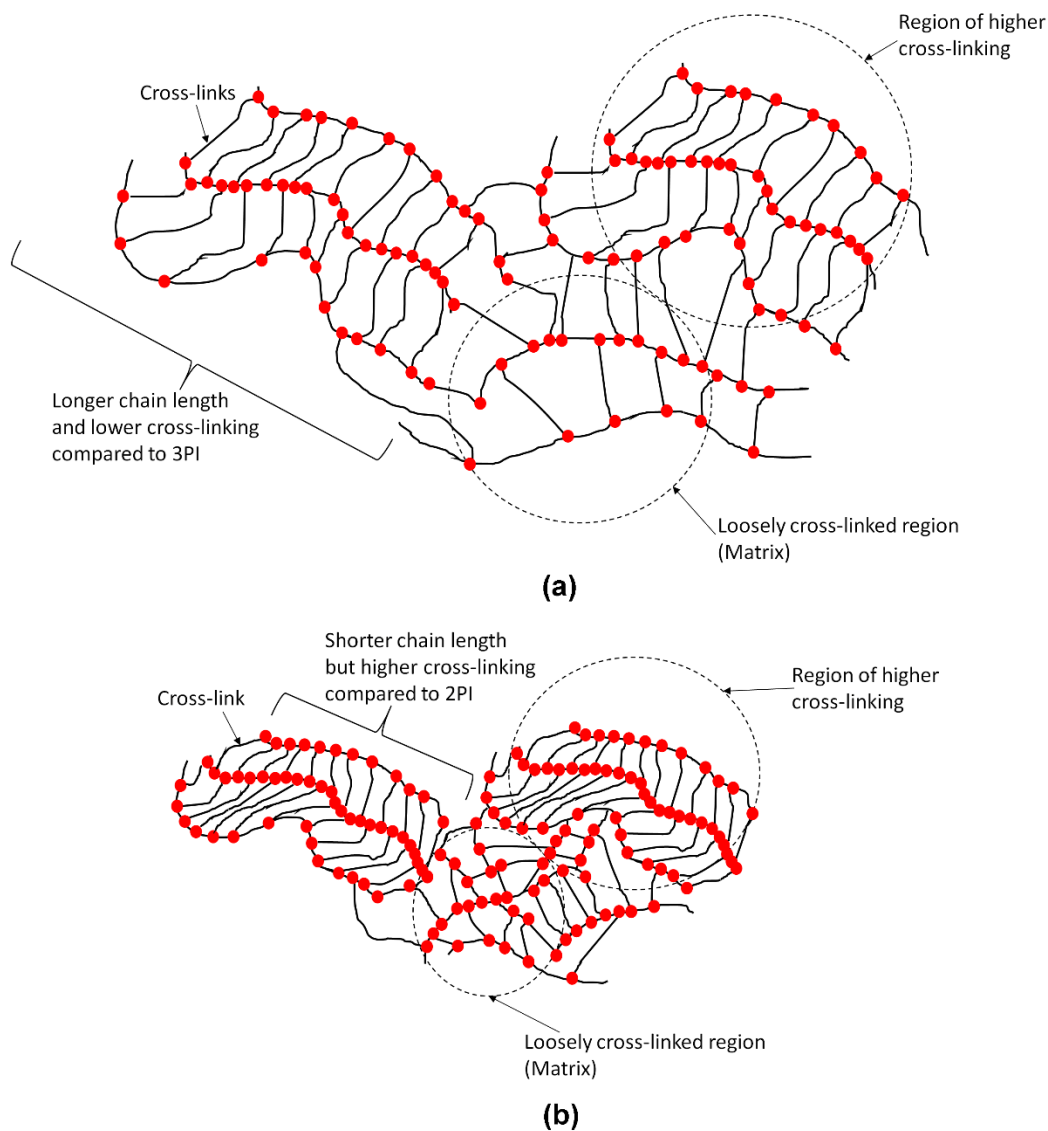


Figure 4.5. Schematic of possible polymer structures for (a) HB45NR2PI and (b) HB45NR3PI (Abedin *et al.*, 2015b)

Therefore, from the DSC study it could be seen that the polymer structure for the hydrophobic 3PI resin might consist of shorter chain lengths but higher cross-linking density compared to the corresponding 2PI resin. Figure 4.5 shows possible network structures for the hydrophobic resins. In the case of the 3PI hydrophilic resin, the polymer structure could consist of shorter polymer chains, more cyclization and lower cross-linking density compared to that for the 2PI hydrophilic resin. The schematic representing the possible polymer structures for the hydrophilic resins is presented in Figure 4.6.

As discussed in previous chapters, dissolved oxygen especially within the hydrophilic resin could impact the kinetic study. The poor DC at 2 h for lower light intensities in the case of the hydrophilic 2PI resin indicates that light intensity can have an adverse impact on the polymerization efficiency of the hydrophilic-rich phase of a dental adhesive. This adverse impact can be overcome by the addition of iodonium salt, since the 3PI hydrophilic resin exhibited substantial DC even at low light intensities. Despite the improved polymerization in the presence of the iodonium salt, the polymer from the hydrophilic resin will be vulnerable to failure/degradation due to shorter polymer chains and poor cross-linking density.

4.5 Conclusion

This study indicates how the light intensity can impact the polymerization efficiency of the hydrophilic dental adhesive resin. It also exhibits how incorporation of iodonium salt impacts the polymerization efficiency and polymer network structure for dental adhesive resins. The outcomes of this study are summarized below:

- Low light intensity negatively impacts the polymerization efficiency of the 2PI hydrophilic dental adhesive resin. Under clinical conditions, there may be regions of the hydrophilic-rich phase exposed to low light intensity. These regions will undergo suboptimal DC making them vulnerable to failure. The optimal light intensity range to obtain good polymerization efficiency within the hydrophilic 2PI resin is 229 – 679 mW/cm².
- For all the hydrophobic resins and 3PI hydrophilic resin, substantial DC was obtained at all light intensities studied here.
- Incorporation of iodonium salt within the adhesive formulation can significantly improve the polymerization efficiency of the hydrophilic resin at lower light intensities, and hence eliminate the dependence of polymerization efficiency on light intensity.
- Iodonium salt leads to shorter chain lengths within the polymer network for the hydrophobic resin. In the case of the hydrophilic resin, iodonium salt leads to shorter polymer chains and promotes cyclization. Possible polymer structures for both hydrophobic and hydrophilic resins, with and without iodonium salt, have been proposed.
- This study also suggests that incorporation of a water compatible multifunctional monomer will significantly improve the durability of the hydrophilic-rich phase of dental adhesives by increasing the cross-linking density.

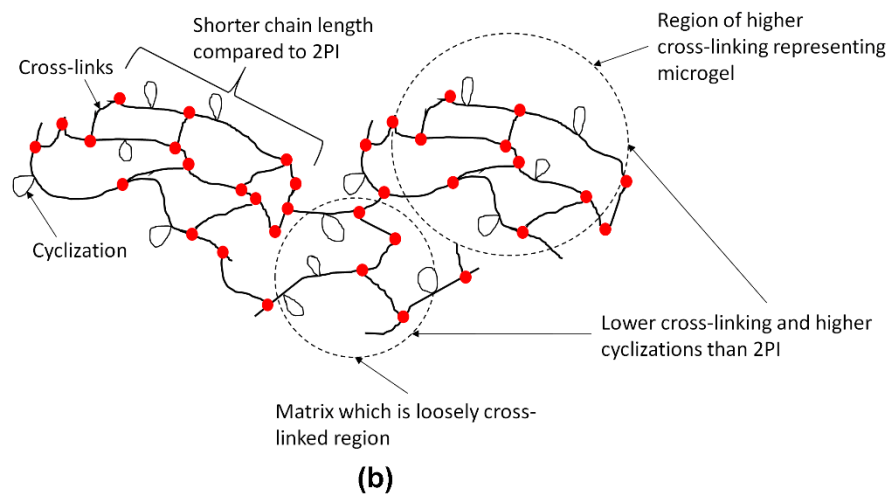
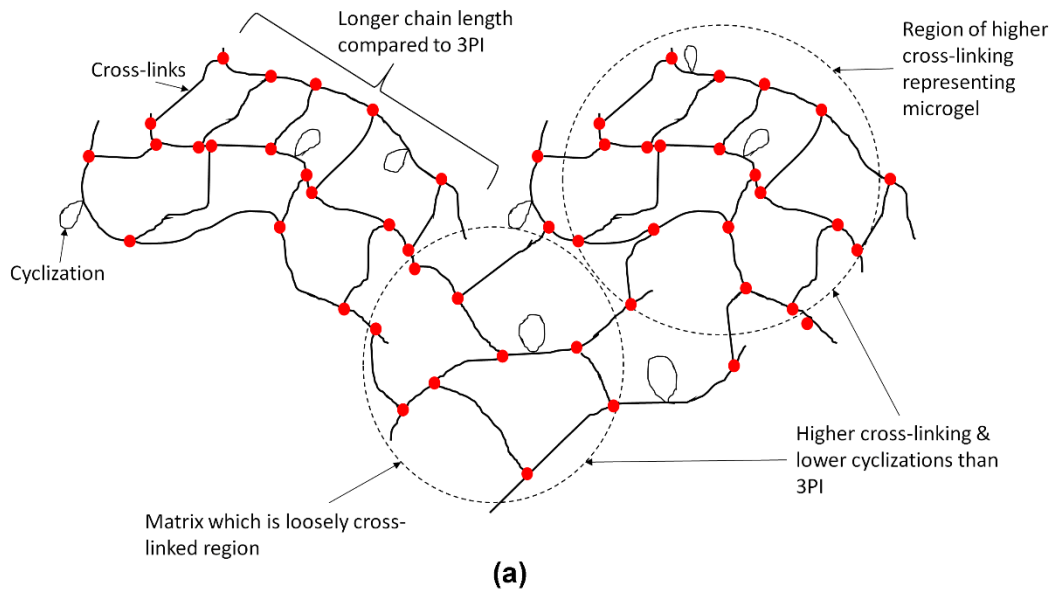


Figure 4.6. Schematic of possible polymer structures for (a) HB95NR2PI and (b) HB95NR3PI (Abedin *et al.*, 2015b)

CHAPTER 5: IMPACT OF PHOTO-INITIATOR PARTITION AND INCORPORATION OF IODONIUM SALT ON THE PHOTO-POLYMERIZATION OF PHYSICALLY PHASE SEPARATED DENTAL ADHESIVE

(This study is based on the journal article: Abedin F., Ye Q., Song L., Ge X., Camarda K., Spencer P., Effect of partition of photo-initiator components and addition of iodonium salt on the photopolymerization of phase-separated dental adhesive, The Journal of the Minerals, Metals and Materials Society, 68(4), 2016, 1090-1099

5.1 Introduction

Previous chapters investigated the characteristics of formulations that mimicked the hydrophilic-rich phase of dental adhesives. These studies showed the trend in changes for reaction kinetics and the network structure of the hydrophilic-rich mimics when parameters like the photo-initiator concentration, water concentration and light intensity were varied. It is equally important to understand how the actual separated phases will behave. There have been very few studies on the physically separated hydrophilic-rich phase of dental adhesives. Ye *et al.* determined the partition concentrations of the mono-methacrylate monomer, cross-linker and water within the hydrophilic-rich phase (Ye *et al.*, 2012). In the subsequent study, the partition concentrations of the photo-initiator components in both the hydrophilic- and hydrophobic-rich phases were determined. The current study explored the impact of the partition concentration of PI components on the photopolymerization of the hydrophobic- and hydrophilic-rich phases. The effect of the hydrophobic and hydrophilic co-initiators was also investigated as well as the impact of the reaction accelerator, DPIHP, on the polymerization behavior of both the phases.

5.2 Materials and Methods

5.2.1 Preparation of physically separated hydrophilic- and hydrophobic-rich phases

The mono-methacrylate monomer, HEMA and the cross-linker, BisGMA were obtained from Sigma Aldrich, Milwaukee, WI. EDMAB as the hydrophobic co-initiator and 2-(dimethylamino)ethyl methacrylate (DMAEMA) as the hydrophilic co-initiator, CQ as the photosensitizer and DPIHP as the reaction accelerator were all obtained from Sigma Aldrich, Milwaukee, WI. At first, a control formulation of the neat resin consisting of HEMA/BisGMA in the ratio of 45:55 wt% was prepared. As mentioned earlier, this formulation also represented the major composition of most of the commercially available dental adhesive resins (Ye *et al.*, 2007a). The control formulations were prepared with various combinations of PI components. Table 5.1 shows the various combinations of PI used to prepare the formulations in this study. Each component of the PI system was added to the control formulation at 0.5 wt% based on the total weight of the neat resin. Deuterium oxide (D₂O, Cambridge Isotope Laboratories

Inc.) was added to the control formulation at 33 wt% based on the total weight of the mixture. The D₂O content exceeded the miscibility limit of the neat resin (Abedin *et al.*, 2015c), and hence the mixture formed after addition of the D₂O was cloudy. Then, the required PI components were added based on the weight of the D₂O so that the concentration of each PI component remained constant at 0.5 wt%. The mixture was vortexed to ensure that the PI components dissolved, and then the mixture was centrifuged at 10,000 rpm for 20 min to separate the hydrophobic- and hydrophilic-rich phases. The hydrophilic-rich phase was collected from the top layer using a pipette, while the interface between the hydrophilic- and hydrophobic-rich phases was discarded, and the hydrophobic-rich phase was collected from the bottom layer. Figure 5.1 shows the schematic for preparing the physically separated hydrophobic- and hydrophilic-rich phases.

Table 5.1. Composition of each components in the resin mixture prior to collection of the two phases by centrifugation (Abedin *et al.*, 2016)

Name of Formulation	wt% of BisGMA	wt% of HEMA	wt% of D ₂ O
EDMAB/DPIHP	36.56 ± 0.04	29.94 ± 0.04	33.50 ± 0.08
DMAEMA/DPIHP	36.46 ± 0.25	29.96 ± 0.21	33.58 ± 0.46
CQ/DPIHP	36.33 ± 0.09	30.14 ± 0.07	33.54 ± 0.16
CQ/DMAEMA	36.61 ± 0.04	29.97 ± 0.03	33.42 ± 0.07
CQ/EDMAB	36.70 ± 0.01	30.02 ± 0.02	33.28 ± 0.03
CQ/DMAEMA/DPIHP	36.52 ± 0.06	29.89 ± 0.05	33.59 ± 0.11
CQ/EDMAB/DPIHP	36.59 ± 0.03	29.94 ± 0.02	33.48 ± 0.04

* CQ, EDMAB, DMAEMA, DPIHP each were added at 0.5 wt% of the total weight of the mixture

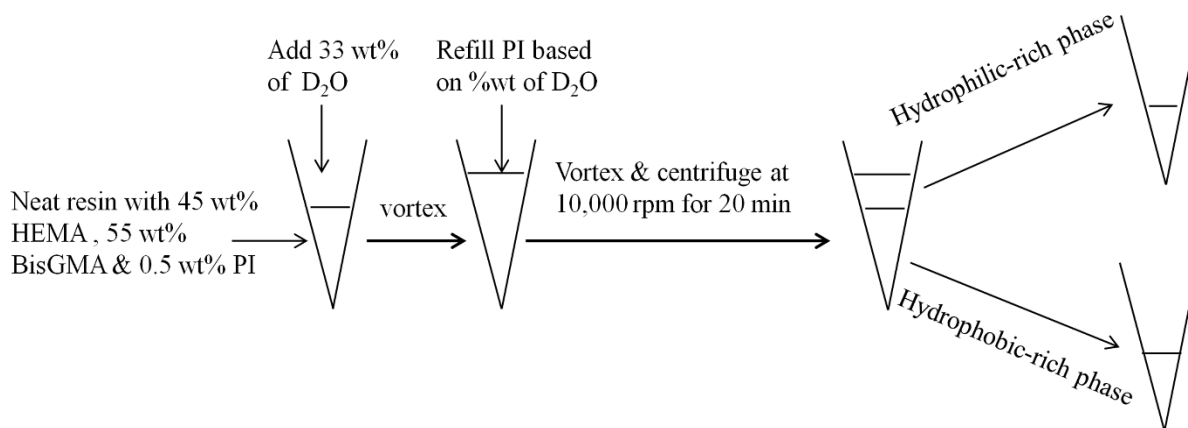


Figure 5.1. Schematic showing steps for preparing hydrophobic- and hydrophilic-rich phases (Abedin *et al.*, 2016)

Table 5.1 shows the concentration of the cross-linker, HEMA and D₂O within the mixture for each combination of PI before centrifugation. The two phases prepared in this manner were used to conduct the polymerization kinetic study.

The hydrophilic- and hydrophobic-rich phases used in the high performance liquid chromatography (HPLC) studies were obtained from neat resins containing only 0.5 wt% of one of the PI components. Although there were four types of PI components, only neat resins containing EDMAB, DMAEMA and DPIHP were prepared separately. In other words, instead of a mixture of PI components, neat resins containing individual PI components were prepared for the HPLC study because this allowed a simpler approach to identify and quantify the PI components within the two phases.

5.2.2 Polymerization kinetic of physically separated hydrophobic- and hydrophilic-rich phases

A polymerization kinetics study of the hydrophobic- and hydrophilic-rich phases was carried out in the same manner as discussed in the previous three chapters. The polymerization kinetics study for the hydrophobic-rich phase was carried out for 1 h and that for the hydrophilic-rich phase for 2 h. The kinetic study was carried out using a PerkinElmer Spectrometer (PerkinElmer, Waltham, MA). The MCT detector was used to collect the data because it allowed high signal to noise ratio. The MCT detector was cooled using the liquid nitrogen, and then 30 μ l of the sample was placed on the ATR crystal which was covered using a plastic coverslip. The coverslip was sealed at the edges with tapes to prevent evaporation of D₂O. The data were collected at a resolution of 4 cm^{-1} . Both the D₂O profile, and the band ratio of C=C at 1637 cm^{-1} to C=O at 1716 cm^{-1} were monitored. The DC was calculated using equation 2.1 in Chapter 2. The rate of polymerization was obtained by differentiating the DC against time graph using Microcal Origin (Version 6.0, Microcal Software, Northampton, MA).

5.2.3 High performance liquid chromatography (HPLC)

5.2.3.1 Reverse-phase chromatography

The major components of an HPLC system are solvent reservoirs, pumps, an injector, a HPLC column and a detector as shown in Figure 5.2. For HPLC, a solution of the analytes is injected, which travels through the column in the mobile phase. The mobile phase can be a solvent or a mixture of solvents. In the column, the analytes interact with the stationary phase differently, leading to their separation. Compounds are identified based on their time of elution. In the case of reverse phase HPLC, the stationary phase is made up of silica particles which have hydrophobic alkyl chains bound to them. For reverse phase chromatography, the interaction between the analyte and stationary phase depends on the

hydrophobicity of the analyte. If the analyte is non-polar, then it will interact with hydrocarbon chains on the silica particles and be delayed. A hydrophilic analyte will have minimal interaction with the alkyl chains on the silica particles, and hence it will mostly travel through the column in the mobile phase. Therefore, a hydrophilic analyte elutes earlier compared to a hydrophobic analyte. Solvents for the mobile phase can be pumped in an isocratic mode or gradient mode. In case of the isocratic mode, the solvent volume proportion is kept constant. In the gradient mode, the solvent volume proportion is varied linearly. Retention time is the time taken for an analyte's peak to appear after the sample is injected. The retention time depends on various factors such as the hydrophobicity of the analyte, the composition of the mobile phase, the type of column, the flow rate and the temperature. The analyte can be detected using a UV light detector. As the analyte passes through the column, it absorbs UV light. It is possible to determine the concentration of an analyte in an unknown solution from the absorption intensity if calibration data for the analyte using the same experimental conditions are available.

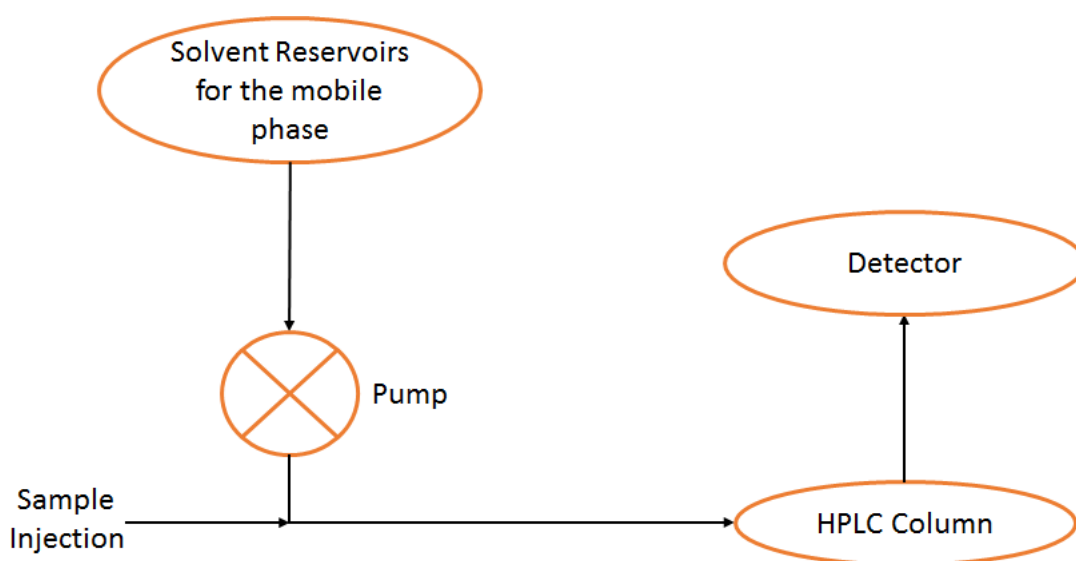


Figure 5.2. Schematic showing major components for high performance liquid chromatography (HPLC)

5.2.3.2 HPLC for determining partition concentrations of PI components in hydrophobic- and hydrophilic-rich phases

A Shimadzu LC-2010 CHT HPLC system equipped with a SPD-M20A photodiode array detector and an autosampler with EZstart chromatography software was used to determine the concentration of DMAEMA, DPIHP and EDMAB in the hydrophobic- and hydrophilic-rich phases. The concentration of CQ was not determined because CQ was found to be unstable in both the phases. The major components of adhesive resin, HEMA and BisGMA ,were quantified in a previous study (Ye *et al.*, 2012). A reverse phase

column (Phenomenex Luna 5 μm C18 4.6 \times 250, Torrance, CA) was used for the HPLC. To quantify EDMAB and DMAEMA, the mobile phase was pumped in an isocratic mode. For the DMAEMA quantification, the mobile phase consisted of 10 mM phosphate buffer solution and acetonitrile (Fisher Scientific) in the ratio of 35:65 vol% respectively. The buffer was prepared using HPLC grade water (Fisher Scientific). For the quantification of EDMAB, the mobile phase was made up of HPLC grade water and acetonitrile in the ratio of 35:65 vol% respectively. For the isocratic method, the flow rate was maintained at 0.5 mL/min. For this method, after 24.99 min the acetonitrile in the mobile phase was increased to 85 vol% which was maintained for 5 min. The hydrophobic- and hydrophilic-rich phases were diluted using HPLC grade ethanol (Acros Organics). After dilution, the samples were filtered using a Millipore centrifuge filter device (Ultrafree[®]-CL, UFC4LCCOO 5000 NMWL, Millipore, Bedford, MA), and centrifuged (Eppendorf MiniSpin Plus, Eppendorf, Hamburg, Germany) at 10,000 rpm. The hydrophobic-rich phase for the determination of EDMAB concentration was diluted by 124 times, and that for DMAEMA was diluted by 120 times. In the case of EDMAB quantification, the hydrophilic-rich phase was not diluted but for the DMAEMA it was diluted by 60 times. For DPIHP quantification, a gradient mode for solvent pumping was used. The mobile phase in this case consisted of 10 mM phosphate buffer and acetonitrile. For DPIHP, the buffer was decreased from 75 vol% to 35 vol% in 20 min. For 5 min the buffer volume was kept constant to 35 vol%. Then, the buffer was increased to 75 vol% in 1 min and kept constant at this volume for 19 min. The peak for DPIHP overlapped with that for HEMA when the isocratic method discussed earlier was used but the gradient method allowed separation of the two peaks. The flow rate for the gradient method was also 0.5 mL/min. The hydrophobic-rich phase for quantification of DPIHP was diluted by 21 times whereas the hydrophilic-rich was diluted by 15 times.

Hydrophobic- and hydrophilic-rich phases without containing any PI were also prepared and diluted to the equivalent levels as hydrophobic-rich and hydrophilic-rich phases containing the PI components. The chromatograms obtained using the phases without containing PI were subtracted from chromatograms of corresponding phases with PI component. Figure 5.3 (a) and (b) shows the DPIHP peak for hydrophobic- and hydrophilic-rich phases before and after the subtraction. This allowed an accurate quantification of the absorption intensity for each PI component. The PI components were identified based on their retention time and their concentrations were determined using the absorption intensity at 208 nm and a calibration graph obtained using known standards. The intensities of the peaks for the PI components were baseline corrected before the subtraction using OriginPro (Version 8.0, OriginLab, Northampton, MA). The calibration graph of absorption intensity against concentration showed a range of linearity of 12-210 $\mu\text{g}/\text{mL}$ in case of the EDMAB, 10-100 $\mu\text{g}/\text{mL}$ for the DMAEMA and 95-413 $\mu\text{g}/\text{mL}$ for

the DPIHP. The linear relationships between absorption intensity and concentration for all three PI components are given below:

$$\text{Intensity} = 4.045[\text{DMAEMA}] - 4.392 \quad R^2 = 0.99 \quad 5.1$$

$$\text{Intensity} = 4.593[\text{EDMAB}] + 17.544 \quad R^2 = 0.99 \quad 5.2$$

$$\text{Intensity} = 3.465[\text{DPIHP}] - 2.264 \quad R^2 = 0.99 \quad 5.3$$

5.2.4 Statistical Analysis

The polymerization kinetic study for each PI combination given in Table 5.1 was carried out in triplicate for each phase, and the HPLC study for each PI component and phase was also carried out in triplicate. The DC and rate maxima for each PI combination and phase were compared using one-way analysis of variance (ANOVA, $p < 0.05$) and t-test ($p < 0.05$). This was done using Microcal Origin (Version 6.0, Microcal Software, Northampton, MA). The concentrations of PI components in each phase were also compared using one-way ANOVA ($p < 0.05$) and t-test ($p < 0.05$).

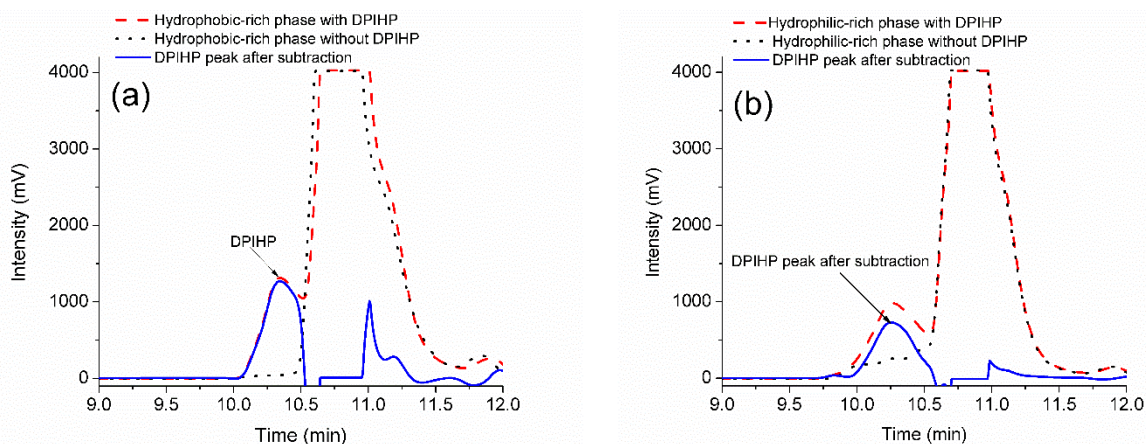


Figure 5.3. Chromatograms of (a) hydrophobic- and (b) hydrophilic-rich phases prepared from resin containing DPIHP, showing DPIHP peak after subtraction (Abedin *et al.*, 2016)

5.3 Results

5.3.1 Polymerization kinetics results

The hydrophobic-rich phase representing PI combinations without any photosensitizer, CQ, exhibited poor DC. The PI combinations without CQ included EDMAB/DPIHP and DMAEMA/DPIHP. The rate maxima of the hydrophobic-rich phase for these two PI combinations were significantly lower than for the same phase with PI combinations containing CQ, except for CQ/DMAEMA. Therefore, the

photosensitizer plays a vital role in generating radicals for the polymerization reaction (one-way ANOVA, t-test, $p < 0.05$). For the PI combination, CQ/DMAEMA both the hydrophobic- and hydrophilic-rich phases exhibited poor DC and a low rate maxima, showing that DMAEMA was an inefficient co-initiator compared to EDMAB. Significantly higher DC and rate maxima were observed for the hydrophobic-rich phase in the case of PI combinations, CQ/EDMAB, CQ/EDMAB/DPIHP and CQ/DMAEMA/DPIHP when compared to the other PI combinations (one-way ANOVA, t-test, $p < 0.05$). The highest DC for the hydrophobic-rich phase was observed in the case of CQ/EDMAB/DPIHP. The DC in this case was significantly higher than that for CQ/EDMAB and CQ/DMAEMA/DPIHP (t-test, $p < 0.05$). The rate maxima of the hydrophobic-rich phase representing the PI combination CQ/EDMAB and CQ/EDMAB/DPIHP were similar (no statistical difference, t-test, $p < 0.05$). Figure 5.4 shows the representative results of the kinetic study for the hydrophobic-rich phase. Table 5.2 shows the average DC and rate maxima of the hydrophobic-rich phase for all PI combinations.

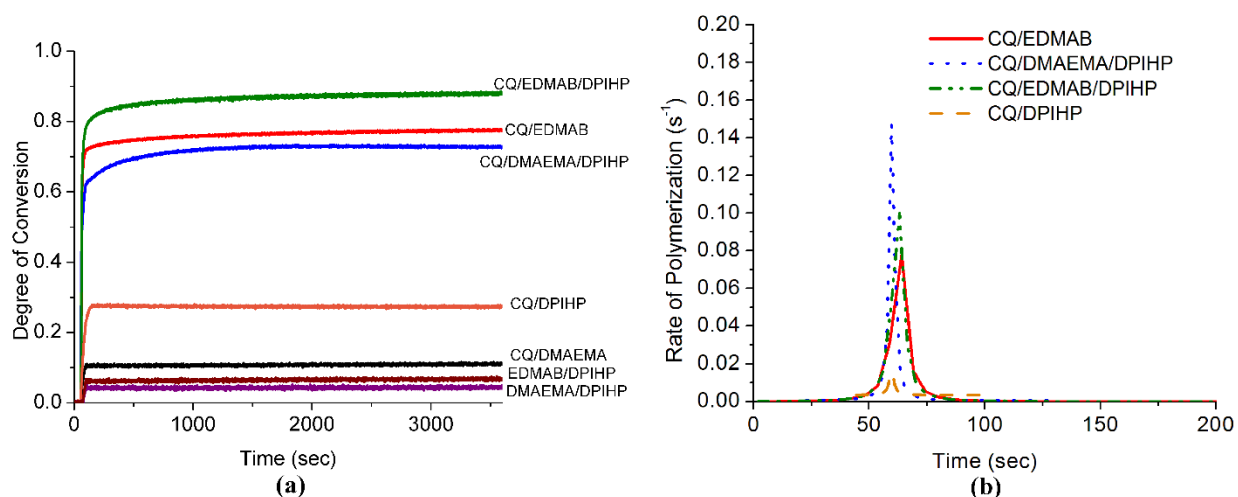


Figure 5.4. Representative polymerization kinetics result for the hydrophobic-rich phase showing (a) DC against time and (b) rate maxima against time (Abedin *et al.*, 2016)

The hydrophilic-rich phase representing the PI combinations DMAEMA/DPIHP and EDMAB/DPIHP failed to polymerize. The hydrophilic-rich phase representing CQ/EDMAB and CQ/DMAEMA also showed poor polymerization which improved significantly when the iodonium salt, DPIHP, was added. Hence, the DC and rate maxima of the hydrophilic-rich phase were significantly higher for PI combinations CQ/EDMAB/DPIHP and CQ/DMAEMA/DPIHP when compared to CQ/EDMAB and CQ/DMAEMA (one-way ANOVA, t-test, $p < 0.05$). It was observed that the DC and rate maxima of the hydrophilic-rich phase were higher for the PI combination CQ/DMAEMA/DPIHP compared to that for CQ/EDMAB/DPIHP.

Table 5.2. Degree of conversion and rate maxima for hydrophobic-rich phase (Abedin *et al.*, 2016)

Formulation Name	Degree of Conversion (DC) after 1 hr	Rate Maxima (s^{-1}) $\times 10^2$
EDMAB/DPIHP	0.068 \pm 0.009	0.52 \pm 0.02
DMAEMA/DPIHP	0.045 \pm 0.013	0.45 \pm 0.02
CQ/DPIHP	0.267 \pm 0.006	1.64 \pm 0.15
CQ/DMAEMA	0.104 \pm 0.008	0.77 \pm 0.11
CQ/EDMAB	0.771 \pm 0.007	8.07 \pm 1.37
CQ/DMAEMA/DPIHP	0.747 \pm 0.029	16.1 \pm 2.1
CQ/EDMAB/DPIHP	0.878 \pm 0.007	9.74 \pm 0.45

The hydrophilic-rich phase representing CQ/DPIHP exhibited a poor DC, which was significantly lower than that of the corresponding hydrophobic-rich phase (t-test, $p < 0.0001$). The DC and rate maxima of the hydrophilic-rich phase for CQ/DPIHP were significantly higher than those of the corresponding phases representing CQ/DMAEMA and CQ/EDMAB (one-way ANOVA, t-test, $p < 0.05$). Figure 5.5 shows the representative results of the kinetic study for the hydrophilic-rich phase. Table 5.3 shows the average DC and rate maxima of the hydrophilic-rich phase for all the PI combinations.

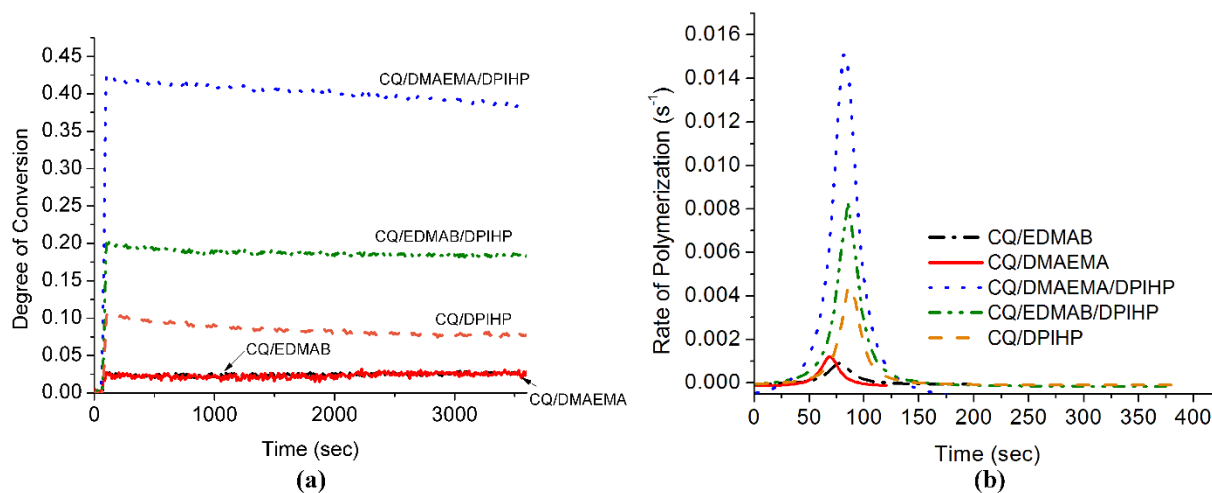


Figure 5.5. Representative polymerization kinetics result for the hydrophilic-rich phase showing (a) DC against time and (b) rate maxima against time (Abedin *et al.*, 2016)

Table 5.3. Degree of conversion and rate maxima for hydrophilic-rich phase (Abedin *et al.*, 2016)

Formulation Name	Degree of Conversion (DC) after 1.5 hr	Rate Maxima (s ⁻¹)× 10 ⁴
CQ/DPIHP	0.087 ± 0.027	46.4 ± 8.4
CQ/DMAEMA	0.024 ± 0.001	13.8 ± 3.9
CQ/EDMAB	0.028 ± 0.018	13.9 ± 10.1
CQ/DMAEMA/DPIHP	0.322 ± 0.034	142 ± 16
CQ/EDMAB/DPIHP	0.201 ± 0.082	94.3 ± 33.1

* The formulations containing EDMAB/DPIHP and DMAEMA/DPIHP did not polymerize

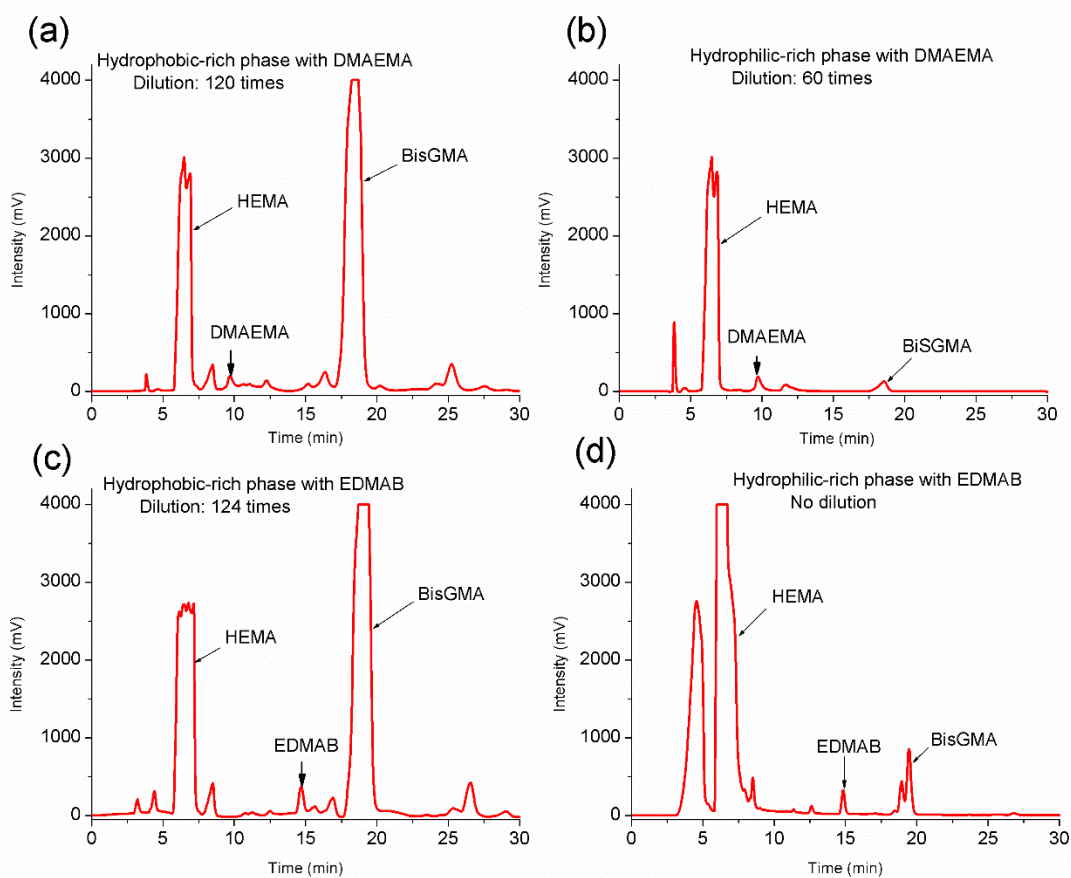


Figure 5.6. Chromatograms of hydrophobic- and hydrophilic-rich phases for (a), (b) DMAEMA and (c), (d) EDMAB (Abedin *et al.*, 2016)

5.3.2 Results from high performance liquid chromatography (HPLC)

EDMAB and DPIHP were present in the hydrophobic-rich phase at significantly greater concentrations than DMAEMA (one-way ANOVA, t-test, $p < 0.05$) as shown in Table 5.4. The concentration of EDMAB in the hydrophilic-rich phase was significantly lower than DMAEMA and DPIHP (one-way

ANOVA, t-test, $p < 0.05$). On the other hand, the partition concentration of the DPIHP in the hydrophilic-rich phase was significantly higher than DMAEMA (one-way ANOVA, t-test, $p < 0.05$). Table 5.4 shows the average partition concentrations of EDMAB, DMAEMA and DPIHP in both hydrophobic- and hydrophilic-rich phases. Table 5.4 also shows the partition ratio of these components in the hydrophilic-rich phase. Figure 5.6 shows the representative chromatograms for the PI components EDMAB and DMAEMA for both the hydrophobic- and hydrophilic-rich phases, and Figure 5.7 presents a chromatogram for DPIHP. It can be seen from Table 5.4 that the partition ratio of EDMAB in the hydrophilic-rich phase was very low which explains the poor polymerization of this phase for CQ/EDMAB.

Table 5.4. Partition concentration of DMAEMA, DPIHP and EDMAB in hydrophobic- and hydrophilic-rich phase (Abedin *et al.*, 2016)

Photo-initiator Component	Content in Hydrophobic-rich Phase (wt%)	Content in Hydrophilic-rich Phase (wt%)	Partition ratio (h'philic / h'phobic)
DMAEMA	0.492 ± 0.003	0.251 ± 0.004	0.510
DPIHP	0.698 ± 0.007	0.286 ± 0.003	0.410
EDMAB	1.063 ± 0.026	0.007 ± 0.000	0.007

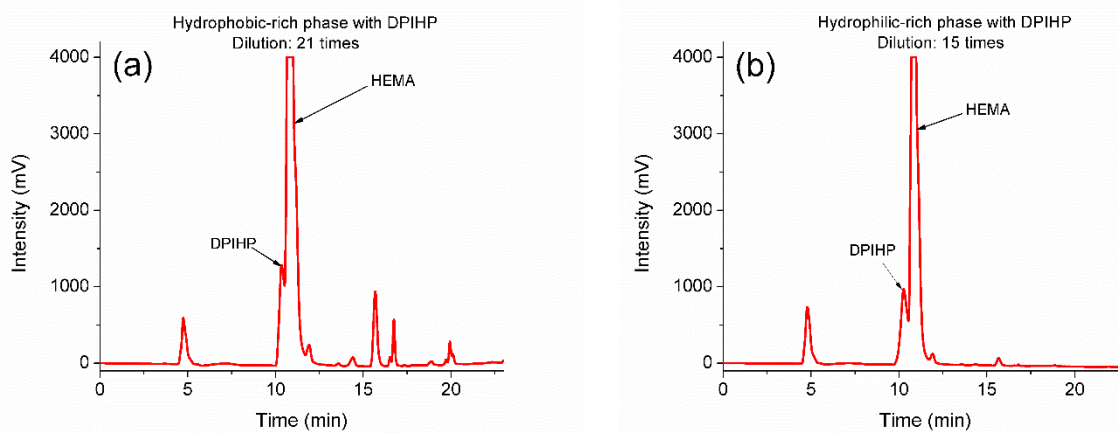


Figure 5.7. Chromatograms of DPIHP for the (a) hydrophobic-rich phase and (b) hydrophilic-rich phase (Abedin *et al.*, 2016)

5.4 Discussion

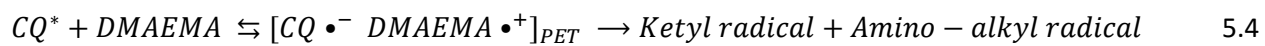
For the formulation containing CQ/DPIHP, the CQ after reaching the excited state immediately after irradiation reacts with the monomer to produce ketyl and alkyl radicals (Cook and Chen, 2011). For a detailed understanding, the readers are directed to the proposed reaction mechanism for the CQ system by Cook *et al.* (Cook and Chen, 2011). The reaction between the monomer and the excited CQ is slow and

reversible which accounts for the poor polymerization of both the phases for CQ/DPIHP. The iodonium salt oxidizes the ketyl radicals resulting in the regeneration of CQ and production of phenyl radicals which are active in the initiation. CQ is hydrophobic in nature and hence it is possible that it partitions at lower concentration within the hydrophilic-rich phase. This may result in a lower concentration of radicals within the hydrophilic-rich phase as compared to the hydrophobic-rich phase, and moreover the monomer concentration is much higher in the hydrophobic-rich phase (Ye *et al.*, 2012), enhancing the possibility of reaction between CQ and monomers to generate radicals in the latter phase. Therefore, the hydrophilic-rich phase is much less reactive than the hydrophobic-rich phase.

For the PI system consisting of CQ and tertiary amine, electrons are transferred from the tertiary amine to the excited CQ after irradiation to generate photo-induced electron transfer (PET) species (Cook and Chen, 2011). Aminoalkyl and ketyl radicals are formed when proton transfer within the PET species takes place. Aminoalkyl radicals participate in the initiation reaction and ketyl radicals in the termination reaction. The reaction for PET formation is a reversible reaction. For the PI combination CQ/EDMAB, it can be seen from Table 5.4 that the partition ratio of EDMAB is very low, and CQ may also be present in a low concentration within the hydrophilic-rich phase. The low concentrations of both the photosensitizer, CQ, and co-initiator, EDMAB, in the hydrophilic-rich phase may account for the poor polymerization of this phase.

In the case of the PI system consisting of CQ and DMAEMA, it can be seen that the partition ratio of the DMAEMA is higher compared to that of EDMAB. Despite the presence of DMAEMA in higher concentration within the hydrophilic-rich phase, the polymerization of this phase was poor. This is most likely due to the lack of CQ in the hydrophilic-rich phase and possibly due to the reduction of reactive species triggered by back electron transfer in PET species within this phase. Although the concentration of DMAEMA in the hydrophobic-rich phase is significantly higher than that in the hydrophilic-rich phase (Table 5.4), the polymerization of the hydrophobic-rich phase in this case is still very poor, and a significantly lower DC was observed as compared to that of the corresponding phase for CQ/EDMAB. Although one reason for the sub-optimal polymerization of the hydrophobic-rich phase for CQ/DMAEMA could be the lower concentration of DMAEMA as compared to EDMAB in this phase (Table 5.4), the major reason could be enhanced back electron transfer within PET species in the case of DMAEMA as compared to EDMAB, reducing the concentration of reactive species. The equation 5.4 below shows the PET formation due to transfer of electron from DMAEMA and CQ (Cook and Chen, 2011). The back electron transfer occurs in the reverse direction as shown in the equation 5.4. For the 3PI system where the third

component is the iodonium salt (DPIHP), the ketyl and aminoalkyl radicals are oxidized by the DPIHP regenerating CQ in the process and producing phenyl radicals. As mentioned earlier, the terminating ketyl radicals are replaced by radicals active in initiation (Cook and Chen, 2011). The oxidation by DPIHP also reduces the possibility of back electron transfer within PET species (Cook and Chen, 2011). Hence, the overall concentration of the effective radicals for the 3PI system is higher than the 2PI system, as discussed earlier. In the case of the hydrophilic-rich phase, it is possible that the addition of DPIHP reduces back electron transfer substantially causing significant increase in the DC of this phase despite very low concentration of CQ. As a result 20.1% DC for the CQ/EDMAB/DPIHP and 32.2% for the CQ/DMAEMA/DPIHP were observed for the hydrophilic-rich phase. This also explains the higher polymerization rate of the hydrophilic-rich phase for the 3PI system when compared to the corresponding 2PI system. Since the concentration of the DMAEMA in the hydrophilic-rich phase is higher than the EDMAB (Table 5.4), it is possible that the concentration of effective radicals is higher in the hydrophilic-rich phase for CQ/DMAEMA/DPIHP as compared to CQ/EDMAB/DPIHP. This could lead to an enhanced DC and polymerization rate for this phase in the case of CQ/DMAEMA/DPIHP as compared to CQ/EDMAB/DPIHP.



This increased concentration of effective radicals also accounts for the significantly higher DC of the hydrophobic-rich phase in the presence of DPIHP as compared to the corresponding formulations without DPIHP. It is also possible that DPIHP is more effective in reducing back electron transfer in the case of the DMAEMA as compared to the EDMAB. This becomes evident when DC of the hydrophobic-rich phase for the 3PI system is compared with their corresponding 2PI system. The DC of the hydrophobic-rich phase with CQ/DMAEMA is poor, but the addition of the DPIHP to this PI system increased the DC significantly. When the DC for CQ/EDMAB/DPIHP and CQ/EDMAB of the hydrophobic-rich phase are compared, it can be seen that they are similar. Moreover, Table 5.4 shows that the concentration of the DMAEMA in the hydrophobic-rich phase is lower than that for the EDMAB, but the DC of this phase is similar when these co-initiators are used with CQ and DPIHP.

This study indicates the importance of the photo-initiating system on the rate of polymerization and DC for model dental adhesive phases. The results indicate that DMAEMA alone is an inefficient co-initiator as compared to EDMAB. However, when DMAEMA is used with DPIHP, its performance becomes equivalent to EDMAB. CQ/DMAEMA and CQ/EDMAB are not efficient PI systems for both or at least one of the adhesive phases. As mentioned earlier, the addition of DPIHP improves the polymerization of both

the phases especially the hydrophilic-rich phase. Despite the improved polymerization of the hydrophilic-rich phase due to the DPIHP, the DC was still poor which would make this phase vulnerable to failure. The poor, DC was primarily due to the low partition concentration of the hydrophobic photosensitizer, CQ and/or co-initiator EDMAB. This can be avoided if an efficient water compatible photosensitizer and co-initiator are partially incorporated into the dental adhesive PI system. Chapter 2 showed that partial incorporation of a hydrophilic photosensitizer, QTX in addition to the hydrophobic CQ substantially improved the DC of the hydrophilic-rich mimic when the PI components were present in low concentrations, as compared to the corresponding formulation when CQ was solely used as the photosensitizer (Abedin *et al.*, 2015c).

The previous chapters showed the presence of the secondary gel effect in the case of the hydrophilic-rich mimics. In this investigation, no secondary rate maxima were observed for the hydrophilic-rich phase. The hydrophilic-rich phase was produced by physical separation of a mixture of neat resin and D₂O which was beyond its miscibility limit. An earlier study showed that the cross-linker, BisGMA was present in a very low concentration, i.e. approximately 302 µg/mL, in the physically separated hydrophilic-rich phase (Ye *et al.*, 2012). This quantity of BisGMA could be much lower than the concentration of BisGMA in the hydrophilic-rich mimics which were studied in the earlier chapters. The presence of cross-linker in minor quantities and also the low DC due to the incompatibility of the PI components could significantly reduce microgel formation and hence impair secondary gel effect.

5.5 Conclusion

This study shows the importance of the PI system on the polymerization of model adhesives that are used in the wet environment of the mouth. The results from this study provide clear evidence to support the importance of a PI system that is compatible with both the hydrophobic and hydrophilic-rich phases. This investigation provides direction for the development of more efficient and durable dental adhesives. The outcomes of this study are given below:

- Incorporation of DPIHP can significantly improve the polymerization of the hydrophilic-rich phase.
- DMAEMA is an inefficient co-initiator for both the hydrophilic- and hydrophobic-rich phases when used with CQ alone.
- The inefficiency of DMAEMA may be due to the enhanced back electron transfer within the PET species but the addition of DPIHP significantly improves its performance.

- DPIHP has greater impact in reducing the back electron transfer when the DMAEMA is used as the co-initiator as compared to the EDMAB.
- Despite the improved DC of the hydrophilic-rich phase due to the presence of the DPIHP, the polymerization of this phase was still low due to the incompatibility of the photosensitizer and/or co-initiator with the hydrophilic-rich phase.
- The polymerization of the hydrophilic-rich phase can be significantly improved to obtain substantial DC by including DPIHP as well as partially incorporating hydrophilic photosensitizer and co-initiator in the adhesive PI systems.

**PART II: COMPUTATIONAL DESIGN OF WATER COMPATIBLE PHOTOSENSITIZER FOR
DENTAL ADHESIVE APPLICATIONS**

CHAPTER 6: DYES AS PHOTSENSITIZERS FOR DENTAL ADHESIVES

6.1 Introduction

Previous chapters have explored the characteristics of model hydrophilic-rich phases of dental adhesives in terms of polymerization behavior under varying parameters such as light intensity, PI and D₂O concentrations. The effect of addition of an iodonium salt and the concentration of each PI component in the hydrophobic- and hydrophilic-rich phases on the polymerization kinetics have also been explored. These studies have also provided critical aspects for designing experiments to explore the potential of existing photosensitizers to be used in dental adhesive formulations. This study forms phase I of the computer aided molecular design (CAMD) methodology discussed in Chapter 1. This chapter represents the following forward problem steps in CAMD as discussed in Figure 1.3:

- Model building set
- Measurement of target properties

The critical aspects for the experimental work in CAMD which were obtained from earlier investigations were:

- The polymerization kinetics study for the hydrophilic adhesive formulations should be carried out for at least 2 h to capture the secondary rate maxima although the physically separated hydrophilic-rich phase for the monomer system BisGMA/HEMA might not show any secondary gel effect.
- To evaluate the performance of the existing photosensitizers on the polymerization of the hydrophobic- and hydrophilic-rich phases of dental adhesive, the D₂O concentration should be kept constant since water concentration could impact the polymerization rate.
- To eliminate the influence of light intensity on the polymerization of the hydrophilic-rich phase, it was important to keep the light intensity constant and in the range of 229 – 679 mW/cm².
- To obtain DC of the hydrophilic-rich phase, it was important to incorporate iodonium salt, DPIHP, in the PI system since no polymerization was observed for the physically separated hydrophilic-rich phase for CQ/EDMAB and CQ/DMAEMA PI system without DPIHP.
- The existing photosensitizers should be used in addition to CQ to prevent negative impact on the polymerization of the hydrophobic-rich phase.

- Both hydrophobic and hydrophilic co-initiators should be incorporated in the PI system to improve the compatibility of PI system with the hydrophilic-rich phase.

The objective of this and the subsequent Chapter are to design a hydrophilic photosensitizer suitable for application in dental adhesives. The incorporation of a hydrophilic photosensitizer will enhance the DC of the hydrophilic-rich phase. It is likely that with the enhanced DC, there will be a reduction in the degradation of the hydrophilic-rich phase and a concomitant reduction in the release of methacrylic acid. Methacrylic acid may be partially responsible for the demineralization of the surrounding dentin and enamel. Moreover, higher DC of the hydrophilic-rich phase will ensure better seal at the hybrid layer and hence reduce the extent of exposed collagen for degradation and possible direct attachment of the *Streptococcus mutans* (Larson *et al.*, 2010). Therefore, an enhanced DC will likely translate to an improvement in the adhesive durability and an increase in the lifetime of the composite restoration.

In this chapter, the polymerization kinetics of both the hydrophobic- and hydrophilic-rich phases will be investigated in the presence of CQ and a new photosensitizer. The new photosensitizers investigated were mostly dyes. The molar extinction coefficient of these photosensitizers and also their photon absorption efficiency (PAE) were evaluated to understand their photosensitizing ability. Therefore, the target properties measured here were: DC, polymerization rate, molar extinction coefficient (ξ) and PAE.

6.2 Materials and methods

The compounds which were investigated for their performance as a photosensitizer were: New Fuchsin, Victoria blue B, Methylene blue chloride, Eosin Y disodium salt, Bromophenol blue sodium salt, Erythrosin B, [3-(3,4-dimethyl-9-oxo-9H-thioxanthen-2-yloxy)-2-hydroxypropyl]trimethylammonium chloride (QTX), Fluorescein sodium salt and Rose bengal sodium salt. All these compounds were purchased from Sigma Aldrich (St. Louis, MO, USA) and used as received. The dental monomers were HEMA and BisGMA which were also obtained from Sigma Aldrich (St. Louis, MO, USA). The hydrophobic photosensitizer was CQ and the hydrophobic co-initiator was EDMAB. DMAEMA was used exclusively as the hydrophilic co-initiator and DPIHP as a reaction accelerator. These PI components were also obtained from Sigma Aldrich (St. Louis, MO, USA).

6.2.1 Rational selection of photosensitizer molecules to form the model building set

The molecular structures of the new photosensitizers that have been investigated are shown in Figure 6.1. The new photosensitizers were selected such that their maximum absorption wavelength fell within the visible range. This is because the light curing unit (LCU) for dental applications operates in the visible range. Since the final goal was to design candidate water compatible visible light photosensitizers, the molecules chosen to form the model building were also hydrophilic in nature. The molecules selected were such that they possessed a wide variety of functional moieties since this would increase the range of functional groups for the combinatorial optimization problem to choose from to generate new molecules. The molecules in the model building set should also possess some structural similarities to ensure development of accurate structure-property relationships (QSPRs). Also to avoid complication, it was ensured that all the molecules in the model building set were available commercially. The molecules that were chosen all have photosensitizing capability.

6.2.2 Preparation of hydrophobic- and hydrophilic-rich phases

The physically separated hydrophobic- and hydrophilic-rich phases were prepared in the same way as discussed in Chapter 5 and shown in Figure 5.1. In this case, the PI components and composition in the formulation from which the two phases are collected are given in Table 6.1. Briefly, the control formulation consisting of BisGMA and HEMA in the ratio of 55:45 wt% was prepared. The PI components were added in the same wt% as shown in Table 6.1 but the wt% was based on the total weight of the neat resin. Then, approximately 33 wt% of D₂O (Cambridge Isotope Laboratories, Andover, MA, USA) was added to produce a mixture beyond the miscibility limit of D₂O. The PI components were then replenished based on the weight of D₂O added. The mixture was vortexed to ensure dissolution of the PI components. The mixture was then separated into the two phases by centrifugation followed by collection of the phases. The concentration of HEMA, BisGMA and D₂O in the final mixture is summarized in Table 6.2. The mixture for each type of new photosensitizer was prepared in triplicate.

Table 6.1. Components of PI and their approximate wt% in the final mixture before phase separation

Name of PI Component	wt%
CQ	0.5
New photosensitizer	0.25
EDMAB	0.25
DMAEMA	0.5
DPIHP	0.5

6.2.3 Photo-polymerization kinetics study

The polymerization kinetic studies for the two phases were carried out separately in the same way as discussed in Chapter 5. Briefly, 30 μl of each phase per new photosensitizer was added onto the ATR crystal of the PerkinElmer Spectrometer Frontier (PerkinElmer, Waltham, MA). The polymerization kinetics study was carried out at a resolution of 4 cm^{-1} . A plastic coverslip was placed on the sample and its edges were sealed using tapes. This was done to prevent the evaporation of D_2O during *in-situ* monitoring of the polymerization kinetics. The polymerization of the hydrophilic-rich phase was monitored for 2 h while the polymerization for the hydrophobic-rich phase was monitored for 1 h. The band ratio profile of C=C at 1637 cm^{-1} to C=O at 1716 cm^{-1} was monitored and used to calculate DC using equation 2.1. For each phase per new photosensitizer, the polymerization kinetic study was carried out in triplicate. The target properties that were determined from this study were DC and polymerization rate for each phase. The polymerization rate was evaluated by differentiating the DC against time graph using Microcal Origin (Version 6.0, Microcal Software, Northampton, MA). D_2O instead of H_2O was used for the same reason as discussed in the earlier chapters.

6.2.4 Determination of molar extinction co-efficient (ξ)

The molar extinction coefficient of a molecule at a given wavelength is the probability of absorption of light by that species (Neumann *et al.*). In this case, the molar extinction coefficient (ξ) was determined at 480 nm which approximately matched the maximum emission wavelength of the halogen LCU (Eacute *et al.*, 2008). With the exception of Victoria blue B and QTX, approximately $9\text{ }\mu\text{M}$ solution of each compound in the model building set was prepared in de-ionized water (DI water). For Victoria blue B and QTX, approximately $27\text{ }\mu\text{M}$ solutions in DI water were prepared because the $9\text{ }\mu\text{M}$ solution produced very low absorption intensity at 480 nm. Then, $200\text{ }\mu\text{l}$ of each solution was transferred to a well in a 96 well flat bottom plate. Using a UV-vis spectrophotometer, Cytation 3 multimode microplate reader (Bio Tek, Winooski, VT), the absorption of each compound at 480 nm was read. This was done in triplicate for each solution. The path length was automatically corrected for 1 cm. The molar extinction coefficient is calculated using the Beer-Lambert law given below:

$$\text{Absorbance} = \xi \times [C_{\text{mol/L}}] \times X_{\text{cm}} \quad 6.1$$

where ξ is the molar extinction co-efficient in $\text{L}/(\text{mol cm})$, $[C]$ is the concentration in mol/L and X is the path length in cm which in this case is 1 cm

6.2.5 Photon absorption efficiency (PAE)

In addition to the molar extinction coefficient, the absorption of light by a photosensitizer also depends on the overlap of the emission spectrum of the LCU and the absorption spectrum of the photosensitizer. PAE determines the overlap between these two spectra and hence can be used as a measure of the efficiency of photosensitizer/LCU combination (Neumann *et al.*; Stahl *et al.*, 2000; Teshima *et al.*, 2003). It is actually a measure of the quantity of photons absorbed by the photosensitizer after irradiation with a LCU of interest (Neumann *et al.*). The UV-vis spectrum of each photosensitizer in the model building set was also obtained using UV-vis spectrophotometer, Cytation 3 multimode microplate reader (Bio Tek, Winooski, VT).

Table 6.2. Composition of mixture before phase separation for each type of photosensitizer in the model building set

Photosensitizer in the model building set	wt% of HEMA	wt% of BisGMA	wt% of D ₂ O	wt% of CQ	wt% of EDMAB	wt% of DMAEMA	wt% of additional photosensitizer	wt% of DPIHP
Bromophenol blue sodium salt	29.31 ± 0.05	35.87 ± 0.06	32.81 ± 0.12	0.52 ± 0.01	0.26 ± 0.01	0.50 ± 0.01	0.25 ± 0.00	0.50 ± 0.00
Eosin Y disodium salt	29.34 ± 0.06	35.94 ± 0.01	32.73 ± 0.05	0.50 ± 0.01	0.25 ± 0.00	0.50 ± 0.01	0.25 ± 0.00	0.50 ± 0.01
Erythrosin B	29.38 ± 0.14	35.92 ± 0.17	32.7 ± 0.30	0.51 ± 0.01	0.26 ± 0.01	0.49 ± 0.00	0.25 ± 0.00	0.49 ± 0.01
Fluorescein sodium salt	29.31 ± 0.02	35.87 ± 0.02	32.84 ± 0.04	0.5 ± 0.01	0.25 ± 0.00	0.49 ± 0.01	0.25 ± 0.00	0.49 ± 0.00
Methylene blue chloride	29.42 ± 0.14	35.95 ± 0.17	32.64 ± 0.30	0.49 ± 0.01	0.25 ± 0.00	0.05 ± 0.00	0.25 ± 0.01	0.50 ± 0.01
New Fuchsin	29.24 ± 0.03	35.74 ± 0.04	33.03 ± 0.08	0.49 ± 0.01	0.25 ± 0.00	0.50 ± 0.00	0.25 ± 0.01	0.50 ± 0.00
QTX	29.24 ± 0.10	35.74 ± 0.11	33.04 ± 0.22	0.49 ± 0.01	0.24 ± 0.01	0.50 ± 0.00	0.25 ± 0.00	0.49 ± 0.01
Rose bengal sodium salt	29.38 ± 0.04	35.86 ± 0.05	32.78 ± 0.08	0.49 ± 0.01	0.25 ± 0.00	0.49 ± 0.00	0.25 ± 0.01	0.49 ± 0.01
Victoria blue B	29.27 ± 0.07	35.74 ± 0.08	33.00 ± 0.14	0.50 ± 0.00	0.25 ± 0.00	0.49 ± 0.00	0.25 ± 0.00	0.49 ± 0.01

The spectrum was obtained using approximately 9 μM solution of each photosensitizer in DI water. In the case of Victoria blue B and QTX, approximately 27 μM solution was used. This was done in triplicate. The

emission spectrum for the halogen LCU Dentsply Spectrum® 800 (SN 9169 Dentsply, Konstanz, Germany) was obtained from the literature (Eacute *et al.*, 2008). The spectral irradiance in mW/cm² of LCU Dentsply Spectrum® 800 (SN 9169 Dentsply, Konstanz, Germany) was converted to the number of photons per square centimeter (cm²) and second (s) using equation 6.2 for each wavelength (Neumann *et al.*):

$$n_{ph\lambda} = \frac{w\lambda}{hc} \quad 6.2$$

where w is the spectral irradiance in mW/cm², λ is the wavelength, h is Planck's constant (6.62607×10^{-30} kgcm²/s) and c is the speed of light in cm/s

Figure 6.2(a) shows the emission spectrum of the LCU Dentsply Spectrum® 800 (SN 9169 Dentsply, Konstanz, Germany) (Eacute *et al.*, 2008) and Figure 6.2(b) shows a representative absorption spectrum of the Eosin Y disodium salt. The $n_{ph\lambda}$ of the LCU for each wavelength is multiplied by the absorption of photosensitizer at the corresponding wavelength. The product of $n_{ph\lambda}$ and absorption was plotted against wavelength and the area under the plot gave a measure of the PAE (Neumann *et al.*). The PAE was normalized for concentration of the solution used to collect the absorption spectra and then the relative normalized PAE was obtained for each photosensitizer.

6.3 Results

6.3.1 Polymerization kinetics study

Incorporation of photosensitizers such as bromophenol blue sodium salt, QTX, rose bengal sodium salt and victoria blue B showed substantial average DC exceeding 50% for the hydrophilic-rich phase. From this study, it is evident that addition of a water compatible photosensitizer will significantly improve the DC of the hydrophilic-rich phase as hypothesized in Chapter 5. New Fuchsin and erythrosine B also led to substantial DC of the hydrophilic-rich phase, approximately 50% and 47% respectively. It was observed that the DC of the hydrophilic-rich phase was sub-optimal in the case of photosensitizers such as fluorescein sodium salt and methylene blue chloride salt. A minimum rate of polymerization of the hydrophilic-rich phase was observed for methylene blue sodium salt. A hydrophilic-rich phase containing QTX exhibited the highest polymerization rate. Compared to previous studies with hydrophilic-rich mimics, discussed in Chapters 2 and 3, the rate of polymerization in this study was much higher. This could be attributed to the absence of DPIHP in the mimics.

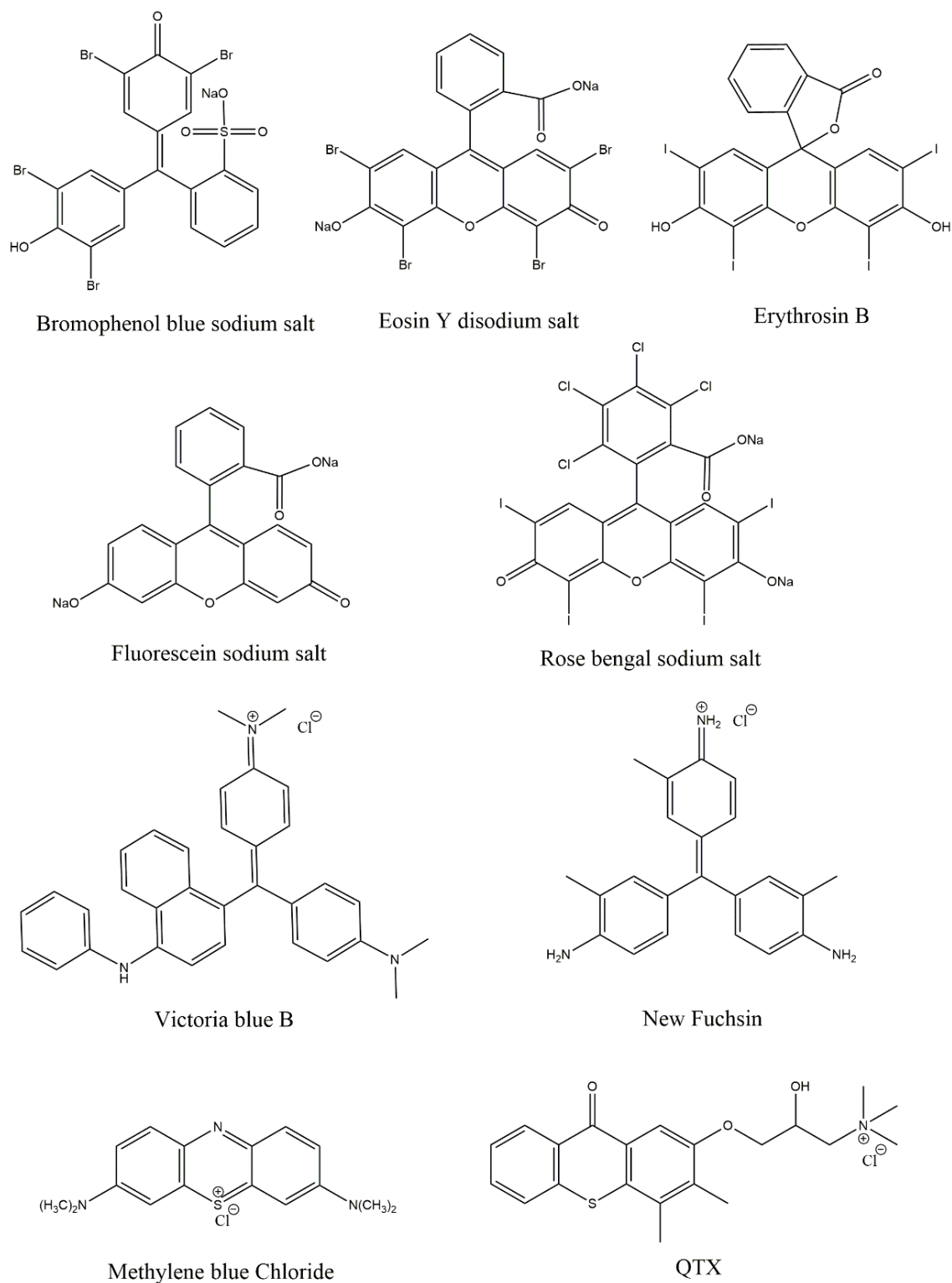


Figure 6.1. Molecular structures of photosensitizers in the model building set

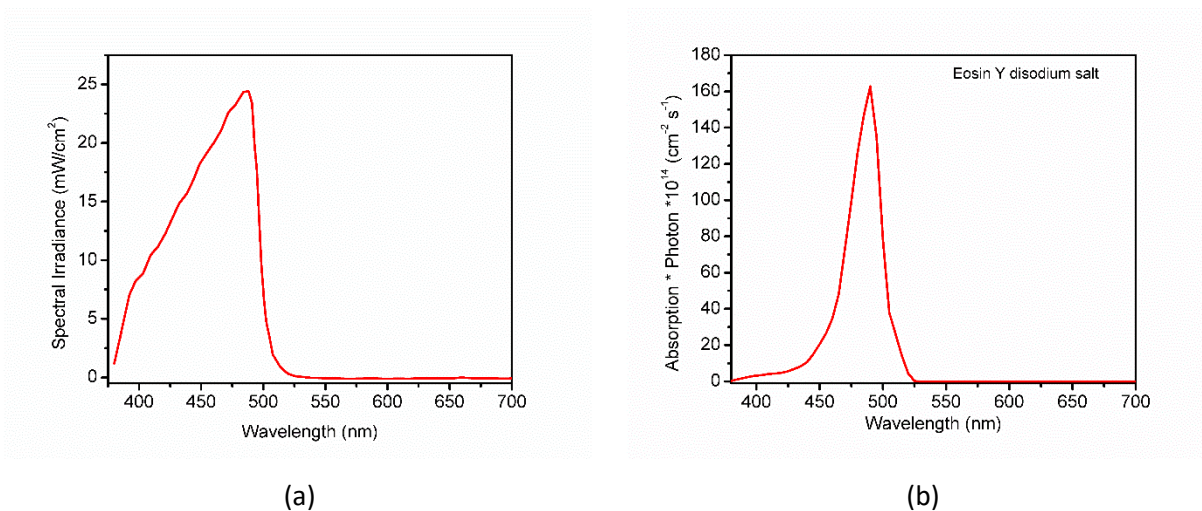


Figure 6.2. (a) Emission spectrum of LCU Dentsply Spectrum® 800 (SN 9169 Dentsply, Konstanz, Germany) (Eacute *et al.*, 2008) and (b) representative absorption spectrum of the photosensitizer Eosin Y disodium salt

A similar rate of polymerization was observed for the hydrophilic-rich phase with the PI system CQ/DMAEMA/DPIHP and CQ/EDMAB/DPIHP in Chapter 5. Figure 6.3 shows the representative polymerization kinetics result for the hydrophilic-rich phase and Table 6.3 summarizes the average DC and polymerization rate for this phase. The polymerization rate of the hydrophilic-rich phase with rose bengal sodium salt exhibited two peaks, and the secondary rate maxima appeared as a shoulder peak. For rose Bengal sodium salt, Table 6.3 shows the rate maxima for the highest peak.

A substantial DC was observed for all the hydrophobic-rich phases, except when fluorescein sodium salt was used as the photosensitizer in addition to CQ. In the presence of the fluorescein sodium salt, the average DC was approximately 20%. The average DC was above 70% in the case of the other photosensitizers in the model building set. In the case of methylene blue chloride, New Fuchsin and Victoria blue B, the average DC of the hydrophobic-rich was above 90%. Figure 6.4 shows representative polymerization kinetics results for the hydrophobic-rich phase. Table 6.4 summarizes the average DC and rate of polymerization for the hydrophobic-rich phase. A minimum polymerization rate was observed in the case of fluorescein sodium salt and the maximum polymerization rate was observed for the bromophenol blue sodium salt for the hydrophobic-rich phase. As mentioned earlier, two rate maxima were observed for the PI system with the rose bengal sodium salt. For the hydrophobic-rich phase, in addition to the rose bengal sodium salt, the photosensitizer Eosin Y disodium salt also exhibited double

peaks. For both these photosensitizers, Table 6.4 shows the average rate corresponding to the highest peak.

Table 6.3. Average DC and polymerization rate of the hydrophilic-rich phase for each photosensitizer in the model building set

Hydrophilic photosensitizer in the formulation before phase separation	Average DC	Average polymerization rate (s^{-1})
Bromophenol blue sodium salt	0.56 ± 0.04	0.021 ± 0.001
Eosin Y disodium salt	0.20 ± 0.07	0.037 ± 0.011
Erythrosin B	0.47 ± 0.08	0.016 ± 0.002
Fluorescein sodium salt	0.08 ± 0.03	0.036 ± 0.002
Methylene blue chloride	0.06 ± 0.01	0.010 ± 0.001
New Fuchsin	0.50 ± 0.07	0.020 ± 0.002
QTX	0.56 ± 0.11	0.066 ± 0.018
Rose Bengal sodium salt	0.54 ± 0.05	0.025 ± 0.007
Victoria blue B	0.58 ± 0.02	0.023 ± 0.002

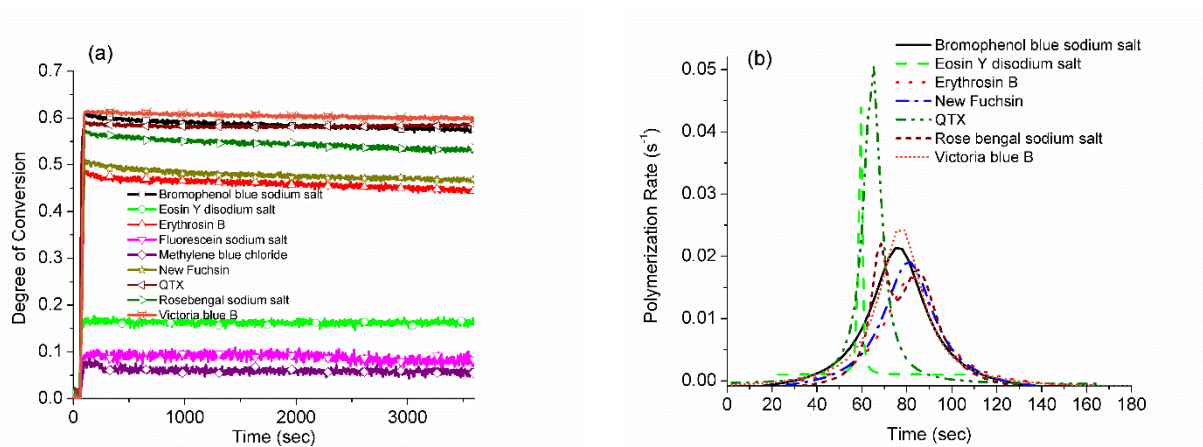


Figure 6.3. Polymerization kinetic result of hydrophilic-rich phase showing (a) DC versus time and (b) polymerization rate against time. The polymerization rate of the hydrophilic-rich phase representing fluorescein sodium salt and methylene blue chloride are not shown because their DC is very low

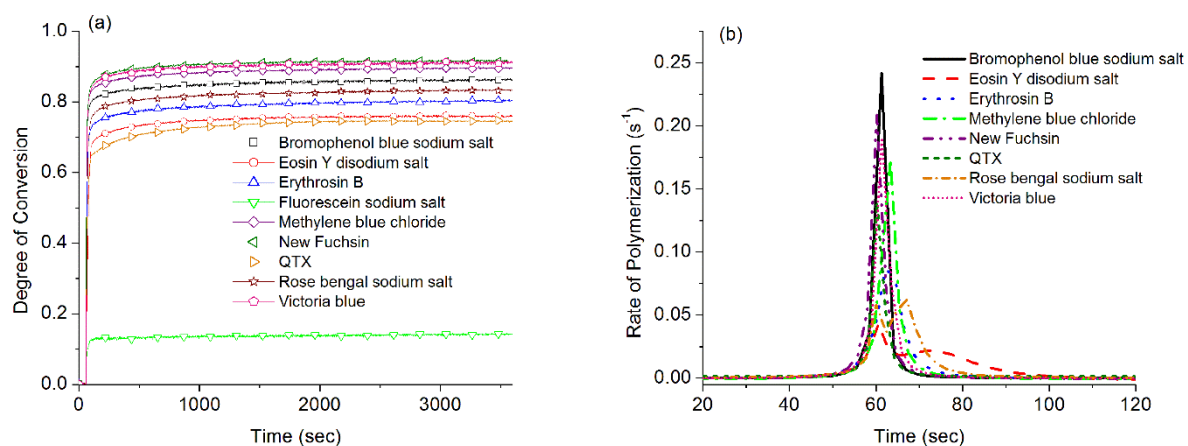


Figure 6.4. Polymerization kinetic result of hydrophobic-rich phase showing (a) DC versus time and (b) polymerization rate against time. The polymerization rate of the hydrophobic-rich phase representing fluorescein sodium salt is not shown because its rate is very low

Table 6.4. Average DC and polymerization rate of the hydrophobic-rich phase for each photosensitizer in the model building set

Hydrophilic photosensitizer in the formulation before phase separation	Average DC	Average polymerization rate (s^{-1})
Bromophenol blue sodium salt	0.88 ± 0.02	0.242 ± 0.001
Eosin Y disodium salt	0.70 ± 0.05	0.046 ± 0.001
Erythrosin B	0.81 ± 0.04	0.091 ± 0.027
Fluorescein sodium salt	0.20 ± 0.05	0.028 ± 0.004
Methylene blue chloride	0.90 ± 0.01	0.175 ± 0.009
New Fuchsin	0.93 ± 0.02	0.199 ± 0.019
QTX	0.74 ± 0.04	0.147 ± 0.043
Rose Bengal sodium salt	0.85 ± 0.02	0.058 ± 0.007
Victoria blue B	0.91 ± 0.01	0.195 ± 0.009

6.3.2 Molar extinction coefficient of photosensitizers

The molar extinction coefficients at 480 nm of the dyes were higher than that for QTX. The photosensitizer molecules exhibited a wide range of molar extinction coefficient starting at approximately 234 L mol⁻¹ cm⁻¹ to 76883 L mol⁻¹ cm⁻¹. The highest molar extinction coefficient at 480 nm was observed for the photosensitizer, new fuchsin and lowest for QTX. This indicates that the probability of new fuchsin molecules transitioning to the excited state after irradiation with halogen LCU will be higher than that for the other molecules in the model building set. Table 6.5 summarizes the maximum absorption wavelength for each photosensitizer in the model building set and their molar extinction coefficients at 480 nm. It could be seen from Table 6.5 that all the molecules in the model building set possessed a peak wavelength in the visible range which was an important criteria for dental adhesive curing.

Table 6.5. Average molar extinction coefficient and peak wavelength of photosensitizers in the model building set

Photosensitizer in the model building set	Peak wavelength (nm)	Average molar extinction coefficient at 480 nm (L/(mol cm))
Bromophenol blue sodium salt	590	14143 ± 510
Eosin Y disodium salt	515	51471 ± 1550
Erythrosin B	525	13750 ± 1674
Fluorescein sodium salt	480	46208 ± 1617
Methylene blue chloride	663	1594 ± 232
New Fuchsin	545	76883 ± 683
QTX	403	235 ± 154
Rose Bengal sodium salt	550	8001 ± 1792
Victoria blue B	615	5269 ± 134

6.3.3 Photon absorption efficiency (PAE)

The photosensitizers exhibited a wide range of relative normalized PAE. New fuchsin had the highest relative normalized PAE showing that it had the highest capability to absorb photons among all the molecules in the model building set when irradiated with the halogen LCU. Figure 6.5 shows the representative absorption spectrum and the graphs used to determine the relative normalized PAE of the

photosensitizers. Table 6.6 summarizes the average relative normalized PAE for each photosensitizer molecule. Methylene blue chloride, QTX and victoria blue B exhibited very low average relative normalized PAE (Table 6.6).

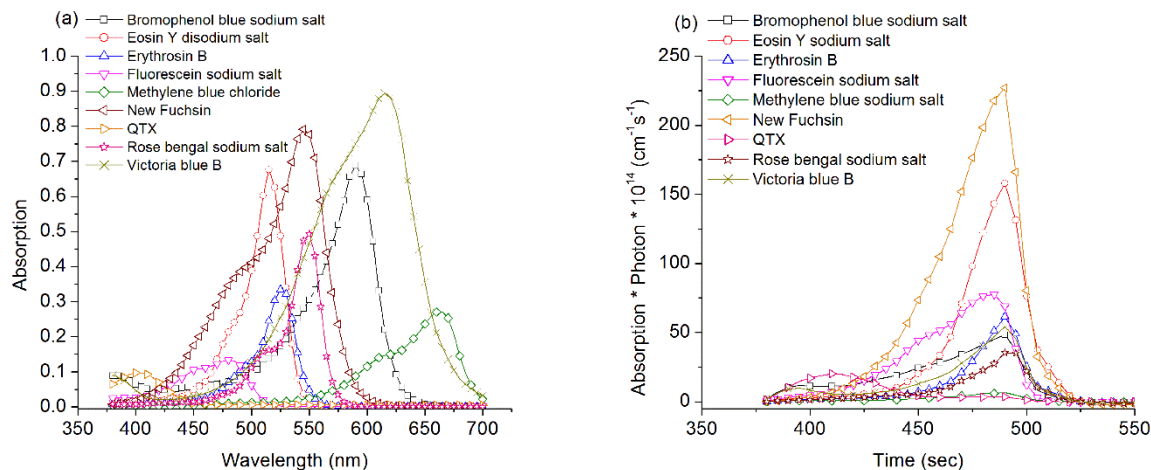


Figure 6.5. (a) Absorption spectrum and (b) graph showing the product of emission spectrum of the LCU and absorption spectrum of each photosensitizer molecule in the model building set. The concentration of the solution was 9 μM except in case of QTX and victoria blue B. In case of the latter two the concentration was 27 μM

Table 6.6. Summary of average relative normalized PAE of each photosensitizer in the model building set

Photosensitizer	Relative normalized PAE
Bromophenol blue sodium salt	3.14 ± 0.08
Eosin Y disodium salt	6.30 ± 0.36
Erythrosin B	2.19 ± 0.07
Fluorescein sodium salt	4.42 ± 0.07
Methylene blue chloride	0.29 ± 0.04
New Fuchsin	10.65 ± 0.07
QTX	0.36 ± 0.03
Rose Bengal sodium salt	1.46 ± 0.03
Victoria blue B	0.85 ± 0.02

6.4 Discussion

It can be seen that in the case of the fluorescein sodium salt, the molar extinction coefficient at 480 nm was high but the relative normalized PAE was moderate. Despite high molar extinction coefficient and moderate relative normalized PAE, the DC and polymerization rate of both the hydrophobic- and hydrophilic-rich phases for the fluorescein sodium salt (Table 6.4) was low. It could be assumed that the photo-polymerization within the hydrophobic-rich phase was mostly initiated by CQ since it would be present in a high concentration within this phase and in a very low concentration within the hydrophilic-rich phase. Since the addition of fluorescein sodium salt led to poor polymerization of the hydrophobic-rich, it could be that it interfered with CQ in triggering the radical formation process. Although the polymerization rate of the hydrophilic-rich phase in its presence was much higher compared to most of the other dyes, the average DC was very poor. It could be that the radicals in the presence of fluorescein sodium salt were also not effective or efficient in triggering the polymerization reaction which led to a poor DC of the hydrophilic-rich phase.

The DC of the hydrophobic-rich phase was substantial in the case of all other photosensitizers. This result indicates that the other photosensitizers did not interfere with the performance of the CQ. For the hydrophobic-rich phase, CQ is mostly responsible for initiating the polymerization reaction. In case of methylene blue chloride, new fuchsin and Victoria blue B, the average DC of the hydrophobic-rich phase was close to or higher than 90%. Although the rate of polymerization of the hydrophobic-rich phase for eosin Y disodium salt and rose bengal sodium salt were lower than that of the other compounds, the formation of radicals was sufficient and effective to result in a substantial DC.

Most of the photosensitizers in the model building set led to a much higher polymerization rate for the hydrophilic-rich phase when compared to methylene blue chloride and erythrosine B. It was found that the average DC of the hydrophilic-rich phase for bromophenol blue sodium salt, erythrosine B, new fuchsin, QTX, rose bengal sodium salt and Victoria blue B were substantially high. It is possible that the high DC observed for the hydrophilic-rich phase was contributed by these additional photosensitizers. It should be noted that the relative normalized PAE for QTX, rose bengal sodium salt and Victoria blue B were low indicating that their ability to absorb photons when irradiated with dental halogen LCU was poor as compared to the other photosensitizers, and moreover the molar extinction coefficient of QTX was very low. Despite the low PAE and molar extinction coefficient, it was possible that the radicals produced in these three cases were highly effective in initiating the polymerization reaction leading to a substantial DC. Again, the average DC of the hydrophilic-rich phase for eosin Y disodium salt was only 20%, and thus

it was possible that in this case mostly CQ and DPIHP were responsible for the observed DC. Although the molar extinction coefficient and PAE were both higher for eosin Y disodium salt, the radicals formed might not be as effective as in the case of bromophenol blue sodium salt, erythrosine B, QTX, rose bengal sodium salt and Victoria blue B. Therefore, high molar extinction and PAE of a photosensitizer may not always reflect its performance in the polymerization reaction, and the efficiency of the radicals in triggering the reaction is also an important factor to consider which is captured by the DC. Methylene blue chloride exhibited low molar extinction coefficient and poorest PAE indicating that it could lead to a lower quantity of radicals. Low concentration of radicals or low efficiency of the generated radicals could cause poor DC of the hydrophilic-rich phase for methylene blue chloride. Therefore, the combination of all three of the parameters, i.e. molar extinction coefficient, PAE and DC should be considered in evaluating the performance of a photosensitizer.

6.5 Conclusion

This study evaluates the potential of various photosensitizers to be used in the dental adhesive for improving the DC of the hydrophilic-rich phase. The following summarizes the outcomes of this study:

- It is important to consider the interaction between CQ and the additional photosensitizer since the latter can impair the performance of CQ as in the case of fluorescein sodium salt.
- In addition to the molar extinction coefficient and PAE, the efficiency of the radicals to trigger the photo-polymerization reaction is also important. In this study, the efficiency of the radicals due to the photosensitizers in the model building set is depicted by the DC of the hydrophilic-rich phase. Therefore, combination of all three parameters should be considered to evaluate the performance of the photosensitizer for dental applications.
- This study showed that the addition of an efficient photosensitizer of hydrophilic nature can significantly improve the DC of the hydrophilic-rich phase of dental adhesive.

CHAPTER 7: COMPUTER-AIDED MOLECULAR DESIGN (CAMD) OF WATER-COMPATIBLE VISIBLE LIGHT PHOTSENSITIZER FOR DENTAL ADHESIVE APPLICATION

7.1 Introduction

In the previous chapter, the model building set and the determination of target properties for the computer-aided molecular design of water-compatible photosensitizers have been discussed. In this chapter, the forward problem of CAMD involving the development of quantitative structure property relationships (QSPRs) and the inverse problem involving the optimization formulation have been discussed. CAMD is a cost effective and efficient technique to predict candidate molecular structures which possess near optimal properties. In this technique, the molecular structure can be optimized for several properties simultaneously, which is difficult to achieve by the trial and error method. For this method, the target properties should be dependent on the molecular structure. The inverse problem is solved via optimization algorithm which can be either deterministic in nature or stochastic. In this case, Tabu Search has been employed which is a stochastic method.

7.2 Materials and method

7.2.1 Forward problem: Target properties and model building set

The criteria based on which the model building set was chosen were discussed in Chapter 6. Most of the molecules in the model building set were dyes. The structural features with delocalized electrons such as C=N, C=C and aromatic rings allow a photosensitizing capability of the molecules. The target properties for the CAMD were: molar extinction coefficient (ξ), relative normalized photon absorption efficiency (PAE), degree of conversion (DC), polymerization rate (RT) and octanol/water partition coefficient. Molar extinction coefficient dictates the probability of the photosensitizer to be promoted to an excited state after absorption of light, and hence can impact the generation of radicals responsible for initiating the polymerization reaction. The absorption of light by a photosensitizer also depends on the LCU. The efficiency of LCU and photosensitizer combination is measured by PAE. Therefore, PAE can also influence the formation of radicals for initiation of the polymerization reaction. The molar extinction coefficient and PAE are dependent on the photochemistry of the photoinitiator. Although the generation of sufficient reactive species is important, their efficiency to initiate the polymerization reaction also needs to be considered. Degree of conversion (DC) could reflect the effectiveness of the reactive species to trigger the polymerization reaction. Dental adhesive shrinkage after polymerization may compromise the seal at the a/d interface, and a high polymerization rate is usually accompanied by enhanced

shrinkage. So polymerization rate was considered as one of the target properties. Here, only the DC and polymerization rate of the hydrophilic-rich phase was considered since this phase underwent poor polymerization in presence of the conventional PI system (CQ/EDMAB). In this study, the natural logarithm of molar extinction coefficient ($\ln(\xi)$) was used to develop the QSPR for this property. The partition concentration within the hydrophilic-rich phase is an important parameter. Since inadequate radicals could impair the polymerization reaction, it is important to ensure that the photosensitizer is present in sufficient concentration within the hydrophilic-rich phase. Therefore, octanol/water partition coefficient which is a measure of hydrophilicity of a molecule has been included as a target property.

The structures of molecules in the model building set used to determine the first four properties are given in Figure 6.1. The model building set for the target property, octanol/water partition coefficient consisted of Bromophenol blue, Eosin Y, Erythrosin B, Fluorescein, Methylene blue chloride, Rose bengal, Victoria blue B and Victoria blue R (Figure 7.1). Octanol/water partition coefficient of these molecules were obtained from the literature (Pellosi *et al.*, 2012; Sheikh, 1976; Wagner *et al.*, 1998; Wainwright *et al.*). Here, logarithm of the octanol/water partition coefficient ($\log P$) was used to develop the QSPR for this property. Table 7.1 shows the $\log P$ of the molecules in the model building set.

Table 7.1. Summary of $\log P$ of molecules in the model building set

Name of the molecule	$\log P$	Reference
Eosin Y	0.18	(Pellosi et al., 2012)
Fluorescein	-0.32	(Pellosi et al., 2012)
Rose bengal	0.59	(Pellosi et al., 2012)
Erythrosin B	0.46	(Pellosi et al., 2012)
Methylene blue	-0.96	(Wagner et al., 1998)
Bromophenol blue	-2.35	(Sheikh, 1976)
Victoria blue R	1.59	(Wainwright et al., 1999)
Victoria blue B	2.8	(Wainwright et al., 1999)

7.2.2 Connectivity indices as topological descriptors

Here, connectivity indices were used to describe the structure of the molecules in the model building set mathematically. To calculate the connectivity indices of various orders, first hydrogen-suppressed connectivity graph of the molecule is drawn, which consists of only connections between non-hydrogen atoms. Figure 7.2 shows an example of a hydrogen-suppressed graph for one of the dyes such as new fuchsin. The first atomic index, δ for each non-hydrogen atom in a molecule is calculated from the hydrogen suppressed graph, and it is equal to the number of edges from the non-hydrogen atom

(Bicerano, 2002). The second atomic index, δ^v of a non-hydrogen atom in the hydrogen suppressed graph can be obtained from the following equation (Bicerano, 2002):

$$\delta^v = \frac{Z^v - N_H}{Z - Z^v - 1} \quad 7.1$$

where Z^v is the number of valence electrons of a non-hydrogen atom, Z is the total number of valence electrons and the number of electrons in the inner shells, and N_H is the number of hydrogen atoms bonded to the non-hydrogen atom

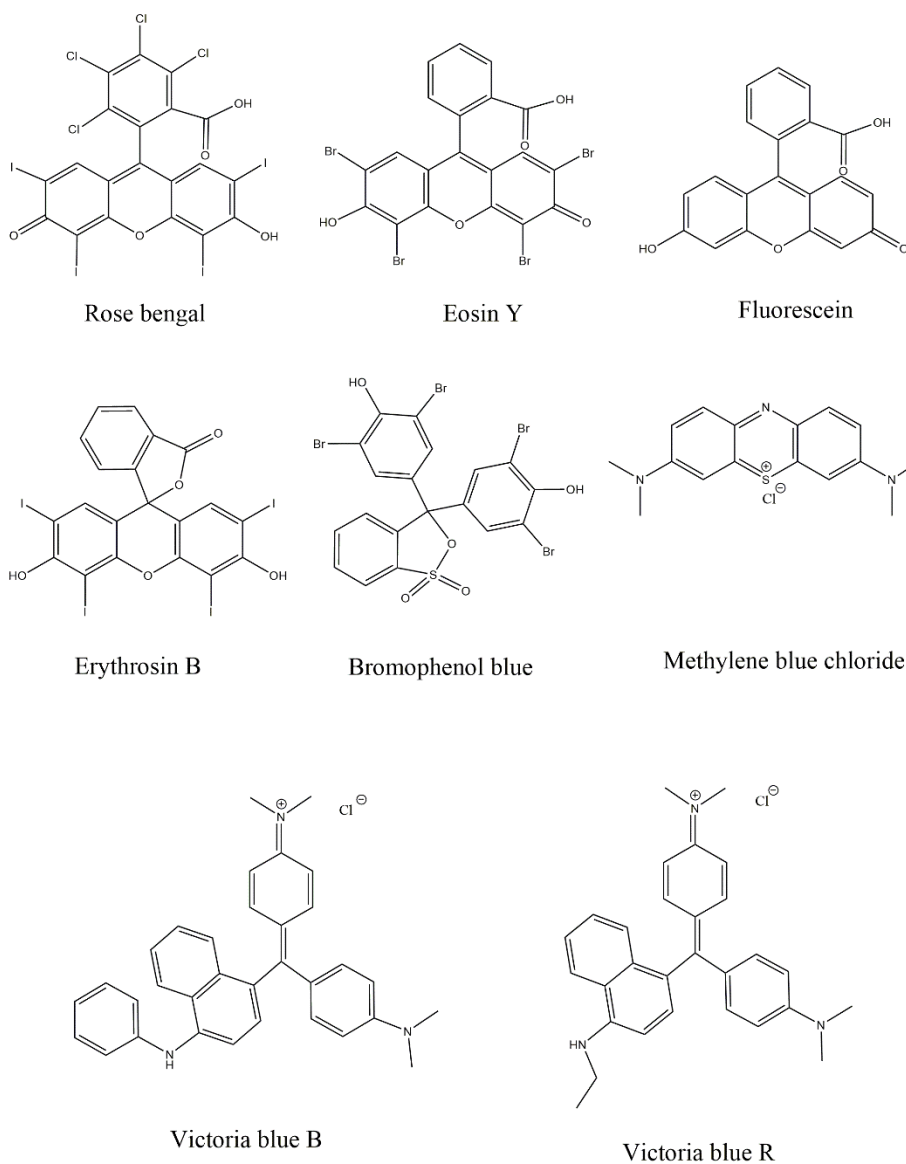


Figure 7.1. Molecular structure of molecules in the model building set for log P

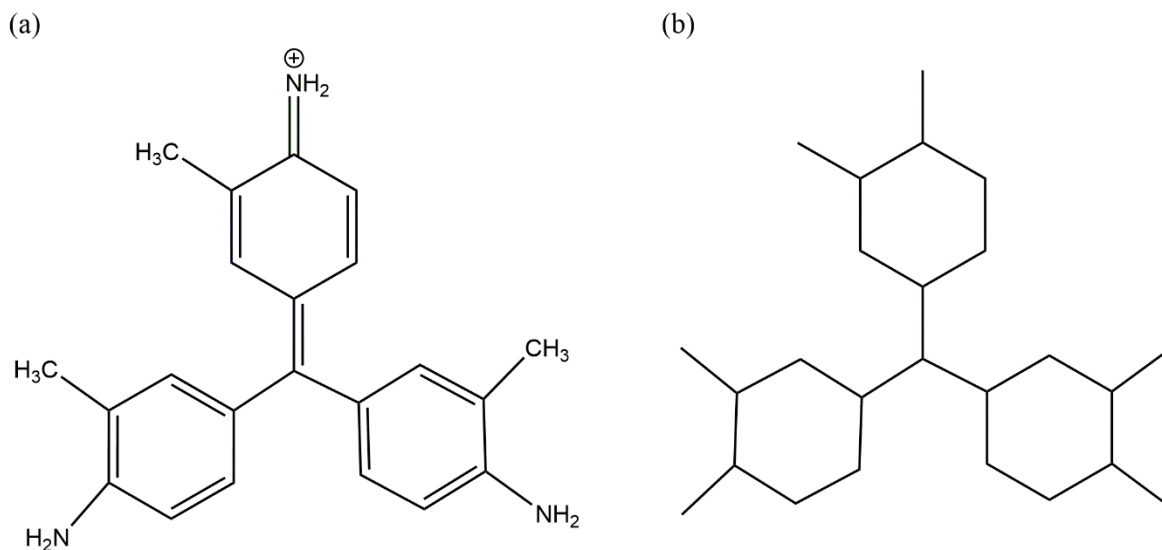


Figure 7.2. (a) Molecular structure and (b) hydrogen suppressed graph of new fuchsin

In this case, the connectivity indices up to fifth order were calculated for the molecules in the model building sets. Here, connectivity indices of anions of bromophenol blue sodium salt, rose bengal sodium salt, eosin Y disodium salt, fluorescein sodium salt, and cations of victoria blue B, new fuchsin, methylene blue chloride and QTX were determined. In case of erythrosine B, the connectivity indices of the neutral molecule were determined. In case of the structures in the model building set for the octanol/water partition coefficient, the connectivity indices of the neutral molecules were determined except for the Victoria blue B and Victoria blue R. For these two molecules, connectivity indices of the cations were evaluated. For the anion, the charged atom will have one excess valence electron, and for the cation the charged atom will be deficient of one electron. The generalized formula for calculating the connectivity indices of a molecule is given below (Roughton, 2013):

$${}^n\chi = \sum_{k=1}^{N_s} \left(\prod_{i=1}^{n+1} \frac{1}{\delta_i} \right)^{\frac{1}{k}} \quad 7.2$$

where ${}^n\chi$ is the connectivity index of n^{th} order, and N_s is the number of subgraphs of path length n

The valence connectivity indices of a molecule is calculated similarly, but δ^v is used instead of δ as shown in equation 7.3. The zeroth order connectivity index for an entire molecule is calculated by summing $1/\delta$ of the non-hydrogen atoms within the molecule and for the zeroth order valence connectivity index $1/\delta^v$ are summed. The first order connectivity index of an entire molecule sums $1/\delta_1 \times \delta_2$ over the edge or bond between non-hydrogen atoms within the molecule where δ_1 is the first

atomic index of one non-hydrogen atom and δ_2 is that of the non-hydrogen atom bonded to the former. In other words, the summation is done over a path length of 1. The first order valence connectivity index of a molecule is calculated similarly, but second atomic indices of non-hydrogen atoms are used instead. The path length over which the summation is done increases with the increase in the order of the connectivity indices. Tables 7.2 and 7.3 show the connectivity indices and valence connectivity indices of the molecules in the model building sets shown in Figures 6.1 and 7.1. The extent of structural information of a molecule that is captured by the connectivity indices increases with its order. Figure 7.3 shows a schematic of the entire forward problem of CAMD in detail. Appendix A shows the source code for calculating the connectivity indices of molecules in Matlab® using a path finding algorithm. The connectivity indices of the molecules were also checked using the software E-dragon 1.0 (Tetko *et al.*).

$${}^n\chi^v = \sum_{k=1}^{N_s} \left(\prod_{i=1}^{n+1} \frac{1}{\delta_i^v} \right)_k^{\frac{1}{2}} \quad 7.3$$

7.2.3 Development of quantitative structure property relationships (QSPRs)

A quantitative structure property relationship (QSPR) is a mathematical equation correlating the molecular descriptors to a target property. In this study, the statistical software package R was used to select the descriptors and develop the QSPRs by linear regression. Descriptors were selected using the Leaps package in R (Lumely, 2009). The process of developing models for target properties in R and the code for the process have been discussed by Roughton *et al.* in detail (Roughton, 2013). Connectivity indices up to fifth order were used and hence there were a total of twelve descriptors. At first, linear regression using all twelve descriptors was carried out, and based on the correlation coefficient, R^2 the number of descriptors was reduced. The number of descriptors was reduced to 5 for reaction rate, 6 for log P and 7 for the rest of the properties (DC, $\ln(\xi)$ and relative normalized PAE). The reduced number of descriptors was used in linear regression and models with lowest Mallows' C_p statistic and good R^2 were finally chosen for all the properties. A model with low C_p statistic indicates that the model possesses higher precision and minimal bias. With the incorporation of more and more descriptors in the model, the C_p statistic decreases but after a certain number of descriptors it begins to increase to account for overfitting and bias (Roughton, 2013; Roughton *et al.*, 2012b). Figure 7.4 shows the graphs for C_p statistic versus the number of descriptors in the case of all five target properties. In all the cases, the model with the minimum C_p statistic was selected. The following expression is used to calculate the Mallows' C_p statistic (Roughton, 2013):

$$C_p = \sum_{i=1}^m (Y_i - \bar{Y}_i)^2 + 2p\sigma^2$$

7.4

where m is the total number of data points, p is the total number of descriptors, Y_i is the experimental data, \bar{Y}_i is the corresponding predicted value for the data, and σ^2 is the residual variance

Table 7.2. Summary of connectivity indices of the molecules used to develop QSPRs

Name of molecule	${}^0\chi$	${}^1\chi$	${}^2\chi$	${}^3\chi$	${}^4\chi$	${}^5\chi$
Bromophenol blue sodium salt	21.508	13.502	13.589	10.803	8.491	6.657
Bromophenol blue	21.137	13.575	13.739	11.958	9.834	8.444
Eosin Y disodium salt	21.033	13.718	13.187	11.951	9.658	8.306
Eosin Y	21.033	13.718	13.187	11.951	9.658	8.306
Erythrosin B	20.662	13.769	13.487	12.931	10.933	9.817
Fluorescein	17.552	12.042	11.354	9.427	8.435	7.497
Fluorescein sodium salt	17.552	12.042	11.354	9.427	8.435	7.497
Methylene blue chloride	14.276	9.542	9.146	7.457	5.913	5.256
New Fuchsin	18.138	11.863	11.161	9.549	6.971	5.927
QTX	19.060	12.171	12.292	9.258	7.857	6.139
Rose Bengal sodium salt	24.514	15.378	15.166	14.086	11.119	9.405
Rose bengal	24.514	15.378	15.166	14.086	11.119	9.405
Victoria blue B	25.070	17.508	15.768	13.364	11.238	9.510
Victoria blue R	22.665	15.490	13.817	11.662	9.824	8.222

To perform CAMD using QSPRs, it is important to ensure that the models are able to accurately predict the target properties of interest. Here, the final models were cross-validated to understand their predictive capability. As mentioned earlier, the predictive squared correlation (Q^2) was used as a measure of the model's predictive capability. Models with Q^2 close to R^2 have good predictive capability. The cross-validation was carried out using the Leave-one-out cross-validation (LOOCV) method using the DAAG package in the R software. In this method, after leaving out each molecule separately from the model building set, the properties were correlated again using the selected descriptors in the final model. The new correlation was then used to predict the property of the molecule that had been left out.

Table 7.3. Summary of valence connectivity indices of the molecules used to develop QSPRs

Name of molecule	${}^0\chi^v$	${}^1\chi^v$	${}^2\chi^v$	${}^3\chi^v$	${}^4\chi^v$	${}^5\chi^v$
Bromophenol blue sodium salt	21.249	12.318	10.599	7.280	5.824	3.337
Bromophenol blue	21.319	12.578	11.224	8.399	7.142	4.729
Eosin Y disodium salt	20.301	11.104	9.332	6.994	5.546	3.482
Eosin Y	20.439	11.174	9.398	7.100	5.574	3.504
Erythrosin B	22.725	12.521	10.996	8.679	7.346	4.687
Fluorescein	12.893	7.567	5.666	4.104	3.037	2.242
Fluorescein sodium salt	12.754	7.498	5.595	4.064	3.007	2.218
Methylene blue chloride	13.147	7.501	6.546	4.631	3.339	2.716
New Fuchsin	15.058	8.395	6.659	4.748	3.014	2.128
QTX	16.867	9.755	9.211	5.966	4.467	3.022
Rose Bengal sodium salt	26.813	14.188	12.492	10.037	7.899	4.699
Rose bengal	26.951	14.257	12.558	10.160	7.935	4.729
Victoria blue B	21.417	12.409	9.591	6.670	4.677	3.298
Victoria blue R	19.737	11.309	8.630	5.984	4.236	2.972

Therefore, here the number of folds over which the cross-validation was done was equal to the total number of molecules in the model building set. The predictive capability of a model is challenged more when the number of folds, k for cross-validation decreases (Roughton, 2013). When the number of folds is less than the number of molecules in the model building set, for each fold equal number of data points are left out, and as k decreases, the number of data points left out increases (Roughton, 2013). In the case of the properties of interest; $\ln(\xi)$, relative normalized PAE, DC and polymerization rate, the number of folds for the cross-validation was 9, while for $\log P$ it was 8. It should also be noted that the R^2 and Q^2 of a model is dependent on the accuracy of the experimental data. Factors such as experimental conditions and sensitivity of the instruments introduce errors in the experimental data which are not taken into account in the QSPRs. Therefore, the predictive ability of the QSPRs will also have limitations especially for complex properties such as the DC and rate of polymerization. This is reflected by the Q^2 for these two properties since the Q^2 for these are not as close to the R^2 as in the case of the other three properties.

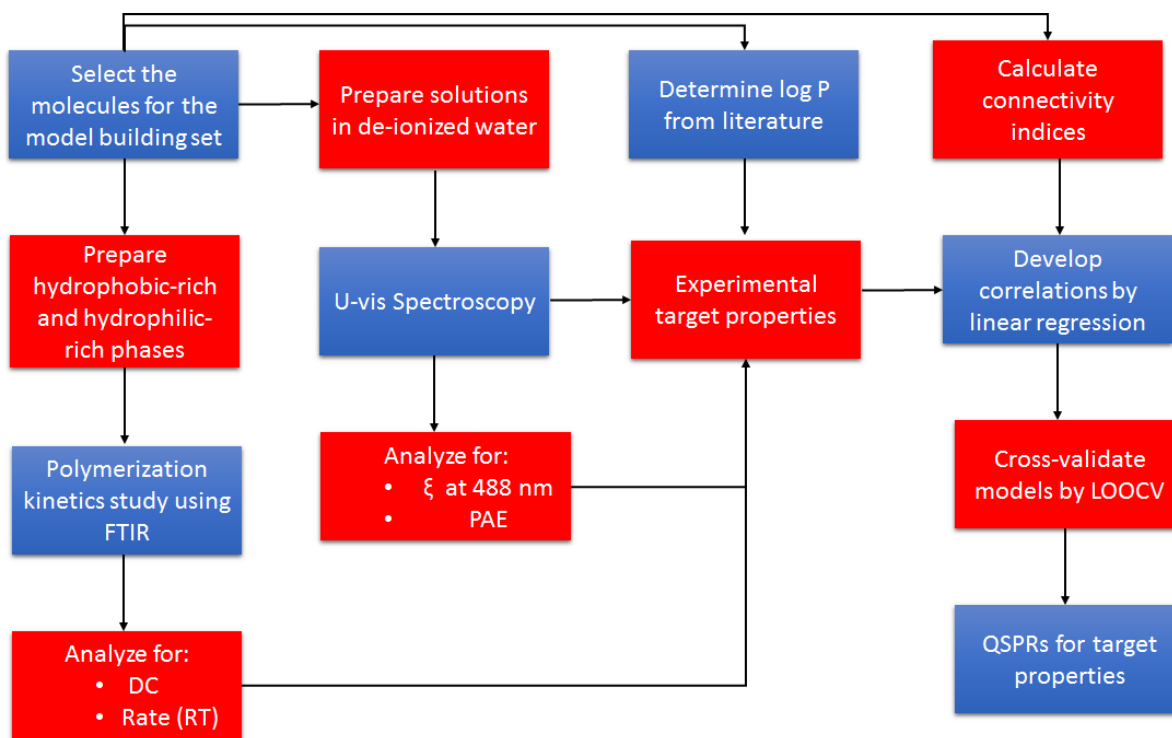


Figure 7.3. Schematic showing steps for the forward problem of CAMD

7.2.4 Inverse problem: CAMD formulation and Tabu Search

Here, an existing design framework by Roughton *et al.* for carbohydrate excipient design known as the “Carbohydrate Excipient Designer” was employed. The existing design framework was written in Visual Basic (VBA) while Microsoft excel was used for the database (Roughton, 2013; Roughton *et al.*, 2012b).

For the design of a photosensitizer, the molecules in the model building set were used to create 42 molecular sub-groups with two free terminals at their ends. These molecular fragments were used to create the new solutions. For the purpose of designing a photosensitizer, the existing design framework “Carbohydrate Excipient Designer” was modified by including the relevant 42 sub-groups. These sub-groups were expressed as an array of group numbers and each group consisted of adjacency matrix of the group, and vectors containing Z and Z' of each non-hydrogen atoms in the group. Finally the number of hydrogen atoms, N_H to which each non-hydrogen atoms in the group was connected was also included as a vector for each sub-group. The structures of the 42 groups used for the photosensitizer design are shown in Appendix B and the ends denoted by ‘X’ in the structures are the connectors.

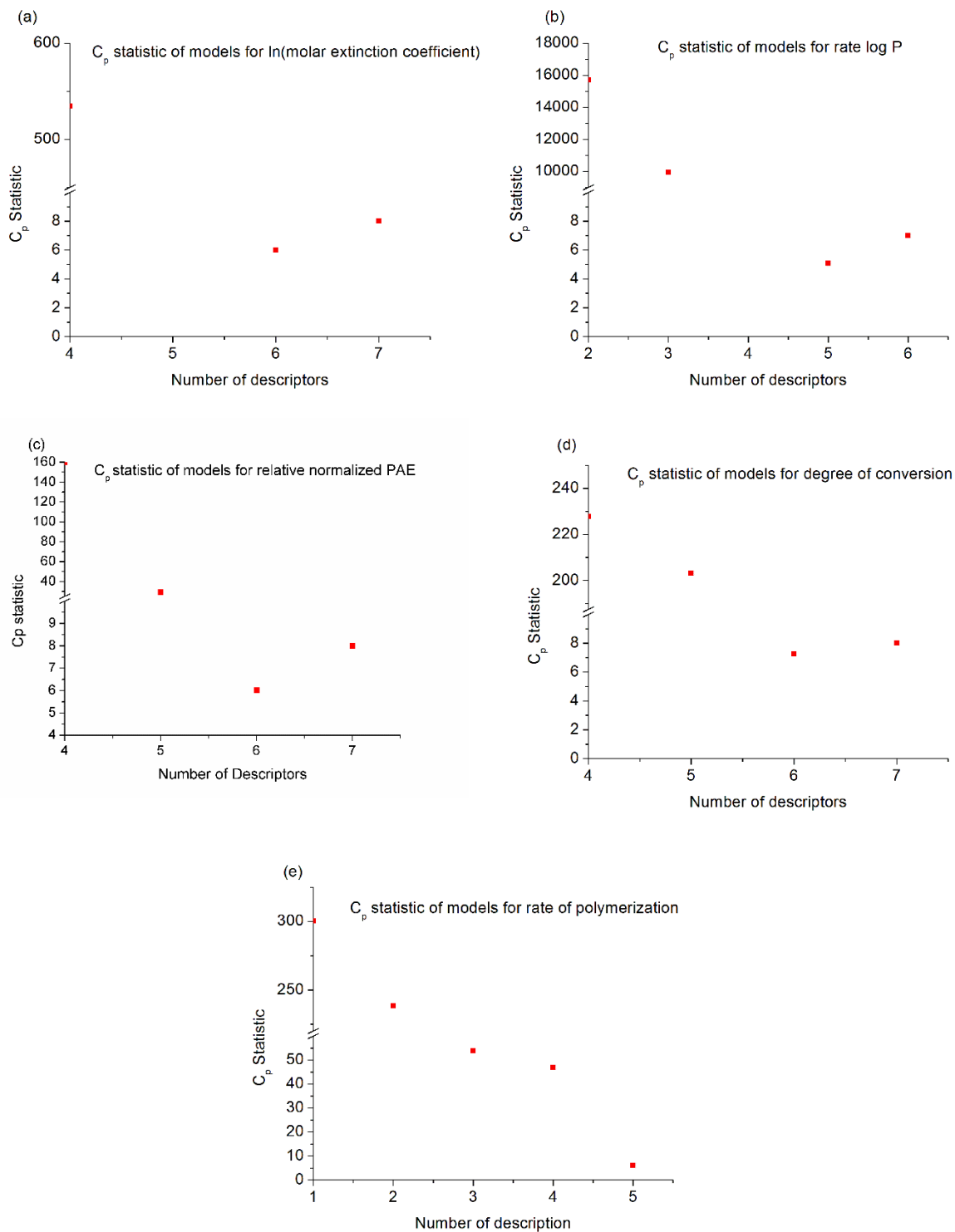


Figure 7.4. Variation of C_p statistic with the number of descriptors in the models for (a) $\ln(\xi)$ (b) $\log P$ (c) relative normalized PAE (d) degree of conversion (DC) and (e) rate of polymerization (RT)

The property calculations were also modified to incorporate QSPRs of relevant target properties. The changes made to the existing design framework are given in Appendix C. To understand the working principle of the design framework in detail, the reader is directed to the previous study by Roughton *et al.* on the design of carbohydrate excipient (Roughton, 2013). The readers are also directed to the same study for the source code (Roughton, 2013). Here, only a brief discussion on the working principle of “Carbohydrate Excipient Designer” will be provided. As already mentioned, the molecular sub-groups acted as the building blocks to create new solutions. For this study a maximum of 6 groups in the solution were allowed from a total of 42 sub-groups. Since the order in which the sub-groups are chosen is important and repeated sub-groups are allowed, the overall number of permutations for this combinatorial problem turns out to be approximately 5489 million. Hence, there can be a maximum 5489 million possibilities to choose from which clearly indicates the need for an optimization technique to determine near optimal solutions. At first, an initial solution is provided by selecting specific random group numbers which are connected to form a molecule. The design framework can also create random initial solutions automatically. Each time a new molecule is generated or an existing solution is modified (discussed in the next section), adjacency matrix, vectors containing Z , Z' and N_H are updated to represent the molecule (Roughton, 2013). This information allows calculation of connectivity indices for the new molecule which are then used to calculate target properties. In this study the terminal groups were kept constant to a hydroxyl group (-OH).

The function “atoms” in the program stores information regarding the total number of non-hydrogen atoms in each sub-group (Roughton, 2013). The function “Name” assigns a name to each excel worksheet representing the molecular structures of the sub-group in terms of adjacency matrix, vectors containing Z , Z' and N_H (Roughton, 2013). The function “terminus” assigns hydroxyl groups to the right end terminals of the molecule (Roughton, 2013). The sub-routine “BuildMolecule” builds up a molecule by joining the selected groups and adding hydroxyl groups to the first and last groups (Roughton, 2013). Here, the adjacency matrix, vectors containing Z , Z' and N_H are updated to represent the structure of the molecule built (Roughton, 2013). In the sub-routine, “GetConnectivity” the adjacency matrix and vectors containing Z , Z' and N_H of a molecule are used to calculate connectivity indices and valence connectivity indices until fifth order (Roughton, 2013). During this process, array containing simple connectivity indices, δ and simple valence connectivity indices, δ^v for each non-hydrogen atom in the molecule were calculated.

7.2.4.1 Optimization formulation and objective function

The QSPRs, calculation of connectivity indices, constraints to ensure feasible molecular structures and the objective function were all formulated together as a mixed integer non-linear program (MINLP). The MINLP was solved by a stochastic algorithm, Tabu Search as discussed below. The generalized optimization formulation has already been discussed in Chapter 1. For this problem, the differences between the properties of candidate solutions and target values were first normalized, and then each property was scaled based on their importance. Degree of conversion (DC) was given a maximum weight of 0.4, and log P carried the next highest weight which was 0.3. The rest of the three properties carried an equal and lowest weight of 0.1. The reason for selecting this scaling factor is that it yielded candidate molecules which exhibited a substantial degree of conversion and they were hydrophilic in nature, while at the same time keeping the other three properties to a reasonable values around the target values. There are other means of ensuring that DC will always be above the target value by removing DC from the objective function and introducing it in a constraint such that DC cannot be less than the target value. The degree of conversion (DC) was given the highest scaling factor because high DC is vital to ensure a stronger bond at the a/d interface and seal of the demineralized dentin from the detrimental oral environment. To trigger the photo-polymerization reaction, it is equally important to ensure the presence of photosensitizer in sufficient concentration. Therefore, log P was given the second highest scaling factor. DC and log P were directly linked to the durability of a/d interface. The rationale for the selection of target values is discussed later. The actual objective function used to design the photosensitizer is given below:

$$\begin{aligned} \text{Objective function} = & \frac{|\ln(\xi)-9|}{9} \times 0.1 + \frac{|PAE-7|}{7} \times 0.1 + \frac{|\log P+0.55|}{0.55} \times 0.3 + \frac{|DC-0.8|}{0.8} \times 0.4 + \\ & \frac{|RT-0.003|}{0.003} \times 0.1 \end{aligned} \quad 7.5$$

7.2.4.2 Tabu Search algorithm

Tabu Search is a stochastic search algorithm capable of yielding locally near-optimal solutions (Roughton *et al.*, 2012b). Solving the CAMD problem with a stochastic optimization technique provides multiple near optimal solutions instead of a global solution. In this study, Tabu Search was employed to solve the MINLP. The entire process of the Tabu Search algorithm implemented here is summarized in a schematic by Roughton *et al.* (Roughton, 2013). The sub-routine “InitialSolution” creates an initial solution for the candidate molecule. The connectivity indices of the initial solution was then used to calculate the target properties followed by the objective function. This forms the current solution and the initial

solution in the Tabu list. The Tabu list stores an array containing groups within the solution and zeroth order connectivity index for checking against Tabu criterion.

In the first iteration, the number of neighbors of the current solution is determined randomly between 1 and maximum allowable number of neighbors which is set. The “MakeNeighbor” function creates neighbors of the current solution by making local moves such as swap, insert, delete and replace.

- Swap: The positions of two random groups in the current solution are swapped
- Insert: A random group is inserted in between two random groups in the current solution
- Delete: A random group is deleted from the current solution
- Replace: A random group in the current solution is replaced with another random group

To determine whether the neighbors are Tabu, the differences between zeroth order connectivity indices of the neighbors and members in the Tabu list are checked against the Tabu criterion as shown below (Roughton, 2013):

$$\left| \chi_{\text{current solution}}^0 - \chi_{\text{previous solution}}^0 \right| > \text{Tabu Criterion} \quad 7.6$$

A neighbor becomes Tabu if the difference in the zeroth order connectivity indices is less than the Tabu criterion. If a neighbor passes the Tabu test, it is added to the Tabu list as the first member and then as more neighbors pass the test they are added to the Tabu list which increases. If the number of members in the Tabu list exceeds the maximum allowable limit, then members in it are deleted in the order they have been added. If a neighbor violates the Tabu criterion, its objective function is compared with that of the best solution. If the objective function of the neighbor is better than the current best solution, the neighbor is kept in the list despite being Tabu. This process is called aspiration and prevents good solutions from being discarded (Glover, 1989; Roughton, 2013). If all the neighbors turn out to be Tabu and no solution is found, then a completely new random molecule is created for the current solution by a global move as discussed below:

- Global move: Completely new molecule is built by randomly selecting groups from the entire set of available sub-groups (calling ‘InitialSolution’ sub-routine) and this forms a pseudo-neighbor solution

The current solution is replaced as the best solution if its objective function turns out to be lower than all the previous solutions. This procedure is repeated until maximum allowable number of non-improving iterations. The solution with the lowest objective function value is returned by Tabu search. For the design

of photosensitizers, the maximum number of non-improving iteration was 100, size of the Tabu list was 15, the maximum number neighbors was limited to 4 and the Tabu criterion was 0.2. The design was carried out for 100 runs.

7.2.4.3 Selection of target values for the properties

The target values of the properties are summarized in Table 7.4. The target value for log P was equivalent to that of HEMA (Fujisawa and Masuhara, 1981). Since HEMA was observed to partition at higher concentration within the hydrophilic-rich phase (Ye *et al.*, 2012), photosensitizers with log P close to that of HEMA would partition at a much higher concentration than the CQ in the hydrophilic-rich phase. The target values for relative normalized PAE and $\ln(\xi)$ were kept close to the maximum values observed for the molecules in the model building set. Maximizing these two properties means that the probability of radical formation for photo-polymerization is increased. The target values for DC and polymerization rate (RT) of the hydrophilic-rich phase were obtained from the previous chapters discussing the polymerization kinetics of the hydrophilic-rich mimics. From these studies (Chapters 2 and 3) it was observed that the DC of the mimics varied from approximately 63% to 97% in presence of sufficient photo-initiator concentration (Abedin *et al.*, 2014; Abedin *et al.*, 2015c). Based on these studies, the target value for DC was selected to be 0.8 which was average of the highest and lowest values observed for the mimics. For the target value of the polymerization rate, RT, only the initial rate maxima of the hydrophilic-rich mimics in the previous chapters (Chapters 2 and 3) were considered. The reason for this was that the polymerization shrinkage may be associated with the higher polymerization rate and the secondary rate maxima were much lower compared to the initial rate maxima. From the previous study, it was observed that the initial rate maxima of the hydrophilic-rich mimics varied from $14.3 \times 10^{-4} \text{ s}^{-1}$ to $47 \times 10^{-4} \text{ s}^{-1}$ when the conventional photo-initiators were present in sufficient concentrations (Abedin *et al.*, 2014; Abedin *et al.*, 2015c). Therefore, the target value for the polymerization rate of the hydrophilic-rich phase was set to be close to the average of the highest and lowest initial rates observed for the mimics mentioned earlier. The target value was selected to be $30 \times 10^{-4} \text{ s}^{-1}$ which was much lower than the polymerization rate of the physically separated hydrophilic-rich phase for most molecules in the model building set.

7.3 Results and discussion

7.3.1 Quantitative structure property relationships (QSPRs)

The QSPR for the relative photon absorption efficiency (PAE) which is a measure of the photosensitizer/LCU efficiency is as follows:

$$\text{Relative Normalized PAE} = 34.3226 - (1.7485 \times \chi^0) - (8.0407 \times \chi^2) + (6.1803 \times \chi^3) + (5.108 \times \chi^5) + (9.9007 \times \chi^v) - (26.9838 \times \chi^v) \quad 7.7$$

Adjusted $R^2 = 0.9996$ and $Q^2 = 0.9861$

Figure 7.5 (a) shows the parity chart for the PAE. The QSPR for $\ln(\xi)$ where ξ is a measure of the probability of the photosensitizer to absorb light and hence be promoted to the excited state is given below (Abedin *et al.*, 2015a):

$$\ln(\xi) = 32.22723 - (4.60663 \times \chi^0) + (0.63374 \times \chi^1) - (0.62536 \times \chi^3) + (4.81887 \times \chi^4) + (3.95277 \times \chi^v) - (15.07572 \times \chi^v) \quad 7.8$$

Adjusted $R^2 = 0.99999$ and $Q^2 = 0.99272$

The use of connectivity indices instead of the group contribution method for the prediction of $\log P$ led to a more accurate QSPR for this case. The QSPR for this property is given by equation 7.9 (Abedin *et al.*, 2015a):

$$\log P = -9.08869 + (1.61343 \times \chi^1) - (7.88886 \times \chi^4) + (6.86586 \times \chi^5) + (0.98095 \times \chi^v) - (1.487 \times \chi^v) \quad 7.9$$

Adjusted $R^2 = 0.99996$ and $Q^2 = 0.99813$

The parity charts for $\ln(\xi)$ and $\log P$ are shown in Figure 7.5 (b) and (c) respectively. DC is a measure of the effectiveness of the reactive species in carrying out the polymerization reaction. The QSPR for this property is summarized below:

$$\text{DC} = -5.1037 - (1.3282 \times \chi^1) + (2.1164 \times \chi^2) - (3.0557 \times \chi^4) + (2.9822 \times \chi^5) + (0.7338 \times \chi^v) - (1.1734 \times \chi^v) \quad 7.10$$

Adjusted $R^2 = 0.9896$ and $Q^2 = 0.8633$

The QSPR for the polymerization rate (RT) which is associated with the polymerization shrinkage is given by the equation 7.11. The parity charts for DC and RT are exhibited in the Figure 7.5 (d) and (e) respectively. It can be seen that for all the properties $Q^2 \approx R^2$, indicating that the QSPRs can accurately predict the properties. Also from the parity charts, it can be seen that the predicted and experimental values are very close.

$$RT = -0.0393 + (0.0176 \times \chi^0) - (0.0559 \times \chi^1) + (0.0383 \times \chi^2) - (0.0286 \times \chi^3) + (0.0299 \times \chi^4) \quad 7.11$$

Adjusted R² = 0.9742 and Q² = 0.9169

7.3.2 Candidate photosensitizers using CAMD

As mentioned earlier, the modified “Carbohydrate excipient designer” has been allowed to run 100 times, and out of these the four best solutions are summarized in Figure 7.6. The properties of these candidate molecules along with the target values are summarized in Table 7.4. It can be seen that the predicted DC of the hydrophilic-rich phase for the candidate molecules are significantly higher than that observed in Chapter 5 for CQ/DMAEMA/DPIHP and CQ/EDMAB/DPIHP (Abedin *et al.*, 2016). The log P values of the candidate molecules also indicate that they are hydrophilic in nature. These results indicate that the proposed candidates may bring about substantial improvement in the performance of the PI system of dental adhesives for the hydrophilic-rich phase. From the molecular structures of the candidate molecules (Figure 7.6), it can be seen that the functional group represented by the iminium ion (C=NH₂⁺) is common. It is possible that the presence of the structural feature, iminium ion, can have a substantial positive impact on the polymerization of the hydrophilic-rich phase and result in an enhanced degree of conversion (DC).

Table 7.4. Summary of the properties for the candidate molecules

Photosensitizer	ln(ξ)	log P	Relative Normalized PAE	DC	Rate (s ⁻¹)	Objective
Target	9.00	-0.55	7.00	0.80	0.0030	0.00
Candidate 1	15.28	-0.47	13.10	0.76	0.0061	0.32
Candidate 2	14.24	-0.70	12.93	0.48	0.0019	0.33
Candidate 3	16.25	-0.37	13.83	0.79	0.0006	0.36
Candidate 4	11.66	-0.29	9.63	0.67	0.0076	0.42

7.4 Conclusion

This study provides direction towards the development of novel photosensitizers for dental adhesive applications. The photosensitizer structures proposed were specially designed for efficient performance in the over-wet condition. The outcomes from this study are summarized below:

- A design framework for photosensitizers was developed along with QSPRs of relevant properties.

- Novel structures for photosensitizer molecules were proposed which had been predicted to possess superior performance in the hydrophilic-rich phase.

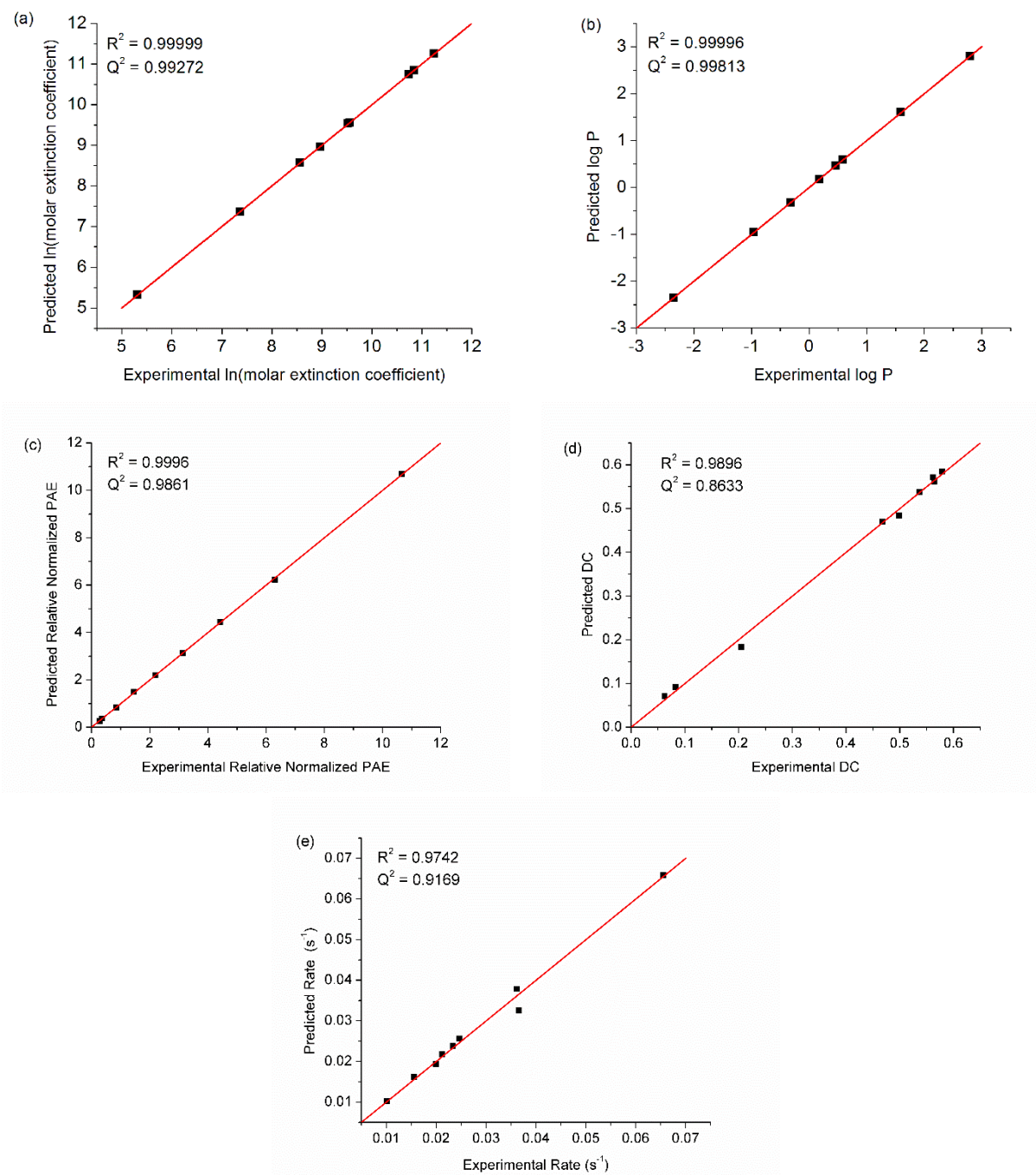


Figure 7.5. Variation of predicted value with experimental value for (a) $\ln(\xi)$ (b) $\log P$ (c) relative normalized PAE (d) degree of conversion (DC) and (e) rate of polymerization (RT)

- The proposed structures contained iminium ions indicating that the functional group, $C=NH_2^+$ could lead to a formation of efficient reactive species responsible for higher DC in the hydrophilic-rich phase.

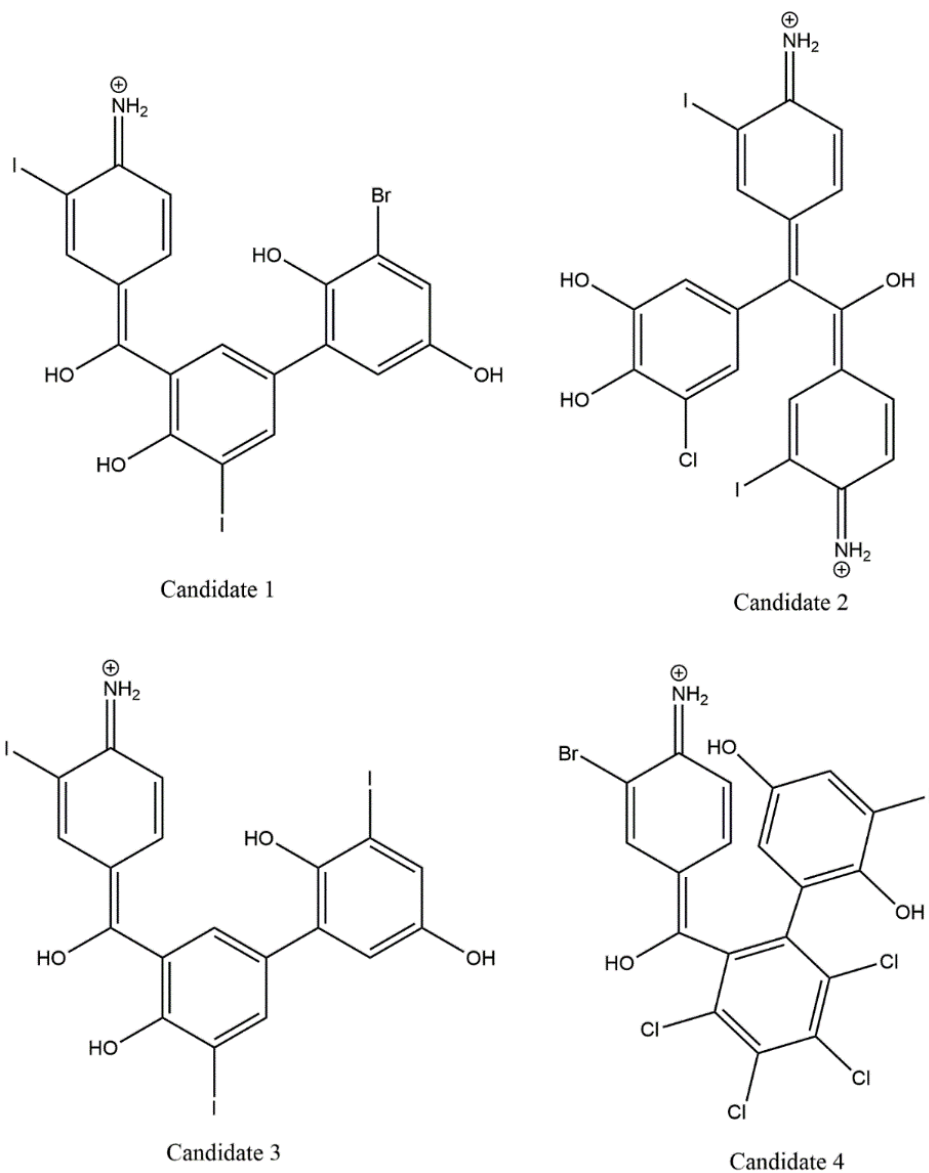


Figure 7.6. Structures of four best candidate photosensitizer molecules given by CAMD for dental adhesive application

CHAPTER 8: CONCLUSIONS AND FUTURE DIRECTIONS

The clinical lifetime of dental composite restoration is inferior compared to that of the amalgam, and the primary cause of failure was identified to be secondary caries. Since the resin for composite restorations is too viscous, a layer of less viscous adhesive is applied to facilitate the bonding between the tooth and restoration. Ideally the adhesive should provide a seal for the demineralized dentin from the oral environment. This is not achieved at the a/d interface due to several reasons such as incomplete infiltration, phase separation, sub-optimal polymerization, plasticization, degradation of the polymer and the collagen. The phase separation of the adhesive resin results in a hydrophilic-rich phase within the hybrid layer which forms a vulnerable region for failure. The goal of this study was to improve the lifetime of the hydrophilic-rich phase by characterizing the hydrophilic-rich phase to understand the impact of variable experimental conditions on its polymerization kinetics and glass transition temperature, and developing a computational design framework for water compatible visible light photosensitizer.

In this study, the characteristics of hydrophilic-rich phase of dental adhesive in terms of polymerization kinetics under varying water concentration, photo-initiator concentration and light intensity were determined. This study reports for the first time the characteristics of hydrophilic-rich phase of dental adhesives in detail. This study is innovative because it has identified characteristics of the hydrophilic-rich phase which had not been observed previously. The presence of secondary rate maxima in case of hydrophilic-rich phase mimics was identified for the first time, and based on these studies the polymerization mechanism of dental adhesives in an over-wet condition was proposed. The DC of the hydrophilic-rich phase was found to be dependent on the photo-initiator concentration and not on the cross-linker, i.e. BisGMA concentration, although the latter may impact the reactivity of monomers during the polymerization. It was determined that the polymerization of the hydrophilic-rich phase of model dental adhesives could be lowered when irradiated at low light intensity making the DC poor. This was in distinct contrast to the widely studied hydrophobic-rich phase where the impact of light intensity was subtle. The influence of light intensity on the DC of the hydrophilic-rich phase can be reduced substantially by incorporating iodonium salt in the PI system. The conventional PI system, CQ/EDMAB led to no polymerization of the physically separated hydrophilic-rich phase but incorporation of iodonium salt improved it substantially. The polymerization of this phase was still lower than the hydrophobic-rich phase due to the lack of the photosensitizer and co-initiator in this phase. Comparison of the polymerization kinetics between the hydrophobic- and hydrophilic-rich phases have shown that the polymerization efficiency of the latter is much lower. These studies also clearly indicate that the hydrophilic-rich phase

contains loosely cross-linked regions which may enhance the diffusion of oral fluid, promoting degradation and plasticization of the polymer and colonization of cariogenic bacteria at the a/d interface. Hence, these investigations clearly indicate that the hydrophilic-rich phase is susceptible to failure due to the lack of DC and cross-linking density. The study showed that the incorporation of an iodonium salt and water compatible PI system will improve the DC of the hydrophilic-rich phase of dental adhesives enhancing its lifetime.

To address the lack of water compatibility of the current PI system, several candidate hydrophilic visible light photo-sensitizers were proposed specifically designed for dental applications. These molecular structures were obtained by computer-aided molecular design (CAMD). This was another novel aspect of this study since new molecular structures were designed to meet the requirements of the hydrophilic-rich phase of dental adhesives. The molecules proposed contained iminium ions, indicating that this structural feature could play an important role in the efficiency of the reactive species. Synthesis chemists can obtain structural insight for water compatible photosensitizers from this work.

Some aspects of the hydrophilic-rich phase have been left unexplored and thus further investigations are required to fully understand the characteristics of the hydrophilic-rich phase. The hydrophilic-rich phase was not directly investigated for its cross-linking density when polymerized under various parameters such as water concentration and iodonium salt, and hence future studies could include this property. Moreover, future investigations on the mechanical properties and degradation of the hydrophilic-rich phase could be carried out to understand the extent of vulnerability of this region. The computational design framework could include more relevant target properties. Some further relevant properties of photosensitizers are: toxicity, solubility, quantity of radicals generated and their stability in the hydrophilic-rich phase. QSPRs for these properties can be developed and included in the CAMD problem to obtain comprehensive optimized molecular structures. The radicals generated and their stability can be quantified using electron spin resonance (ESR) spectroscopy.

Although enhancing the degree of conversion of the hydrophilic-rich phase can significantly enhance the a/d bond integrity by improving the seal at the interface and reducing the diffusion of oral fluid, the resultant polymer will be linear with cyclizations and have very little cross-linking. Incorporation of hydrophilic cross-linker will certainly improve the cross-linking density of the hydrophilic-rich phase and hence its lifetime. Therefore, design and synthesis of a water compatible cross-linker for dental adhesive application is the overall goal to address the frequent failure of composite restorations. An esterase resistant cross-linker will further reduce the degradation caused by the enzyme, salivary

esterase. This was not addressed in this study due to the lack of timeframe. The next step could be to develop a computational design framework for esterase resistant water compatible cross-linker specifically for the dental adhesives.

The overall study conducted here provides directions towards reducing vulnerability of the hydrophilic-rich phase of dental adhesives, and hence for improving the lifetime of dental composite restorations.

REFERENCES

- Abedin, F., Roughton, B., Spencer, P., Ye, Q., Camarda, K., 2015a. Computational Molecular Design of Water Compatible Dentin Adhesive System. PSE2015 ESCAPE25, 233.
- Abedin, F., Ye, Q., Camarda, K., Spencer, P., 2015b. Impact of light intensity on the polymerization kinetics and network structure of model hydrophobic and hydrophilic methacrylate based dental adhesive resin. *Journal of Biomedical Materials Research Part B: Applied Biomaterials*, n/a-n/a.
- Abedin, F., Ye, Q., Good, H.J., Parthasarathy, R., Spencer, P., 2014. Polymerization- and solvent-induced phase separation in hydrophilic-rich dentin adhesive mimic. *Acta Biomaterialia* 10, 3038-3047.
- Abedin, F., Ye, Q., Parthasarathy, R., Misra, A., Spencer, P., 2015c. Polymerization Behavior of Hydrophilic-Rich Phase of Dentin Adhesive. *Journal of Dental Research*.
- Abedin, F., Ye, Q., Song, L., Ge, X., Camarda, K., Spencer, P., 2016. Effect of Partition of Photo-Initiator Components and Addition of Iodonium Salt on the Photopolymerization of Phase-Separated Dental Adhesive. *JOM*, 1-10.
- Allen, N.S., 1996. Photoinitiators for UV and visible curing of coatings: Mechanisms and properties. *Journal of Photochemistry and Photobiology A: Chemistry* 100, 101-107.
- Almeida, J.F., Ferreira, P., Lopes, A., Gil, M.H., 2011. Photocrosslinkable biodegradable responsive hydrogels as drug delivery systems. *International Journal of Biological Macromolecules* 49, 948-954.
- Anseth, K.S., Shastri, V.R., Langer, R., 1999. Photopolymerizable degradable polyanhydrides with osteocompatibility. *Nat Biotech* 17, 156-159.
- Anseth, K.S., Wang, C.M., Bowman, C.N., 1994. Reaction behaviour and kinetic constants for photopolymerizations of multi(meth)acrylate monomers. *Polymer* 35, 3243-3250.
- Bailey, B.M., Hui, V., Fei, R., Grunlan, M.A., 2011. Tuning PEG-DA hydrogel properties via solvent-induced phase separation (SIPS). *Journal of materials chemistry* 21, 18776-18782.
- Bernardo, M., Luis, H., Martin, M.D., Leroux, B.G., Rue, T., Leitão, J., DeRouen, T.A., 2007. Survival and reasons for failure of amalgam versus composite posterior restorations placed in a randomized clinical trial. *The Journal of the American Dental Association* 138, 775-783.
- Besse, V., Pluart, L., Cook, W.D., Pham, T.N., Madec, P.J., 2013. Polymerization kinetics of phosphonic acids and esters using an iodonium initiator. *Journal of Polymer Science Part A: Polymer Chemistry* 51, 5046-5055.
- Beyazit, S., Ambrosini, S., Marchyk, N., Palo, E., Kale, V., Soukka, T., Tse Sum Bui, B., Haupt, K., 2014. Versatile synthetic strategy for coating upconverting nanoparticles with polymer shells through localized photopolymerization by using the particles as internal light sources. *Angewandte Chemie International Edition* 53, 8919-8923.
- Bicerano, J., 2002. Prediction of polymer properties, Third ed. Marcel Dekker Inc.
- Biswas, A.K., Barik, S., Sen, A., Das, A., Ganguly, B., 2014. Design of Efficient Metal-Free Organic Dyes Having an Azacyclazine Scaffold as the Donor Fragment for Dye-Sensitized Solar Cells. *The Journal of Physical Chemistry C* 118, 20763-20771.
- Bogdanov, B., Nikolić, S., Trinajstić, N., 1989. On the three-dimensional Wiener number. *Journal of mathematical chemistry* 3, 299-309.
- Boots, H.M.J., Kloosterboer, J.G., Serbutoviez, C., Touwslager, F.J., 1996. Polymerization-Induced Phase Separation. 1. Conversion-Phase Diagrams. *Macromolecules* 29, 7683-7689.
- Bose, S., Bogner, R.H., 2010. Solventless visible light-curable coating: I. Critical formulation and processing parameters. *International Journal of Pharmaceutics* 393, 32-40.
- Brambilla, E., Ionescu, A., Gagliani, M., Cochis, A., Arciola, C.R., Rimondini, L., 2012. Biofilm formation on composite resins for dental restorations: An in situ study on the effect of chlorhexidine mouthrinses. *International Journal of Artificial Organs* 35, 792-799.

Burke, F.J.T., Wilson, N.H.F., Cheung, S.W., Mjör, I.A., 2001. Influence of patient factors on age of restorations at failure and reasons for their placement and replacement. *Journal of Dentistry* 29, 317-324.

Cadenaro, M., Antonioli, F., Sauro, S., Tay, F.R., Di Lenarda, R., Prati, C., Biasotto, M., Contardo, L., Breschi, L., 2005. Degree of conversion and permeability of dental adhesives. *European Journal of Oral Sciences* 113, 525-530.

Cadenaro, M., Pashley, D.H., Marchesi, G., Carrilho, M., Antonioli, F., Mazzoni, A., Tay, F.R., Di Lenarda, R., Breschi, L., 2009. Influence of chlorhexidine on the degree of conversion and E-modulus of experimental adhesive blends. *Dental Materials* 25, 1269-1274.

Camarda, K.V., Maranas, C.D., 1999. Optimization in Polymer Design Using Connectivity Indices. *Industrial & Engineering Chemistry Research* 38, 1884-1892.

Carrilho, M., Carvalho, R.M., Tay, F., Yiu, C., Pashley, D.H., 2005. Durability of resin-dentin bonds related to water and oil storage. *American Journal of Dentistry* 18, 315-319.

Catel, Y., Besse, V., Zulauf, A., Marchat, D., Pfund, E., Pham, T.-N., Bernache-Assolant, D., Degrange, M., Lequeux, T., Madec, P.-J., Le Pluart, L., 2012. Synthesis and evaluation of new phosphonic, bisphosphonic and difluoromethylphosphonic acid monomers for dental application. *European Polymer Journal* 48, 318-330.

Catel, Y., Degrange, M., Pluart, L.L., Madec, P.J., Pham, T.N., Chen, F., Cook, W.D., 2009. Synthesis, photopolymerization, and adhesive properties of new bisphosphonic acid monomers for dental application. *Journal of Polymer Science Part A: Polymer Chemistry* 47, 5258-5271.

Chang, H.-H., Guo, M.-K., Kasten, F.H., Chang, M.-C., Huang, G.-F., Wang, Y.-L., Wang, R.-S., Jeng, J.-H., 2005. Stimulation of glutathione depletion, ROS production and cell cycle arrest of dental pulp cells and gingival epithelial cells by HEMA. *Biomaterials* 26, 745-753.

Chavali, S., Lin, B., Miller, D.C., Camarda, K.V., 2004. Environmentally-benign transition metal catalyst design using optimization techniques. *Computers & Chemical Engineering* 28, 605-611.

Chen, Y.C., Lin, R.Z., Qi, H., Yang, Y., Bae, H., Melero-Martin, J.M., Khademhosseini, A., 2012. Functional human vascular network generated in photocrosslinkable gelatin methacrylate hydrogels. *Advanced functional materials* 22, 2027-2039.

Consonni, V., Todeschini, R., Pavan, M., 2002. Structure/Response Correlations and Similarity/Diversity Analysis by GETAWAY Descriptors. 1. Theory of the Novel 3D Molecular Descriptors. *Journal of Chemical Information and Computer Sciences* 42, 682-692.

Cook, W.D., 1993. Photopolymerization kinetics of oligo (ethylene oxide) and oligo (methylene) oxide dimethacrylates. *Journal of Polymer Science Part A: Polymer Chemistry* 31, 1053-1067.

Cook, W.D., Chen, F., 2011. Enhanced photopolymerization of dimethacrylates with ketones, amines, and iodonium salts: The CQ system. *Journal of Polymer Science Part A: Polymer Chemistry* 49, 5030-5041.

Coşkun, M., Demirelli, K., Ahmetzade, M.A., 1997. Synthesis, Characterization, and Polymerization of New Hydroxyethyl Methacrylate Containing Cyclobutane Ring. *Journal of Macromolecular Science, Part A* 34, 429-438.

Davidson-Kaban, S.S., Davidson, C.L., Feilzer, A.J., de Gee, A.J., Erdilek, N., 1997. The effect of curing light variations on bulk curing and wall-to-wall quality of two types and various shades of resin composites. *Dental Materials* 13, 344-352.

Davis, K.A., Burdick, J.A., Anseth, K.S., 2003. Photoinitiated crosslinked degradable copolymer networks for tissue engineering applications. *Biomaterials* 24, 2485-2495.

Deligeorgi, V., Mjor, I., Wilson, N., 2001. An overview of reasons for the placement and replacement of restorations. *Prim Dent Care* 8, 5-11.

Dennison, J.B., Yaman, P., Seir, R., Hamilton, J.C., 2000. Effect of variable light intensity on composite shrinkage. *The Journal of Prosthetic Dentistry* 84, 499-505.

Discacciati, J.A.C., Neves, A.D., Oréface, R.L., Pimenta, F.J.G.S., Sander, H.H., 2004. Effect of light intensity and irradiation time on the polymerization process of a dental composite resin. *Materials Research* 7, 313-318.

Donovan, T.E., Marzola, R., Becker, W., Cagna, D.R., Eichmiller, F., McKee, J.R., Metz, J.E., Albouy, J.P., 2015. Annual review of selected scientific literature: Report of the Committee on Scientific Investigation of the American Academy of Restorative Dentistry. *Journal of Prosthetic Dentistry* 114, 756-809.

Eacute, Rez, M., iacute, a del, M., Eacute, Rez, O.C., Oacute, N, F., Lucena, M., lacute, N, C., Pulgar, R., 2008. Stability and Reproducibility of Radiometric Properties of Light Curing Units (LCUs). Part I: QTH LCUs. *Dental Materials Journal* 27, 284-291.

Eliades, G., Vougiouklakis, G., Palaghias, G., 2001. Heterogeneous distribution of single-bottle adhesive monomers in the resin–dentin interdiffusion zone. *Dental Materials* 17, 277-283.

Eljack, F.T., Eden, M.R., 2008. A systematic visual approach to molecular design via property clusters and group contribution methods. *Computers & Chemical Engineering* 32, 3002-3010.

Ely, C., Schneider, L.F.J., Ogliari, F.A., Schmitt, C.C., Corrêa, I.C., Lima, G.d.S., Samuel, S.M.W., Piva, E., 2012. Polymerization kinetics and reactivity of alternative initiators systems for use in light-activated dental resins. *Dental Materials* 28, 1199-1206.

Emami, N., Söderholm, K.-J.M., Berglund, L.A., 2003. Effect of light power density variations on bulk curing properties of dental composites. *Journal of Dentistry* 31, 189-196.

Encinas, M.V., Rufs, A.M., Bertolotti, S.G., Previtali, C.M., 2009. Xanthene dyes/amine as photoinitiators of radical polymerization: A comparative and photochemical study in aqueous medium. *Polymer* 50, 2762-2767.

Eslick, J.C., Ye, Q., Park, J., Topp, E.M., Spencer, P., Camarda, K.V., 2009. A computational molecular design framework for crosslinked polymer networks. *Computers & Chemical Engineering* 33, 954-963.

Estrada, E., 1995. Three-Dimensional Molecular Descriptors Based on Electron Charge Density Weighted Graphs. *Journal of Chemical Information and Computer Sciences* 35, 708-713.

Falconi, M., Teti, G., Zago, M., Pelotti, S., Breschi, L., Mazzotti, G., 2007. Effects of HEMA on type I collagen protein in human gingival fibroblasts. *Cell biology and toxicology* 23, 313-322.

Ferracane, J.L., 2011. Resin composite—State of the art. *Dental Materials* 27, 29-38.

Folić, M., Adjiman, C.S., Pistikopoulos, E.N., 2008. Computer-Aided Solvent Design for Reactions: Maximizing Product Formation. *Industrial & Engineering Chemistry Research* 47, 5190-5202.

Fouassier, J.P., Allonas, X., Burget, D., 2003. Photopolymerization reactions under visible lights: principle, mechanisms and examples of applications. *Progress in Organic Coatings* 47, 16-36.

Fouassier, J.P., Morlet-Savary, F., 1996. Photopolymers for laser imaging and holographic recording: design and reactivity of photosensitizers. *Optical engineering* 35, 304-312.

Franco, E.B., Santos, P.A.d., Mondelli, R.F.L., 2007. The effect of different light-curing units on tensile strength and microhardness of a composite resin. *Journal of Applied Oral Science* 15, 470-474.

Fredenslund, A., Jones, R.L., Prausnitz, J.M., 1975. Group-contribution estimation of activity coefficients in nonideal liquid mixtures. *AIChE Journal* 21, 1086-1099.

Fujisawa, S., Masuhara, E., 1981. Determination of partition coefficients of acrylates, methacrylates, and vinyl monomers using high performance liquid chromatography (HPLC). *Journal of biomedical materials research* 15, 787-793.

Gani, R., Harper, P.M., Hostrup, M., 2005. Automatic Creation of Missing Groups through Connectivity Index for Pure-Component Property Prediction. *Industrial & Engineering Chemistry Research* 44, 7262-7269.

Gani, R., Nielsen, B., Fredenslund, A., 1991. A group contribution approach to computer-aided molecular design. *AIChE Journal* 37, 1318-1332.

Ganster, B., Fischer, U.K., Moszner, N., Liska, R., 2008. New Photocleavable Structures. Diacylgermane-Based Photoinitiators for Visible Light Curing. *Macromolecules* 41, 2394-2400.

- Gao, F., Yang, Y.-y., 2000. Visible Light Dye-Sensitized Photosensitive Systems: A Comprehensive Study on Photoimaging. *Journal of Photopolymer Science and Technology* 13, 265-268.
- Gao, X., Nie, J., 2007. Low-temperature photopolymerization and post-cure characteristics of acrylates. *Polymer International* 56, 707-710.
- Glover, F., 1989. Tabu search-part I. *ORSA Journal on computing* 1, 190-206.
- Grinstein, S., Swallow, C.J., Rotstein, O.D., 1991. Regulation of cytoplasmic pH in phagocytic cell function and dysfunction. *Clinical Biochemistry* 24, 241-247.
- Hahnel, S., Rosentritt, M., Bürgers, R., Handel, G., 2008. Surface properties and in vitro *Streptococcus mutans* adhesion to dental resin polymers. *Journal of Materials Science: Materials in Medicine* 19, 2619-2627.
- Hashimoto, M., Nagano, F., Endo, K., Ohno, H., 2011. A review: Biodegradation of resin–dentin bonds. *Japanese Dental Science Review* 47, 5-12.
- He, H., Li, L., Lee, L.J., 2006. Photopolymerization and structure formation of methacrylic acid based hydrogels in water/ethanol mixture. *Polymer* 47, 1612-1619.
- He, H., Li, L., Lee, L.J., 2008. Photopolymerization and structure formation of methacrylic acid based hydrogels: The effect of light intensity. *Reactive and Functional Polymers* 68, 103-113.
- Hofmann, N., Hugo, B., Klaiber, B., 2002. Effect of irradiation type (LED or QTH) on photo-activated composite shrinkage strain kinetics, temperature rise, and hardness. *European Journal of Oral Sciences* 110, 471-479.
- Holde, K.E.V., Johnson, W.C., Ho, P.S., 2006. *Principles of Physical Biochemistry*, Second ed. Pearson Education Inc., New Jersey.
- Horie, K., Otagawa, A., Muraoka, M., Mita, I., 1975. Calorimetric investigation of polymerization reactions. V. Crosslinked copolymerization of methyl methacrylate with ethylene dimethacrylate. *Journal of Polymer Science: Polymer Chemistry Edition* 13, 445-454.
- Ionescu, A., Wutscher, E., Brambilla, E., Schneider-Feyrer, S., Giessibl, F.J., Hahnel, S., 2012. Influence of surface properties of resin-based composites on in vitro *Streptococcus mutans* biofilm development. *European Journal of Oral Sciences* 120, 458-465.
- Ishihara, M., Obara, K., Nakamura, S., Fujita, M., Masuoka, K., Kanatani, Y., Takase, B., Hattori, H., Morimoto, Y., Ishihara, M., 2006. Chitosan hydrogel as a drug delivery carrier to control angiogenesis. *Journal of Artificial Organs* 9, 8-16.
- Ito, S., Hashimoto, M., Wadgaonkar, B., Svizero, N., Carvalho, R.M., Yiu, C., Rueggeberg, F.A., Foulger, S., Saito, T., Nishitani, Y., Yoshiyama, M., Tay, F.R., Pashley, D.H., 2005. Effects of resin hydrophilicity on water sorption and changes in modulus of elasticity. *Biomaterials* 26, 6449-6459.
- Jakubiak, J., Nie, J., Lindén, L.Å., Rabek, J., 2000. Crosslinking photocopolymerization of acrylic acid (and N-vinylpyrrolidone) with triethyleneglycol dimethacrylate initiated by camphorquinone/ethyl-4-dimethylaminobenzoate. *Journal of Polymer Science Part A: Polymer Chemistry* 38, 876-886.
- Jokstad, A., Bayne, S., Blunck, U., Tyas, M., Wilson, N., 2001. Quality of dental restorations FDI Commission Project 2–95*. *International Dental Journal* 51, 117-158.
- Keir, L., Hall, L., 1986. *Molecular connectivity in structure-activity analysis*. NY: John Wiley & Sons.
- Keizer, H.M., Sijbesma, R.P., Jansen, J.F.G.A., Pasternack, G., Meijer, E.W., 2003. Polymerization-Induced Phase Separation Using Hydrogen-Bonded Supramolecular Polymers. *Macromolecules* 36, 5602-5606.
- Klapdohr, S., Moszner, N., 2005. New inorganic compounds for dental filling composites. *Monatshefte für Chemie* 136, 21-45.
- Kopecek, J., 2009. Hydrogels: From soft contact lenses and implants to self-assembled nanomaterials. *Journal of Polymer Science Part A: Polymer Chemistry* 47, 5929-5946.
- Kopperud, S.E., Tveit, A.B., Gaarden, T., Sandvik, L., Espelid, I., 2012. Longevity of posterior dental restorations and reasons for failure. *European Journal of Oral Sciences* 120, 539-548.

Lardner, A., 2001. The effects of extracellular pH on immune function. *Journal of Leukocyte Biology* 69, 522-530.

Larsen, B.L., Rasmussen, P., Fredenslund, A., 1987. A modified UNIFAC group-contribution model for prediction of phase equilibria and heats of mixing. *Industrial & Engineering Chemistry Research* 26, 2274-2286.

Larson, M.R., Rajashankar, K.R., Patel, M.H., Robinette, R.A., Crowley, P.J., Michalek, S., Brady, L.J., Deivanayagam, C., 2010. Elongated fibrillar structure of a streptococcal adhesin assembled by the high-affinity association of α - and PPII-helices. *Proceedings of the National Academy of Sciences* 107, 5983-5988.

Lee, S.-K., Kim, T.-W., Son, S.-A., Park, J.-K., Kim, J.-H., Kim, H.-I., Kwon, Y.H., 2013. Influence of light-curing units on the polymerization of low-shrinkage composite resins. *Dental Materials Journal* 32, 688-694.

Levin, L., Coval, M., Geiger, S.B., 2007. Cross-sectional radiographic survey of amalgam and resin-based composite posterior restorations. *Quintessence International* 38.

Li, L., Lee, L.J., 2005. Photopolymerization of HEMA/DEGDMA hydrogels in solution. *Polymer* 46, 11540-11547.

Lima, G.d.S., Ogliari, F.A., Souza e Silva, M.G., Münchow, E.A., Petzhhold, C.L., Piva, E., 2013. Benzodioxoles as alternative coinitiators for radical polymerization in a model-dental adhesive resin. *Journal of Applied Polymer Science* 127, 4160-4167.

Lohbauer, U., Rahiotis, C., Krämer, N., Petschelt, A., Eliades, G., 2005. The effect of different light-curing units on fatigue behavior and degree of conversion of a resin composite. *Dental Materials* 21, 608-615.

Lovelh, L.G., Newman, S.M., Bowman, C.N., 1999. The Effects of Light Intensity, Temperature, and Comonomer Composition on the Polymerization Behavior of Dimethacrylate Dental Resins. *Journal of Dental Research* 78, 1469-1476.

Lovell, L.G., Berchtold, K.A., Elliott, J.E., Lu, H., Bowman, C.N., 2001a. Understanding the kinetics and network formation of dimethacrylate dental resins. *Polymers for Advanced Technologies* 12, 335-345.

Lovell, L.G., Lu, H., Elliott, J.E., Stansbury, J.W., Bowman, C.N., 2001b. The effect of cure rate on the mechanical properties of dental resins. *Dental Materials* 17, 504-511.

Lovell, L.G., Newman, S.M., Donaldson, M.M., Bowman, C.N., 2003. The effect of light intensity on double bond conversion and flexural strength of a model, unfilled dental resin. *Dental Materials* 19, 458-465.

Lumely, T., 2009. Package 'Leaps'.

Luo, K., 2006. The morphology and dynamics of polymerization-induced phase separation. *European Polymer Journal* 42, 1499-1505.

Malacarne, J., Carvalho, R.M., de Goes, M.F., Svizero, N., Pashley, D.H., Tay, F.R., Yiu, C.K., Carrilho, M.R.d.O., 2006. Water sorption/solubility of dental adhesive resins. *Dental Materials* 22, 973-980.

Malda, J., Visser, J., Melchels, F.P., Jüngst, T., Hennink, W.E., Dhert, W.J., Groll, J., Hutmacher, D.W., 2013. 25th anniversary article: engineering hydrogels for biofabrication. *Advanced Materials* 25, 5011-5028.

Mallavia, R., Amat-Guerri, F., Fimia, A., Sastre, R., 1994. Synthesis and Evaluation as a Visible-Light Polymerization Photoinitiator of a New Eosin Ester with an O-Benzoyl- α -oxoimine Group. *Macromolecules* 27, 2643-2646.

Marrero, J., Gani, R., 2001. Group-contribution based estimation of pure component properties. *Fluid Phase Equilibria* 183-184, 183-208.

Menczel, J.D., Prime, R.B., 2014. *Thermal analysis of polymers: fundamentals and applications*. John Wiley & Sons.

Monroe, B.M., Weed, G.C., 1993. Photoinitiators for free-radical-initiated photoimaging systems. *Chemical Reviews* 93, 435-448.

Moszner, N., Hirt, T., 2012. New polymer-chemical developments in clinical dental polymer materials: Enamel-dentin adhesives and restorative composites. *Journal of Polymer Science Part A: Polymer Chemistry* 50, 4369-4402.

Musanje, L., Ferracane, J.L., Sakaguchi, R.L., 2009. Determination of the optimal photoinitiator concentration in dental composites based on essential material properties. *Dental Materials* 25, 994-1000.

Neumann, M.G., Miranda, W.G., Jr., Schmitt, C.C., Rueggeberg, F.A., Correa, I.C., Molar extinction coefficients and the photon absorption efficiency of dental photoinitiators and light curing units. *Journal of Dentistry* 33, 525-532.

NIH, 2000. Oral health in America: A report of the surgeon general. National Institute of Dental and Craniofacial Research, National Institutes of Health, pp. 1-332.

Norrish, R., Smith, R., 1942. Catalyzed polymerization of methyl methacrylate in the liquid phase. *Nature* 150, 336-337.

Nwabunma, D., Chiu, H.-W., Kyu, T., 2000. Morphology Development and Dynamics of Photopolymerization-Induced Phase Separation in Mixtures of a Nematic Liquid Crystal and Photocuratives. *Macromolecules* 33, 1416-1424.

Opdam, N.J.M., Bronkhorst, E.M., Roeters, J.M., Loomans, B.A.C., 2007. A retrospective clinical study on longevity of posterior composite and amalgam restorations. *Dental Materials* 23, 2-8.

Paranjpe, A., Bordador, L.C.F., Wang, M.-y., Hume, W.R., Jewett, A., 2005. Resin Monomer 2-Hydroxyethyl Methacrylate (HEMA) is a Potent Inducer of Apoptotic Cell Death in Human and Mouse Cells. *Journal of Dental Research* 84, 172-177.

Park, J., Ye, Q., Topp, E.M., Misra, A., Kieweg, S.L., Spencer, P., 2010. Effect of photoinitiator system and water content on dynamic mechanical properties of a light-cured bisGMA/HEMA dental resin. *Journal of Biomedical Materials Research Part A* 93A, 1245-1251.

Park, J.G., Ye, Q., Topp, E.M., Kostoryz, E.L., Wang, Y., Kieweg, S.L., Spencer, P., 2008. Preparation and properties of novel dentin adhesives with esterase resistance. *Journal of applied polymer science* 107, 3588-3597.

Park, S.S., Won, Y.S., Choi, Y.C., Kim, J.H., 2009. Molecular design of organic dyes with double electron acceptor for dye-sensitized solar cell. *Energy & Fuels* 23, 3732-3736.

Pashley, D.H., Tay, F.R., Breschi, L., Tjäderhane, L., Carvalho, R.M., Carrilho, M., Tezvergil-Mutluay, A., 2011a. State of the art etch-and-rinse adhesives. *Dental Materials* 27, 1-16.

Pashley, D.H., Tay, F.R., Imazato, S., 2011b. How to increase the durability of resin-dentin bonds. *Compendium of continuing education in dentistry (Jamesburg, N.J. : 1995)* 32, 60-64, 66.

Pashley, D.H., Tay, F.R., Yiu, C., Hashimoto, M., Breschi, L., Carvalho, R.M., Ito, S., 2004. Collagen Degradation by Host-derived Enzymes during Aging. *Journal of Dental Research* 83, 216-221.

Pellosi, D.S., Estevão, B.M., Semensato, J., Severino, D., Baptista, M.S., Politi, M.J., Hioka, N., Caetano, W., 2012. Photophysical properties and interactions of xanthene dyes in aqueous micelles. *Journal of Photochemistry and Photobiology A: Chemistry* 247, 8-15.

Podgórski, M., 2012. Structure–property relationship in new photo-cured dimethacrylate-based dental resins. *Dental Materials* 28, 398-409.

Price, R.B., DÉRand, T., Sedarous, M., Andreou, P., Loney, R.W., 2000. Effect of Distance on the Power Density from Two Light Guides. *Journal of Esthetic and Restorative Dentistry* 12, 320-327.

Randic, M., 1975. Characterization of molecular branching. *Journal of the American Chemical Society* 97, 6609-6615.

Randic, M., 1995. Molecular profiles Novel geometry-dependent molecular descriptors. *New journal of chemistry* 19, 781-791.

Roughton, B.C., 2013. Development of Computer-Aided Molecular Design Methods for Bioengineering Applications. The University of Kansas.

Roughton, B.C., Christian, B., White, J., Camarda, K.V., Gani, R., 2012a. Simultaneous design of ionic liquid entrainers and energy efficient azeotropic separation processes. *Computers & Chemical Engineering* 42, 248-262.

Roughton, B.C., Topp, E.M., Camarda, K.V., 2012b. Use of glass transitions in carbohydrate excipient design for lyophilized protein formulations. *Computers & Chemical Engineering* 36, 208-216.

Rueggeberg, F.A., Jordan, D.M., 1993. Effect of light-tip distance on polymerization of resin composite. *International Journal of Prosthodontics* 6.

Santerre, J.P., Shajii, L., Leung, B.W., 2001. Relation of Dental Composite Formulations To Their Degradation and the Release of Hydrolyzed Polymeric-Resin-Derived Products. *Critical Reviews in Oral Biology & Medicine* 12, 136-151.

Santini, A., Miletic, V., 2008. Quantitative micro-Raman assessment of dentine demineralization, adhesive penetration, and degree of conversion of three dentine bonding systems. *European Journal of Oral Sciences* 116, 177-183.

Schneider, L.F.J., Consani, S., Sakaguchi, R.L., Ferracane, J.L., 2009. Alternative photoinitiator system reduces the rate of stress development without compromising the final properties of the dental composite. *Dental Materials* 25, 566-572.

Schneider, L.F.J., Pfeifer, C.S.C., Consani, S., Prael, S.A., Ferracane, J.L., 2008. Influence of photoinitiator type on the rate of polymerization, degree of conversion, hardness and yellowing of dental resin composites. *Dental Materials* 24, 1169-1177.

Sheikh, M.I., 1976. Renal handling of phenol red. II. The mechanism of substituted phenolsulphophthalein (PSP) dye transport in rabbit kidney tubules in vitro. *The Journal of physiology* 256, 175-195.

Sheldon, T.J., Adjiman, C.S., Cordiner, J.L., 2005. Pure component properties from group contribution: Hydrogen-bond basicity, hydrogen-bond acidity, Hildebrand solubility parameter, macroscopic surface tension, dipole moment, refractive index and dielectric constant. *Fluid Phase Equilibria* 231, 27-37.

Siddhaye, S., Camarda, K.V., Topp, E., Southard, M., 2000. Design of novel pharmaceutical products via combinatorial optimization. *Computers & Chemical Engineering* 24, 701-704.

Silikas, N., Eliades, G., Watts, D.C., 2000. Light intensity effects on resin-composite degree of conversion and shrinkage strain. *Dental Materials* 16, 292-296.

Sodré, C.S., Albuquerque, P.P.A.C., Isolan, C.P., Moraes, R.R., Schneider, L.F., 2015. Relative photon absorption determination and the influence of photoinitiator system and water content on C=C conversion, water sorption/solubility of experimental self-etch adhesives. *International Journal of Adhesion and Adhesives* 63, 152-157.

Spagnuolo, G., D'Antò, V., Cosentino, C., Schmalz, G., Schweikl, H., Rengo, S., 2006. Effect of N-acetyl-L-cysteine on ROS production and cell death caused by HEMA in human primary gingival fibroblasts. *Biomaterials* 27, 1803-1809.

Spencer, P., Wang, Y., 2002. Adhesive phase separation at the dentin interface under wet bonding conditions. *Journal of Biomedical Materials Research* 62, 447-456.

Spencer, P., Ye, Q., Park, J., Topp, E.M., Misra, A., Marangos, O., Wang, Y., Bohaty, B.S., Singh, V., Sene, F., 2010. Adhesive/dentin interface: the weak link in the composite restoration. *Annals of biomedical engineering* 38, 1989-2003.

Stahl, F., Ashworth, S.H., Jandt, K.D., Mills, R.W., 2000. Light-emitting diode (LED) polymerisation of dental composites: flexural properties and polymerisation potential. *Biomaterials* 21, 1379-1385.

Struebing, H., Ganase, Z., Karamertzanis, P.G., Sioukrou, E., Haycock, P., Piccione, P.M., Armstrong, A., Galindo, A., Adjiman, C.S., 2013. Computer-aided molecular design of solvents for accelerated reaction kinetics. *Nat Chem* 5, 952-957.

Tamilavan, V., Kim, A.Y., Kim, H.-B., Kang, M., Hyun, M.H., 2014. Structural optimization of thiophene-(N-aryl)pyrrole-thiophene-based metal-free organic sensitizer for the enhanced dye-sensitized solar cell performance. *Tetrahedron* 70, 371-379.

Tay, F.R., Hashimoto, M., Pashley, D.H., Peters, M.C., Lai, S.C.N., Yiu, C.K.Y., Cheong, C., 2003. Aging Affects Two Modes of Nanoleakage Expression in Bonded Dentin. *Journal of Dental Research* 82, 537-541.

Teshima, W., Nomura, Y., Tanaka, N., Urabe, H., Okazaki, M., Nahara, Y., 2003. ESR study of camphorquinone/amine photoinitiator systems using blue light-emitting diodes. *Biomaterials* 24, 2097-2103.

Tetko, I.V., Gasteiger, J., Todeschini, R., Mauri, A., Livingstone, D., Ertl, P., Palyulin, V.A., Radchenko, E.V., Zefirov, N.S., Makarenko, A.S., Tanchuk, V.Y., Prokopenko, V.V., Virtual Computational Chemistry Laboratory – Design and Description. *Journal of Computer-Aided Molecular Design* 19, 453-463.

Thomas, L.C., 2005. Modulated DSC paper # 2, Modulated DSC basics: calculation and calibration of MDSC signals. TA Instruments Technical Paper TP 007.

Toledano, M., Osorio, R., Osorio, E., Aguilera, F.S., Yamauti, M., Pashley, D.H., Tay, F., 2007. Durability of resin–dentin bonds: Effects of direct/indirect exposure and storage media. *Dental Materials* 23, 885-892.

Toledano, M., Yamauti, M., Osorio, E., Monticelli, F., Osorio, R., 2012. Characterization of Micro- and Nanophase Separation of Dentin Bonding Agents by Stereoscopy and Atomic Force Microscopy. *Microscopy and Microanalysis* 18, 279-288.

Valmikinathan, C.M., Mukhatyar, V.J., Jain, A., Karumbaiah, L., Dasari, M., Bellamkonda, R.V., 2012. Photocrosslinkable chitosan based hydrogels for neural tissue engineering. *Soft Matter* 8, 1964-1976.

Van Landuyt, K.L., De Munck, J., Snauwaert, J., Coutinho, E., Poitevin, A., Yoshida, Y., Inoue, S., Peumans, M., Suzuki, K., Lambrechts, P., Van Meerbeek, B., 2005. Monomer-Solvent Phase Separation in One-step Self-etch Adhesives. *Journal of Dental Research* 84, 183-188.

Venkatasubramanian, V., Chan, K., Caruthers, J.M., 1994. Computer-aided molecular design using genetic algorithms. *Computers & Chemical Engineering* 18, 833-844.

Wagner, S.J., Skripchenko, A., Robinette, D., Foley, J.W., Cincotta, L., 1998. Factors affecting virus photoinactivation by a series of phenothiazine dyes. *Photochemistry and photobiology* 67, 343-349.

Wainwright, M., Burrow, S.M., Guinot, S.G.R., Phoenix, D.A., Waring, J., Uptake and cell-killing activities of a series of Victoria blue derivatives in a mouse mammary tumour cell line. *Cytotechnology* 29, 35-43.

Wang, T., Mu, X., Li, H., Wu, W., Nie, J., Yang, D., 2013. The photocrosslinkable tissue adhesive based on copolymeric dextran/HEMA. *Carbohydrate Polymers* 92, 1423-1431.

Wang, Y., Spencer, P., 2003. Hybridization Efficiency of the Adhesive/Dentin Interface with Wet Bonding. *Journal of Dental Research* 82, 141-145.

Wang, Y., Spencer, P., Yao, X., Ye, Q., 2006. Effect of coinitiator and water on the photoreactivity and photopolymerization of HEMA/camphoquinone-based reactant mixtures. *Journal of Biomedical Materials Research Part A* 78A, 721-728.

Wang, Z.-S., Cui, Y., Dan-oh, Y., Kasada, C., Shinpo, A., Hara, K., 2008. Molecular Design of Coumarin Dyes for Stable and Efficient Organic Dye-Sensitized Solar Cells. *The Journal of Physical Chemistry C* 112, 17011-17017.

Yamamoto, A., Tsubota, K., Takamizawa, T., Kurokawa, H., Rikuta, A., Ando, S., Takigawa, T., Kuroda, T., Miyazaki, M., 2006. Influence of light intensity on dentin bond strength of self-etch systems. *Journal of Oral Science* 48, 21-26.

Ye, Q., Park, J., Laurence, J.S., Parthasarathy, R., Misra, A., Spencer, P., 2011. Ternary Phase Diagram of Model Dentin Adhesive Exposed to Over-wet Environments. *Journal of Dental Research* 90, 1434-1438.

Ye, Q., Park, J., Parthasarathy, R., Pamatmat, F., Misra, A., Laurence, J.S., Marangos, O., Spencer, P., 2012. Quantitative analysis of aqueous phase composition of model dentin adhesives experiencing phase separation. *Journal of Biomedical Materials Research Part B: Applied Biomaterials* 100B, 1086-1092.

Ye, Q., Park, J., Topp, E., Spencer, P., 2009. Effect of photoinitiators on the in vitro performance of a dentin adhesive exposed to simulated oral environment. *Dental Materials* 25, 452-458.

Ye, Q., Park, J.G., Topp, E., Wang, Y., Misra, A., Spencer, P., 2008. In vitro Performance of Nano-heterogeneous Dentin Adhesive. *Journal of Dental Research* 87, 829-833.

Ye, Q., Spencer, P., Wang, Y., Misra, A., 2007a. Relationship of solvent to the photopolymerization process, properties, and structure in model dentin adhesives. *Journal of Biomedical Materials Research Part A* 80A, 342-350.

Ye, Q., Wang, Y., Williams, K., Spencer, P., 2007b. Characterization of photopolymerization of dentin adhesives as a function of light source and irradiance. *Journal of Biomedical Materials Research Part B: Applied Biomaterials* 80B, 440-446.

Yu, Q., Nauman, S., Santerre, J., Zhu, S., 2001. UV photopolymerization behavior of dimethacrylate oligomers with camphorquinone/amine initiator system. *Journal of applied polymer science* 82, 1107-1117.

Zhang, Y., Kranbuehl, D.E., Sautereau, H., Seytre, G., Dupuy, J., 2008. Study of UV Cure Kinetics Resulting from a Changing Concentration of Mobile and Trapped Radicals. *Macromolecules* 41, 708-715.

NOMENCLATURE

Abbreviations and symbols with their meaning are given below:

a/d	Adhesive/dentin
CQ	Camphorquinone
EDMAB	Ethyl 4-(dimethylamino) benzoate
HEMA	2-hydroxyethyl methacrylate
BisGMA	Bisphenol A glycerolate dimethacrylate
DMAEMA	2-(dimethylamino)ethyl methacrylate
DPIHP	Diphenyl iodonium hexafluorophosphate
D ₂ O	Deuterium oxide
QTX	[3-(3,4-Dimethyl-9-oxo-9H-thioxanthen-2-yloxy)-2-hydroxypropyl]trimethylammonium chloride
PI	Photo-initiator
NR	Neat resin
PB	Phase boundary
PIPS	Polymerization-induced phase separation
SIPS	Solvent-induced phase separation
HPLC	High performance liquid chromatography
DSC	Differential scanning calorimetry
MTDSC	Modulated temperature differential scanning calorimetry
FTIR	Fourier transform infrared spectrophotometer
PET	Photo-induced electron transfer
T _g	Glass transition temperature
[C]	Concentration
λ	Wavelength
X	Path length for UV-vis spectroscopy
n _{phλ}	Number of photons per square centimeter and per second
LCU	Light curing unit
nm	Nano meter
w	Spectral irradiance
mW/cm ²	Milliwatt per centimeter square
h	Planck's constant
c	Speed of light
μM	Micro molar
R ²	Correlation coefficient
Q ²	Predictive squared correlation
C _p	Mallow's statistic
LOOCV	Leave-one-out cross-validation
QSPRs	Quantitative structure property relationships
CAMD	Computer-aided molecular design
DC	Degree of conversion
PAE	Photon absorption efficiency
RT	Rate of polymerization
ξ	Molar extinction coefficient
ⁿ χ	Connectivity indices of n th order
ⁿ χ ^v	Valence connectivity indices of n th order

δ	Simple connectivity indices
δ^v	Valence simple connectivity indices
Z	Total number of electrons on the inner shells and valence shell of a non-hydrogen atom
Z^v	Number of electrons on the valence shell of a non-hydrogen atom
N_H	Number of hydrogen atoms connected to a non-hydrogen atom
N_s	Number of sub-graphs of path length n
log P	Logarithm of octanol/water partition coefficient

APPENDIX: A. SOURCE FOR CALCULATION OF CONNECTIVITY INDICES AND VALENCE CONNECTIVITY INDICES IN MATLAB®

```
function calcDescriptor
%
% adjacency matrix
% adjM = [0 1 0 0; 1 0 1 1; 0 1 0 0; 0 1 0 0];
adjM = xlsread('Molecule4_DC0.8_Weight.xlsx');
%
E = xlsread('extra_Molecule4_DC0.8_Weight.xlsx');
% number of hydrogen bonded to an atom
% numH = [3 0 0 0];
numH = E(1,:);
%
% atomic number
% del = [6 6 8 9];
del = E(2,:);
%
% valance electron
% delV = [4 4 6 7];
delV = E(3,:);
%
% simple valance connectivity index
avv = (delV - numH) ./ (del - delV - 1);
%
% simple connectivity indices
av = sum(adjM,2)';
%
% chi0 is the zeroth connectivity index
% chi0 = SUM(1 / sqrt(av(i)))
```

```

temp1 = 1 ./ (av .^ 0.5); % temporary vector for chi0 calculation
chi0 = sum(temp1);
disp('Chi0 = ')
disp(chi0)
%
% chi0v is the zeroth valence connectivity index
% chi0v = SUM(1 / sqrt(avv(i)))
temp2 = 1 ./ (avv .^ 0.5); % temporary vector for chi0v calculation
chi0v = sum(temp2);
disp('Chi0v = ')
disp(chi0v)
%
% chi1 is first order connectivity index
[r3,c3] = find(triu(adjM)); % retrieves the row and column number
                % for non zero element in upper adjM
temp3 = 1 ./ ((av(r3) .* av(c3)) .^ 0.5); % temporary vector for chi1
chi1 = sum(temp3);
disp('Chi1 = ')
disp(chi1)
%
% chi1v is first order valance connectivity index
temp4 = 1 ./ ((avv(r3) .* avv(c3)) .^ 0.5); % temporary vector for chi1
chi1v = sum(temp4);
disp('Chi1v = ')
disp(chi1v)
%
% chi2 is second order connectivity index
% chi2v is second order valance connectivity index
m = size(adjM,1);

```



```

disp('Chi3v = ')
disp(chi3v)
%
% chi4 is second order connectivity index
% chi4v is second order valance connectivity index
m = size(adjM,1);
U = adjM;
chi4 = 0;
chi4v = 0;
for ii = 1:1:m
    for jj = 1:1:m
        if jj ~= ii
            if U(ii,jj) > 0
                for kk = 1:1:m
                    if (kk ~= ii) && (kk ~= jj)
                        if U(jj,kk) > 0
                            for ll = 1:1:m
                                if (ll ~= ii) && (ll ~= jj) && (ll ~= kk)
                                    if U(kk,ll) > 0
                                        for mm = 1:1:m
                                            if (mm ~= ii) && (mm ~= jj) && (mm ~= kk) && (mm ~= ll)
                                                if U(ll,mm) > 0
                                                    chi4 = chi4 + (1 / (av(ii) * av(jj) * av(kk) * av(ll) * av(mm)))^0.5);
                                                    chi4v = chi4v + (1 / (avv(ii) * avv(jj) * avv(kk) * avv(ll) * avv(mm)))^0.5);
                                                end
                                            end
                                        end
                                    end
                                end
                            end
                        end
                    end
                end
            end
        end
    end
end
end
end

```



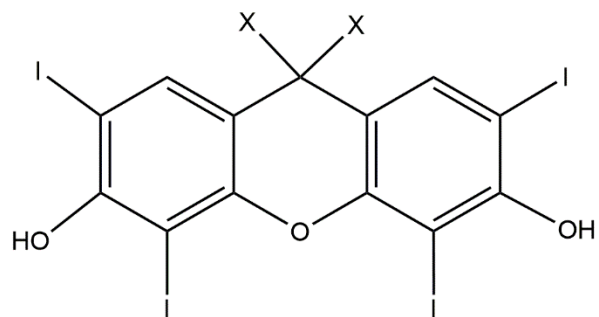
```
disp('Chi5 =')
```

```
disp(chi5)
```

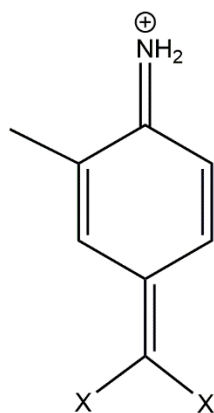
```
disp('Chi5v =')
```

```
disp(chi5v)
```

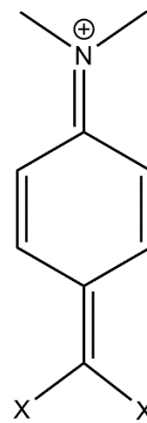
APPENDIX: B. MOLECULAR STRUCTURES OF SUB-GROUPS USED IN CAMD



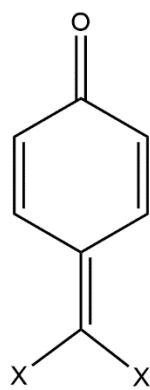
Group 1



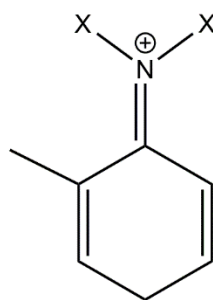
Group 2



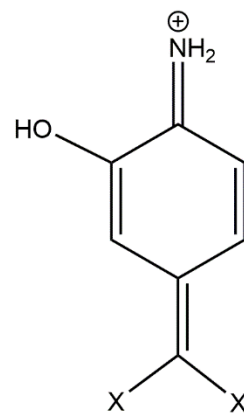
Group 3



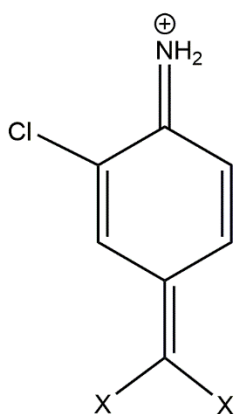
Group 4



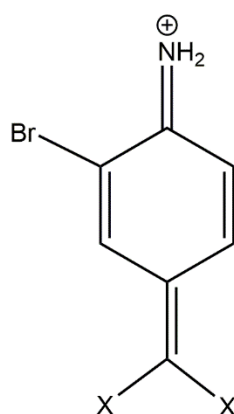
Group 5



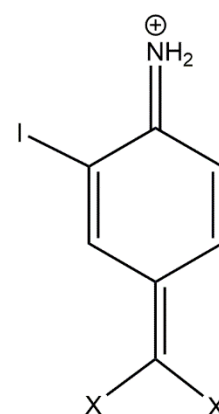
Group 6



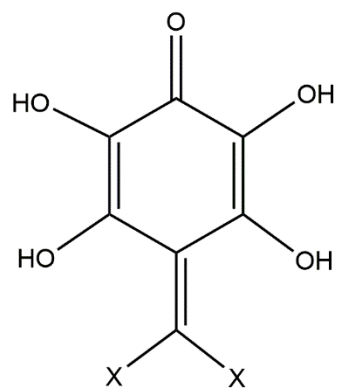
Group 7



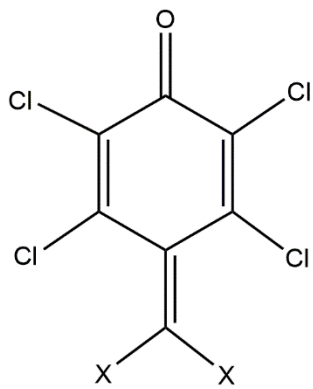
Group 8



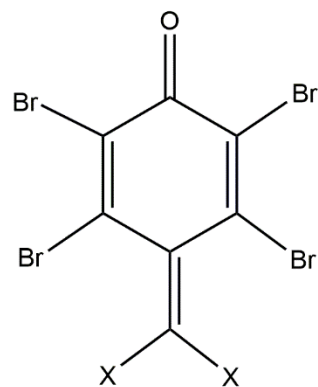
Group 9



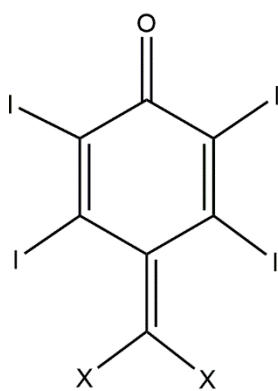
Group 10



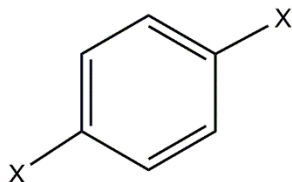
Group 11



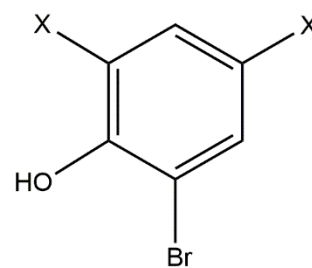
Group 12



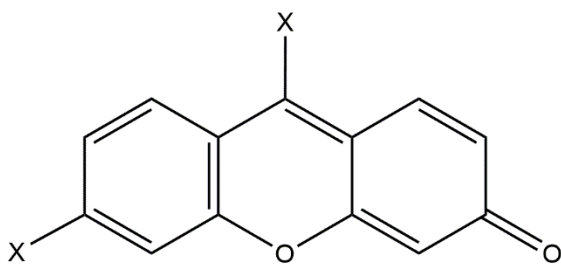
Group 13



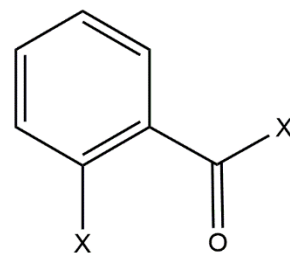
Group 14



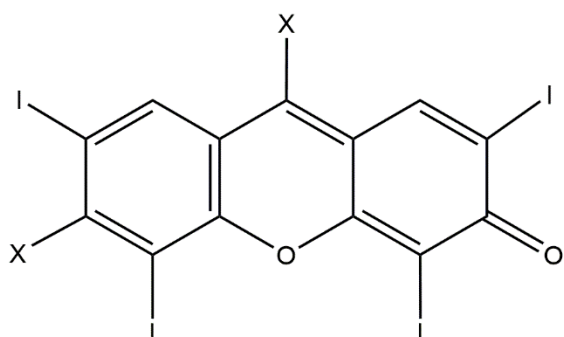
Group 15



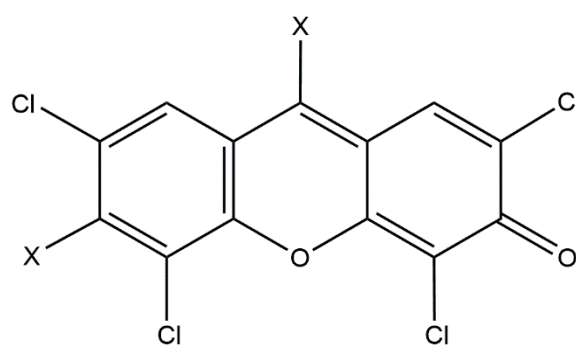
Group 16



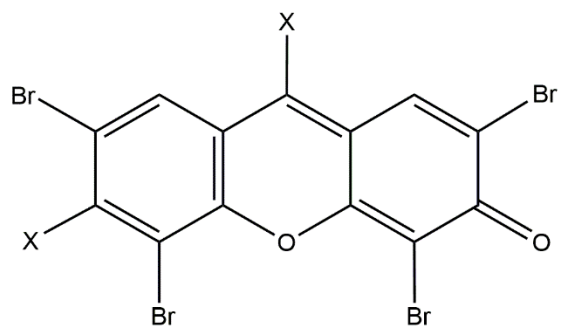
Group 17



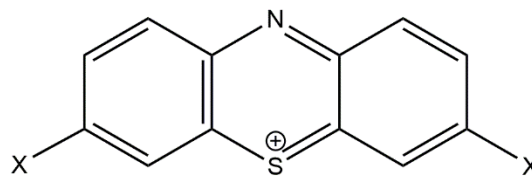
Group 18



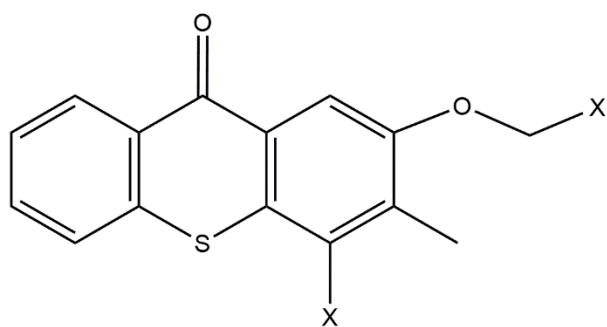
Group 19



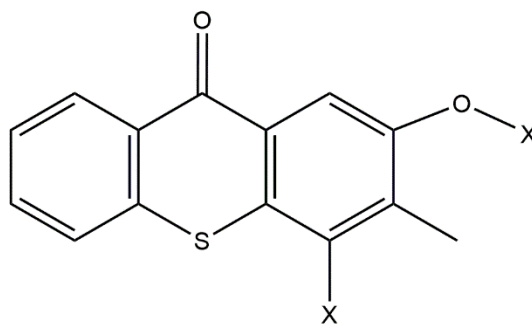
Group 20



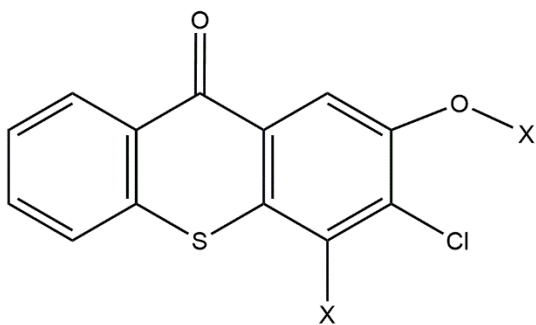
Group 21



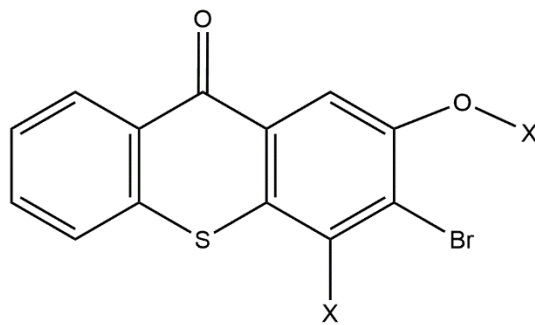
Group 22



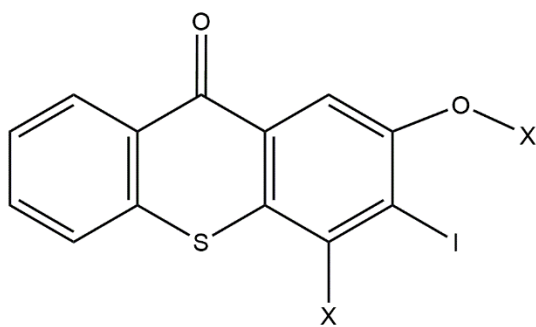
Group 23



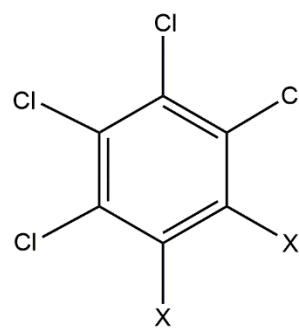
Group 24



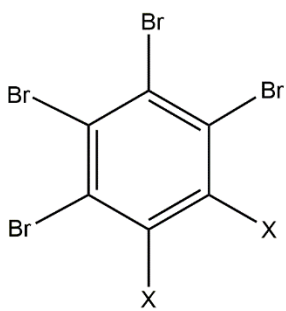
Group 25



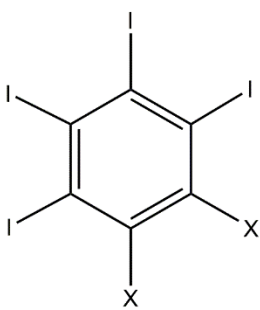
Group 26



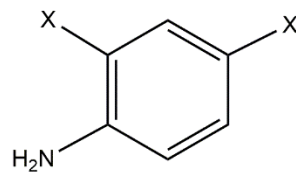
Group 27



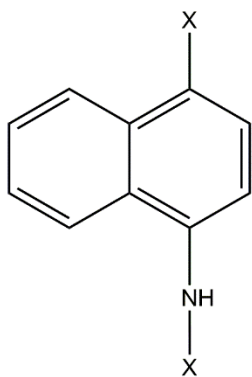
Group 28



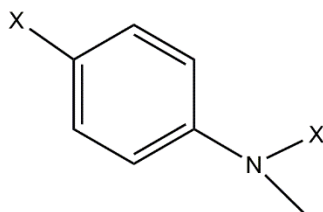
Group 29



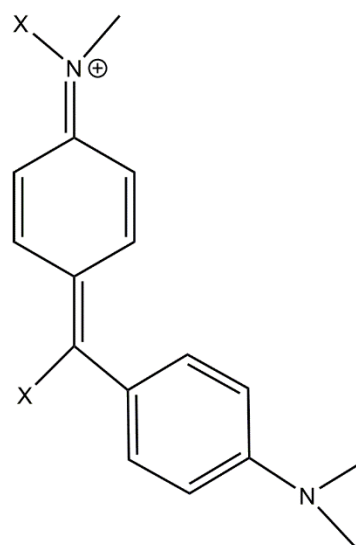
Group 30



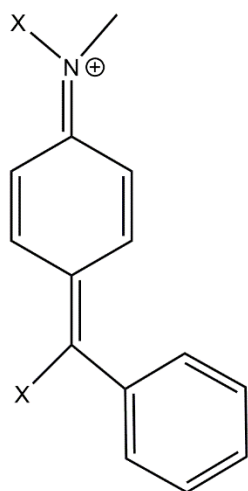
Group 31



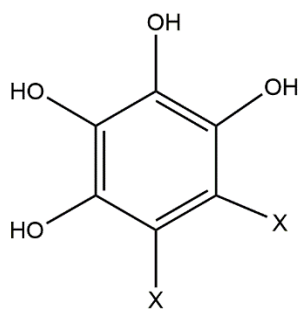
Group 32



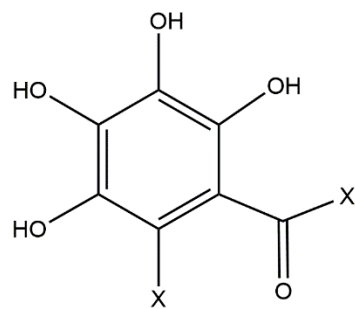
Group 33



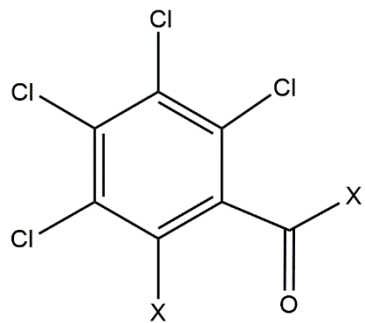
Group 34



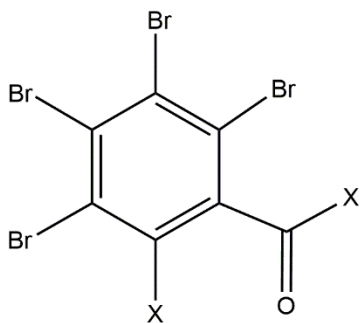
Group 35



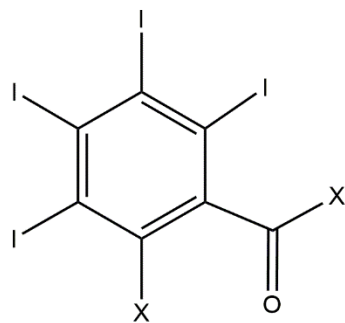
Group 36



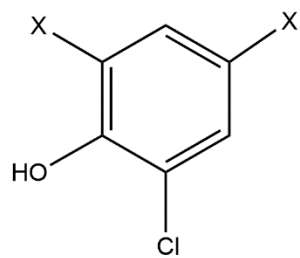
Group 37



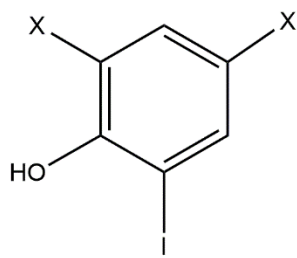
Group 38



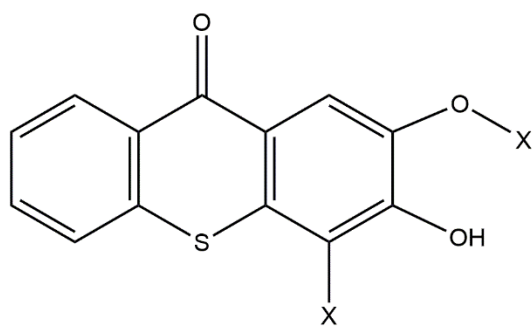
Group 39



Group 40



Group 41



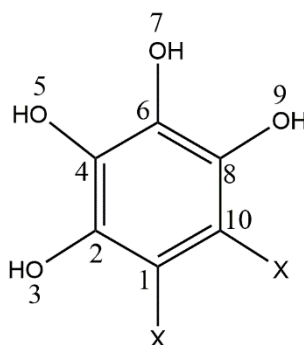
Group 42

APPENDIX: C. CHANGES MADE TO THE EXISTING “CARBOHYDRATE EXCIPIENT DESIGNER” TO ADAPT IT FOR THE DESIGN OF PHOTSENSITIZER

- At first the sub-groups are replaced with relevant groups in terms of adjacency matrix (denoted as ‘AM’ in the excel sheet), vectors for total number of non-hydrogen atoms (n) in the group, total number of electrons in the inner shell and valence shell which is denoted in the excel sheet as ‘d’, number of electrons in the valence shell which is denoted as ‘dv’ and number of hydrogen atoms connected to each non-hydrogen atom in the group and this is denoted as ‘nH’.
- The Figure below shows the screen shot of the excel sheet containing structural information of one such group. The name of the excel sheet representing the example is ‘Group7j’ and it represents the sub-group 35 shown in Appendix B.

	A	B	C	D	E	F	G	H	I	J	K	L	M	N	O	P	Q	R	S
1				0		0 AM													
2	n	d	dv	nH															
3	1	6	4	0		1	0	1	1	0	0	0	0	0	0	0	0	0	0
4	2	6	4	0		0	1	0	0	0	0	0	0	0	0	0	0	0	0
5	3	8	6	1		0	1	0	0	1	1	0	0	0	0	0	0	0	0
6	4	6	4	0		0	0	0	1	0	0	0	0	0	0	0	0	0	0
7	5	8	6	1		0	0	0	1	0	0	1	1	0	0	0	0	0	0
8	6	6	4	0		0	0	0	0	0	1	0	0	0	0	0	0	0	0
9	7	8	6	1		0	0	0	0	0	1	0	0	1	1	0	0	0	0
10	8	6	4	0		0	0	0	0	0	0	0	1	0	0	0	0	0	0
11	9	8	6	1		1	0	0	0	0	0	0	1	0	0	0	0	0	0
12	10	6	4	0															

- The Figure below shows the structure of the sub-group 35 with each non-hydrogen atom numbered.



- The maximum number of groups allowed to create the solution is changed to 6 which is denoted in the program as 'm_max'. The total number of groups available to choose from to build solutions is changed to 42 which is denoted here as 'n'. The Figure below shows that these changes have been made in the Base_Module.

```

Cells(1 + i, 3) = Final_Obj
Cells(1 + i, 4) = GetTickCount - t 'time elapsed while running code(and calculating MW and inserting values in excel - but that
For j = 1 To mol_size
    Cells(1 + i, 4 + j) = mol(j)
Next j
Next i

End Sub

Sub CAMD(mol() As Long, Final_Obj As Double) 'argument mol() As Long, Final_Obj As Double

Dim m As Long, size As Long
Dim i As Long, j As Long
'Dim mol() As Long, Final_Obj As Double 'arguments sometimes
Dim del() As Long, delv() As Long, nH() As Long
Dim AdjM() As Long, chi(0 To 5) As Double, ChiV(0 To 5) As Double
Dim Chi_Avg(0 To 5) As Double, ChiV_Avg(0 To 5) As Double

m_max = 6 'maximum number of groups in molecule
n = 42 ' number of groups
n_minusrings = 0 'number of groups that are non-ring groups, also the first groups by order

'Create initial solution
Call InitialSolution(mol(), m)
m = 5
ReDim mol(1 To m)
mol(1) = 7
mol(2) = 17
mol(3) = 36
mol(4) = 22
mol(5) = 1

'Create adjacency matrix and vectors to store del and delv values

```

- The total number of non-hydrogen atoms in each group is modified based on the groups used for the photosensitizer design. The Figure shows the section in the program within the Base_Module where changes have been made.

```

End Sub

Function atoms(molecule_group As Long) As Long
'Assigns number of atoms in group selected

Select Case molecule_group
Case Is = 1
atoms = 20
Case Is = 2
atoms = 9
Case Is = 3
atoms = 10
Case Is = 4
atoms = 8
Case Is = 5
atoms = 7
Case 6 To 9
atoms = 9
Case 10 To 13
atoms = 12
Case Is = 14
atoms = 6
Case Is = 15
atoms = 8
Case Is = 16
atoms = 15
Case Is = 17
atoms = 8
Case 18 To 20
atoms = 19
Case Is = 21
atoms = 14
Case Is = 22
atoms = 18
Case 23 To 26
atoms = 17

```

- It was ensured that the correct group numbers were assigned against the excel sheet names which contained structural information of the groups. The Figure below shows the section on the program within the Base_module where these changes were made.

The screenshot shows the Microsoft Visual Basic for Applications editor. The Project - VBAProject window on the left lists several sheets (Sheet5 to Sheet90) and a ThisWorkbook object. The Properties - Base_Modu window shows the Base_Modu Module. The main code window displays the following code:

```

End Select
End Function

Function Name(molecule_group As Long) As String
'Assigns name to group selected

Select Case molecule_group
Case Is = 1
    Name = "Group1"
Case Is = 2
    Name = "Group2a"
Case Is = 3
    Name = "Group2b"
Case Is = 4
    Name = "Group3"
Case Is = 5
    Name = "Group4"
Case Is = 6
    Name = "Group5a"
Case Is = 7
    Name = "Group5b"
Case Is = 8
    Name = "Group5c"
Case Is = 9
    Name = "Group5d"
Case Is = 10
    Name = "Group6a"
Case Is = 11
    Name = "Group6b"
Case Is = 12
    Name = "Group6c"
Case Is = 13
    Name = "Group6d"
Case Is = 14
    Name = "Group6e"
Case Is = 15

```

- The excel sheets containing structural information of groups that were not relevant to the design of photosensitizer were not included as shown in the Figure below.

The screenshot shows the Microsoft Visual Basic for Applications editor. The Project - VBAProject window on the left lists several sheets (Sheet5 to Sheet90) and a ThisWorkbook object. The Properties - Base_Modu window shows the Base_Modu Module. The main code window displays the following code:

```

Case Is = 33
    Name = "Group7h"
Case Is = 34
    Name = "Group7i"
Case Is = 35
    Name = "Group7j"
Case Is = 36
    Name = "Group7k"
Case Is = 37
    Name = "Group7l"
Case Is = 38
    Name = "Group7m"
Case Is = 39
    Name = "Group7n"
Case Is = 40
    Name = "Group7o"
Case Is = 41
    Name = "Group7p"
'Case Is = 42
'Name = "Group8a"
Case Is = 42
    Name = "Group8b"
'Case Is = 44
'Name = "Group8c"
'Case Is = 45
'Name = "Group8d"
'Case Is = 46
'Name = "Group8e"
'Case Is = 47
'Name = "Group8f"
'Case Is = 48
'Name = "Group8g"
'Case Is = 49
'Name = "Group8h"
'Case Is = 50
'Name = "Group8i"
'Case Is = 51

```

- The molecular weight of the groups were modified based on the groups used for the photosensitizer design and the Figure below shows the section within the Properties_Module in the program where these changes were made. As groups are added to build the molecule, their molecular weights are added to yield the final molecular weight of the molecule.

```

Microsoft Visual Basic for Applications - Carbohydrate Expdient Designer_v5_editable - Dental_Adhesive_final.xlsm - [Properties_Module (Code)]
File Edit View Insert Format Debug Run Tools Add-Ins Window Help
Project - VBAPProject (General) MW
Function MW(mol) As Double
Dim sum As Long, size As Long
Dim i As Long
m = UBound(mol)
sum = 34
For i = 1 To m
Select Case mol(i)
Case Is = 1
sum = sum + 716
Case Is = 2
sum = sum + 117
Case Is = 3
sum = sum + 131
Case Is = 4
sum = sum + 104
Case Is = 5
sum = sum + 91
Case Is = 6
sum = sum + 119
Case Is = 7
sum = sum + 138
Case Is = 8
sum = sum + 183
Case Is = 9
sum = sum + 230
Case Is = 10
sum = sum + 168
Case Is = 11
sum = sum + 240
Case Is = 12
sum = sum + 420
Case Is = 13
sum = sum + 608

```

- The target properties for the photosensitizer design was declared in the function obj() within the Properties_Module as 'Prop_extinction' for $\ln(\xi)$, 'Prop_PAE' for relative normalized PAE, 'Prop_logp' for log P, 'Prop_DC' for degree of conversion (DC) and 'Prop_RT' for the rate of polymerization (RT). The correlations for the current problem were included as shown below. The objective function was modified accordingly as shown below.

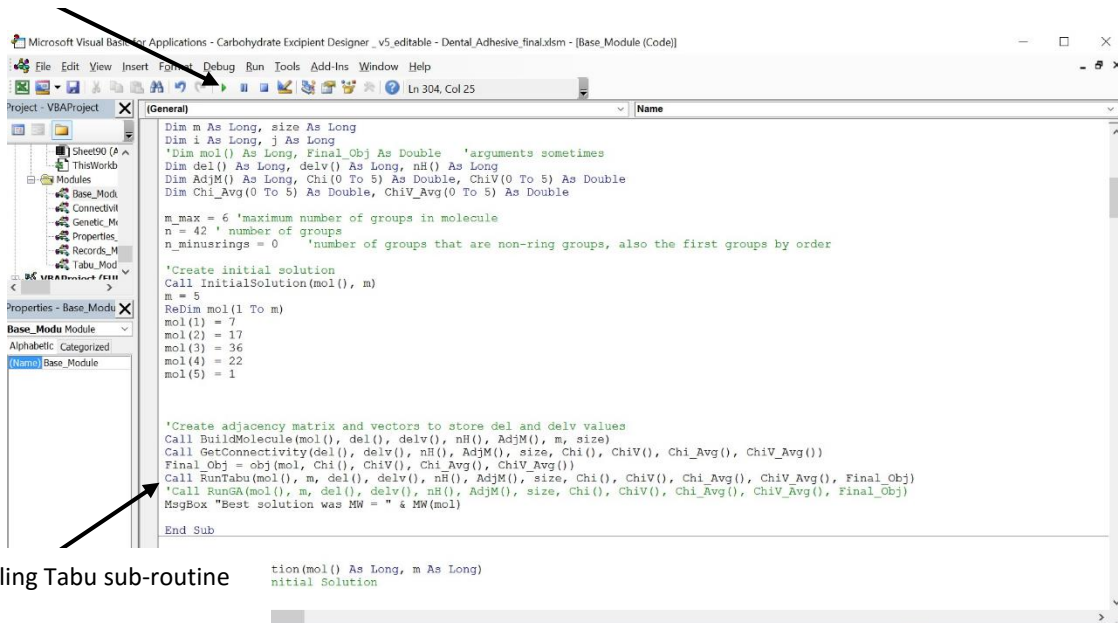
```

Microsoft Visual Basic for Applications - Carbohydrate Expdient Designer_v5_editable - Dental_Adhesive_final.xlsm - [Properties_Module (Code)]
File Edit View Insert Format Debug Run Tools Add-Ins Window Help
Project - VBAPProject (General) obj
Dim Target_MW As Double, Target_A As Double, Prop_DC As Double, Prop_RT As Double
Dim A As Double, alpha As Double, bebest As Double, MW_prot As Double, Tn As Double
Design Targets
Target_MW = 1200
Target1 = 18 '1.64092082073789
Target2 = 18 '0.19286646593339
Process Properties -- Read from user at later date
'ASA = 4152
'bebest = 21
'bebest = 33
'MW_prot = 16.5
'Tn = 42.5
Penalty = 0
Prop_MW = MW(mol)
Prop_extinction = 32.22723179 + 3.95276955 * ChiV(0) - 15.07571983 * ChiV(5) - 4.60662739 * Chi(0) + 0.63374376 * Chi(1) - 0.4253649 * Chi(3) + 4.81887335 * Chi(4)
Prop_PAE = 34.3226 - 1.7455 * Chi(0) - 0.0407 * Chi(2) + 6.1803 * Chi(3) + 5.108 * Chi(5) + 9.9007 * ChiV(2) - 26.9839 * ChiV(5)
Prop_logp = -9.058655281 + 1.613431332 * Chi(1) - 7.566660202 * Chi(6) + 6.868561976 * Chi(5) + 0.985948192 * ChiV(0) - 1.487003961 * ChiV(2)
Prop_DC = -5.1037 - (1.3282 * Chi(5)) + (2.3184 * Chi(2)) - (3.0587 * Chi(4)) + (2.8822 * Chi(5)) - (0.7338 * ChiV(2)) - (1.1734 * ChiV(4))
Prop_RT = -0.0393 + (0.0376 * Chi(0)) - (0.0389 * ChiV(1)) + (0.0383 * ChiV(3)) - (0.0284 * ChiV(5)) + (0.0289 * ChiV(4))
'Penalty Function
'For i = 1 To UBound(mol)
'If i > 1 Then
'If mol(i - 1) > n_minrings And mol(i) > n_minrings Then 'Add penalty if two rings are fused together
'Penalty = 1000
'Exit For
'End If
'End If
'Next i
obj = (Abs(Prop_extinction - 9) / 9) * 0.1 + (Abs(Prop_PAE - 7) / 7) * 0.1 + (Abs(Prop_logp + 0.55) / 0.55) * 0.3 + (Abs(Prop_DC - 0.8) / 0.8) * 0.4 + (Abs(Prop_RT - 0.0031) / 0.0031) * 0.2 + (Abs(Prop_extinction - 9) / 9) * 0.22 + (Abs(Prop_PAE - 7) / 7) * 0.22 + (Abs(Prop_logp + 0.55) / 0.55) * 0.22 + (Abs(Prop_DC - 0.8) / 0.8) * 0.22 + (Abs(Prop_RT - 0.0031) / 0.0031) * 0.22
Function fitness(mol) As Double
'Target_MW = 148
'Lower_MW = 0
'Higher_MW = 296
'alpha = 0.001
'Fitness = Exp(-alpha * (MW(mol) - Target_MW) ^ 2 / (Higher_MW - Lower_MW) ^ 2)
End Function

```

- The “Carbohydrate Excipient Designer” is capable of solving the CAMD problem by Tabu Search as well as by genetic algorithm. For the problem here, only Tabu Search was employed as shown in the Figure below. The program is ran by pressing the start button and then it will show a command box where ‘RUNMANYCAMD()’ needs to be selected and the ‘RUN’ button is clicked to run the program.

Start button



Calling Tabu sub-routine

- For each run, the best solution is displayed on the “Sheet1” of the excel file as shown below. The result for the best solution contains the group number making up the molecule and its objective function value.

Attempt	Obj	t (ms)	molecule
1	1.060854	10389	1
2	0.861308	10920	7 21
3	0.686634	15334	9 21
4	1.15464	11466	6 21
5	0.721149	15397	25 8
6	1.060854	19001	1
7	1.060854	14305	1
8	0.686634	35584	21 9
9	0.721149	19859	25 8
10	1.204144	17285	27 15 2
11	1.185349	10281	12 23 31 27
12	0.977125	11872	26 30
13	0.626063	19625	18 27
14	0.693257	17347	23 9
15	1.060854	9360	1
16	1.244615	15335	8 33
17	0.585228	18580	12 16 3
18	0.867974	7207	14 21
19	0.602612	22683	12 37 15 7
20	0.934771	15772	30 21
21	0.863927	18315	27 30
22	0.840543	16228	27 41 14 41
23			

Best solution for each run is displayed here